DEVELOPMENT OF ANALYTICAL METHODS FOR THE QUANTITATIVE ANALYSIS OF THE ENZYME ABUNDANCE AND ACTIVITY IN THE ARACHIDONIC ACID CASCADE

Dissertation

to obtain the academic degree

Doctor rerum naturalium

(Dr. rer. nat.)

Faculty of Mathematics and Natural Sciences

of the

Bergische Universität Wuppertal

by

Nicole M. Hartung

Frankfurt am Main

- 2022 -

Erste*r Gutachter*in: .... Prof. Dr. Nils Helge Schebb

Zweite*r Gutachter*in: ....Prof. Dr. Julia Bornhorst

Tag der mündlichen Prüfung: 29.04.2022

Tag der Promotion: 29.04.2022

Für meine Familie

Table of Contents

Chapter 1

Introduction and Scope

Several physiological reactions such as inflammation, vascular tone or blood clotting are regulated by a distinct set of oxygenated polyunsaturated fatty acids (PUFA) termed eicosanoids and other oxylipins [1]. Their formation routes include enzymatic conversion via the enzymes of the arachidonic acid (ARA) cascade or autoxidation of mainly n6 (e.g. ARA, linoleic acid) or n3 (eicosapentaenoic acid, docosahexaenoic acid) PUFA, leading to a multitude of structurally diverse products. The three main enzymatic pathways are comprised of the cyclooxygenase (COX), lipoxygenase (LOX) and cytochrome P450 monooxygenase (CYP) enzymes which catalyze the oxygenation to mainly regio- and stereospecific products, while the autoxidation reaction is less specific [2].

The two main enzymes of the COX pathway, COX-1 and -2, both catalyze a dual cyclooxygenase (*bis*-oxygenase) and peroxidase reaction. In the first reaction step, prostaglandin (PG) G_2 is formed from ARA after initial hydrogen abstraction at C13 and reaction with molecular O_2 to form a C11 to C9 endoperoxide concomitant with internal cyclization and peroxidation at C15 with a second O_2 molecule. PGG_2 is then reduced at the heme-containing active site of COX to PGH_2 which serves as substrate for many downstream enzymatic reactions [3]. For example, PGE, PGD and PGI synthases convert the unstable PGH_2 to PGE_2, PGD_2 and PGI_2, respectively, while the thromboxane (Tx) synthase catalyzes the formation of TxA_2 and as side product 12-hydroxy-heptadecatrienoic acid (12-HHT) [4]. However, PGE_2, PGD_2 and 12-HHT can also be formed non-enzymatically under certain conditions [5, 6]. Though the COX isoforms share about 60% sequence identity [7], they differ in their physiological functions. The prostaglandin-endoperoxide synthase 1 (*PTGS1*;

COX-1 gene) is mainly constitutively expressed and involved in homeostatic processes, for example, in the mucosal protection of the gastrointestinal tract [8] or the regulation of blood clotting in platelets [7] and the vascular endothelium [9]. *PTGS2* (COX-2 gene) is constitutively expressed in several organs including the renal medulla and regions of the brain and gut [10] and inducible in the setting of disease, e.g. in colon tissue or macrophages [3]. Its expression is then induced by stimulation with pro-inflammatory noxae, for example, lipopolysaccharide, tumor necrosis factor α or interleukin 1β [3]. Therefore, *PTGS2* expression is elevated during acute and chronic diseases such as arthritis and inflammation [7].

LOX are non-heme iron-containing dioxygenases that convert PUFA to unstable hydroperoxy-FA. The regio- and stereospecific peroxidation is performed by six different isoforms in humans, initially termed with respect to their reaction specificity with ARA (5-LOX, eLOX3, 12-LOX, 12-*R*-LOX, 15-LOX, 15-LOX-2) [11]. Hereby, after a stereospecific hydrogen abstraction at the C3-atom of a *cis,cis*-1,4-pentadiene system the radical migrates to the C5 atom and finally forms hydroperoxyl-FA under molecular O_2 consumption [12]. It can be reduced to hydroxy-FA by, e.g., cellular glutathione peroxidases [13] or, in case of ARA oxygenation by 5-LOX, be further converted to leukotriene (LT) A_4 [14]. Unlike other LOX isoforms, the cellular product formation of 5-LOX is greatly enhanced together with the 5-LOX activating protein (FLAP) which is located at the nuclear membrane by stimulated substrate utilization [15]. Downstream enzymes can further convert LTA_4 to LTB_4 or LTC_4 acting as pro-inflammatory signaling molecules, e.g., by stimulating chemotaxis of neutrophils [16] and as mediators of bronchoconstriction [17], respectively. 12-LOX, also termed "platelet-type" LOX for its high abundance in these cells [18], catalyzes the formation of 12-hydro(pero)xyeicosatetraenoic acid (H(p)ETE) from ARA which is involved in the regulation of platelet functions [19]. Eosinophils are one of the main sources of 15-LOX as well as M2-like macrophages where 15-LOX-2 is also present [12, 20]. While 15-LOX-2 converts ARA exclusively to 15-H(p)ETE, 15-LOX shows dual reaction specificity forming 15- and 12-H(p)ETE in a ratio of

~ 9:1 [21]. Concerted reactions of several LOX isoforms lead to the formation of multiple hydroxylated-FA termed lipoxins, maresins, protectins and resolvins which promote active resolution of inflammation [22]. However, they are controversially discussed regarding their suggested biosynthetic pathways, signaling receptors and formation in biologically active concentrations in humans [23].

The CYP family consists of 57 enzymes in humans [24]. They are highly relevant in the metabolism of xenobiotics, but many are also able to convert fatty acids to oxylipins. Depending on the enzyme, CYP oxidize PUFA at the heme-iron active site via three reaction types forming mid-chain or *ω*-/(*ω*-n)-hydroxy-FA by *bis*-allylic or terminal/subterminal hydroxylation, respectively, as well as *cis*-epoxy-FA by olefin epoxidation [25]. The CYP products are involved in many physiological reactions, for example, the regulation of the vascular tone or sodium reabsorption in the kidneys [26]. Epoxy-FA are readily hydrolyzed by the soluble epoxide hydrolase to *vic*-dihydroxy-FA, which are generally regarded as less biologically active [27].

Not only the enzymatic, but also non-enzymatic autoxidative reactions lead to the large variety of oxylipin structures including hydro(pero)xy-FA, prostanoid-like isoprostanes (IsoP) as well as *cis* and *trans*-epoxy-FA [28-30] which is initiated by *bis*-allylic hydrogen abstraction, the reaction with molecular oxygen and additional rearrangement or cyclization reactions [28]. Though some biological functions of the isoprostanes have been described, they are mainly investigated for their role as biomarkers of oxidative stress arising from disease or environmental factors [31]. For instance, 15-F_{2t}-IsoP (8-*iso*-$PGF_{2\alpha}$) and the 8-*iso*-$PGF_{2\alpha}$/$PGF_{2\alpha}$-ratio are prominent examples of isoprostane biomarkers for oxidative stress [32, 33] and recently, the *trans/cis*-epoxy-PUFA ratio was also shown to serve as such an indicator [30].

This large number of enzymatic and non-enzymatic reactions combined with multiple PUFA substrates lead to the formation of a plethora of oxylipins with distinct physiological functions. Due to their regulatory crosstalk and complex interactions between the different pathways of the ARA cascade it is necessary to analyze the whole oxylipin pattern rather than single compounds. Thus, metabolomics-based analytical approaches are indispensable for understanding their biology [1, 34]. Moreover, changes in the abundances of the enzymes/proteins involved in oxylipin formation affect their concentrations.

Therefore, the parallel analysis of enzyme/protein abundance levels is essential. In the past decades, new methods for protein analysis based on mass spectrometry have emerged [35]. Accompanied by major technological progress regarding instrumentation, sample preparation and quantification techniques as well as bioinformatic tools, LC-MS-based proteomics approaches have largely contributed to the understanding of biological systems [36]. For example, (nearly) complete proteomes of several organisms [37-39] and the regulation of cellular processes by post-translational modifications [40] have been characterized and LC-MS-based proteomics is used for the identification of disease biomarkers [41]. Depending on the aim of the study, several approaches are applicable [42]. In shotgun proteomics, typically high-resolution MS is used for assays aiming at the discovery of proteome changes by high throughput screenings, e.g., protein abundances or posttranslational modifications, without directly targeting a specific set of proteins [36]. The aim of targeted proteomics studies, in contrast, are the absolute quantification of a predefined set of proteins [43]. Therefore, this approach finds wide appreciation in clinical applications especially for biomarker validation and quantification [44] and in the development of precision medicine [45]. Here, measurements in multiple reaction monitoring (MRM) mode on triple quadrupole instruments with low detection limits and wide linear ranges generate reproducible data within and across laboratories [46].

In *chapter 2* of this thesis a targeted proteomics LC-MS/MS method was developed for the quantitative analysis of the COX-2 pathway of the ARA cascade. The method development is comprised of several *in silico* and experimental steps which were carefully described in detail presenting a standard operating procedure for future methods. With this methodology, differences in the COX-2 abundance of three colon carcinoma cell lines and the time-dependent *PTGS2* gene expression in stimulated human macrophages derived from peripheral blood monocytic cells were measured. These correlated well with the respective oxylipin levels formed via the COX branch of the ARA cascade that were measured in parallel with a targeted oxylipin metabolomics method.

A comprehensive oxylipin analysis is essential for understanding how the ARA cascade can be modulated, e.g. by diseases as well as pharmaceuticals or dietary constituents. Among the latter, secondary plant metabolites such as polyphenols are intensely investigated because of their proposed positive effects on human health. They are believed to contribute to the beneficial health effects that are correlated with the intake of fruit and vegetables in many epidemiological studies [47, 48]. Though the detailed effect mechanisms in the human body are still unclear, polyphenols are assumed to exert their positive effects by i.e. anti-oxidant – protecting from oxidative stress – and anti-inflammatory actions, mediated by the modulation of the ARA cascade [49, 50]. However, monitoring the effects on the concentrations of single oxylipins only partially reflects the biological implications, keeping in mind that physiological reactions are rather controlled by the complex interplay of several oxylipins than individual compounds [1, 34]. In *chapter 3* the impact of a library of polyphenols on the 5-LOX pathway during short-term incubations was investigated. The use of cell-free assays together with human neutrophils as biological test systems allowed not only to investigate their individual inhibitory potencies towards the 5-LOX enzyme, but also to assess their effect on the total oxylipin pattern and thus, the complex interactions with the other enzymes of the ARA cascade.

Food ingredients or drugs can not only have direct implications on the enzyme activity but can also affect oxylipin levels by modulating gene expression given sufficient exposure time. In order to further understand how the interference with gene expression contributes to the modulation of the oxylipin pattern, protein levels need to be examined simultaneously. Targeted proteomics methods provide the advantage of multiplexing several enzymes and thus, enable the parallel analysis of the different pathways. This is especially relevant for the analysis of biological systems containing multiple enzymes/proteins of the COX and LOX pathways which play crucial roles in the immune response by forming lipid mediators serving as signaling molecules. For this reason, a targeted proteomics method was developed to enable the parallel analysis of all COX (COX-1 and -2) and relevant LOX pathway enzymes/proteins (5-, 12-, 15-LOX, 15-LOX-2 and FLAP), presented in *chapter 4*. Moreover, different MS modes were carefully evaluated to ensure the most selective and sensitive peptide detection. The analytical scope of the oxylipin metabolomics method was also further extended allowing a quantitative analysis of 198 oxylipins (and 28 additional isoprostanes [51]) and thus, an even more thorough analysis of the oxylipin pattern. With the multi-omics approach comprised of the sensitive oxylipin metabolomics and proteomics methods the ARA cascade was evaluated in different human immune cells, revealing distinct oxylipin and protein signatures.

Overall, the aim of this thesis is to contribute to a more thorough understanding of the ARA cascade regulation by enabling the quantitative analysis of the enzyme/protein abundances together with the analysis of the total oxylipin pattern in a comprehensive multi-omics approach.

1.1 References

1. Gabbs M, Leng S, Devassy JG, Monirujjaman M, and Aukema HM (2015) Advances in Our Understanding of Oxylipins Derived from Dietary PUFAs. *Adv Nutr,* 6(5), 513-540; doi: 10.3945/an.114.007732.
2. Buczynski MW, Dumlao DS, and Dennis EA (2009) Thematic Review Series: Proteomics. An integrated omics analysis of eicosanoid biology. *J Lipid Res,* 50(6), 1015-38; doi: 10.1194/jlr.R900004-JLR200.

3. Smith WL, DeWitt DL, and Garavito RM (2000) Cyclooxygenases: Structural, cellular, and molecular biology. *Annu Rev Biochem,* 69, 145-182; doi: 10.1146/annurev.biochem.69.1.145.
4. Smith WL, Urade Y, and Jakobsson PJ (2011) Enzymes of the Cyclooxygenase Pathways of Prostanoid Biosynthesis. *Chem Rev,* 111(10), 5821-5865; doi: 10.1021/cr2002992.
5. Yu R, Xiao L, Zhao G, Christman JW, and van Breemen RB (2011) Competitive Enzymatic Interactions Determine the Relative Amounts of Prostaglandins E_2 and D_2. *J Pharmacol Exp Ther,* 339(2), 716-725; doi: 10.1124/jpet.111.185405.
6. Matsunobu T, Okuno T, Yokoyama C, and Yokomizo T (2013) Thromboxane A synthase-independent production of 12-hydroxyheptadecatrienoic acid, a BLT2 ligand. *J Lipid Res,* 54(11), 2979-2987; doi: 10.1194/jlr.M037754.
7. Vane JR, Bakhle YS, and Botting RM (1998) Cyclooxygenases 1 and 2. *Annu Rev Pharmacol Toxicol,* 38, 97-120; doi: 10.1146/annurev.pharmtox.38.1.97.
8. Takeuchi K and Amagase K (2018) Roles of Cyclooxygenase, Prostaglandin E-2 and EP Receptors in Mucosal Protection and Ulcer Healing in the Gastrointestinal Tract. *Curr Pharm Des,* 24(18), 2002-2011; doi: 10.2174/1381612824666180629111227.
9. Kirkby NS, Lundberg MH, Harrington LS, Leadbeater PDM, Milne GL, Potter CMF, Al-Yamani M, Adeyemi O, Warner TD, and Mitchell JA (2012) Cyclooxygenase-1, not cyclooxygenase-2, is responsible for physiological production of prostacyclin in the cardiovascular system. *Proc Natl Acad Sci,* 109(43), 17597; doi: 10.1073/pnas.1209192109.
10. Kirkby NS, Zaiss AK, Urquhart P, Jiao J, Austin PJ, Al-Yamani M, Lundberg MH, MacKenzie LS, Warner TD, Nicolaou A, et al. (2013) LC-MS/MS Confirms That COX-1 Drives Vascular Prostacyclin Whilst Gene Expression Pattern Reveals Non-Vascular Sites of COX-2 Expression. *PLoS One,* 8(7), e69524; doi: 10.1371/journal.pone.0069524.
11. Kuhn H, Banthiya S, and van Leyen K (2015) Mammalian lipoxygenases and their biological relevance. *Biochim Biophys Acta, Mol Cell Biol Lipids,* 1851(4), 308-330; doi: 10.1016/j.bbalip.2014.10.002.
12. Haeggstrom JZ and Funk CD (2011) Lipoxygenase and Leukotriene Pathways: Biochemistry, Biology, and Roles in Disease. *Chem Rev,* 111(10), 5866-5898; doi: 10.1021/cr200246d.
13. Christophersen BO (1968) Formation of monohydroxy-polyenic fatty acids from lipid peroxides by a glutathione peroxidase. *Biochim Biophys Acta, Lipids Lipid Metab,* 164(1), 35-46; doi: 10.1016/0005-2760(68)90068-4.
14. Rouzer CA, Matsumoto T, and Samuelsson B (1986) Single protein from human leukocytes possesses 5-lipoxygenase and leukotriene A4 synthase activities. *Proc Natl Acad Sci,* 83(4), 857-861; doi: 10.1073/pnas.83.4.857.
15. Abramovitz M, Wong E, Cox ME, Richardson CD, Li C, and Vickers PJ (1993) 5-lipoxygenase-activating protein stimulates the utilization of arachidonic acid by 5-lipoxygenase. *Eur J Biochem,* 215(1), 105-11; doi: 10.1111/j.1432-1033.1993.tb18012.x.
16. Palmblad J, Malmsten CL, Udén A-M, Rådmark O, Engstedt L, and Samuelsson B (1981) Leukotriene B4 is a Potent and Stereospecific Stimulator of Neutrophil Chemotaxis and Adherence. *Blood,* 58(3), 658-661; doi: 10.1182/blood.V58.3.658.658.
17. Weiss JW, Drazen JM, Coles N, McFadden ER, Weller PF, Corey EJ, Lewis RA, and Austen KF (1982) Bronchoconstrictor Effects of Leukotriene C in Humans. *Science,* 216(4542), 196-198; doi: 10.1126/science.7063880.

18. Hamberg M and Samuelsson B (1974) Prostaglandin Endoperoxides - Novel Transformations of Arachidonic-Acid in Human Platelets. *Proc Natl Acad Sci U S A,* 71(9), 3400-3404; doi: 10.1073/pnas.71.9.3400.
19. Tourdot BE and Holinstat M (2017) Targeting 12-Lipoxygenase as a Potential Novel Antiplatelet Therapy. *Trends Pharmacol Sci,* 38(11), 1006-1015; doi: 10.1016/j.tips.2017.08.001.
20. Ebert R, Cumbana R, Lehmann C, Kutzner L, Toewe A, Ferreirós N, Parnham MJ, Schebb NH, Steinhilber D, and Kahnt AS (2020) Long-term stimulation of toll-like receptor-2 and -4 upregulates 5-LO and 15-LO-2 expression thereby inducing a lipid mediator shift in human monocyte-derived macrophages. *Biochim Biophys Acta, Mol Cell Biol Lipids,* 1865(9), 158702; doi: 10.1016/j.bbalip.2020.158702.
21. Kutzner L, Goloshchapova K, Heydeck D, Stehling S, Kuhn H, and Schebb NH (2017) Mammalian ALOX15 orthologs exhibit pronounced dual positional specificity with docosahexaenoic acid. *Biochim Biophys Acta, Mol Cell Biol Lipids,* 1862(7), 666-675; doi: 10.1016/j.bbalip.2017.04.001.
22. Bannenberg G and Serhan CN (2010) Specialized pro-resolving lipid mediators in the inflammatory response: An update. *Biochim Biophys Acta, Mol Cell Biol Lipids,* 1801(12), 1260-1273; doi: 10.1016/j.bbalip.2010.08.002.
23. Schebb NH, Kühn H, Kahnt AS, Rund KM, O’Donnell VB, Flamand N, Peters-Golden M, Jakobsson P-J, Weylandt KH, Rohwer N, et al. (2022) Formation, Signaling and Occurrence of Specialized Pro-Resolving Lipid Mediators—What is the Evidence so far? *Front Pharmacol,* 13; doi: 10.3389/fphar.2022.838782.
24. Nelson DR, Zeldin DC, Hoffman SMG, Maltais LJ, Wain HM, and Nebert DW (2004) Comparison of cytochrome P450 (CYP) genes from the mouse and human genomes, including nomenclature recommendations for genes, pseudogenes and alternative-splice variants. *Pharmacogenetics,* 14(1), 1-18; doi: 10.1097/01.fpc.0000054151.92680.31.
25. Capdevila JH, Falck JR, and Harris RC (2000) Cytochrome P450 and arachidonic acid bioactivation. Molecular and functional properties of the arachidonate monooxygenase. *J Lipid Res,* 41(2), 163-81; doi: 10.1016/S0022-2275(20)32049-6.
26. Westphal C, Konkel A, and Schunck WH (2015) Cytochrome p450 enzymes in the bioactivation of polyunsaturated Fatty acids and their role in cardiovascular disease. *Adv Exp Med Biol,* 851, 151-87; doi: 10.1007/978-3-319-16009-2_6.
27. Morisseau C and Hammock BD (2005) Epoxide hydrolases: mechanisms, inhibitor designs, and biological roles. *Annu Rev Pharmacol Toxicol,* 45, 311-33; doi: 10.1146/annurev.pharmtox.45.120403.095920.
28. Yin H, Xu L, and Porter NA (2011) Free Radical Lipid Peroxidation: Mechanisms and Analysis. *Chem Rev,* 111(10), 5944-5972; doi: 10.1021/cr200084z.
29. Morrow JD, Hill KE, Burk RF, Nammour TM, Badr KF, and Roberts LJ (1990) A series of prostaglandin F2-like compounds are produced in vivo in humans by a non-cyclooxygenase, free radical-catalyzed mechanism. *Proc Natl Acad Sci,* 87(23), 9383-9387; doi: 10.1073/pnas.87.23.9383.
30. Rund KM, Heylmann D, Seiwert N, Wecklein S, Oger C, Galano JM, Durand T, Chen R, Gueler F, Fahrer J, et al. (2019) Formation of trans-epoxy fatty acids correlates with formation of isoprostanes and could serve as biomarker of oxidative stress. *Prostaglandins Other Lipid Mediat,* 144, 106334; doi: 10.1016/j.prostaglandins.2019.04.004.
31. Ahmed Omar S, Galano J-M, Pavlickova T, Revol-Cavalier J, Vigor C, Lee Jetty C-Y, Oger C, and Durand T (2020) Moving forward with isoprostanes, neuroprostanes and

phytoprostanes: where are we now? *Essays Biochem,* 64(3), 463-484; doi: 10.1042/ebc20190096.

32. van 't Erve TJ, Kadiiska MB, London SJ, and Mason RP (2017) Classifying oxidative stress by F2-isoprostane levels across human diseases: A meta-analysis. *Redox Biol,* 12, 582-599; doi: 10.1016/j.redox.2017.03.024.
33. van't Erve TJ, Lih FB, Jelsema C, Deterding LJ, Eling TE, Mason RP, and Kadiiska MB (2016) Reinterpreting the best biomarker of oxidative stress: The 8-iso-prostaglandin F2α/prostaglandin F2α ratio shows complex origins of lipid peroxidation biomarkers in animal models. *Free Radical Biol Med,* 95, 65-73; doi: 10.1016/j.freeradbiomed.2016.03.001.
34. Gladine C, Ostermann AI, Newman JW, and Schebb NH (2019) MS-based targeted metabolomics of eicosanoids and other oxylipins: Analytical and inter-individual variabilities. *Free Radical Biol Med,* 144, 72-89; doi: 10.1016/j.freeradbiomed.2019.05.012.
35. Aebersold R and Mann M (2003) Mass spectrometry-based proteomics. *Nature,* 422(6928), 198-207; doi: 10.1038/nature01511.
36. Bantscheff M, Lemeer S, Savitski MM, and Kuster B (2012) Quantitative mass spectrometry in proteomics: critical review update from 2007 to the present. *Anal Bioanal Chem,* 404(4), 939-965; doi: 10.1007/s00216-012-6203-4.
37. Picotti P, Clément-Ziza M, Lam H, Campbell DS, Schmidt A, Deutsch EW, Röst H, Sun Z, Rinner O, Reiter L, et al. (2013) A complete mass-spectrometric map of the yeast proteome applied to quantitative trait analysis. *Nature,* 494(7436), 266-270; doi: 10.1038/nature11835.
38. Schubert Olga T, Mouritsen J, Ludwig C, Röst Hannes L, Rosenberger G, Arthur Patrick K, Claassen M, Campbell David S, Sun Z, Farrah T, et al. (2013) The Mtb Proteome Library: A Resource of Assays to Quantify the Complete Proteome of Mycobacterium tuberculosis. *Cell Host Microbe,* 13(5), 602-612; doi: 10.1016/j.chom.2013.04.008.
39. Kusebauch U, Campbell DS, Deutsch EW, Chu CS, Spicer DA, Brusniak M-Y, Slagel J, Sun Z, Stevens J, Grimes B, et al. (2016) Human SRMAtlas: A Resource of Targeted Assays to Quantify the Complete Human Proteome. *Cell,* 166(3), 766-778; doi: 10.1016/j.cell.2016.06.041.
40. Pagel O, Loroch S, Sickmann A, and Zahedi RP (2015) Current strategies and findings in clinically relevant post-translational modification-specific proteomics. *Expert Rev Proteomics,* 12(3), 235-253; doi: 10.1586/14789450.2015.1042867.
41. He T (2019) Implementation of Proteomics in Clinical Trials. *Proteomics Clin Appl,* 13(2), 1800198; doi: 10.1002/prca.201800198.
42. Gillet LC, Leitner A, and Aebersold R (2016) Mass Spectrometry Applied to Bottom-Up Proteomics: Entering the High-Throughput Era for Hypothesis Testing. *Annu Rev Anal Chem,* 9(1), 449-472; doi: 10.1146/annurev-anchem-071015-041535.
43. Gallien S, Duriez E, and Domon B (2011) Selected reaction monitoring applied to proteomics. *J Mass Spectrom,* 46(3), 298-312; doi: 10.1002/jms.1895.
44. Rifai N, Gillette MA, and Carr SA (2006) Protein biomarker discovery and validation: the long and uncertain path to clinical utility. *Nat Biotechnol,* 24(8), 971-983; doi: 10.1038/nbt1235.
45. Van Eyk JE and Snyder MP (2019) Precision Medicine: Role of Proteomics in Changing Clinical Management and Care. *J Proteome Res,* 18(1), 1-6; doi: 10.1021/acs.jproteome.8b00504.

46. Addona TA, Abbatiello SE, Schilling B, Skates SJ, Mani DR, Bunk DM, Spiegelman CH, Zimmerman LJ, Ham A-JL, Keshishian H, et al. (2009) Multi-site assessment of the precision and reproducibility of multiple reaction monitoring–based measurements of proteins in plasma. *Nat Biotechnol,* 27(7), 633-641; doi: 10.1038/nbt.1546.
47. Aggarwal BB and Shishodia S (2006) Molecular targets of dietary agents for prevention and therapy of cancer. *Biochem Pharmacol,* 71(10), 1397-1421; doi: 10.1016/j.bcp.2006.02.009.
48. Arts IC and Hollman PC (2005) Polyphenols and disease risk in epidemiologic studies. *Am J Clin Nutr,* 81(1), 317S-325S; doi: 10.1093/ajcn/81.1.317S.
49. Garcia-Lafuente A, Guillamon E, Villares A, Rostagno MA, and Martinez JA (2009) Flavonoids as anti-inflammatory agents: implications in cancer and cardiovascular disease. *Inflamm Res,* 58(9), 537-52; doi: 10.1007/s00011-009-0037-3.
50. Yarla NS, Bishayee A, Sethi G, Reddanna P, Kalle AM, Dhananjaya BL, Dowluru KSVGK, Chintala R, and Duddukuri GR (2016) Targeting arachidonic acid pathway by natural products for cancer prevention and therapy. *Semin Cancer Biol,* 40–41, 48-81; doi: 10.1016/j.semcancer.2016.02.001.
51. Rund KM, Ostermann AI, Kutzner L, Galano JM, Oger C, Vigor C, Wecklein S, Seiwert N, Durand T, and Schebb NH (2018) Development of an LC-ESI(-)-MS/MS method for the simultaneous quantification of 35 isoprostanes and isofurans derived from the major n3- and n6-PUFAs. *Anal Chim Acta,* 1037, 63-74; doi: 10.1016/j.aca.2017.11.002.

Chapter 2

Combined Targeted Proteomics and Oxylipin Metabolomics for Monitoring of the COX-2 Pathway

The important role of inducible cyclooxygenase-2 (COX-2) in several diseases necessitates analytical tools enabling thorough understanding of its modulation. Analysis of a comprehensive oxylipin pattern provides detailed information about changes in enzyme activities. In order to simultaneously monitor gene expression levels, a targeted proteomics method for human COX-2 is developed. With limits of detection and quantification down to 0.25 and 0.5 fmol (on column) the method enables sensitive quantitative analysis via LC-MS/MS within a linear range up to 2.5 pmol. Three housekeeping proteins are included in the method for data normalization. A tiered approach for method development comprised of in silico and experimental steps is described for choosing unique peptides and selective and sensitive SRM transitions while avoiding isobaric interferences. This method combined with a well-established targeted oxylipin metabolomics method allows to investigate the role of COX-2 in the human colon carcinoma cell lines HCT-116, HT-29, and HCA-7. Moreover, the developed methodology is used to demonstrate the time-dependent prostanoid formation and COX-2 enzyme synthesis in lipopolysaccharide-stimulated human primary macrophages. The described approach is a helpful tool which will be further used as standard operation procedure, ultimately aiming at comprehensive targeted proteomics/oxylipin metabolomics strategies to examine the entire arachidonic acid cascade.

Reprinted from Hartung NM, Ostermann AI, Immenschuh S, Schebb NH (2021) Combined targeted proteomics and oxylipin metabolomics for monitoring of the COX-2 pathway. *Proteomics*, 21 (3-4), 1900058; doi: 10.1002/pmic.201900058;

Author contributions: NMH designed research, performed experiments and wrote the manuscript; AIO designed research and performed experiments, SI performed experiments; NHS designed research and wrote the manuscript.

2.1 Introduction

Cyclooxygenases (COX) belong, next to the lipoxygenases (LOX) and cytochrome P450 monooxygenases (CYP), to the three main enzymatic branches of the arachidonic acid (ARA) cascade. Eicosanoids and other oxylipins formed here from polyunsaturated fatty acids function as potent lipid mediators and are involved in the regulation numerous physiological functions, for example, in the regulation of the vascular tone, blood clotting, or immune response [1]. Different COX isoforms catalyze the formation of prostaglandin (PG) H_2 from ARA. PGH_2 in turn can be converted to other prostanoids by a multitude of downstream enzymes. Prostaglandin E synthases form PGE_2 and thromboxane A synthase catalyzes the formation of thromboxane A_2 (TxA_2) and 12-hydroxyheptadecatrienoic acid (12-HHT) [2], though non-enzymatic formation of PGE_2 and 12-HHT from PGH_2 is also possible under certain conditions [3, 4]. COX-1 (derived from the PTGS1 gene) is mainly responsible for tissue homeostasis, for example, in the stomach and kidney, and is constitutively expressed in many cell types [5]. Although constitutive COX-2 (derived from the PTGS2 gene) expression is found in few tissues (e.g., brain), its expression is mainly regulated by growth factors, cytokines (such as tumor necrosis factor *α* or interleukin 1*β*) and pro-inflammatory stimuli, for example, through the NF*κ*b-pathway [6]. Elevated COX-2 gene expression has been reported in colon and several other cancers [7, 8] as well as during diseases that are accompanied by chronic inflammation such as atherosclerosis [9]. This central role of COX-2 in the mediation of inflammatory responses has made it a major target for drug development in the past years [10]. Moreover, COX-2 inhibition by natural products such as food ingredients with potentially anti-inflammatory properties has been intensely investigated [11, 12]. Since the direct COX products PGG_2 and PGH_2 are unstable, their effects on the modulation of COX-2 activity are frequently only measured as changes of PGE_2 levels. Though, a comprehensive analysis of the whole oxylipin profile using targeted oxylipin metabolomics enables further characterization of their mode of action, revealing, for example, additional inhibitory properties on other ARA cascade enzymes or increased formation of other oxylipins due to substrate shunts [13, 14]. However, no conclusions can be drawn concerning the mechanisms responsible for the changes only from the oxylipin profile. Parallel analysis of enzyme activity and abundance is required in order to fully comprehend effect mechanisms, since reduced oxylipin levels may result from direct enzyme inhibition or reduced gene expression. This issue is often addressed by classical western blot analyses, which are labor-intensive and only lead to semi-quantitative results.

In the recent years, liquid chromatography-tandem mass spectrometry (LC-MS/MS) based targeted proteomics has increasingly become the method of choice for quantitative analysis of protein abundance on triple quadrupole instruments via selected reaction monitoring (SRM) [15]. The main advantages are the ability to quantify absolute protein levels [15] and higher sample throughput by multiplexing of many target proteins. Until now, only few proteomic assays have been reported that specifically aim at analyzing the ARA cascade [16-18], also partly in combination with different omics strategies. However, the two SRM based methods among these do not target human COX-2 [17, 18], for example, the comprehensive multiplexed proteomics SRM method from Sabido et al. covering several enzymes of the ARA cascade is limited to the mouse proteome [18].

Therefore, our aim was to develop a targeted LC-MS/MS based proteomics method for human COX-2 which we can utilize together with our well-established targeted oxylipin metabolomics method [19, 20]. This enables us to thoroughly investigate of the effect mechanisms involved in the modulation of the oxylipin profile.

Here, we present the detailed development of a targeted SRM based proteomics method for human COX-2. This step-by-step description of our tiered approach can serve as instruction for further SRM method development.

Finally, the successful parallel investigation of different human colon carcinoma cell lines and lipopolysaccharide (LPS)-stimulated primary macrophages with both, targeted proteomics and oxylipin metabolomics methods enabled us to correlate prostanoid levels and COX-2 abundance.

2.2 Experimental Section

2.2.1 Materials

FCS (superior standardized) and L-glutamine were purchased from Biochrom (Berlin, Germany), human AB serum was from c.c. pro. GmbH (Thuringia, Germany) and macrophage-colony stimulating factor (M-CSF) from PeproTech, Inc. (Rocky Hill, NJ, USA). Protease-inhibitor mix M (AEBSF, Aprotinin, Bestatin, E-64, Leupeptin, and Pepstatin A) as well as MS approved trypsin (> 6.000 U/g, from porcine pancreas) were from SERVA Electrophoresis GmbH (Heidelberg, Germany) and celecoxib was obtained from Santa Cruz Biotechnology, Inc. (Dallas, TX, USA). Lipopolysaccharide serotype 0111:B4 was obtained from Invivogen (San Diego, CA, USA). Oxylipin standards and crude COX-2 were from Cayman Chemical (Ann Arbor, MI, USA), unlabeled and heavy labeled (lys: uniformly labeled (U)-$^{13}C_6$; U-$^{15}N_2$; arg: U-$^{13}C_6$; U-$^{15}N_4$) peptide standards were purchased from JPT Peptides (Berlin, Germany). Acetonitrile (HPLC-MS-grade), acetone (HPLC grade) methanol, and acetic acid (Optima LC/MS grade) as well as BCA assay reagent A were obtained from Fisher Scientific (Schwerte, Germany). Copper sulfate pentahydrate was from Merck (Darmstadt, Germany) and dithiothreitol was from AppliChem (Darmstadt, Germany). Ammonium hydrogen carbonate, sodium deoxycholate, and urea were obtained from Carl Roth. DMEM, RPMI 1640 medium, penicillin/streptomycin (5000 units penicillin and 5 mg streptomycin per mL), porcine trypsin, indomethacin, and iodoacetamide as well as all other chemicals were purchased from Sigma (Schnellendorf, Germany).

2.2.2 Cell cultivation

Human colon carcinoma cell lines HCT-116 and HT-29 were obtained from the German Collection of Microorganisms and Cell Cultures GmbH (DSMZ, Braunschweig, Germany) and HCA-7 cells were obtained from the European Collection of Cell Cultures (ECACC, Salisbury, UK). Cells were maintained in DMEM with 10% FCS, 100 U/mL penicillin, 100 µg/mL streptomycin and 2 mM L-glutamine in 60.1 mm² dishes in a humidified incubator at 37 °C and 5% CO_2.

Primary human macrophages were prepapmred as described [21]. In brief, peripheral blood mononuclear cells (PBMC) isolated from healthy donors by density centrifugation were differentiated for seven days with 25 ng/ml recombinant human macrophage-colony stimulating factor (M-CSF) in RPMI 1640 medium containing 5% AB-serum, 100 U/mL penicillin, and 10 mg/mL streptomycin. The study was approved by the Ethical Committee of the Hannover Medical School.

For determination of the oxylipin profile and COX-2 abundance, colon carcinoma cells were seeded at densities of 1.5 mio cells per 10 mL and 2.4 mio cells were seeded in case of the primary macrophages. HCT-116, HT-29, and HCA-7 cells were harvested 48 h after seeding. HCA-7 cells were incubated with 5 µM indomethacin or 3 µM celecoxib after a 24 h preincubation period and harvested 24 h post incubation. Possible cytotoxic effects of the test compounds were evaluated by resazurin (alamar blue) assay [22] and no significant effects were found after an incubation time of 24 h. Cells were washed with 5% FCS in PBS, collected by scraping and centrifugation, and finally washed in PBS containing protease inhibitor and pelleted. Primary macrophages were treated with 1 µg/mL lipopolysaccharide (LPS) in the presence of 1% serum and 12.5 ng/mL M-CSF, and incubated cells as well as their culture medium supernatants (for oxylipin analysis) were collected after 0 – 24 h of LPS incubation, as well as the 24 h control without LPS. Cells were washed twice with PBS, scraped from the plate and transferred to a reaction tube, washed again, and were resuspended in PBS. All pellets and supernatants were immediately stored at -80 °C until further use.

2.2.3 LC-MS/MS based Oxylipin Quantification

For the investigation of the oxylipin profile approx. 5 – 10 mio cells and cell culture media of the primary macrophages were analyzed as described [19, 20]. In brief, the cell pellets were resuspended in PBS and sonicated, protein content was determined via bicinchoninic acid (BCA) assay. Internal standards (IS) as well as antioxidant solution were added to 500 µL of cell culture supernatant and the cell lysate before proteins were precipitated in methanol at -80 °C for at least 30 min. The samples were purified via solid phase extraction (SPE) on a non-polar (C8) / strong anion exchange mixed mode material (Bond Elut Certify II, 200 mg, Agilent Waldbronn, Germany) and finally analyzed by LC-MS/MS in negative electrospray ionization (ESI(-)) mode on a 1290 Infinity II LC System (Agilent, Waldbronn, Germany) coupled with a 5500 QTRAP mass spectrometer (Sciex, Darmstadt, Germany). The oxylipin levels were quantified by an external calibration with internal standards.

2.2.4 Targeted LC-MS/MS Based Proteomics

Cell pellets were re-dissolved in 5% (*w*/*v*) sodium deoxycholate (SDC) containing protease inhibitor mix, sonicated, and finally centrifuged (4 °C, 15,000 × *g*, 20 min) in order to remove cellular debris (**Fig. 2.1**). Protein concentration in each cell suspension was determined using BCA assay. Four volumes of ice-cold acetone were then added to each sample and protein was precipitated by overnight-freezing (-30 °C). Next, the pellet was washed twice

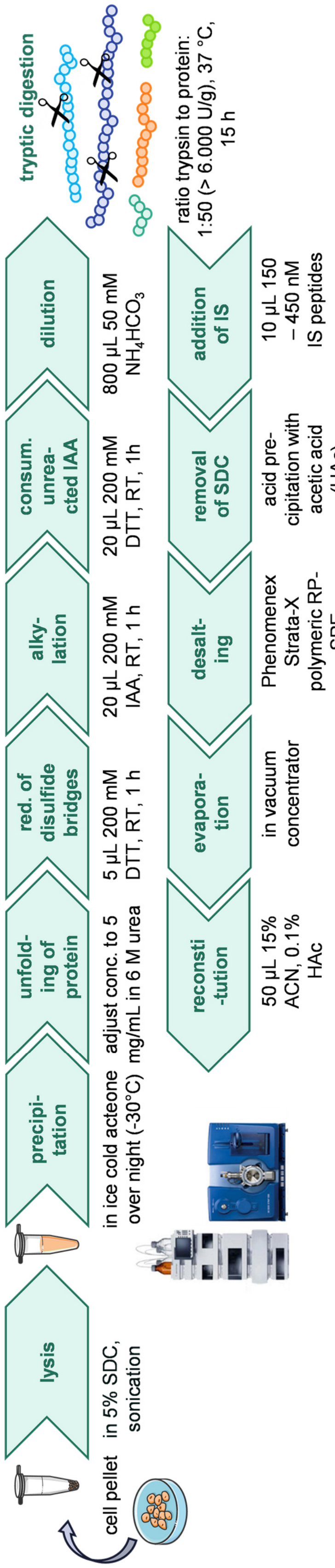

Fig. 2.1: Sample preparation work flow for cell lysis and tryptic digest based on a modified protocol from Kinter and Sherman [24].

with fresh ice-cold acetone by centrifugation (4 °C, 15,000 × *g*, 15 min) and dried under N_2 current [23].

It was re-dissolved in 6 M urea to a final concentration of 5 mg/mL. 100 µL of this solution were incubated with 5 µL of 200 mM dithiothreitol (DTT, in 50 mM NH_4HCO_3) for 1 h while gently shaking for reduction of disulfide bridges. Resulting free sulfhydryl groups were alkylated with 20 µL 200 mM iodo-acetamide (IAA, in 50 mM NH_4HCO_3) for 1 h while shaking in the dark to prevent re-formation of disulfide bridges. Finally, 20 µL 200 mM DTT were added to the mixture and gently shaken for 1 h to consume unreacted IAA [24]. 800 µL 50 mM NH_4HCO_3 were added before the protein digestion with 100 µL of 100 µg/mL trypsin in 50 mM HAc at a trypsin-to-protein ratio of 1:50 for 15 h (pH ~ 7.8). Addition of concentrated acidic acid to reduce the pH to 3 – 4 stopped the digestion and led to the precipitation of SDC [25]. 10 µL of 150/300/450 nM heavy labeled peptides (lys: U-$^{13}C_6$; U-$^{15}N_2$; arg: U-$^{13}C_6$; U-$^{15}N_4$; corresponding to each of the analyte peptides) were then added, serving as IS, and SDC was removed by centrifugation (4 °C, 15,000 × *g*, 10 min). Next, samples were subjected to SPE (Strata-X 33 µm Polymeric Reversed Phase 100 mg per 3mL, Phenomenex LTD, Aschaffenburg, Germany). Cartridges were activated with 3 mL methanol and equilibrated with 3 mL 1% HAc. Samples were diluted in 1.2 mL 1% HAc on the column, washed with 3 mL 5% MeOH, 1% HAc. Finally, peptides were eluted in 2 mL of 70% ACN, 0.1% HAc. Peptides were concentrated using a vacuum concentrator, re-dissolved in 15% ACN, 0.1% HAc, and centrifuged (4 °C, 15,000 × *g*, 10 min) before LC-MS/MS analysis (**Fig. 2.1**).

Peptides were separated on a Zorbax Eclipse Plus C18 reversed phase column (2.1 × 150 mm, particle size 1.8 µm, pore size 95 Å, Agilent) at 40 °C, with an upstream inline filter (3 mm, 1290 infinity II inline filter, Agilent) and a SecurityGuard Ultra C18 cartridge as precolumn (2.1 × 2 mm, Phenomenex LTD), with a 1290 Infinity II System (Agilent). Peptides were separated with a gradient consisting of 95/5% water/acetonitrile (mobile phase A) and 5/95% water/acetonitrile (mobile phase B), both acidified with 0.1% acetic acid at a flow rate of 0.3 mL/min as follows: 0% B at 0 min, 0% B at 1 min, 35% B at 30.5 min, 100% B at 30.6 min, 100% B at 33.5 min, 0% B at 33.7 min and 0% B at 38 min. Mass spectrometric detection was performed on a 5500 QTRAP instrument (Sciex) in ESI(+)-mode, with the following settings: ion spray voltage: 4500 V, capillary temperature: 700 °C, curtain gas N_2: 50 psi, nebulizer gas (GS1) N_2: 30 psi, drying gas (GS2) N_2: 70 psi, generated with N_2 generator Ecoinert (DTW, Bottrop, Germany). Declustering potential, exit potential, and collision cell exit potential were set to 80 V, 10 V and 12.50 V, respectively, and collision energies were optimized for each of the peptides. CAD gas was set to medium. Peptides were measured in scheduled SRM where the detection window was set to ± 45 s at the expected retention time and a cycle time of 0.4 s.

Data analysis was performed with Multiquant (Sciex, Version 3.0.2). Peptide concentrations were determined via an external calibration with internal standards prepared in 15% ACN, 0.1% HAc using the same peptide sequences as unlabeled and heavy labeled peptides and consideration of the absolute protein content. The COX-2 abundance levels were also normalized to each of the housekeeper protein levels.

2.3 Results

A targeted proteomics LC-MS/MS method was developed with the aim of comprehensively investigating the ARA cascade together with our established targeted oxylipin metabolomics method, that is, on enzyme abundance and activity level. Enzyme activity in the cells was determined based on several prostanoids formed downstream of the direct COX products PGG_2/PGH_2, which are unstable. The detailed method development for the targeted proteomics method is described here based on COX-2 enzyme. Both, oxylipin metabolomics and proteomics methods, were then utilized to characterize the COX(-2) branch of the ARA cascade in different cell types, that is, in different human colon carcinoma cell lines and LPS-stimulated human primary macrophages.

2.3.1 Peptide Selection and SRM Method Development

In the first step of targeted proteomics method development, unique peptides unambiguously identifying the target protein that are well detectable in the mass spectrometer, so called “proteotypic peptides” (PTPs) [26], needed to be selected for the target enzyme COX-2 (prostaglandin G/H synthase 2, UniProtKB accession no. P35354), as well as the three housekeeping proteins (peptidyl-prolyl cis-trans isomerase B, PPIB, P23284; glyceraldehyde-3-phosphate dehydrogenase, GAPDH, P04406; actin, cytoplasmic 1, *β*-actin /actin, cytoplasmic 2, *γ*-actin, P60709 / P63261) and COX-1 (prostaglandin G/H synthase 1, P23219). Detailed method development is described here for

COX-2, the other proteins were evaluated accordingly. An *in silico* tryptic digestion of the amino acid (aa) sequence of COX-2 without its N-terminal signal peptide (using peptide mass and peptide cutter [27]) led to 54 peptides with lengths between 2 and 27 aa (**Tab. 2.1**). The N-terminal signal peptide is found, for example, in proteins that are translocated within the cell to the endoplasmic reticulum and is often removed in the mature protein. Suitable peptides from the *in silico* digest were selected for the proteomics method in consideration of certain criteria. First, peptides with less than 7 and more than 22 aa were excluded from further evaluation, leaving a total of 26 peptides. The uniqueness was evaluated for the remaining peptides with NCBI BLAST [28] and the peptide uniqueness checker on NeXtProt [29]. Tryptic digestion of the COX-2 sequence only yielded one non-unique peptide LILIGETIK (**Tab. 2.1**) which is also part of the COX-1 aa sequence. It was included to be used as dual COX-1/2 indicator. The peptides theoretical cleavage probability was assessed with ExPASy Peptide Cutter [27] and cleavage prediction with decision trees (CP-DT) [30], excluding eight of the remaining peptides with an estimated cleavage probability of <95% or <70%, respectively. Of the remaining 18 peptides, one with a potential site of non-synonymous single nucleotide polymorphism (nsSNP) leading to single amino acid variants (SAV) and thus, sequence variations in the peptides, was excluded as reported on UniProtKB [31]. Peptides with potential posttranslational modifications (PTMs) were also unfavored, and five of the remaining peptides were excluded because they contain a PTM site reported on UniProtKB [31] and Phosphosite Plus [32].

Tab. 2.1 (pages 21 – 23): Evaluation of COX-2 peptides from *in silico* tryptic digest (without signal peptide sequence) for the targeted proteomics method. Peptides were selected based on peptide length (7 – 22 aa), uniqueness, cleavage probability calculated with peptide cutter (≥ 95%) or cleavage prediction with decision trees (CP-DT; ≥ 70%), occurrence of single nucleotide polymorphisms (SNPs) or posttranslational modifications (PTMs), as well as unfavored amino acids (C, M, N, Q, W; max. 2) and predicted retention time (RT; 3 – 30 min). Peptides fulfilling all criteria are shown in bold, those selected for method are also underlined.

Peptide sequence	Pos.	[M+H]+	Length [aa]	Uniqueness[a)]	C-term. cleav. prob.[b)] [%]	Overall cleav. prob.[c)] [%]	SNPs[d)]	PTMs[e)]	Unfavoured aa	Pred. RT [min][f)]
ANPCCSHPCQNR	18-29	1329.5	12	unique	100	-			2 x C, 2 × N, 1 × Q	0.6
GVCMSVGFDQYK	30-41	1333.6	12	unique	100	84			1 x C, 1 × M, 1 × Q	13.7
CDCTR	42-46	597.2	5	-	100	86			1 x C	-
TGFYGENCSTPEFLTR	47-62	1821.8	16	unique	100	88		N53: gl	1 x C, 1 × N	16.6
IK	63-64	260.2	2	-	100	87				-
LFLK	65-68	520.3	4	-	50	13				-
PTPNTVHYILTHFK	69-82	1667.9	14	unique	100	14			1 × N	15.4
GFWNVVNNIPFLR	83-95	1575.8	13	unique	80	94			3 × N, 1 × W	24.4
NAIMSYVLTSR	96-106	1254.7	11	unique	100	92			1 × N, 1 × M	16.6
SHLIDSPPTYNADYGYK	107-123	1940.9	17	unique	100	91		Y120: p	1 × N	12.7
SWEAFSNLSYYTR	124-136	1623.7	13	unique	100	94		N130: gl	1 × N, 1 × W	19
ALPPVPDDCPTPLGVK	137-152	1618.9	16	unique	94	89			1 x C	14.4
GK	153-154	204.1	2	-	93	82				-
K	155-155	147.1	1	-	76	80				-
QLPDSNEIVEK	156-166	1271.6	11	unique	95	77			1 × N, 1 × Q	10.4
LLLR	167-170	514.4	4	-	100	84				-
R	171-171	175.1	1	-	73	89				-
K	172-172	147.1	1	-	100	84				-
FIPDPQGSNMMFAFFAQHFTHQFFK	173-197	3020.4	25	unique	100	81			1 × N, 2 × M, 3 × Q	-
TDHK	198-201	500.2	4	-	64	81				-
R	202-202	175.1	1	-	95	76				-
GPAFTNGLGHGVDLNHIYGETLAR	203-226	2509.3	24	unique	100	80			2 × N	-
QR	227-228	303.2	2	-	100	17	228: R → H		1 × Q	-
K	229-229	147.1	1	-	84	17				-

Tab. 2.1 continued.

Peptide sequence	Pos.	[M+H]+	Length [aa]	Uniqueness[a)]	C-term. cleav. prob.[b)] [%]	Overall cleav. prob.[c)] [%]	SNPs[d)]	PTMs[e)]	Unfavoured aa	Pred. RT [min][f)]
LR	230-231	288.2	2	-	100	84				-
LFK	232-234	407.3	3	-	88	69				-
DGK	235-237	319.2	3	-	100	68				-
MK	238-239	278.2	2	-	100	81			1 × M	-
YQIIDGEMYPPTVK	240-253	1653.8	14	unique	100	86			1 × M, 1 × Q	17.2
DTQAEMIYPPQVPEHLR	254-270	2024.0	17	unique	100	91			1 × M, 2 × Q	16.4
FAVGQEVFGLVPGLMMYATIWLR	271-293	2598.4	23	unique	100	94			2 × M, 1 × Q, 1 × W	-
EHNR	294-297	555.3	4	-	100	89			1 × N	-
VCDVLK	298-303	676.4	6	-	100	81			1 x C	-
QEHPEWGDEQLFQTSR	304-319	1986.9	16	unique	100	84			3 × Q, 1 × W	13.7
LILIGETIK	320-328	999.6	9	P23219	100	94				16.9
IVIEDYVQHLSGYHFK	329-344	1948.0	16	unique	100	94			1 × Q	16.8
LK	345-346	260.2	2	-	100	81				-
FDPELLFNK	347-355	1122.6	9	unique	100	81			1 × N	18.4
QFQYQNR	356-362	983.5	7	unique	100	95			1 × N, 3 × Q	5.1
IAAEFNTLYHWHPLLPDTFQIHDQK	363-387	3034.5	25	unique	100	91			1 × N, 2 × Q, 1 × W	-
YNYQQFIYNNSILLEHGITQFVESFTR	388-414	3324.6	27	unique	100	91		N396: gl	3 × N, 1 × Q	-
QIAGR	415-419	544.3	5	-	100	90			1 × Q	-
VAGGR	420-424	459.3	5	-	100	85				-
NVPPAVQK	425-432	852.5	8	unique	100	88	428: P → A		1 × N, 1 × Q	5.3
VSQASIDQSR	433-442	1090.5	10	unique	100	86			2 × Q	4.7
QMK	443-445	406.2	3	-	100	82			1 × M, 1 × Q	-
YQSFNEYR	446-453	1106.5	8	unique	85	86		Y446: p	1 × N, 1 × Q	8.9
K	454-454	147.1	1	-	79	82				-

Tab. 2.1 continued.

Peptide sequence	Pos.	$[M+H]^+$	Length [aa]	Uniqueness[a)]	C-term. cleav. prob.[b)] [%]	Overall cleav. prob.[c)] [%]	SNPs[d)]	PTMs[e)]	Unfavoured aa	Pred. RT [min][f)]
R	455-455	175.1	1	-	100	79				-
FMLK	456-459	538.3	4	-	50	14			1 × M	-
PYESFEELTGEK	460-471	1428.7	12	unique	80	14				14.4
EMSAELEALYGDIDAVELYPALLVEK	472-497	2881.4	26	unique	26	10	488: E → G; 511: V→ A		1 × M	-
PR	498-499	272.2	2	-	36	3				-
PDAIFGETMVEVGAPFSLK	500-518	2008.0	19	unique	100	27			1 × M	24.9
GLMGNVICSPAYWK	519-532	1538.7	14	unique	100	21		C526: n	1 x C, 1 × N, 1 × M, 1 × W	18.9
PSTFGGEVGFQIINTASIQSLICNNVK	533-559	2837.5	27	unique	94	22			1 x C, 3 × N, 2 × Q	-
GCPFTSFSVPDPELIK	560-575	1736.9	16	unique	100	95		S565: ac	1 x C	19.3
TVTINASSSR	576-585	1035.5	10	unique	100	91		N580: gl	1 × N	5.3
SGLDDINPTVLLK	586-598	1384.8	13	unique	93	87	587: G → R		1 × N	18.1
ER	599-600	304.2	2	-	100	86				-
STEL	601-604	449.2	4	-	-	91				-

a)from BLAST[28] and NeXtprot[29]

b)calculated from peptide cutter[27]

c)calculated from CP-DT[30]

d)SNPs from UniProtKB [31]

e)PTMs from UniProtKB[31] and Phosphosite Plus[32] (ac – acetylation, gl – glycosylation, n – nitrosylation, p – phosphorylation)

f)predicted RT from SSRCalc[36]

-: not evaluated

The occurrence of aa prone to modifications, such as cysteine (C), asparagine (N), glutamine (Q, especially N-terminal), methionine (M) and tryptophan (W) are unfavored [33-35]. Maximal two of these aa were tolerated, because they commonly occur, leaving a final number of six peptides to choose from (**Tab. 2.1**). In order to ensure optimal detection of the peptides, chromatographic retention should lay in an acceptable range. This was calculated based on the hydrophobicity index defined in a calculated retention time between 3 and 30 min using the Sequence Specific Retention Calculator (SSRCalc) [36]. Only one of the peptides did not lie within the accepted range. If a signal peptide sequence exists, the first peptide of the remaining sequence should be excluded. Also, the last peptide in the sequence is unfavored, because it mostly does not contain a C-terminal arg or lys residue.

After the *in silico* evaluation, the six remaining peptides were assessed in trypsinized crude recombinant human COX-2 protein via LC-MS/MS. Several transitions were selected per peptide, derived from literature data (SRMAtlas [37]) and product ion spectra. For this initial screening, the transitions were measured with a standard CE of 25 V. IVIEDYVQHLSGYHFK and YQIIDGEMYPPTVK peptides were excluded based on their insufficient MS sensitivity or chromatographic behavior, that is, poor peak shape. Three COX-2 specific peptides VSQASIDQSR, NAIMSYVLTSR, FDPELLFNK as well as the COX-1/2 unspecific peptide LILIGETIK were finally chosen for further method development (**Tab. 2.1**). MS parameters of the final peptides were optimized in order to achieve highest sensitivity. DP only had little influence on the 5500 QTRAP instrument and was kept at 80 V for all peptides.

As expected, variation of the CE had the most effect on signal intensity (**Fig. 7.1**). With the optimized MS parameters, the transition ranking matched well to those from SRMAtlas (experimental and predicted data; **Tab. 7.1**). The same criteria were applied in order to choose PTPs for the housekeeping proteins and COX-1, which led to the selection of two or three peptides per protein (**Tab. 7.2**,

Tab. 7.3). Heavy labeled peptides for each of the corresponding peptide sequences were used as IS.

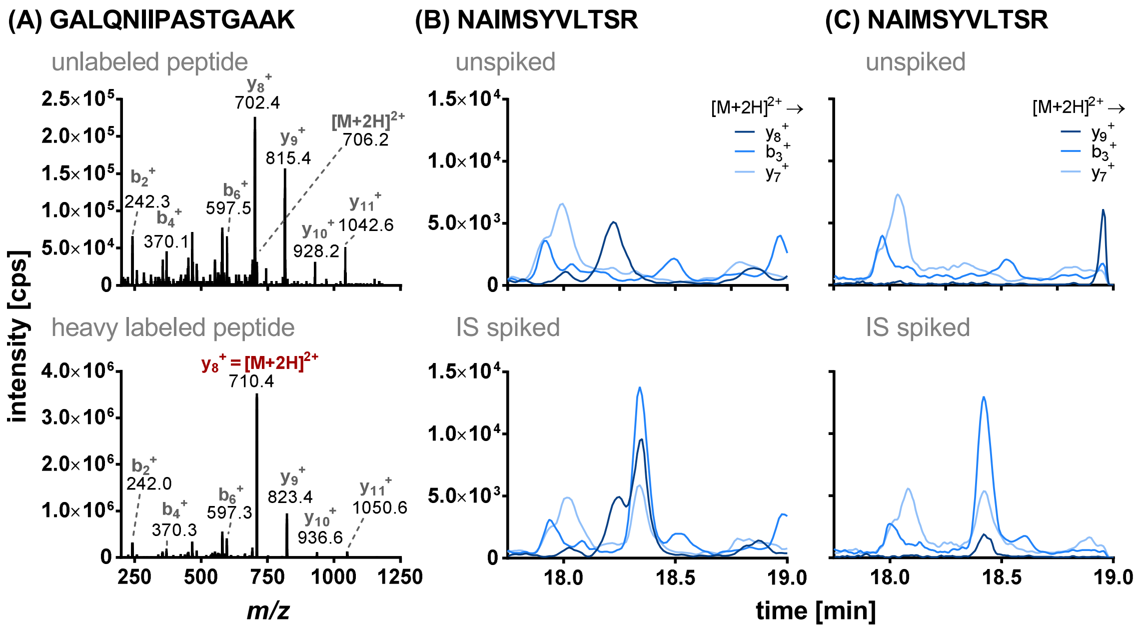

Fig. 2.2: Evaluation of transitions for internal standard (IS) peptides containing heavy labeled lysine (U-$^{13}C_6$; U-$^{15}N_2$) or arginine (U-$^{13}C_6$; U-$^{15}N_4$). **(A)** Comparison of MS/MS spectra of GALQNIIPASTGAAK (from GAPDH) as unlabeled (top) and heavy labeled peptide (bottom) in 100 nM standards show that the *m/z* of both $[M+2H]^{2+}$ and y_8^+ shift to 710.4 for heavy labeled peptide, making them inseparable and thus unsuitable for analysis. Matrix interferences also limit choice of transitions. Shown are **(B)** transitions of heavy labeled NAIMSYVLTSR (from COX-2) peptide (corresponding to transitions of unlabeled peptide) with matrix interference on $[M+2H]^{2+} \rightarrow y_8^+$ transition as well as **(C)** alternative heavy labeled peptide transitions without matrix interference in unspiked (top) and IS spiked (bottom) HCA-7 lysate (10 nM).

The same transitions were chosen for the heavy labeled and unlabeled peptides. However, mass shifts caused by the heavy labeled aa sometimes restricted this approach, as did isobaric matrix interference on the transitions (**Fig. 2.2**), so that every transition of all unlabeled and labeled peptides was evaluated in reference matrix (HCA-7 cell lysate). Finally, three transitions were selected for each of the peptides, one serving as quantifier and the others as qualifiers, and constant ratios between the transitions additionally ensure the peptides' identity in the samples (**Tab. 2.2**, **Tab. 7.4**, **Tab. 7.5**).

Protein abundance levels of COX-2 and the housekeeping proteins were evaluated by multiple PTPs (**Fig. 2.3**) and their concentrations were determined via external calibration with IS, the gold standard for quantification via LC-MS/MS. The heavy labeled peptides used as IS are spiked during sample preparation (**Fig. 2.1**). Evaluation of the IS recovery revealed that that the differences between pre- and post-SPE addition of IS were only ≈ 10% thus, indicating that the low apparent IS recovery (≈ 30-70%) is caused by ion suppression (**Fig. 7.2**). In order to assure easy integration of IS during analysis they were therefore added at high concentrations of approx. 100-fold LLOQ (30 – 90 nM). The calibration ranges were set according to the expected concentrations in samples. For COX-2 peptides the linear calibrations were prepared in the range of pM levels to 500 nM, and the linear calibration for peptides of housekeepers ranged from 1 nM up to 1 µM (**Tab. 2.2**, **Tab. 7.4**).

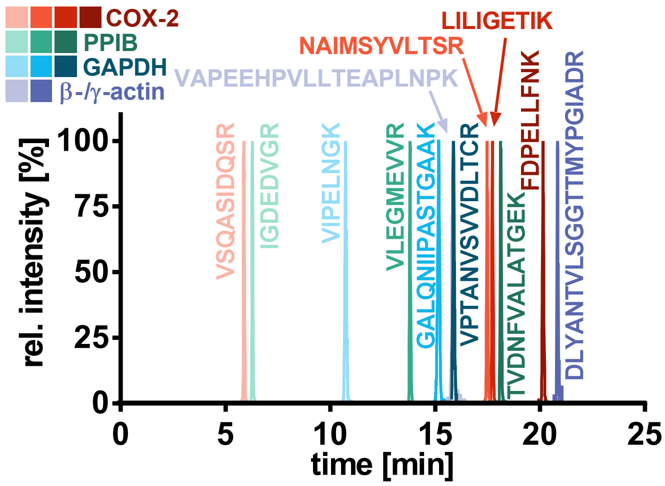

Fig. 2.3: Chromatographic separation of peptides from COX-2 as well as the housekeeping proteins PPIB, GAPDH and β-/γ-actin. The peptides (approx. 100 nM) were separated on an RP-C18 phase (2.1 × 150 mm, 1.8 µm, 95 Å) with a gradient consisting of H2O/ACN/HAc and detected on a 5500 QTRAP instrument (Sciex) in positive electrospray ionization (ESI+) mode.

The linearity of the covered range is demonstrated by a resulting $R^2 \geq 0.998$ from $1/x^2$ weighted linear regressions, the accuracies were within ± 20% for all calibrators. The limits of detection (LOD) and lower limits of quantification (LLOQ) were determined for COX-2 peptides at signal-to-noise (S/N) ratios of three and five, respectively, with accuracies of ± 20%. COX-2 peptides could be detected in the pM range, for example, the LOD for FDPELLFNK was 50 pM and the LLOQ at 100 pM (equivalent to 0.5 fmol or 561 fg peptide, 34 pg COX-2 protein on column; **Fig. 7.3**). No LOD and LLOQ were determined for the housekeeper peptides, since they are always present at sufficient concentrations. Their CEs were set slightly higher compared to their optimized CE in order to reduce the ion current reaching the secondary electron multiplier detector unit in the mass spectrometer. However, at levels exceeding 1 µM the linear slope of the detector response decreased due to ion suppression and a quadratic regression of levels up to 10 µM allowed robust quantification (**Fig. 7.4, Tab. 7.4**). Robustness of the method was evaluated by repeated analysis of samples from an HCA-7 pool which was evenly aliquoted á ≈ 5 mio cells. Intraday precision was < 10 %, and interday precision was <15% (**Tab. 7.6**). For unambiguous identification of the target peptides in samples, several criteria needed to be met: 1) exact RT alignment of all transitions of unlabeled target peptides, 2) exact co-elution of unlabeled target peptides and corresponding heavy labeled IS peptides, and 3) the relative signal intensity ratios between the transitions in the sample must match those in the peptide standards without matrix for labeled and unlabeled peptides, respectively (at least one of the qualifier transitions must lie within ± 20% of the area of the quantifier transition; Fig. 2.5).

2.3.2 Prostanoid Formation and COX-2 Abundance

A comprehensive set of prostanoids was quantified in HCT-116, HT-29, and HCA-7 cells. The lowest PGE_2 concentration of 0.35 ± 0.05 pmol/mg protein was detected in HCT-116 cells, while 1.8 ± 0.1 pmol/mg protein was found in HT-29 cells and the highest concentration of 26 ± 2 pmol/mg protein was determined in HCA-7 cells, exceeding the concentrations found in the other cells by more than ten times (**Fig. 2.4 (A) i)**). Also, other prostanoids such as PGD_2, TxB_2 and 12-HHT were found with pronounced differences between the cell lines. 12-HHT concentrations ranged from 29.2 ± 0.4 fmol/mg protein in HCT-116 cells to 5.5 ± 0.9 pmol/mg in HCA-7 cells, though the differences between HT-29 (1.9 ± 0.2 pmol/mg) and HCA-7 were less pronounced (**Fig. 2.4 (A) ii), Tab. 7.7**).

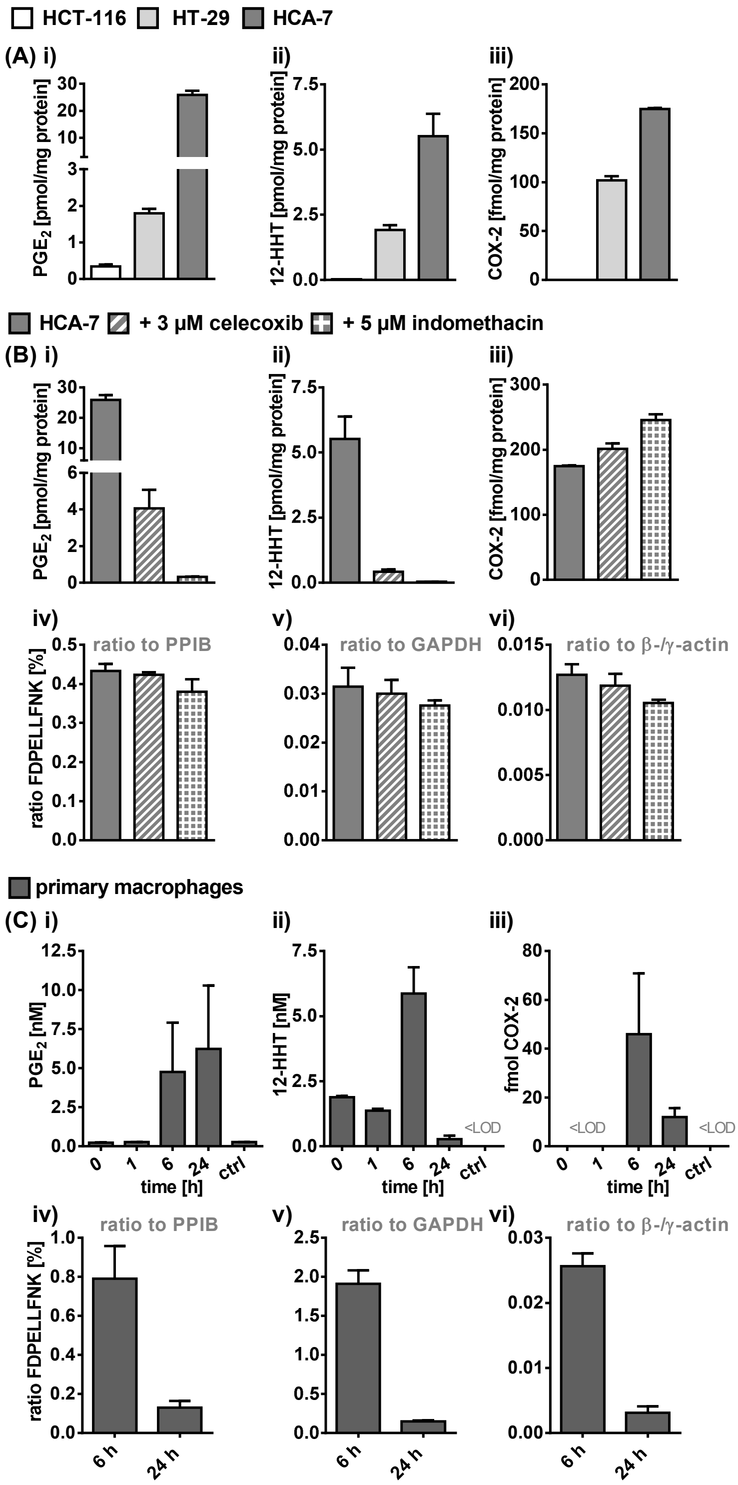

Fig. 2.4: Analysis of COX(-2) pathway. PGE_2 and 12-HHT levels were determined via targeted LC-MS/MS based oxylipin metabolomics in **(A) i,ii)** human colon carcinoma cell lines HCT-116, HT-29, and HCA-7, **(B) i,ii)** untreated HCA-7 cells, HCA-7 cells treated with 3 µM celecoxib or 5 µM indomethacin and **(C) i,ii)** in the culture medium of human primary macrophages treated with 1 µg/mL LPS for up to 24 h (control: 24 h without LPS).

COX-2 abundance levels were determined as peptide FDPELLFNK in **(A) iii)** and **(B) iii)** in the colon cells (normalized to protein content) and in **(C) iii)** LPS treated macrophages. COX-2 protein level was normalized to PPIB peptide VLEGMEVVR, GAPDH peptide GALQNIIPASTGAAK and β-/γ-actin peptide VAPEEHPVLLTEAPLNPK (from left to right) in **(B) iv-vi)** differently treated HCA-7 cells as well as **(C) iv-vi)** LPS treated macrophages.

$PGF_{2\alpha}$ concentrations were about similar in HT-29 and HCA-7 cells, while this lipid mediator was below LOD in HCT-116 cells (**Tab. 7.7**). Regarding gene expression, no COX-2 specific peptides were detected in HCT-116 cells with the targeted proteomics method and only the COX isoform-unspecific peptide LILIGETIK was found, which is also formed upon tryptic digest of COX-1. All COX-2 PTPs and the isoform unspecific peptide LILIGETIK were detected in HT-29 and HCA-7 cells (**Fig. 2.4 (A) iii)**) and the COX-2 abundance was correlated to PGE_2 concentrations here. Interestingly, the differences in COX-2 levels were less pronounced than the product formation. No COX-1 specific peptides were detectable under the same conditions in any colon cells (**Tab. 7.5**, **Fig. 7.5**). After 24 h incubation of HCA-7 cells with the COX-2 inhibitor celecoxib (3 µM) and the COX-1/2 inhibitor indomethacin (5 µM) at sub-cytotoxic levels (**Fig. 7.6**) prostanoid levels strongly decreased, for example, a 6 – 13-fold reduction of PGE_2 and 12-HHT (**Fig. 2.4 (B) i-ii), Tab. 7.7**). The COX-2 levels (normalized to different housekeeping proteins PPIB, GAPDH and *β*/*γ* actin) were not affected by the inhibitors (**Fig. 2.4 (B) iv-vi), Fig. 7.7 (A)**). Human primary macrophages were stimulated with 1 µg/mL LPS and time-dependent changes in prostanoid formation as well as COX-2 abundance were analyzed for up to 24 h. A strong increase of prostanoid levels in the culture medium was detected after 6 h, the highest concentrations were found 24 h post incubation start in case of PGE_2, $PGF_{2\alpha}$, and TxB_2 with a 12 – 25-fold increase (**Fig. 2.4 (C) i-ii)**). 12-HHT and PGD_2 concentrations peaked already after 6 h, and 12-HHT concentrations markedly reduced from 6 ± 1 nM to 0.3 ± 0.1 nM after 24 h (**Tab. 7.7**). COX-2 PTPs were only detected after 6 and 24 h of LPS incubation, and, in contrast to the PGE_2 formation, the enzyme abundance levels peaked at 6 h (**Fig. 2.4 (C) iii-vi), Fig. 7.7 B**). The isoform-unspecific peptide LILIGETIK was detected at all time points and in untreated control, indicating COX-1 abundances which was supported by the detection of specific COX-1 peptides (**Tab. 7.5**). Neither an increase of prostanoids nor COX-2 abundance was detected in the control.

The parallel investigation of oxylipin formation and gene expression by targeted oxylipin metabolomics and proteomics methods allows a thorough characterization of the ARA cascade and the modulation thereof. We could show that different levels of COX-2 correlate with the levels of prostanoids in three colon carcinoma cell lines. Constant COX-2 abundance with at the same time decreased prostanoid levels in HCA-7 cells treated with COX(-1/-2) inhibitors indicate that these directly act on enzyme activity level. Lastly, the analysis revealed a time delay between the peak of COX-2 abundance and its maximal activity based on PGE_2 formation in LPS-stimulated human macrophages.

2.4 Discussion

2.4.1 Peptide Selection

Based on current literature [33-35, 38-40], we describe a tiered approach for the selection of peptides and method development of a quantitative SRM method for COX-2 alongside three housekeeping proteins (PPIB, GAPDH and *β*/*γ* actin) and COX-1, highlighting the crucial parts. Using the following steps and selection rules, this approach can be used as blueprint for the whole ARA cascade or all other proteins of interest.

In the first step, an *in silico* tryptic digest gave us all peptides which can theoretically result from the COX-2 sequence. We only chose peptides for further evaluation with lengths > 7 and < 23 aa. Peptides with less than 6 – 8 aa are generally regarded as unfavored due to their higher unlikelihood of being unique [33, 39, 40] and the total peptide length (up to 20 – 25 aa) is restricted by the upper mass range of the instrument, typically 1250 *m/z* [40]. The uniqueness of the peptides is their most important characteristic. Although

COX-2 shares 60 – 65% sequence identity with COX-1 [41] they only have one common tryptic peptide LILIGETIK, and all the remaining COX-2 peptides (>7 aa) are COX-2 specific (**Tab. 2.1**). This peptide can serve as parallel COX-1/2 indicator and was therefore included in the further evaluations. For other proteins it is more challenging to find unique peptides, as shown in this study for the aa sequence of the cytoskeletal protein *β*-actin, which we used here as housekeeping protein. Many tryptic peptides match several other actin proteins present in the cytoskeleton or muscles. In this case, we were able to select two peptides which both exclusively occur in *β*/*γ*-actin (**Tab. 7.2**). Next, we evaluated the peptides' cleavage probability based on two methods: ExPASy Peptide Cutter [27] which calculates C-terminal cleavage probability under consideration of the experimentally determined "Keil"-rules [42] and CP-DT, a machine learning based approach [30]. The "Keil"-rules suggest *inter alia* to avoid sequences containing neighboring basic aa (KR, KK, or RR) or proline residues next to cleavage sites (KP, RP) as they may result in missed cleavages [34, 39]. However, recent reports suggest that these rules are outdated [30, 43], and a more accurate prediction can be achieved with CP-DT [30]. Comparison of both methods applied to the COX-2 aa sequence shows only a partly overlap of the predicted cleavage probabilities, for example, between the aa no. 227 – 229 ("QRK"), CP-DT predicts a very low overall cleavage probability of 17% for the resulting "QR" and "K", while ExPASy calculates C-terminal cleavage probabilities of 100% and 84%, although the Keil rules should apply (**Tab. 2.1**). However, between the aa no. 456 – 499, CP-DT predicts cleavage probabilities <15%, and ExPASy results are also relatively low (26 – 80%; **Tab. 2.1**). Thus, different cut-offs were applied: predicted cleavage probabilities from ExPASy Peptide Cutter were set to ≥95% and for CP-DT ≥70%. Of the remaining peptides, we removed all that contain known sites of nsSNP. For COX-2, these sites could be easily avoided, as only five natural variants occurring in four tryptic peptides were reported in UniProtKB (**Tab. 2.1**) [31]. Genetic variations caused by nsSNP in protein coding regions lead to changes in the aa sequence, and about half of polymorphic variations are “disease-associated” [44]. In cell culture experiments different treatments of cells within a cell line (and thus, same DNA) are compared, hence, the occurrence of nsSNPs might not be a problem. However, our method should also be applicable to primary blood cells, for example, PBMC, neutrophils, or macrophages from different donors where a non-isobaric variation of the aa sequence of the target peptide is crucial. All peptides containing known sites of PTMs were excluded for COX-2 (**Tab. 2.1**) as they can be present in modified and unmodified forms. However, for the housekeeping proteins GAPDH and *β*/*γ*-actin no peptides without PTM sites exist which fulfill the remaining criteria (**Tab. 7.2**). The large number of reported PTM sites is linked to stronger regulation and diverse functions of these proteins [45]. Possibly, this is also due to more investigations regarding these abundant proteins and new PTM sites of COX-2 remain to be identified. For GAPDH and *β*/*γ*-actin, we selected peptides with as few PTM sites as possible or with little experimental evidence from shotgun approaches. Theoretically, for an exact quantification of the protein levels, all possible peptides resulting from the different types and numbers of PTMs must be analyzed together and summed. But for the housekeeping proteins, only the transitions of the unmodified peptides were considered. Independent of the protein of interest, circumvention of aa that might be susceptible to artifactual modifications including methionine and tryptophan (oxidation), cysteine (oxidation, potentially incomplete carbamidomethylation), asparagine, and glutamine (deamidation, N-terminal pyroglutamate formation) [33, 40] in the peptide sequence is very challenging.

Tab. 2.2 (right, page 33): (A) Unlabeled and **(B)** heavy labeled (lys: U-$^{13}C_6$; U-$^{15}N_2$; arg: U-$^{13}C_6$; U-$^{15}N_4$) COX-2 peptide data (UniProtKB accession no. P35354). For each peptide, different CAD fragment ions used for qualification and quantification (underlined) with their Q1 and Q3 *m/z* are shown with retention time (RT, median ± range, n =35), relative ratios to quantifier transition as well as collision energies (CE). For unlabeled peptides **(A)** linear calibration range is shown for quantifier transitions, as well as the transitions of the corresponding heavy labeled peptides used internal standards (IS) for the quantification. Accuracy of calibrators was within a range of ±20%. The spiking levels of the heavy labeled peptides (concentrations in vial) are in shown **(B)**.

(A)	Peptide	Transitions	Q1 *m/z*	Q3 *m/z*	RT [min]	Rel. Ratio to quantifier [%]	CE (V)	IS Transitions	Calibration Range [nM]
	VSQASIDQSR								
		$M^{2+} \rightarrow y_7^+$	**545.8**	**776.4**			**28**	**$M^{2+} \rightarrow y_7^+$**	**0.25 - 500**
		$M^{2+} \rightarrow y_4^+$	545.8	505.2	5.42 ± 0.07	84	28		
		$M^{2+} \rightarrow y_5^+$	545.8	618.3		46	27		
	NAIMSYVLTSR								
		$M^{2+} \rightarrow b_3^+$	**627.8**	**299.1**			**26**	**$M^{2+} \rightarrow b_3^+$**	**0.25 - 500**
		$M^{2+} \rightarrow y_8^+$	627.8	956.3	16.90 ± 0.14	41	26		
		$M^{2+} \rightarrow y_7^+$	627.8	825.3		27	30		
	LILIGETIK								
		$M^{2+} \rightarrow b_{2+}$	**500.3**	**227.2**			**21**	**$M^{2+} \rightarrow b_{3+}$**	**0.1 - 500**
		$M^{2+} \rightarrow y_7^+$	500.3	773.3	17.19 ± 0.14	57	20		
		$M^{2+} \rightarrow y_6^+$	500.3	660.3		25	22		
	FDPELLFNK								
		$M^{2+} \rightarrow b_2^+$	561.8	263.1		219	22		
		$M^{2+} \rightarrow y_7^+$	**561.8**	**860.4**	19.70 ± 0.08		**24**	**$M^{2+} \rightarrow y_7^{++}$**	**0.1 - 500**
		$M^{2+} \rightarrow y_5^+$	561.8	634.3		42	30		

(B)	Peptide IS	Transitions	Q1 *m/z*	Q3 *m/z*	RT [min]	Rel. Ratio to quantifier [%]	CE (V)	Spiking level in vial [nM]
	VSQASIDQSR							
		$M^{2+} \rightarrow y_6^+$	550.8	715.4		105	28	
		$M^{2+} \rightarrow y_7^+$	**550.8**	**786.4**	5.42 ± 0.07		**28**	30
		$M^{2+} \rightarrow y_5^+$	550.8	628.3		43	25	
	NAIMSYVLTSR							
		$M^{2+} \rightarrow b_3^+$	**632.8**	**299.2**			**26**	
		$M^{2+} \rightarrow y_7^+$	632.8	832.5	16.90 ± 0.15	30	30	30
		$M^{2+} \rightarrow y_9^+$	632.8	1079.6		17	25	
	LILIGETIK							
		$M^{2+} \rightarrow b_2^+$	504.3	227.2		402	20	
		$M^{2+} \rightarrow b_3^+$	**504.3**	**340.3**	17.18 ± 0.14		**20**	30
		$M^{2+} \rightarrow y_8^+$	504.3	894.6		6	15	
	FDPELLFNK							
		$M^{2+} \rightarrow y_7^{++}$	**565.8**	**434.8**			**24**	
		$M^{2+} \rightarrow y_3^+$	565.8	416.2	19.71 ± 0.10	8	36	30
		$M^{2+} \rightarrow y_4^+$	565.8	529.3		5	36	

Of all tryptic peptides between 7 and 22 aa length in the COX-2 sequence, only two contain none of the unfavored aa. For this reason, we tolerated max. two of these aa during peptide selection. Finally, detectability of the peptides in the LC-MS/MS system was evaluated beforehand based on the aa sequence to further filter for suitable peptides. We found the predicted RT using SSRCalc [36] quite accurate, most RTs of the final peptides were within a range of ± 1 min, maximum ± 2.5 min of the predicted ones on our system (**Tab. 2.1, Tab. 2.2**) and we were indeed not able to detect the very hydrophilic peptide ANPCCSHPCQNR with a predicted RT of 0.6 min in a tryptic digest of crude recombinant human COX-2 protein. If peptides are too hydrophilic, RTs can be instable, sequences containing too many hydrophobic aa may result in broad peaks in reversed phase chromatography, low ion intensities in ESI ionization, and reduced solubility during sample preparation.

The use of a protein standard proved to be helpful in the final step of peptide selection, where three COX-2 specific peptides needed to be chosen from the remaining six peptides (including COX-1/-2 unspecific peptide; **Tab. 2.1**). Many groups use their own experimental data from shotgun approaches to search for appropriate abundant peptides. However, if such data is not available, the digestion of the protein of interest is a useful alternative where the chromatographic and mass-spectrometric properties of the peptides can be directly compared. Here, two of the six peptides showed insufficient MS sensitivity or chromatographic behavior and were excluded, leaving three COX-2 specific and one COX-1/2 specific peptide as PTPs for the final method (**Tab. 2.2**).

2.4.2 SRM Method Development

In the next step, we selected precursor-fragment-ion transitions with the aim of choosing the most intense, highly selective, and interference-free ones. We only used transitions that result from CAD based fragmentation at the peptide backbone releasing mainly intense y- or b-type ions. The most intense transitions were selected based on data from SRMAtlas [37] and experimentally from MS/MS spectra of the respective peptide standards. Fragment ions with *m/z* exceeding those of the precursor ions were preferred, because there is no interference from singly charged background ions which cannot fragment to *m/z* higher than the precursor. CEs of several transitions were optimized for increased sensitivity and the final transition ranking was generally in good agreement with the data from SRMAtlas, even for predicted transitions (**Tab. 7.1**). Thus, we conclude that this approach facilitates SRM development workflow. Because of their identical physicochemical properties [15] the same transitions were selected for the corresponding heavy labeled and unlabeled peptides. However, this was not always possible due to mass shifts caused by the heavy labeled aa. For example, in case of GALQNIIPASTGAAK (from GAPDH), the intense transition $[M+2H]^{2+} \rightarrow y_8^+$ (*m/z* 706.4 → *m/z* 702.4) is used to detect the unlabeled peptide. Due to the mass shift in the heavy labeled peptide (+8 Da), the corresponding transition results in a pseudo-SRM (*m/z* 710.4→ *m/z* 710.4). Both ion types cannot be separated in the triple quadrupole mass spectrometer, and another transition must be selected (**Fig. 2.2 (A)**).

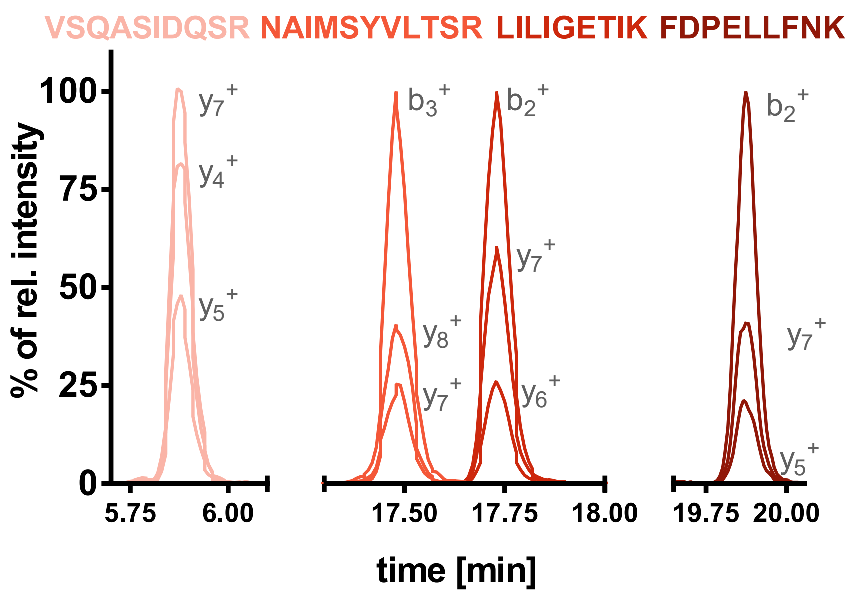

Fig. 2.5: Exemplary signal intensity ratios of quantifier and qualifier transitions in unlabeled COX-2 peptide standards (10 – 80 nM).

Even though a unique peptide and a defined precursor-fragment-ion transition provide a high degree of specificity, in a complex matrix background containing numerous other peptides, (nearly) isobaric interferences are not unlikely. For this reason, we evaluated each transition of the unlabeled and heavy labeled peptides in the biological matrix of interest. For example, in HCA-7 cell lysate we found background signals interfering with the $[M+2H]^{2+} \rightarrow y_8^+$ transition of heavy labeled NAIMSYVLTSR (from COX-2).

Thus, it was substituted with a less sensitive but interference-free alternative transition (**Fig. 2.2 (B),(C)**). Peptides containing the same aa in different orders (each with unique sequences), isobaric (L=I) or nearly isobaric aa exchanges (e.g., W=SV=EG=AD) which cannot be separated on quadrupole instruments lead to (nearly) isobaric precursor *m/z* [46]. However, identification of the correct peptide is supported by monitoring several transitions. This higher sequence coverage provides additional specificity by comparing the area ratios in samples to matrix-free standards (Fig. 2.5) and exact retention time alignment of all transitions [34, 35].

High intra- and interday precisions (< 15%) demonstrated the reproducibility and robustness of the method despite severe ion suppression up to 70% of the IS peak area (**Tab. 7.6**, **Fig. 7.2**). This is most likely a result of the large sample amount (50 µg total protein injected) used for analysis, which is required in order to sensitively detect the target protein in sample matrix. The LOD and LLOQ for the COX-2 peptides were in the pM range (LOD: 25-250 pM in vial, corresponding to 0.125-1.25 fmol on column) and comparable to other reports of SRM assays of peptides on the same sensitive instrument (QTRAP 5500) with LODs in the medium to high amol range [47-49]. The abundances of the proteins (and thus, peptides) targeted with the developed method are present at greatly different concentrations, since COX-2 is often only expressed upon stimuli and rapidly degraded while the housekeeping proteins PPIB, GAPDH and *β*-/*γ*-actin are always present in high concentrations, for example, GAPDH belonged to the most abundantly expressed proteins in 11 cell lines [50].

Generally, the differences in protein abundances are about seven orders of magnitude in human cells [50, 51]. A linear calibration ranging up to 500 nM is sufficient in order to determine COX-2 peptides (**Tab. 2.2**). However, despite the large dynamic range of the triple quadrupole instrument, ion suppression restricted the linear calibration range for housekeeper peptides to 1 µM. Here, the use of a quadratic fitted calibration allowed us to quantify peptides occurring at higher levels (**Tab. 7.4**). Hence, we were able to simultaneously quantify COX down to the pM range and housekeeping proteins in the µM range.

2.4.3 Evaluation of COX(-2) Pathway in Cell Culture Models

The developed targeted proteomics method was applied to characterize COX-2 abundance in parallel to COX activity in three human colon carcinoma cell lines HCT-116, HT-29, and HCA-7. Because of the central role of COX-2 in colorectal cancer [7, 52] it is interesting to study the ARA cascade in these cells producing different levels of prostanoids (**Fig. 2.4 (A) i-ii), Tab. 7.7**). Among the investigated compounds (ARA-derived prostanoids), PGE_2 and 12-HHT showed the highest levels and were detectable in all cell lines and may therefore serve as indicators of COX activity. While no COX-2 specific peptides could be detected in HCT-116 cells, all COX-2 specific peptides were found in HT-29 and HCA-7 cells and the COX-2 abundance levels correlated with the oxylipin levels. The COX-1/2 unspecific peptide LILIGETIK showing the highest intensity and thus sensitivity was found in all colon cells. However, no COX-1 specific peptides were detectable (**Fig. 7.5**). COX-1 abundance has been previously reported in HCT-116 cells [53, 54]. The low level of COX-2 in HCT-116 cells (**Fig. 2.4 (A) iii)**) is in line with studies reporting no (or a weak) COX-2 (PTGS2) gene expression [53-56]. HCA-7 cells are well-known for their COX-2 overexpression [14, 53, 54, 56], while the extent of COX-1gene expression in this cell line is not as clear [53, 54, 57]. The reported lower COX-2 levels in HT-29 [53, 58, 59] compared to HCA-7 cells are in line with our results [56, 59]. Parallel analysis of enzyme activity and protein levels are especially helpful when investigating the modulation of metabolic pathways such as the ARA cascade. Here, we showed that a 24 h incubation with indomethacin and celecoxib at concentrations approximately ten times higher than their previously determined IC_{50} values [14] lead to a marked reduction of prostanoid levels in HCA-7 cells compared to untreated control (**Fig. 2.4 (B) i-ii), Tab. 7.7**). The similar COX-2 levels (normalized to those of the housekeeping proteins) revealed that the inhibitors did not introduce changes in COX-2 formation. Here, the use of single peptides (**Fig. 2.4 (B) iv-vi)**) or the mean of all specific peptides per protein (**Fig. 7.7 (A) ii-iv)**) lead to similar results.

Housekeeping proteins are assumed to be expressed in cells at constant levels, and therefore are commonly used as internal loading controls in western blot or PCR analysis. However, protein abundances depend on the model organism or cell line and can be influenced by a variety of factors, for example, the physiological state of the cell and experimental conditions. Thus, the existence of a universal housekeeping protein is questionable. In order to address this limitation, we selected a set of housekeeping proteins derived from three different biological processes: PPIB in protein folding, GAPDH in glycolysis, and *β*-/*γ*-actin in the cytoskeleton. In contrast to the classic western blot approach, targeted proteomics easily allows multiplexing of numerous target proteins and the use of a set of housekeeping proteins for quantitative proteomics SRM approaches has been described [60, 61]. Lee et al. [62] proposed the use of a selection of housekeeping proteins ("barcode") comprising a set of stably formed proteins derived from various biological pathways with different levels as well as molecular weights that can be used as sum for normalization of spectral count data. Our approach allows us to compare the normalization of COX-2 to each of the housekeeping proteins and detect relevant changes in their abundance. Here, their similar results indicate that all can be used in this experimental setting. Yet, the SRM method can be further extended in the future.

Time-dependent changes in the COX pathway caused by LPS stimulation were investigated in human primary macrophages. One of the strengths of our oxylipin metabolomics approach is the parallel analysis of a set of COX-derived products (PGD_2, PGE_2, PGF_{2a}, TxB_2, and 12-HHT; **Fig. 2.4 (C) i-ii), Tab. 7.7**) enabling a comprehensive assessment of downstream enzyme activities. Interestingly, the time course of 12-HHT formation differed from the other oxylipins, declining after 24 h. This suggests a more rapid degradation/further conversion of this COX-activity indicator, for example, to 12-keto-HHT [63, 64]. Moreover, oxylipin analysis in the culture medium revealed that the relative fold changes of PGE_2 in the time-dependent concentration increase distinctly differed between the two donors, that is, 10 and 40-fold between 24 h and 0 h, respectively, despite similar basal levels. At the same time, the relative fold changes of the other prostanoids were comparable between both donors. This finding might be attributed by varying abundance and/or activities of downstream prostaglandin E synthases of the individuals. Consistently, the changes in COX-2 abundance levels were similar in the cells from both donors (after normalization to housekeeping proteins). COX-2 abundance increased during LPS-stimulation and was detectable after 6 h of LPS treatment, where it peaked and was declined after 24 h of total incubation time (**Fig. 2.4 (C) iii-vi), Fig. 7.7 (B)**). All COX-2 specific peptides showed similar fold changes between 6 h and 24 h (0.3 – 0.5). The presence of the COX-1/2-specific peptide LILIGETIK at all time points as well as the COX-1 specific peptides indicated the presence of COX-1 in the cells independent of the stimulus.

Time dependent changes in COX-2 abundance have been reported in similar test systems of LPS-stimulated monocyte derived PMA-differentiated macrophages (human U937 and THP-1 cell lines). The mRNA levels rapidly and strongly increased until about 2 – 4 h after incubation start and then declined. They were followed by progressing gene expression which further increased for up to ≈ 24 h while COX-1 transcription and expression remained unchanged [65-67]. The longer lasting detectability of COX-2 protein compared to our results might be explained by differences between primary macrophages and cell-line derived macrophages, which are often derived from cancerous states. In line with our results, PGE_2 levels concurrently raised alongside with enzyme abundance and were also highest after about 24 h [65-67].

Conclusively, we could show that combined oxylipin metabolomics and proteomics analysis is a powerful tool to thoroughly investigate the ARA cascade, enabling parallel monitoring of oxylipin formation and enzyme abundance levels as well as their modulation. Here, we present a detailed workflow for targeted proteomics method development including the selection of suitable unique peptides for the proteins of interest and SRM transitions for the measurement. Multiple *in silico* tools assist the researcher in method development, however, our results show that experimental verification of each transition is indispensable since isobaric matrix interferences disrupt the specificity of the analysis. Alongside with the protein of interest, targeting a set of housekeeping proteins in the multiplexed method additionally represents a suitable tool as internal loading control for data normalization, as we could show for the analysis of COX-2 abundance in human colon carcinoma cells and LPS-triggered primary macrophages. In the future, the inclusion of all key enzymes of the ARA cascade in the method will enable us to extensively characterize and understand biological mechanisms involved in the modulation of the ARA cascade induced by, for example, diseases, drugs, or food ingredients.

Associated data

Proteomics data is available through PASSEL (http://www.peptideatlas.org/passel/) at PASS01623.

2.5 References

1. Buczynski MW, Dumlao DS, and Dennis EA (2009) Thematic Review Series: Proteomics. An integrated omics analysis of eicosanoid biology. *J Lipid Res,* 50(6), 1015-38; doi: 10.1194/jlr.R900004-JLR200.
2. Ricciotti E and FitzGerald GA (2011) Prostaglandins and Inflammation. *Atertio Thromb Vasc Biol,* 31(5), 986-1000; doi: 10.1161/Atvbaha.110.207449.
3. Yu R, Xiao L, Zhao G, Christman JW, and van Breemen RB (2011) Competitive Enzymatic Interactions Determine the Relative Amounts of Prostaglandins E_2 and D_2. *J Pharmacol Exp Ther,* 339(2), 716-725; doi: 10.1124/jpet.111.185405.
4. Matsunobu T, Okuno T, Yokoyama C, and Yokomizo T (2013) Thromboxane A synthase-independent production of 12-hydroxyheptadecatrienoic acid, a BLT2 ligand. *J Lipid Res,* 54(11), 2979-2987; doi: 10.1194/jlr.M037754.
5. Vane JR, Bakhle YS, and Botting RM (1998) Cyclooxygenases 1 and 2. *Annu Rev Pharmacol Toxicol,* 38, 97-120; doi: 10.1146/annurev.pharmtox.38.1.97.
6. Morita I (2002) Distinct functions of COX-1 and COX-2. *Prostaglandins Other Lipid Mediators,* 68-9, 165-175; doi: 10.1016/S0090-6980(02)00029-1.
7. Rohwer N, Kuhl AA, Ostermann AI, Hartung NM, Schebb NH, Zopf D, McDonald FM, and Weylandt KH (2020) Effects of chronic low-dose aspirin treatment on tumor prevention in three mouse models of intestinal tumorigenesis. *Cancer Med.*; doi: 10.1002/cam4.2881.
8. Fosslien E (2000) Biochemistry of cyclooxygenase (COX)-2 inhibitors and molecular pathology of COX-2 in neoplasia. *Crit Rev Clin Lab Sci,* 37(5), 431-502; doi: 10.1080/10408360091174286.
9. Cipollone F and Fazia ML (2006) COX-2 and Atherosclerosis. *J Cardiovasc Pharmacol,* 47, S26-S36.
10. Zarghi A and Arfaei S (2011) Selective COX-2 Inhibitors: A Review of Their Structure-Activity Relationships. *Iran J Pharm Res,* 10(4), 655-683.
11. Nomikos T, Fragopoulou E, and Antonopoulou S (2007) Food ingredients and lipid mediators. *Curr Nutr Food Sci,* 3(4), 255-76.
12. Garcia-Lafuente A, Guillamon E, Villares A, Rostagno MA, and Martinez JA (2009) Flavonoids as anti-inflammatory agents: implications in cancer and cardiovascular disease. *Inflamm Res,* 58(9), 537-52; doi: 10.1007/s00011-009-0037-3.
13. Gottschall H, Schmöcker C, Hartmann D, Rohwer N, Rund K, Kutzner L, Nolte F, Ostermann AI, Schebb NH, and Weylandt KH (2018) Aspirin alone and combined with a statin suppresses eicosanoid formation in human colon tissue. *J Lipid Res,* 59(5), 864-871; doi: 10.1194/jlr.M078725.
14. Willenberg I, Meschede AK, Gueler F, Jang MS, Shushakova N, and Schebb NH (2015) Food Polyphenols Fail to Cause a Biologically Relevant Reduction of COX-2 Activity. *PLoS One,* 10(10), e0139147; doi: 10.1371/journal.pone.0139147.
15. Kirkpatrick DS, Gerber SA, and Gygi SP (2005) The absolute quantification strategy: a general procedure for the quantification of proteins and post-translational modifications. *Methods,* 35(3), 265-273; doi: 10.1016/j.ymeth.2004.08.018.
16. Hanáková Z, Hošek J, Kutil Z, Temml V, Landa P, Vaněk T, Schuster D, Dall'Acqua S, Cvačka J, Polanský O, et al. (2017) Anti-inflammatory Activity of Natural Geranylated Flavonoids: Cyclooxygenase and Lipoxygenase Inhibitory Properties and Proteomic Analysis. *J Nat Prod,* 80(4), 999-1006; doi: 10.1021/acs.jnatprod.6b01011.

17. Tahir A, Bileck A, Muqaku B, Niederstaetter L, Kreutz D, Mayer RL, Wolrab D, Meier SM, Slany A, and Gerner C (2017) Combined Proteome and Eicosanoid Profiling Approach for Revealing Implications of Human Fibroblasts in Chronic Inflammation. *Anal Chem,* 89(3), 1945-1954; doi: 10.1021/acs.analchem.6b04433.
18. Sabido E, Quehenberger O, Shen Q, Chang CY, Shah I, Armando AM, Andreyev A, Vitek O, Dennis EA, and Aebersold R (2012) Targeted Proteomics of the Eicosanoid Biosynthetic Pathway Completes an Integrated Genomics-Proteomics-Metabolomics Picture of Cellular Metabolism. *Mol Cell Proteomics,* 11(7); doi: 10.1074/Mcp.M111.014746.
19. Rund KM, Ostermann AI, Kutzner L, Galano JM, Oger C, Vigor C, Wecklein S, Seiwert N, Durand T, and Schebb NH (2018) Development of an LC-ESI(-)-MS/MS method for the simultaneous quantification of 35 isoprostanes and isofurans derived from the major n3- and n6-PUFAs. *Anal Chim Acta,* 1037, 63-74; doi: 10.1016/j.aca.2017.11.002.
20. Kutzner L, Rund KM, Ostermann AI, Hartung NM, Galano JM, Balas L, Durand T, Balzer MS, David S, and Schebb NH (2019) Development of an Optimized LC-MS Method for the Detection of Specialized Pro-Resolving Mediators in Biological Samples. *Front Pharmacol,* 10; doi: 10.3389/fphar.2019.00169.
21. Vijayan V, Pradhan P, Braud L, Fuchs HR, Gueler F, Motterlini R, Foresti R, and Immenschuh S (2019) Human and murine macrophages exhibit differential metabolic responses to lipopolysaccharide - A divergent role for glycolysis. *Redox Biol.,* 22; doi: 10.1016/j.redox.2019.101147.
22. O'Brien J, Wilson I, Orton T, and Pognan F (2000) Investigation of the Alamar Blue (resazurin) fluorescent dye for the assessment of mammalian cell cytotoxicity. *Eur J Biochem,* 267(17), 5421-5426; doi: 10.1046/j.1432-1327.2000.01606.x.
23. Botelho D, Wall MJ, Vieira DB, Fitzsimmons S, Liu F, and Doucette A (2010) Top-Down and Bottom-Up Proteomics of SDS-Containing Solutions Following Mass-Based Separation. *J Proteome Res,* 9(6), 2863-2870; doi: 10.1021/pr900949p.
24. Kinter M and Sherman NE (2000) Protein sequencing and identification using tandem mass spectrometry. Wiley-Interscience series on mass spectrometry. New York: Wiley.
25. Zhou J, Zhou TY, Cao R, Liu Z, Shen JY, Chen P, Wang XC, and Liang SP (2006) Evaluation of the application of sodium deoxycholate to proteomic analysis of rat hippocampal plasma membrane. *J Proteome Res,* 5(10), 2547-2553; doi: 10.1021/pr060112a.
26. Mallick P, Schirle M, Chen SS, Flory MR, Lee H, Martin D, Raught B, Schmitt R, Werner T, Kuster B, et al. (2007) eComputational prediction of proteotypic peptides for quantitative proteomics. *Nat Biotechnol,* 25(1), 125-131; doi: 10.1038/nbt1275.
27. Gasteiger E, Hoogland C, Gattiker A, Duvaud Se, Wilkins MR, Appel RD, and Bairoch A, (2005) Protein Identification and Analysis Tools on the ExPASy Server, in The Proteomics Protocols Handbook, Walker JM, Editor. Humana Press: Totowa, NJ, 571-607.
28. Johnson M, Zaretskaya I, Raytselis Y, Merezhuk Y, McGinnis S, and Madden TL (2008) NCBI BLAST: a better web interface. *Nucleic Acids Res,* 36(suppl_2), W5-W9; doi: 10.1093/nar/gkn201.
29. Schaeffer M, Gateau A, Teixeira D, Michel PA, Zahn-Zabal M, and Lane L (2017) The neXtProt peptide uniqueness checker: a tool for the proteomics community. *Bioinformatics,* 33(21), 3471-3472; doi: 10.1093/bioinformatics/btx318.
30. Fannes T, Vandermarliere E, Schietgat L, Degroeve S, Martens L, and Ramon J (2013) Predicting Tryptic Cleavage from Proteomics Data Using Decision Tree Ensembles. *J Proteome Res,* 12(5), 2253-2259; doi: 10.1021/pr4001114.

31. The UniProti Consortium (2018) UniProt: a worldwide hub of protein knowledge. *Nucleic Acids Res,* 47(D1), D506-D515; doi: 10.1093/nar/gky1049.
32. Hornbeck PV, Zhang B, Murray B, Kornhauser JM, Latham V, and Skrzypek E (2015) PhosphoSitePlus, 2014: mutations, PTMs and recalibrations. *Nucleic Acids Res,* 43(D1), D512-D520; doi: 10.1093/nar/gku1267.
33. Hoofnagle AN, Whiteaker JR, Carr SA, Kuhn E, Liu T, Massoni SA, Thomas SN, Townsend RR, Zimmerman LJ, Boja E, et al. (2016) Recommendations for the Generation, Quantification, Storage, and Handling of Peptides Used for Mass Spectrometry-Based Assays. *Clin Chem,* 62(1), 48-69; doi: 10.1373/clinchem.2015.250563.
34. Lange V, Picotti P, Domon B, and Aebersold R (2008) Selected reaction monitoring for quantitative proteomics: a tutorial. *Mol Syst Biol,* 4; doi: 10.1038/Msb.2008.61.
35. Gallien S, Duriez E, and Domon B (2011) Selected reaction monitoring applied to proteomics. *J Mass Spectrom,* 46(3), 298-312; doi: 10.1002/jms.1895.
36. Krokhin OV and Spicer V (2009) Peptide Retention Standards and Hydrophobicity Indexes in Reversed-Phase High-Performance Liquid Chromatography of Peptides. *Anal Chem,* 81(22), 9522-9530; doi: 10.1021/ac9016693.
37. Kusebauch U, Campbell DS, Deutsch EW, Chu CS, Spicer DA, Brusniak M-Y, Slagel J, Sun Z, Stevens J, Grimes B, et al. (2016) Human SRMAtlas: A Resource of Targeted Assays to Quantify the Complete Human Proteome. *Cell,* 166(3), 766-778; doi: 10.1016/j.cell.2016.06.041.
38. Maiolica A, Junger MA, Ezkurdia I, and Aebersold R (2012) Targeted proteome investigation via selected reaction monitoring mass spectrometry. *J Proteomics,* 75(12), 3495-3513; doi: 10.1016/j.jprot.2012.04.048.
39. Liebler DC and Zimmerman LJ (2013) Targeted Quantitation of Proteins by Mass Spectrometry. *Biochemistry,* 52(22), 3797-3806; doi: 10.1021/bi400110b.
40. Kamiie J, Ohtsuki S, Iwase R, Ohmine K, Katsukura Y, Yanai K, Sekine Y, Uchida Y, Ito S, and Terasaki T (2008) Quantitative Atlas of Membrane Transporter Proteins: Development and Application of a Highly Sensitive Simultaneous LC/MS/MS Method Combined with Novel In-silico Peptide Selection Criteria. *Pharm Res,* 25(6), 1469-1483; doi: 10.1007/s11095-008-9532-4.
41. Smith WL, DeWitt DL, and Garavito RM (2000) Cyclooxygenases: Structural, cellular, and molecular biology. *Annu Rev Biochem,* 69, 145-182; doi: 10.1146/annurev.biochem.69.1.145.
42. Keil B (1992) Specificity of Proteolysis. Berlin Heidelberg: Springer-Verlag.
43. Rodriguez J, Gupta N, Smith RD, and Pevzner PA (2008) Does trypsin cut before proline? *J Proteome Res,* 7(1), 300-305; doi: 10.1021/pr0705035.
44. Stenson PD, Mort M, Ball EV, Howells K, Phillips AD, Thomas NST, and Cooper DN (2009) The Human Gene Mutation Database: 2008 update. *Genome Med,* 1; doi: 10.1186/gm13.
45. White MR and Garcin ED (2017) D-Glyceraldehyde-3-Phosphate Dehydrogenase Structure and Function. Macromolecular Protein Complexes: Structure and Function, ed. Harris JR and Marles-Wright J. Cham: Springer International Publishing.
46. Sherman J, McKay MJ, Ashman K, and Molloy MP (2009) How specific is my SRM?: The issue of precursor and product ion redundancy. *Proteomics,* 9(5), 1120-1123; doi: 10.1002/pmic.200800577.
47. Ebhardt HA, Sabidó E, Hüttenhain R, Collins B, and Aebersold R (2012) Range of protein detection by selected/multiple reaction monitoring mass spectrometry in an

unfractionated human cell culture lysate. *Proteomics,* 12(8), 1185-1193; doi: 10.1002/pmic.201100543.

48. Faktor J, Sucha R, Paralova V, Liu Y, and Bouchal P (2017) Comparison of targeted proteomics approaches for detecting and quantifying proteins derived from human cancer tissues. *Proteomics,* 17(5), 1600323; doi: 10.1002/pmic.201600323.
49. Matsumoto M, Matsuzaki F, Oshikawa K, Goshima N, Mori M, Kawamura Y, Ogawa K, Fukuda E, Nakatsumi H, Natsume T, et al. (2017) A large-scale targeted proteomics assay resource based on an in vitro human proteome. *Nat Methods,* 14(3), 251-258; doi: 10.1038/nmeth.4116.
50. Geiger T, Wehner A, Schaab C, Cox J, and Mann M (2012) Comparative Proteomic Analysis of Eleven Common Cell Lines Reveals Ubiquitous but Varying Expression of Most Proteins. *Mol Cell Proteomics,* 11(3); doi: 10.1074/mcp.M111.014050.
51. Beck M, Schmidt A, Malmstroem J, Claassen M, Ori A, Szymborska A, Herzog F, Rinner O, Ellenberg J, and Aebersold R (2011) The quantitative proteome of a human cell line. *Mol Syst Biol,* 7(1), 549; doi: 10.1038/msb.2011.82.
52. Eberhart CE, Coffey RJ, Radhika A, Giardiello FM, Ferrenbach S, and Dubois RN (1994) Up-regulation of cyclooxygenase 2 gene expression in human colorectal adenomas and adenocarcinomas. *Gastroenterology,* 107(4), 1183-1188; doi: 10.1016/0016-5085(94)90246-1.
53. Liu Q, Chan STF, and Mahendran R (2003) Nitric oxide induces cyclooxygenase expression and inhibits cell growth in colon cancer cell lines. *Carcinogenesis,* 24(4), 637-642; doi: 10.1093/carcin/bgg014.
54. Smith ML, Hawcroft G, and Hull MA (2000) The effect of non-steroidal anti-inflammatory drugs on human colorectal cancer cells: evidence of different mechanisms of action. *Eur J Cancer,* 36(5), 664-674; doi: 10.1016/S0959-8049(99)00333-0.
55. Kutchera W, Jones DA, Matsunami N, Groden J, McIntyre TM, Zimmerman GA, White RL, and Prescott SM (1996) Prostaglandin H synthase 2 is expressed abnormally in human colon cancer: Evidence for a transcriptional effect. *Proc Natl Acad Sci U S A,* 93(10), 4816-4820; doi: 10.1073/pnas.93.10.4816.
56. Shao JY, Sheng HM, Inoue H, Morrow JD, and DuBois RN (2000) Regulation of constitutive cyclooxygenase-2 expression in colon carcinoma cells. *J Biol Chem,* 275(43), 33951-33956; doi: 10.1074/jbc.M002324200.
57. Goldman AP, Williams CS, Sheng HM, Lamps LW, Williams VP, Pairet M, Morrow JD, and DuBois RN (1998) Meloxicam inhibits the growth of colorectal cancer cells. *Carcinogenesis,* 19(12), 2195-2199; doi: 10.1093/carcin/19.12.2195.
58. Hanif R, Pittas A, Feng Y, Koutsos MI, Qiao L, StaianoCoico L, Shiff SI, and Rigas B (1996) Effects of nonsteroidal anti-inflammatory drugs on proliferation and on induction of apoptosis in colon cancer cells by a prostaglandin-independent pathway. *Biochem Pharmacol,* 52(2), 237-245; doi: 10.1016/0006-2952(96)00181-5.
59. Sharma RA, Gescher A, Plastaras JP, Leuratti C, Singh R, Gallacher-Horley B, Offord E, Marnett LJ, Steward WP, and Plummer SM (2001) Cyclooxygenase-2, malondialdehyde and pyrimidopurinone adducts of deoxyguanosine in human colon cells. *Carcinogenesis,* 22(9), 1557-60; doi: 10.1093/carcin/22.9.1557.
60. Kinter CS, Lundie JM, Patel H, Rindler PM, Szweda LI, and Kinter M (2012) A Quantitative Proteomic Profile of the Nrf2-Mediated Antioxidant Response of Macrophages to Oxidized LDL Determined by Multiplexed Selected Reaction Monitoring. *PLoS One,* 7(11); doi: 10.1371/journal.pone.0050016.
61. Whiteaker JR, Lin CW, Kennedy J, Hou LM, Trute M, Sokal I, Yan P, Schoenherr RM, Zhao L, Voytovich UJ, et al. (2011) A targeted proteomics-based pipeline for

verification of biomarkers in plasma. *Nat Biotechnol,* 29(7), 625-U108; doi: 10.1038/nbt.1900.

62. Lee W and Lazar IM (2014) Endogenous Protein "Barcode" for Data Validation and Normalization in Quantitative MS Analysis. *Anal Chem,* 86(13), 6379-6386; doi: 10.1021/ac500855q.
63. Hecker M and Ullrich V (1988) 12(S)-Hydroxy-5,8,10 (Z,E,E)-heptadecatrienoic acid (HHT) is preferentially metabolized to its 12-keto derivative by human erythrocytes in vitro. *Eicosanoids,* 1(1), 19-25.
64. Liu Y, Yoden K, Shen R-F, and Tai H-H (1985) 12-L-hydroxy-5,8,10-heptadecatrienoic acid (HHT) is an excellent substrate for NAD+-dependent 15-hydroxyprostaglandin dehydrogenase. *Biochem Biophys Res Commun,* 129(1), 268-274; doi: 10.1016/0006-291X(85)91432-9.
65. Barrios-Rodiles M, Tiraloche G, and Chadee K (1999) Lipopolysaccharide modulates cyclooxygenase-2 transcriptionally and posttranscriptionally in human macrophages independently from endogenous IL-1 beta and TNF-alpha. *J Immunol,* 163(2), 963-969.
66. Grkovich A, Johnson CA, Buczynski MW, and Dennis EA (2006) Lipopolysaccharide-induced cyclooxygenase-2 expression in human U937 macrophages is phosphatidic acid phosphohydrolase-1-dependent. *J Biol Chem,* 281(44), 32978-32987; doi: 10.1074/jbc.M605935200.
67. Noma T, Takahashi-Yanaga F, Arioka M, Mori Y, and Sasaguri T (2016) Inhibition of GSK-3 reduces prostaglandin E2 production by decreasing the expression levels of COX-2 and mPGES-1 in monocyte/macrophage lineage cells. *Biochem Pharmacol,* 116, 120-129; doi: 10.1016/j.bcp.2016.07.014.

Chapter 3

Impact of Food Polyphenols on Oxylipin Biosynthesis in Human Neutrophils

The intake of food polyphenols is associated with beneficial impacts on health. Besides anti-oxidative effects, anti-inflammatory properties have been suggested as molecular modes of action, which may result from modulations of the arachidonic acid (ARA) cascade. Here, we investigated the effects of a library of food polyphenols on 5-lipoxygenase (5-LOX) activity in a cell-free assay, and in human neutrophils. Resveratrol, its dimer (ε-viniferin), and its imine analogue (IRA) potently blocked the 5-LOX-mediated LT formation in neutrophils with IC_{50} values in low µM-range. Among the tested flavonoids only the isoflavone genistein showed potent 5-LOX inhibition in neutrophils (IC_{50} = 0.4 ± 0.1 µM), however was ineffective on isolated 5-LOX. We exclude an interference with the 5-LOX-activating protein (FLAP) in HEK_5-LOX/±FLAP cells and suggest global effects on intact immune cells. Using LC-MS based targeted oxylipin metabolomics, we analyzed the effects of 5-LOX-inhibiting polyphenols on all branches of the ARA cascade in Ca^{2+}-ionophore-challenged neutrophils. While ε-viniferin causes a clear substrate shunt towards the remaining ARA cascade enzymes (15-LOX, cyclooxygenase – COX-1/2, cytochrome P450), resveratrol inhibited the COX-1/2 pathway and showed a weak attenuation of 12/15-LOX activity. IRA had no impact on 15-LOX activity, but elevated the formation of COX-derived prostaglandins, having no inhibitory effects on COX-1/2. Overall, we show that food polyphenols have the ability to block 5-LOX activity and the oxylipin pattern is modulated with a remarkable compound/structural specificity. Taken the importance of polyphenols for a healthy diet and their concentration in food supplements into account, this finding justifies further investigation.

Reprinted from Hartung NM*, Fischer J*, Ostermann AI, Willenberg I, Rund KM, Schebb NH, Garscha U (2019) Impact of food polyphenols on oxylipin biosynthesis in human neutrophils. *Biochim Biophys Acta, Mol Cell Biol Lipids*, 1864 (10), 1536-1544; doi: 10.1016/j.bbalip.2019.05.002; Copyright (2019), with permission from Elsevier.

* Authors contributed equally to this work.

Author contributions: NMH and JF designed research, performed experiments and wrote the manuscript; AIO, KR and IW designed research and performed experiments; NHS and UG designed research and wrote the manuscript.

3.1 Introduction

Inflammatory diseases, such as asthma or inflammatory bowel disease, as well as chronic pain conditions are major health problems in the western world with an increasing number of people being affected. Ideally, acute inflammation is a protective immune response towards tissue imbalances such as infections, lesions and osmotic stress with the aim to restore tissue homeostasis. However, exuberant and non-resolved immune-responses may lead to chronic inflammation with concomitant negative impacts on physical health [1]. The resolution process can be influenced by diverse factors including sex, age and food intake. Furthermore, fat content and fat composition of the diet have an impact on the transition from inflammation to resolution [2-4].

It is popularly known that intake of fruits and vegetables is associated with healthiness and well-being [5]. Plenty epidemiologic studies confirm that a diet rich in vegetables reduces the risk for cancer and cardiovascular events [6, 7]. The positive effects are partially attributed to secondary plant metabolites such as polyphenols, which are found in fruit, vegetables and traditionally fermented products such as coffee, black tea and cocoa. They comprise a wide class of structurally diverse compounds [8], roughly grouped as flavonoids, such as the catechin epigallocatechin-gallate (EGCG) found in green tea, the soy isoflavone genistein or the flavone apigenin extracted from parsley, but also non-flavonoids such as resveratrol (a stilbene) found in wine [9]. Many of the polyphenols have been reported to have anti-inflammatory properties [10] and particularly resveratrol possesses the ability to downregulate inflammatory responses by inhibition of pro-inflammatory cytokines [11], induction of the inducible NO synthase (iNOS) [12, 13], and regulation of pro-inflammatory gene expression [14-17]. Apart from this and the anti-oxidative effects of polyphenols that are attributed to their radical scavenging properties, the anti-inflammatory properties are believed to contribute to their positive effects on human health.

Inflammatory processes are tightly regulated by distinct lipid mediators (LMs) that on the one hand initiate inflammation but on the other hand preferably lead to self-resolution [18, 19]. Prostaglandins (PGs) and leukotrienes (LTs) are arachidonic acid (ARA) derived oxylipins acting as lipid mediators involved in acute inflammation and formed via cyclooxygenase-1/2 (COX-1/2) and 5-lipoxygenase (5-LOX) pathways. Among the PGs, PGE_2 is a pro-inflammatory LM that promotes fever, pain and inflammation [20]. LTs are potent chemotactic and vasoactive compounds that possess establishing roles in asthma and allergy [18]. Although generally associated with inflammation, few eicosanoids display anti-inflammatory properties, such as the CYP450-formed epoxyeicosatrienoic acids (EpETrE) [21], COX-derived prostacyclin PGI_2 and 5/15-LOX-generated lipoxins (LXs) [22]. Additionally, over the last two decades a novel group of LMs was found to trigger the resolution process. Aside from ARA, also other PUFA are converted by COX, LOX and CYP enzymes. On the one hand, they reduce the formation of ARA derived pro-inflammatory mediators by substrate competition, on the other hand they give rise for a distinct set of oxylipins with pronounced bioactivity. For example, eicosapentaenoic acid (EPA) derived epoxy-FA show strong anti-inflammatory and anti-arrhythmic activity [23]. Combined conversion by different enzymes of these pathways can lead to multiple hydroxylated EPA and docosahexaenoic acid (DHA). Some of these are called specialized pro-resolving mediators (SPMs), which actively resolve inflammation such as the E- and D- series of resolvins (Rvs), protectins and maresins [22].

Scattered reports show that single polyphenols have modulating effects on ARA-derived LM formation, particularly influencing COX-activity and expression levels [15, 16, 24]. But also LOXs seem to be targets for certain polyphenols as e.g. resveratrol inhibits the 5-LOX in neutrophils with an IC_{50} value in a low micromolar range [25]. However, a comprehensive view of the impact of polyphenols on the LM profile in immune cells is missing. In inflammatory processes, neutrophils generate vast amounts of chemotactic leukotrienes in order to initiate infiltration and to maintain an immune response. Here, we evaluate the effect of a small library of polyphenols on 5-LOX product formation in Ca^{2+}-ionophore challenged neutrophils isolated from human peripheral blood. The effects of a modulation of 5-LOX inhibition were thoroughly evaluated by means of targeted metabolomics and the obtained oxylipin patterns were compared to validated 5-LOX-pathway inhibitors (zileuton, MK886). We found that resveratrol, its dimer (*ε*-viniferin), and its imine analogue (IRA) potently inhibit LT formation in neutrophils. Surprisingly, the subsequent impact on other PUFA-derived LMs is specific for each polyphenol and a substrate shift to other branches of the ARA-cascade is not a foregone conclusion.

3.2 Experimental Section

3.2.1 Materials

Acetonitrile (HPLC–MS grade), acetic acid and methanol (Optima LC/MS grade) were purchased from Fisher Scientific (Schwerte, Germany). Disodium hydrogen phosphate, EDTA, disodium salt dihydrate (≥99%, p.a), sodium dodecylsulfate (SDS), Tris Pufferan and *n*-hexane (HPLC grade) were obtained from Carl Roth (Karlsruhe, Germany). D-Glucose and arachidonic acid (ARA) were purchased from Hartmann Analytics (Braunschweig, Germany). Oxylipins and deuterated oxylipins utilized as internal standards ($^2H_4$-6-keto-$PGF_{1α}$, $^2H_5$-RvD2, $^2H_5$-LxA_4, $^2H_5$-RvD1, $^2H_4$-TxB_2, $^2H_{11}$-5(*R,S*)-5-F_{2t}-IsoP, $^2H_4$-PGE_2, $^2H_4$-PGD_2, $^2H_4$-LTB_4, $^2H_4$-9,10-DiHOME, $^2H_{11}$-14,15-DiHETrE, $^2H_6$-20-HETE, $^2H_4$-9-HODE, $^2H_8$-12-HETE, $^2H_8$-5-HETE, $^2H_{11}$-14(15)-EpETrE, $^2H_4$-9(10)-EpOME), PGB_1, purified human recombinant COX-2, MK886 as well as t-AUCB (≥ 90%) were obtained from Cayman Chemical (Biomol, Hamburg, Germany). Resveratrol (≥ 99%), genistein (≥ 98%) and 2-[[(2-hydroxyphenyl)methylene] amino]-phenol (IRA; CAS: 1761-56-4) [27] were purchased from Sigma, and *ε*-viniferin (≥ 90%) was obtained from

Actichem (Montauban, France). Bovine serum albumin (BSA), glutathione, saccharose, Nonident P-40, sodium orthovanadate and sodium fluoride were obtained from AppliChem (Darmstadt, Germany); L-glutamine from BioChem GmbH (Karlsruhe, Germany). Dulbecco's modified Eagle's high glucose medium with glutamine, geneticin, nitrocellulose membranes, penicillin/streptomycin-solution and trypsin-EDTA were delivered by GE Healthcare Life Science (Freiburg, Germany). Hygromycin B and Histopague-1077 were from Merck (Darmstadt, Germany). ATP was from Roche (Mannheim, Germany) and zileuton from Sequoia Research Products (Oxford, UK). Dulbecco's Buffer Substance (PBS) and Tetramethylethylenediamine (TEMED) were purchased from VWR (Darmstadt, Germany). Ethyl acetate (Chromasolv HPLC grade), glycerol (98%), calcium chloride, hydrochloric acid, triton-x 100 and β-glycerolphosphat disodium salt hydrate, Ca^{2+}-ionophore A23187, butylated hydroxytoluene (BHT, ≥ 99%), dextrane, fetal calf serum (FCS), non-essential amino acids, phenylmethanesulfonyl fluoride, soybean trypsin inhibitor, lysozyme, leupeptin, as well as all other chemicals were obtained from Sigma-Aldrich (Taufkirchen, Germany).

3.2.2 Cell Isolation and Cells

The ethical review committee of the University Hospital Jena, Germany approved experiments with human blood cells. Peripheral human blood from healthy fasted donors was obtained as leukocyte concentrate (buffy coats) from the University Hospital in Jena, Germany. Neutrophils and monocytes were isolated as described [28]. Briefly, leukocyte concentrates (buffy coats) were subjected to dextran sedimentation and centrifuged on lymphocyte separation medium. Peripheral blood mononuclear cells (PBMCs) were washed in PBS (pH 7.4), monocytes were separated through adherence to culture flasks, and finally resuspended in PBS (pH 7.4). Contaminating erythrocytes were removed via hypotonic lysis. Neutrophils were washed twice with ice-cold PBS and resuspended in PBS (pH 7.4; purity > 96-97%). HEK293-cells were cultured as monolayer at 37 °C and 5% CO_2 in DMEM supplemented with 10% heat-inactivated FCS, 100 U/mL penicillin and 100 U/mL streptomycin. HEK293-cells stably expressing 5-LOX±FLAP were selected using geneticin 400 µg/mL ± 200 µg/mL hygromycin B, respectively, as described [29].

3.2.3 Human 5-LOX Expression, Purification and Enzyme Activity Assays

Eschericha coli (BL21) was transformed with pT3-5-LOX plasmid and cells were cultured at 37 °C. 5-LOX expression was induced by isopropyl-β-D-1-thiogalactopyranoside (IPTG) at 30 °C overnight, and recombinant 5-LOX was purified by ATP-agarose as described [30]. Isolated 5-LOX was resuspended in PBS-EDTA (PBS; pH 7.4; 1 mM EDTA) and adjusted to a 5-LOX activity with 1000 ng/mL of 5-LOX products. Samples were preincubated with the test compounds or vehicle control (0.1% DMSO) for 15 min on ice and subsequently stimulated with 20 µM ARA and 2 mM $CaCl_2$ for 10 min at 37 °C. The reaction was stopped by adding 1 mL MeOH and samples were transferred on ice. Upon addition of 530 µL of acidified PBS and 200 ng PGB_1 as internal standard, 5-LOX metabolites were purified by solid phase extraction on C18 columns (100 mg; United Chemical Technologies, Bristol, PA, USA) and 5-LOX products (LTB_4, all-*trans* isomers of LTB_4 and 5-H(p)ETE) were analyzed by reversed-phase LC-UV using Nova-Pak C18 Radial-PAK column (60 Å, 5 × 100 mm, 4 µm) (Waters, Eschborn, Germany) [31].

3.2.4 Determination of 5-Lipoxygenase Product Formation in Intact Cells

In order to determine 5-LOX product formation in intact cells, freshly isolated human neutrophils (5×10^6) or HEK_5-LOX and HEK_5-LOX/FLAP cells (1×10^6) were resuspended in 1 mL PGC-buffer (PBS, pH 7.4; 0.1% Glucose; 1 mM $CaCl_2$) and preincubated with the indicated test compounds, zileuton (5 µM), MK886 (0.3 µM) or vehicle control (0.1% DMSO) for 15 min at 37 °C. Neutrophils and HEK cells were stimulated with Ca^{2+}-ionophore (2.5 µM) or

Ca^{2+}-ionophore (2.5 µM) and ARA (3 µM), respectively, for 10 min at 37 °C. The reaction was stopped with 1 mL ice-cold methanol and the samples were analyzed by HPLC as described above.

3.2.5 Direct COX-2 Inhibition by the Test Compounds

Direct COX-2 inhibition was determined as described [32], utilizing purified human recombinant COX-2. The cell-free COX-2 assay was conducted in a 96-well plate. The test compound was dissolved in DMSO (final DMSO concentration 0.8%) and added to 100 mM TRIS buffer (pH 8) containing 50 ng COX-2 protein/mL (0.5 U/mL), 1 µM hematin and 2 mM L-epinephrin. After 10 min preincubation at 37 °C the reaction was started by the addition of 5 µM ARA. After 10 min HCl (2 N) was added to terminate the enzyme reaction. PGE_2 product formation was determined by means of LC-MS.

3.2.6 LC-MS-based Oxylipin Quantification

For targeted metabolomics analysis, human neutrophils (5×10^6 cells) derived from three healthy human subjects were incubated as described above. Cells were pelleted by centrifugation (900 × *g*, 10 min at 4 °C) and washed with 500 µL ice cold PBS (centrifugation at 10.000 × *g* for 5 min at 4 °C). Both supernatants were collected and pooled. For analysis of the total oxylipin profile, 500 µL of methanol was added to a 500 µL aliquot of the combined supernatants. The total oxylipin profile was analyzed according to Rund et al. and Kutzner et al. with slight modifications [33, 34]. Briefly, upon addition of 1 pmol internal standards and antioxidant solution (2 µg BHT, 2 µg EDTA, 1 nmol t-AUCB, 1 nmol indomethacin) samples were centrifuged (20.000 × *g*, 10 min, 4 °C) and the supernatant was diluted to 3 mL with 0.1 M disodium hydrogen phosphate buffer (pH 6.0). Extraction was carried out on a non-polar (C8) / strong anion exchange mixed mode material (Bond Elut Certify II, 200 mg, Agilent Waldbronn, Germany), and elution of analytes was carried out with ethyl acetate/*n*-hexane (75:25 *v:v*) containing 1% acetic acid.

After reconstitution in 50 µL of methanol, oxylipins were quantified by liquid chromatography-tandem mass spectrometry (LC-MS) in negative electrospray ionization mode utilizing a QqQ mass spectrometer (QTrap6500, Sciex, Darmstadt, Germany). Oxylipin formation induced by A23187 was quantified by subtracting the concentration in unstimulated incubations from the stimulated ones for each of the polyphenols and the control incubations for each human subject. Relative changes in oxylipin formation induced by the test compounds were calculated for each human subject, using the mean of DMSO controls (n=3) as reference. Only those analytes were included which were found in samples of all human subjects and were ≥ 2x LLOQ in the stimulated control. If an analyte was < 2 × LLOQ in the stimulated control but showed an increase which was ≥ 2 x LLOQ in at least one of the incubations, relative changes were also calculated. If more than 50% of the stimulated controls did not exceed the LLOQ, the mean concentration was set to half of LLOQ. If the oxylipin concentration of was < LLOQ in a sample, it was set to half of LLOQ for calculation.

3.2.7 Lactate Dehydrogenase (LDH) Assay

The effect of the selected polyphenols on cell membrane integrity was determined by LDH release assay. Neutrophils (5×10^6) were incubated with 10 µM of the test compounds, DMSO as vehicle control and 0.2% Triton X-100 as full lysis control for 30 minutes. LDH release from disintegrated cells was measured by CytoxTox96 KIT (PROMEGA, Madison, WI, USA) according to the manufacturer’s instructions. The values are presented as percentage of the full lysis control.

3.2.8 SDS-Page and Western Blot Analysis

Cell lysates were prepared from 20 × 10^6 human neutrophils from three different human male surrogates by treatment with Saemann lysis buffer (TBS pH 7.4; NP-40 1%; Na_3VO_4 1 mM; NaF 10 mM; $Na_4P_2O_7$ 5 mM; β- glycerolphosphate 25 mM; EDTA 5 mM; leupeptin 1 mg/mL; STI 6 mg/mL; PMSF 100 mM). Protein separation was performed on 10% and 16% polyacrylamide gels. Proteins were blotted on nitrocellulose membranes and incubated with primary antibodies against 5-LOX (rabbit anti-5-LOX, 1:1000, supplied by O. Rådmark, Karolinska Institutet, Stockholm, Sweden), COX-1-enzyme (rabbit anti-COX-1, 1:1000, Cell Signaling Technology, Danvers, MA, USA), 15-LOX-1 (mouse anti-15-LOX-1, monoclonal antibody 1:800, Abcam, Cambridge, MA, USA), 12-LOX (mouse anti-12-LOX, 1:200, Santa Cruz Biotechnology Inc., Dallas, USA) and FLAP (rabbit anti-FLAP polyclonal antibody, 1:1000, Abcam, Cambridge, MA, USA). Protein expression was normalized to β-Actin (rabbit anti-β-Actin 1:1000 and mouse anti-β-Actin 1:1000, monoclonal antibodies, Cell Signaling Technology, Danvers, MA, USA). Detection was subsequently performed using IRDye 800CW labeled anti-mouse and/or anti-rabbit secondary antibodies (IRD Dye 800 CW goat anti-mouse 1:10000, IRD Dye 680 LT goat anti-mouse 1:40000, IRD dye 800 CW goat anti-rabbit 1:15000, IRD dye 680 LT goat-anti rabbit 1:80000, LI-COR Bioscience, Lincoln, NE, USA). Immunoreactive bands were visualized applying Odyssey infrared imager (LI-COR Bioscience, Lincoln, NE, USA).

3.2.9 Statistic

For the inhibition curves results were calculated as mean ± standard error of the mean from n independent experiments, where n represents the number of performed experiments on different days or from different donors. The IC_{50} values were calculated from five different concentrations visualized in semi-logarithmic graphs applying GraphPad Prism (GraphPad Software Inc., San Diego, CA, USA). Statistical analyses were conducted by one-way ANOVA followed by a Tukey post-hoc test applying GraphPad InStat (GraphPad Software Inc., San Diego, CA, USA). P-values < 0.05 were considered significant.

3.3 Results

3.3.1 Effect of Polyphenols on 5-LOX Activity in Neutrophils

Food-derived polyphenols are commonly known for their anti-inflammatory properties and a correlation between the intake of the corresponding plant-products and beneficial health effects was shown before [6]. LTB_4, formed via the 5-LOX pathway, is one of the prominent chemoattractant lipid mediators during inflammation. Here, we tested a small library of polyphenols including 6 flavonoids (apigenin, EGCG, genistein, naringenin, nobiletin, wogonin), resveratrol and its dimer (*ε*-viniferin), tetramer (hopeaphenol), and imine analogue (IRA) (**Fig. 3.1**) on their potency to inhibit the 5-LOX activity in neutrophils. The polyphenols were not cytotoxic at the tested concentrations as determined by the LDH assay (**Fig. 7.8**).

Genistein, resveratrol and its imine analogue IRA displayed the highest inhibitory potency and suppressed the 5-LOX product formation to ~ 50% at a concentration of 1 µM (**Fig. 3.2**). Additionally, the resveratrol-dimer *ε*-viniferin had a vast effect on 5-LOX activity at a concentration of 10 µM, as it completely abolished the LT formation in neutrophils (**Fig. 7.9**). In contrast, most of the flavonoids and the resveratrol-tetramer (hopeaphenol) did not reduce the 5-LOX product formation. Based on these findings, genistein, resveratrol, IRA, and *ε*-viniferin were selected for further investigations.

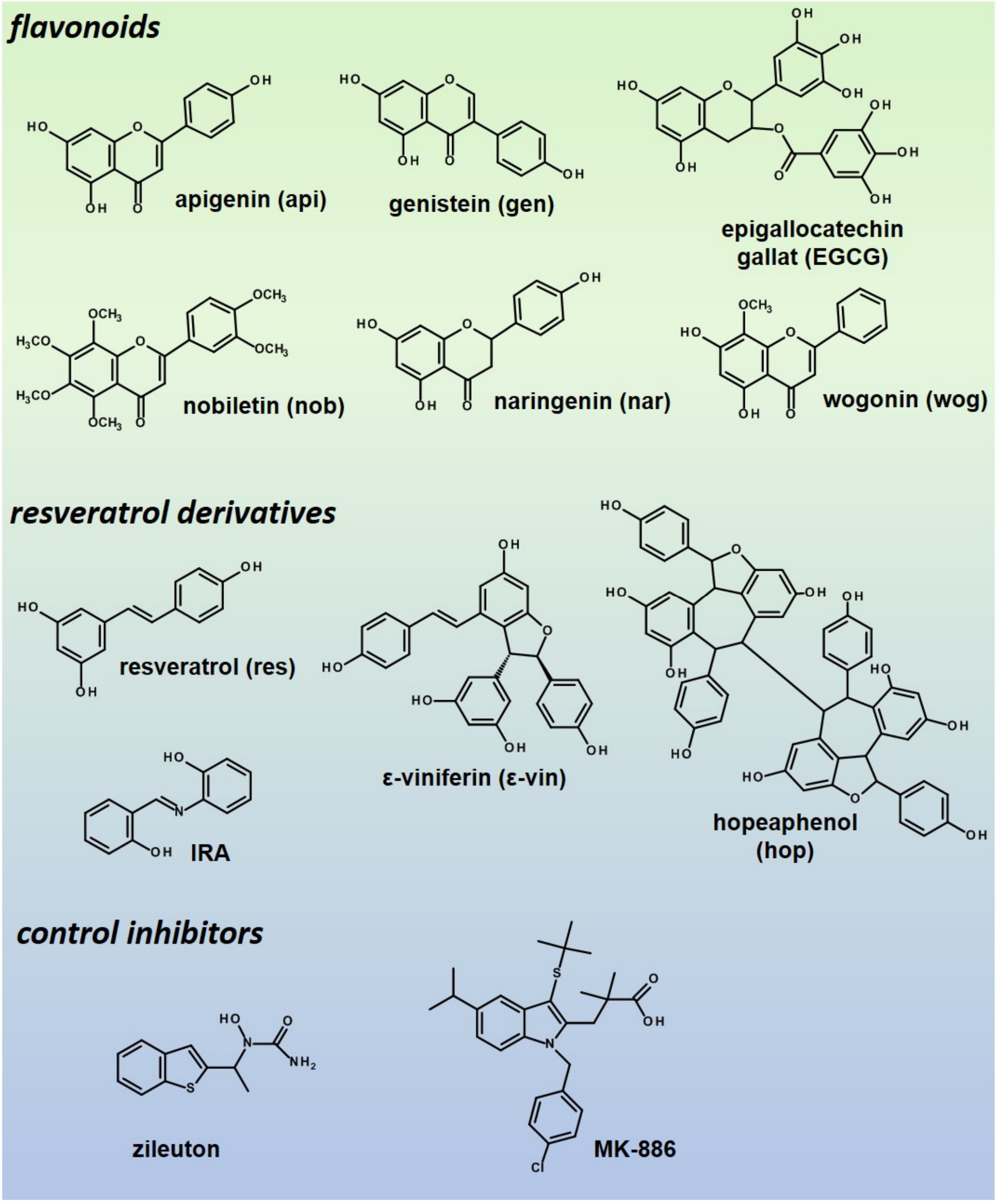

Fig. 3.1: Library of explored polyphenolic compounds. **(A)** Chemical structures of investigated plant-derived flavonoids and **(B)** resveratrol derivatives as well as structures of the control inhibitors zileuton and MK886.

First, we aimed to distinguish whether the inhibitory effects on the LT formation are mediated through direct 5-LOX inhibition or via superordinate cellular targets. Therefore, we tested the effect of the selected polyphenols towards 5-LOX activity on either recombinant isolated 5-LOX enzyme or in human neutrophils in a concentration-dependent manner.

IRA, resveratrol and ε-viniferin induced a robust decline in 5-LOX activity on the recombinant 5-LOX enzyme, with ε-viniferin being the strongest inhibitor with an IC_{50} value of 0.8 ± 0.3 µM (**Tab. 3.1**).

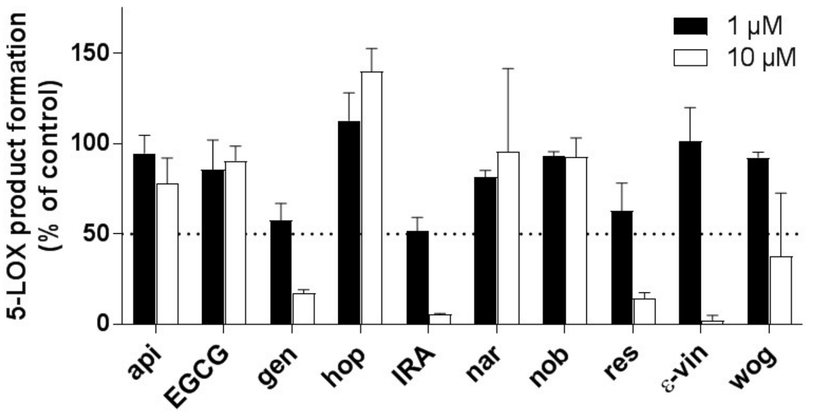

Fig. 3.2: Polyphenols differ in their inhibitory potency towards 5-LOX activity in a cell-based assay. Inhibition of 5-LOX product formation by the indicated polyphenolic compounds at concentrations of 1 µM and 10 µM in A23187-challenged human neutrophils (5 × 10^6). Data are expressed as percentage of vehicle control (DMSO; 0.1%), mean ± SEM; n = 3.

These data support a direct inhibition of 5-LOX by resveratrol, its dimer and its imine analogue, which is in line with previous studies for resveratrol [25]. In neutrophils, resveratrol and its imine-analogue IRA inhibited 5-LOX activity 2-3-fold more potently compared to the isolated 5-LOX enzyme with IC_{50} values of 4.3 ± 1.7 µM and 1.8 ± 0.6 µM, respectively (**Tab. 3.1**). In contrast, the flavonoid genistein failed to inhibit 5-LOX product formation in the cell-free assay even at high concentrations, but strongly reduced the 5-LOX activity in intact neutrophils with an IC_{50} of 0.4 ± 0.1 µM (**Fig. 3.3 A, Tab. 3.1**) suggesting a global cellular interference rather than a direct 5-LOX inhibition.

Tab. 3.1: Inhibition of 5-LOX product formation by selected polyphenols. IC_{50} values of the indicated compounds were determined on isolated recombinant 5-LOX or intact human neutrophils. Data are expressed as means ± SEM (µM); n = 3 – 7.

	5-LOX activity IC50 ± SEM [µM]	
	Recombinant 5-LOX	**Intact neutrophils**
Genistein	> 10	0.4 ± 0.1
IRA	3.8 ± 1.6	1.8 ± 0.6
Resveratrol	7.3 ± 2.2	4.3 ± 1.7
ε-Viniferin	0.8 ± 0.3	3.1 ± 1.4

Consequently, we tested an interplay of genistein with the 5-LOX-activating protein (FLAP), which is essential for cellular LT formation. The effect of the flavonoid towards 5-LOX product formation was investigated in HEK 293 cells stably expressing 5-LOX with and without FLAP [29]. Genistein had only marginal inhibitory potency on both cell lines and 5-LOX product formation was slightly reduced at 10 µM in HEK_5-LOX and HEK_5-LOX/FLAP (**Fig. 3.3 B**). Consequently, genistein can be excluded as 5-LOX and FLAP-inhibitor.

3.3.2 Total Oxylipin Profile

In order to investigate whether the 5-LOX pathway-interfering polyphenols and IRA influence the formation of other LMs that derive from the COX, CYP or other LOX branches of the ARA cascade, we analyzed the impact of IRA, resveratrol, *ε*-viniferin and genistein on the total oxylipin profile in neutrophils by targeted oxylipin metabolomics.

Neutrophils were incubated with the test polyphenols at two concentrations (1 and 10 µM) and the direct 5-LOX inhibitor zileuton (5 µM) and the FLAP inhibitor MK886 (0.3 µM) were used as controls. In total, 192 oxylipins were targeted by the metabolomics approach. Among them, 50 could be detected and relative changes could be calculated for 29 oxylipins (see **Experimental Section**).

Besides 5-LOX products, metabolites formed via the 12- and 15-LOX, COX as well as CYP pathways and autoxidation products were quantified in the A23187 challenged human neutrophils. In line with the 5-LOX activity pretests, inhibition of the 5-LOX pathway was observed (**Tab. 3.2**). At a concentration of 10 µM, all four polyphenols potently reduced the 5-LOX product formation. Here again, *ε*-viniferin showed the strongest inhibition, which was comparable to MK886 (0.3 µM) leading to a nearly complete reduction of all 5-LOX products (e.g. 5-HETE, LTB_4, 6-*trans*-LTB_4 and 12-*epi*-6-*trans*-LTB_4). IRA, the imine analogue of resveratrol, was the second most potent test compound and showed the same trend, resulting in a remaining activity of these products of 6 –36% of control. Compared to ε-viniferin and IRA, resveratrol was less potent and reduced the formation of 5-HETE and LTB_4 to 26 and 45% of control, respectively. Among the four tested polyphenols, genistein had only moderate inhibitory potential against 5-LOX as LTB_4 formation was only reduced to 56% of the control in 10 µM incubations. Inhibition of 5-LOX enzyme was supported by reduced levels of all downstream metabolites of 5-H(p)ETE and LTB_4, i.e. 5-oxo-ETE, 20-OH-LTB_4 and 20-COOH-LTB_4. The same reduction was found for the formation of 5-LOX products of EPA (C20:5n3), i.e. 5-HEPE, as well as mead acid (C20:3 n9), i.e. 5-HETrE.

12-LOX activity in neutrophil incubations can be associated to impurities of platelets, which highly express 12-LOX, or to eosinophil-derived 12/15-LOX activity. However, IRA, resveratrol, and ε-viniferin hardly affected the formation of 12-LOX products (12-HETE, 12-HEPE and 14-HDHA). Only genistein showed moderate effects as it reduced the 12-HETE formation at 10 µM to 40%. Inhibition of the 5-LOX pathway resulted in a two- to threefold elevation of 15-LOX products (15-HETE and 15-HEPE). Pretreatment of neutrophils with MK886 (0.3 µM), zileuton (5 µM), ε-viniferin, and IRA shifted the substrate to the 15-LOX pathway. Interestingly, resveratrol seemed to have an additional effect on 15-LOX as the formation of 15-HETE and 15-HEPE was reduced to 86 and 77% in 10 µM incubations. Genistein on the other hand, reduced the 15-LOX activity quite prominently to roughly 30%, which suggests a global effect on all LOXs. Oxylipins formed via cross talk-activity from 5- and 15-LOX were downregulated by all test compounds (**Tab. 3.2**).

Tab. 3.2 (right, page 61): Results from LC-MS-based targeted metabolomics analysis are shown in % of control (mean ± SD). Oxylipin formation induced by A23187 was quantified by subtracting the concentration in unstimulated incubations from the stimulated ones for each of the polyphenols and controls, where neutrophils were incubated with DMSO. Relative changes in oxylipin formation mediated by the test compounds were calculated for each human subject, using the mean of controls (n = 3) as reference.

formation pathway	concentration [µM]	genistein 0.1	genistein 10	IRA 0.1	IRA 10	resveratrol 0.1	resveratrol 10	ε-viniferin 0.1+	ε-viniferin 10	5-LOX pathway inhibitors: MK886 0.3	5-LOX pathway inhibitors: zileuton 5.0
5-LOX	5-HETE	83 ± 5	34 ± 18	83 ± 34	12 ± 9	78 ± 4	26 ± 19	95 ± 6	2 ± 2	1 ± 0	31 ± 16
	LTB_4	95 ± 4	56 ± 37	92 ± 18	36 ± 24	94 ± 1	45 ± 38	90 ± 8	2 ± 2	0 ± 0	46 ± 27
	6-*trans*-LTB_4	89 ± 7	35 ± 25	86 ± 29	8 ± 6	89 ± 4	25 ± 20	95 ± 9	1 ± 1	0 ± 0	23 ± 14
	12-epi-6-*trans*-LTB_4[1]	90 ± 7	32 ± 24	86 ± 32	6 ± 5	89 ± 3	22 ± 19	94 ± 6	1 ± 1	0 ± 0	19 ± 13
	5-oxo-ETE	82 ± 12	40 ± 31	83 ± 38	31 ± 20	85 ± 23	30 ± 28	91 ± 9	1 ± 1 *	1 ± 1 *	38 ± 27
	20-OH-LTB_4	99 ± 1	79 ± 29	101 ± 12	26 ± 15	98 ± 4	57 ± 38	102 ± 5	6 ± 3	0 ± 0	68 ± 22
	20-COOH-LTB_4	96 ± 6	84 ± 21	104 ± 13	22 ± 8	79 ± 9	67 ± 31	96 ± 6	11 ± 7	2 ± 1	88 ± 30
	5-HEPE	84 ± 2	27 ± 18	87 ± 38	12 ± 8	79 ± 0	23 ± 17	99 ± 11	1 ± 2 *	1 ± 0 *	33 ± 19
	LTB_5	99 ± 6	62 ± 37	97 ± 18	38 ± 24	89 ± 7	47 ± 41	86 ± 16	3 ± 2	0 ± 0 *	55 ± 32
	5(S)-HETrE	78 ± 4	28 ± 14	79 ± 32	9 ± 7 *	70 ± 3	20 ± 16	92 ± 3	1 ± 0 *	1 ± 0 *	20 ± 12
12-LOX	12-HETE	90 ± 5	40 ± 23	97 ± 31	63 ± 12	85 ± 4	70 ± 35	107 ± 5	85 ± 46	117 ± 28	124 ± 23
	12-HEPE	91 ± 5	42 ± 25	100 ± 29	62 ± 13	88 ± 5	70 ± 39	110 ± 15	79 ± 38	120 ± 30	122 ± 21
	14-HDHA	92 ± 8	51 ± 24	99 ± 28	17 ± 5 *	77 ± 16	33 ± 14 *	95 ± 3	28 ± 16 *	36 ± 12 *	40 ± 26 *
15-LOX	15-HETE	76 ± 14	28 ± 11	96 ± 47	139 ± 20	77 ± 6	86 ± 23	109 ± 20	259 ± 134	349 ± 93	296 ± 48
	15-HEPE	78 ± 18	27 ± 8 *	94 ± 57 *	95 ± 4	76 ± 5	77 ± 37 *	98 ± 10	218 ± 142	263 ± 106	231 ± 38
	13-HODE[2]	76 ± 20	18 ± 12	66 ± 41	34 ± 3	63 ± 12	23 ± 21	79 ± 18	17 ± 18 *	20 ± 22 *	14 ± 20 *
	15(S)-HETrE	86 ± 10	34 ± 13	86 ± 37	27 ± 7	75 ± 8	29 ± 14	95 ± 3	27 ± 23 *	49 ± 9	64 ± 18
5,15-LOX	5,15-DiHETE	95 ± 1	36 ± 24	90 ± 25	9 ± 6	88 ± 2	25 ± 20	98 ± 3	2 ± 2	2 ± 1	33 ± 18
	LxA_4	99 ± 7	38 ± 19	84 ± 19	6 ± 5	80 ± 8	20 ± 20	92 ± 1	1 ± 1 *	1 ± 1 *	18 ± 12
	6(S)-LxA_4	101 ± 3	41 ± 22	88 ± 17	12 ± 6 *	84 ± 14	25 ± 25 *	84 ± 0	10 ± 7 *	10 ± 7 *	22 ± 20 *
	RvD5	93 ± 3	33 ± 17 *	73 ± 21	24 ± 2 *	81 ± 3	24 ± 2 *	92 ± 3	24 ± 2 *	24 ± 2 *	24 ± 2 *
COX	PGD_2	92 ± 14 *	82 ± 32 *	91 ± 15 *	312 ± 159	91 ± 16 *	71 ± 50 *	96 ± 6 *	537 ± 376	319 ± 157	374 ± 178
	PGE_2	86 ± 7	43 ± 3	100 ± 25	191 ± 24	82 ± 3	21 ± 15	112 ± 4	414 ± 217	227 ± 73	227 ± 60
	TxB_2	80 ± 11	44 ± 6	103 ± 31	204 ± 75	76 ± 4	21 ± 15	84 ± 0	79 ± 45	226 ± 98	203 ± 67
	12-HHTrE	89 ± 6	40 ± 3	102 ± 20	183 ± 28	89 ± 2	18 ± 10	101 ± 6	71 ± 35	205 ± 72	186 ± 49
CYP	20-HETE	68 ± 16	51 ± 11	102 ± 25	548 ± 55	77 ± 6	169 ± 30	116 ± 26	623 ± 260	1898 ± 829	519 ± 92
	20-HEPE	76 ± 42 *	76 ± 42 *	76 ± 42 *	245 ± 127 *	76 ± 42 *	106 ± 10 *	111 ± 15 *	323 ± 194 *	848 ± 407	267 ± 147 *
misc	8-HETE	84 ± 7	40 ± 21	88 ± 33	25 ± 5	77 ± 8	34 ± 17	104 ± 8	24 ± 15	33 ± 16	51 ± 7
	11-HETE	79 ± 8	28 ± 11	85 ± 31	63 ± 12	71 ± 4	26 ± 14	104 ± 12	50 ± 28	91 ± 17	93 ± 7

[1]: 12-*epi*-6-*trans*-LTB_4 concentration was determined via 6-*trans*-LTB_4
[2]: background signal was subtracted in all incubations
+: calculated from n=2 in 0.1 µM ε-viniferin incubation
*: analyte < LLOQ in at least one of the samples

< 25%	25 - 50	50 - 75	75 - 100	100 - 125	125 - 150	150 - 175	≥ 175

According to 5-LOX inhibition, the formation of 5,15-DiHETE, LxA_4, 6(*S*)-LxA_4 and RvD5 was strongly suppressed by MK886, zileuton and all resveratrol derivatives at 10 µM to a range of 1 – 33% of vehicle control. In contrast, genistein showed the lowest inhibitory potency, consistent with its reduction of 5-LOX metabolites.

Regarding the COX-derived metabolites, different effects were found for the test compounds. While resveratrol potently inhibited PGD_2, PGE_2, TxB_2 and 12-HHT formation at 10 µM, incubation with its imine analogue IRA (10 µM) lead to an approximately two- to fourfold elevation of their formation, which was comparable to the effects evoked by the 5-LOX pathway inhibitors zileuton and MK886. Interestingly, treatment with *ε*-viniferin increased the formation of PGD_2 and PGE_2 in A23187 challenged neutrophils even more potently than IRA, MK886 and zileuton, while the formation of TxB_2 and 12-HHT seemed to be less affected and rather slightly reduced. Again, genistein inhibited the formation of all COX products less specifically.

Cytochrome P450 monooxygenases (CYP) can metabolize PUFAs on the ω-end of the fatty acid to hydroxy-fatty acids (hydroxyeicosatetraenoic acid – HETE; hydroxyeicosapenatenoic acid - HEPE) [35]. Increased formation of 20-HETE and 20-HEPE was detected in incubations with 5-LOX pathway inhibitors (MK886, zileuton) and resveratrol derivatives. Incubations with MK886, zileuton, *ε*-viniferin and IRA (both 10 µM) showed an up to twenty-fold increase of 20-HETE formation and an up to 8.5-fold elevation of 20-HEPE compared to vehicle control. Thus, an inhibition of the 5-LOX pathway effectively promotes the biosynthesis of CYP450-derived monohydroxylated fatty acids. Interestingly, in the incubations with resveratrol the formation of ω-hydroxylated metabolites of ARA and EPA was only moderately affected. As expected, genistein showed inhibiting effects on the formation of both mono-hydroxylated fatty acids (20-HETE / 20-HEPE), which probably cannot be related to a direct CYP450 inhibition (**Tab. 3.2**).

Monohydroxylation at carbon 8 of ARA leading to 8- and 11-HETE is attributed to either autoxidation [36] or CYP-metabolism [35]. Here, the tested polyphenols only moderately influenced the formation of 8-HETE as the reduction ranges from 24 to 40% at the higher test concentration. This effect was comparable to the control inhibitor zileuton and MK886 that reduced the 8-HETE formation to 50 and 30%, respectively. The impact of polyphenols on 11-HETE formation was even less potent.

Expression of ARA-metabolizing enzymes and FLAP in human neutrophils was demonstrated by immunoblotting. 5-LOX-enzyme, COX-1-enzyme and FLAP were clearly expressed throughout all donors, whereas 15-LOX-1 was detected only in two of three donors. Expression of 15-LOX in human neutrophils has been questioned and attributed to eosinophil contamination during preparation of the neutrophils [37]. Platelet 12-LOX could be confirmed by immunoblotting as well, which can be explained by the presence of thrombocytes in the neutrophil preparation (**Fig. 3.4**).

3.4 Discussion

Beneficial health effects of food polyphenols have been discussed and are believed to be mediated, at least partly, by anti-inflammatory effects [10]. Neutrophils are key cells in the innate immune response as they express and release cytokines, initiate ROS formation, and generate high amounts of chemotactic LTs to attract further phagocytic cells to clear the inflammation [38]. Especially the 5-LOX-mediated LT formation is one of the key events in inflammatory processes [39]. In order to investigate the effect of food polyphenols on the LT formation, a small library of 10 polyphenols (**Fig. 3.1**) was tested for their inhibitory potency against the 5-LOX pathway in human neutrophils. The food polyphenols that were investigated comprise a group of flavonoids (genistein, apigenin, epigallcocatechin gallate, nobiletin, naringenin, wogonin) and stilbenoids (resveratrol, IRA, *ε*-viniferin, hopeaphenol). Genistein, resveratrol, its dimer *ε*-viniferin as well as its imine analogue (IRA) showed potent inhibition of 5-LOX product formation in neutrophils with IC_{50} values ranging from 0.4 to 4.3 µM. These four polyphenols were chosen in order to determine the impact on LM formation generated in other branches of the ARA cascade by targeted oxylipin metabolomics.

Of all tested flavonoids, only genistein lead to a pronounced decrease of 5-LOX product formation in intact neutrophils (IC_{50} = 0.4 ± 0.1 µM). Interestingly, genistein had no effect on the purified 5-LOX enzyme, which consequently excludes a direct 5-LOX inhibition. FLAP inhibitors show the same behaviour as they only attenuate the LT formation in intact neutrophils and lose their potency in homogenates or when tested on isolated 5-LOX. However, FLAP inhibition by genistein can be excluded as the 5-LOX product formation in HEK_5-LOX and HEK_5LOX/FLAP cells was barely affected (**Fig. 3.3**), which in turn is in clear contrast to FLAP inhibitors [29]. Thus, we conclude that inhibition of LT formation in neutrophils by genistein is potentially rather attributed to global cellular interference than to modulation of the 5-LOX pathway. Consistently, Lepley et al. found only weak effect of genistein on recombinant 5-LOX (IC_{50} = 11.7 ± 2.1 µM) [40]. Interestingly, targeted oxylipin metabolomics demonstrated that genistein reduced the formation of other oxylipins from all branches of the ARA cascade to the same extent (**Tab. 3.2**). However, similar to 5-LOX, it was reported before that genistein failed to directly inhibit COX-1 and 2 [41]. Plenty of molecular functions are confirmed for genistein, including its antioxidative properties and especially its inhibitory potency against tyrosine kinases [42]. Together, genistein rather interferes with the ARA cascade on a superior level than directly inhibits LM-biosynthesizing enzymes.

In contrast to flavonoids, stilbene derivatives potently inhibited the 5-LOX product formation in calcium-ionophore stimulated human neutrophils (**Fig. 3.2, Tab. 3.1**), except for large resveratrol tetramer hopeaphenol, which was potentially prevented to enter the cells. Our data are in line with previous studies for resveratrol (IC_{50} = 1.4 – 8.9 µM) [25]. Results from the cell free assays confirmed a direct 5-LOX inhibition as resveratrol, IRA and ε-viniferin inhibited the isolated recombinant 5-LOX in a low mircomolar-range. As expected, downstream metabolites of the 5-LOX pathway such as 20-OH-LTB_4, 20-COOH-LTB_4 and 5-oxo-ETE as well as oxylipins formed via cross talk-activity of 5- and 15-LOX (e.g. 5,15-DiHETE) were reduced by resveratrol, IRA, and ε-viniferin in the same manner.

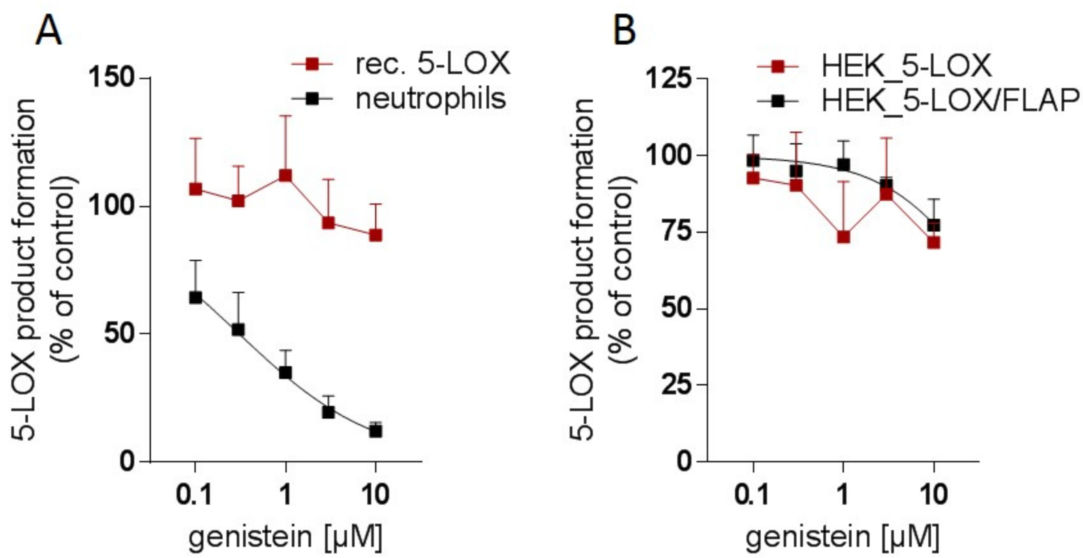

Fig. 3.3: Genistein's modulating effect towards 5-LOX-activity in intact neutrophils is not mediated via FLAP inhibition. **(A)** Inhibition of 5-LOX product formation on isolated, recombinant 5-LOX enzyme and in human neutrophils. **(B)** Modulation of 5-LOX activity in HEK293 cells expressing 5-LOX or 5-LOX and FLAP by genistein. Cells were pre-incubated with genistein (or 0.1% DMSO as vehicle) for 10 min at 37 °C with subsequent stimulation with 2.5 µM A23187 or 2.5 µM A23187 plus 3 µM ARA for 10 min at 37 °C in human neutrophils and HEK_5-LOX±FLAP, respectively. Recombinant 5-LOX enzyme was pre-treated with genistein for 10 min on ice and finally activated with 20 µM ARA and 2 mM $CaCl_2$. 5-LOX products were analyzed by HPLC. Data are shown as percentage of vehicle control, mean ± SEM; n = 3.

Comparable results were obtained by control inhibitors zileuton and MK886 as both efficiently block the 5-LOX pathway and thus the LT formation. Oxylipin profiles of neutrophils treated by zileuton and MK886 indicate a substrate shift, a so called shunt, to other branches of the ARA cascade, as metabolites generated by 15-LOX, COX, and CYP450 were differentially elevated (**Tab.**

3.2), a phenomenon that is frequently reported [43]. Zileuton directly inhibits 5-LOX by chelating the iron at the active site and is reported to have only little effect on other ARA cascade enzymes (e.g. 12-LOX) [44]. MK886, a FLAP inhibitor of the first generation binds FLAP within the nuclear membrane, inhibits the 5-LOX/FLAP protein complex assembly and thus potently blocks the cellular LT formation. While it also shows inhibitory potency against other members of the MAPEG (membrane associated proteins in eicosanoid and glutathione metabolism) family (e.g. LTC_4-synthase), MK886 does not interfere with LOXs, COXs and CYP450-enzymes [45, 46].

Note, while zileuton and MK886 evoke an obvious substrate shunt to other pathways of the ARA cascade, inhibition of the 5-LOX pathway by resveratrol, IRA, and *ε*-viniferin results in a distinct pattern of the oxylipin profile in A23187-challenged neutrophils. Firstly, resveratrol slightly decreased the formation of 15-LOX derived 15-HETE and 15-HEPE, which is in contrast to its imine analogue that hardly influenced the amounts of these metabolites, and to the resveratrol dimer *ε*-viniferin, which even induced the formation of 15-LOX derived metabolites to about 2 – 2.5-fold compared to the control. So far, studies regarding modulation of the 15-LOX pathway by polyphenols are scarce and unconvincing. Experiments were mainly carried out on soybean 15-LOX or rabbit reticulocytes lipoxygenase 15-LOX utilizing linoleic acid as substrate, where resveratrol was shown to inhibit the 15-LOX activity with IC_{50} values of 40 µM, and 32 µM, respectively [47, 48]. Nevertheless, knowledge about the impact of polyphenols on the human 15-LOX pathway is of superior interest as 15-LOX is part of the enzymatic machinery that biosynthesizes a vast proportion the pro-resolving LM (protectins, resolvins) [22]. It is therefore astonishing that resveratrol has an inhibitory effect on 15-LOX whereas *ε*-viniferin, which also presents itself as typical 5-LOX pathway inhibitor, lead to a substrate shunting and increased 15-HETE / 15-HEPE levels (**Tab. 3.2**).

Secondly, while resveratrol inhibited the formation of COX-derived PGD_2 and PGE_2 to 71 and 21%, respectively, *ε*-viniferin and IRA induced a dramatic increase in the biosynthesis of both metabolites. Resveratrol was shown before to directly inhibit COX-1 and 2 in enzyme assays with IC_{50} of 0.43 µM and 0.49 µM, and also to reduce the PGE_2 formation in human LPS-stimulated monocytes [41]. Therefore, it is surprising that the imine analogue and the resveratrol dimer obviously lose the ability to inhibit COX. Furthermore, ε-viniferin but not IRA, seems to have the potential to selectively block the thromboxane synthase (TXAS), a downstream enzyme in the COX-branch of the ARA-cascade and reduced the amounts of generated TXB_2 and 12-HHTrE. Consistently, we earlier reported that *ε*-viniferin inhibits COX-1 and 2 in cell-free assays with IC_{50} of 1.6 and 11 µM, respectively, but was incapable of inhibiting PGE_2 synthesis in LPS-stimulated human monocytes or human colon adenocarcinoma cells (HCA-7 cells) [41], suggesting a cellular inactivation of *ε*-viniferin towards COX-inhibition. Originally, among others, synthetic IRA was developed as resveratrol analogue with the aim of enhancing its radical scavenging properties and thus acting as a more potent antioxidant [27]. IRA was shown to enhance COX-2 expression in HCA-7 cells after 24 h incubation, but decreased PGE_2-levels were detected in the cell supernatants [26]. These results are not necessarily in contrast to our finding as PGE_2-concentrations were analyzed without prior stimulation and substrate release.

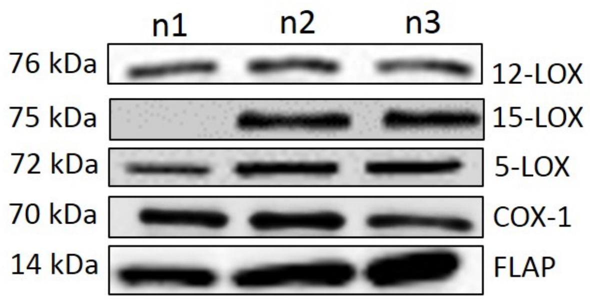

Fig. 3.4: Expression of ARA-metabolizing enzymes in human neutrophils. Expression of p12-LOX, 15-LOX-1, 5-LOX, COX-1 and FLAP was determined by Western blot analysis. Cell lysates were obtained from 5 × 10^6 human neutrophils derived from three independent, healthy donors.

Probably increased COX-2 expression levels also stimulate PGE_2 formation in activated cells. In immune cells the IRA strongly shunted the ARA cascade towards PG formation (**Tab. 3.2**) indicating no inhibitory effect on COX. Indeed, in a in a cell-free assay IRA did not block COX-2 activity (**Tab. 7.8**).

Regarding the CYP branch of the ARA cascade, IRA, *ε*-viniferin and the control inhibitors zileuton and MK886 shunt the ARA cascade towards formation of CYP derived terminal hydroxy-PUFAs (20-HETE and 20-HEPE). Resveratrol had only minor impact, indicating an inhibitory action on these enzymes as well, which highlights the distinct mode of action of different stilbene polyphenols.

It is not conclusively determined which of the > 50 CYP450 isoforms are expressed in neutrophils. However, it is known that CYP4F3A plays an important role as LTB_4-hydroxylase in these cells [49] by inactivating LTB_4 via terminal hydroxylation. Though LTB_4 is the most preferred substrate, CYP4F3A is also capable of converting arachidonic acid to 20-HETE [50, 51]. In our data, a strong decrease of LTB_4 especially after treatment with MK886 and *ε*-viniferin, IRA and zileuton, correlates with increased levels of 20-HETE and 20-HEPE. The lack of the preferred substrate LTB_4 therefore might result in an enhanced conversion of ARA and EPA to their ω-monohydroxylated metabolites.

Resveratrol and its derivatives had only minor effects on 12-LOX product formation (12-HETE and 12-HEPE). Furthermore, zileuton and MK886, the potent 5-LOX pathway inhibitors, did not influence the 12-LOX pathway at all. Interestingly, whereas a clear substrate shunt to other branches (15-LOX, COX, CYP450) was observed with zileuton or MK886, this was not the case for the 12-LOX. This may be explained by the fact that the platelet-type 12-LOX cannot benefit from the release of ARA within the leukocyte cells. Furthermore, formation of 8- and 11-HETE was inhibited by all test polyphenols nearly to the same extent with a slightly higher potency of resveratrol against 11-HETE formation. 11-HETE can be formed by CYP450 enzymes [35] but also by autoxidation [36]. Thus, potential enzyme inhibition and anti-oxidative actions of the test compounds by e.g. radical scavenging [52], seem to be likely. Previous reports already confirmed significant radical scavenging capacities for resveratrol and *ε*-viniferin [53].

The polyphenol concentration *in vivo* reached after food intake depends on many factors. Varying content in fruits and vegetables is influenced by e.g. environmental factors, storage, processing, ripeness etc. Furthermore, most compounds are present in plants as glycosides and need to be hydrolyzed by enzymes in the intestine and colon microbiota prior to absorption [9]. In intestine and liver, the aglycones are then rapidly conjugated by phase II metabolism yielding e.g. sulfated and glucuronidated products [54], which can be eliminated urinary or biliary. For instance, resveratrol is rapidly transformed and detected mainly as its glucuronide and sulfate conjugates within 1 h after oral administration in plasma and urine [55, 56]. Polyphenol plasma concentrations have been reported in the low µM range and can be elevated by a directed diet. For example, plasma levels of resveratrol (including glucuronated and sulfated resveratrol) increased from 0.71 to 1.7 µmol/L in a 15 d controlled daily consumption of red wine [57] and reached about 2 µmol/L upon administration of a radio-labeled resveratrol supplement (25 mg) [56]. Interestingly, the resveratrol oligomers are conjugated slower compared to resveratrol. While resveratrol is conjugated almost completely by human liver microsomes, ε-viniferin is glucuronidated only partly and hopeaphenol does not seem to be substrate for human glucuronosyltransferases [54]. One can assume that the other tested polyphenols undergo rapid phase II metabolism, as e.g. a large portion of genistein circulates in human blood as form of its sulfate and glucuronide [58]. It should be noted that the unconjugated polyphenol concentration in the gut tissue can reach higher levels compared to the blood concentration [59]. Moreover, polyphenol metabolism and thus plasma levels may also depend on individual diet, genetics and metabolism [59], and the concentration of polyphenols in human blood following a polyphenol rich diet could be in the range investigated in our study (low µM range). Despite biologic activity and relevant levels of biotransformation products, they were not part of this study and should be addressed in the future.

The analysis of the inhibition mechanism of polyphenols is of interest as inhibition of distinct branches of the ARA cascade modulates the balance of pro- and anti-inflammatory LMs. The modulation of this balance could be another layer in the complex molecular mechanisms by which polyphenols influence health and well-being. Genistein, IRA, resveratrol and ε-viniferin each seem to interfere with the cellular signaling pathways in neutrophils in a distinct fashion on multiple levels. When compared to 5-LOX pathway inhibitors (zileuton and MK-886), their inhibitory potential is not pronounced, as it is the case for genistein and resveratrol. Genistein seems to act on a "global level", affecting several branches of the ARA cascade. Resveratrol selectively inhibits enzymes of the ARA cascade (5-LOX, 15-LOX, COX), while strong 5-LOX inhibition by ε-viniferin and IRA appears to result in a prominent substrate shift accompanied by an enhanced product formation in certain pathways (15-LOX, COX, CYP). The results show that polyphenols and IRA have potent effects on the ARA cascade in our test system and targeted LC-MS based oxylipin metabolomics is indispensable for monitoring several pathways in parallel, allowing a comprehensive understanding of their implications and cross-talk between the different branches. Further investigations are needed to understand the individual mode of action of food polyphenols, particularly structure-activity relationships and their implications for the potential effects on human health.

3.5 References

1. Serhan CN and Savill J (2005) Resolution of inflammation: the beginning programs the end. *Nat Immunol,* 6(12), 1191-7; doi: 10.1038/ni1276.
2. Halade GV and Kain V (2017) Obesity and Cardiometabolic Defects in Heart Failure Pathology. *Compr Physiol,* 7(4), 1463-1477; doi: 10.1002/cphy.c170011.
3. Varghese M, Griffin C, and Singer K (2017) The Role of Sex and Sex Hormones in Regulating Obesity-Induced Inflammation. *Adv Exp Med Biol,* 1043, 65-86; doi: 10.1007/978-3-319-70178-3_5.
4. Rea IM, Gibson DS, McGilligan V, McNerlan SE, Alexander HD, and Ross OA (2018) Age and Age-Related Diseases: Role of Inflammation Triggers and Cytokines. *Front Immunol,* 9, 586; doi: 10.3389/fimmu.2018.00586.

5. Glade MJ (1999) Food, nutrition, and the prevention of cancer: a global perspective. American Institute for Cancer Research/World Cancer Research Fund, American Institute for Cancer Research, 1997. *Nutrition,* 15(6), 523-6.
6. Arts IC and Hollman PC (2005) Polyphenols and disease risk in epidemiologic studies. *Am J Clin Nutr,* 81(1 Suppl), 317S-325S; doi: 10.1093/ajcn/81.1.317S.
7. Law MR and Morris JK (1999) By how much does fruit and vegetable consumption reduce the risk of ischaemic heart disease: response to commentary. *Eur J Clin Nutr,* 53(11), 903-4; doi: 10.1038/sj.ejcn.1600944.
8. Crozier A, Jaganath IB, and Clifford MN (2009) Dietary phenolics: chemistry, bioavailability and effects on health. *Nat Prod Rep,* 26(8), 1001-43; doi: 10.1039/b802662a.
9. Manach C, Scalbert A, Morand C, Remesy C, and Jimenez L (2004) Polyphenols: food sources and bioavailability. *Am J Clin Nutr,* 79(5), 727-47; doi: 10.1093/ajcn/79.5.727.
10. Garcia-Lafuente A, Guillamon E, Villares A, Rostagno MA, and Martinez JA (2009) Flavonoids as anti-inflammatory agents: implications in cancer and cardiovascular disease. *Inflamm Res,* 58(9), 537-52; doi: 10.1007/s00011-009-0037-3.
11. Pervaiz S (2003) Resveratrol: from grapevines to mammalian biology. *FASEB J,* 17(14), 1975-85; doi: 10.1096/fj.03-0168rev.
12. Das S, Alagappan VK, Bagchi D, Sharma HS, Maulik N, and Das DK (2005) Coordinated induction of iNOS-VEGF-KDR-eNOS after resveratrol consumption: a potential mechanism for resveratrol preconditioning of the heart. *Vascul Pharmacol,* 42(5-6), 281-9; doi: 10.1016/j.vph.2005.02.013.
13. Imamura G, Bertelli AA, Bertelli A, Otani H, Maulik N, and Das DK (2002) Pharmacological preconditioning with resveratrol: an insight with iNOS knockout mice. *Am J Physiol Heart Circ Physiol,* 282(6), H1996-2003; doi: 10.1152/ajpheart.01013.2001.
14. Bollmann F, Art J, Henke J, Schrick K, Besche V, Bros M, Li H, Siuda D, Handler N, Bauer F, et al. (2014) Resveratrol post-transcriptionally regulates pro-inflammatory gene expression via regulation of KSRP RNA binding activity. *Nucleic Acids Res,* 42(20), 12555-69; doi: 10.1093/nar/gku1033.
15. Das S and Das DK (2007) Anti-inflammatory responses of resveratrol. *Inflamm Allergy Drug Targets,* 6(3), 168-73; doi: 10.2174/187152807781696464.
16. Jang M, Cai L, Udeani GO, Slowing KV, Thomas CF, Beecher CW, Fong HH, Farnsworth NR, Kinghorn AD, Mehta RG, et al. (1997) Cancer chemopreventive activity of resveratrol, a natural product derived from grapes. *Science,* 275(5297), 218-20; doi: 10.1126/science.275.5297.218.
17. Koeberle A and Werz O (2014) Multi-target approach for natural products in inflammation. *Drug Discov Today,* 19(12), 1871-82; doi: 10.1016/j.drudis.2014.08.006.
18. Haeggstrom JZ and Funk CD (2011) Lipoxygenase and leukotriene pathways: biochemistry, biology, and roles in disease. *Chem Rev,* 111(10), 5866-98; doi: 10.1021/cr200246d.
19. Serhan CN (2014) Pro-resolving lipid mediators are leads for resolution physiology. *Nature,* 510(7503), 92-101; doi: 10.1038/nature13479.
20. Koeberle A and Werz O (2015) Perspective of microsomal prostaglandin E2 synthase-1 as drug target in inflammation-related disorders. *Biochem Pharmacol,* 98(1), 1-15; doi: 10.1016/j.bcp.2015.06.022.
21. Morisseau C and Hammock BD (2013) Impact of soluble epoxide hydrolase and epoxyeicosanoids on human health. *Annu Rev Pharmacol Toxicol,* 53, 37-58; doi: 10.1146/annurev-pharmtox-011112-140244.

22. Serhan CN, Chiang N, Dalli J, and Levy BD (2014) Lipid mediators in the resolution of inflammation. *Cold Spring Harb Perspect Biol,* 7(2), a016311; doi: 10.1101/cshperspect.a016311.
23. Westphal C, Konkel A, and Schunck WH (2015) Cytochrome p450 enzymes in the bioactivation of polyunsaturated Fatty acids and their role in cardiovascular disease. *Adv Exp Med Biol,* 851, 151-87; doi: 10.1007/978-3-319-16009-2_6.
24. Hong J, Smith TJ, Ho CT, August DA, and Yang CS (2001) Effects of purified green and black tea polyphenols on cyclooxygenase- and lipoxygenase-dependent metabolism of arachidonic acid in human colon mucosa and colon tumor tissues. *Biochem Pharmacol,* 62(9), 1175-83; doi: 10.1016/S0006-2952(01)00767-5.
25. Kimura Y, Okuda H, and Kubo M (1995) Effects of stilbenes isolated from medicinal plants on arachidonate metabolism and degranulation in human polymorphonuclear leukocytes. *J Ethnopharmacol,* 45(2), 131-9; doi: 10.1016/0378-8741(94)01206-F.
26. Wang S, Willenberg I, Krohn M, Hecker T, Meckelmann S, Li C, Pan Y, Schebb NH, Steinberg P, and Empl MT (2017) Growth-Inhibiting Activity of Resveratrol Imine Analogs on Tumor Cells In Vitro. *PLoS One,* 12(1), e0170502; doi: 10.1371/journal.pone.0170502.
27. Lu J, Li C, Chai YF, Yang DY, and Sun CR (2012) The antioxidant effect of imine resveratrol analogues. *Bioorg Med Chem Lett,* 22(17), 5744-5747; doi: 10.1016/j.bmcl.2012.06.026.
28. Boyum A (1968) Isolation of mononuclear cells and granulocytes from human blood. Isolation of monuclear cells by one centrifugation, and of granulocytes by combining centrifugation and sedimentation at 1 g. *Scand J Clin Lab Invest Suppl,* 97, 77-89.
29. Gerstmeier J, Weinigel C, Barz D, Werz O, and Garscha U (2014) An experimental cell-based model for studying the cell biology and molecular pharmacology of 5-lipoxygenase-activating protein in leukotriene biosynthesis. *Biochim Biophys Acta,* 1840(9), 2961-9; doi: 10.1016/j.bbagen.2014.05.016.
30. Fischer L, Szellas D, Radmark O, Steinhilber D, and Werz O (2003) Phosphorylation- and stimulus-dependent inhibition of cellular 5-lipoxygenase activity by nonredox-type inhibitors. *FASEB J,* 17(8), 949-51; doi: 10.1096/fj.02-0815fje.
31. Steinhilber D, Herrmann T, and Roth HJ (1989) Separation of lipoxins and leukotrienes from human granulocytes by high-performance liquid chromatography with a Radial-Pak cartridge after extraction with an octadecyl reversed-phase column. *J Chromatogr,* 493(2), 361-6; doi: 10.1016/S0378-4347(00)82742-5.
32. Willenberg I, Meschede AK, and Schebb NH (2015) Determining cyclooxygenase-2 activity in three different test systems utilizing online-solid phase extraction-liquid chromatography-mass spectrometry for parallel quantification of prostaglandin E(2), D(2) and thromboxane B(2). *J Chromatogr A,* 1391, 40-8; doi: 10.1016/j.chroma.2015.02.059.
33. Kutzner L, Rund KM, Ostermann AI, Hartung NM, Galano JM, Balas L, Durand T, Balzer MS, David S, and Schebb NH (2019) Development of an Optimized LC-MS Method for the Detection of Specialized Pro-Resolving Mediators in Biological Samples. *Front Pharmacol,* 10, 169; doi: 10.3389/fphar.2019.00169.
34. Rund KM, Ostermann AI, Kutzner L, Galano J-M, Oger C, Vigor C, Wecklein S, Seiwert N, Durand T, and Schebb NH (2017) Development of an LC-ESI(-)-MS/MS method for the simultaneous quantification of 35 isoprostanes and isofurans derived from the major n3- and n6-PUFAs. *Anal Chim Acta*; doi: 10.1016/j.aca.2017.11.002.
35. Capdevila JH, Falck JR, and Harris RC (2000) Cytochrome P450 and arachidonic acid bioactivation. Molecular and functional properties of the arachidonate monooxygenase. *J Lipid Res,* 41(2), 163-81; doi: 10.1016/S0022-2275(20)32049-6.

36. Porter NA, Lehman LS, Weber BA, and Smith KJ (1981) Unified Mechanism for Poly-Unsaturated Fatty-Acid Autoxidation - Competition of Peroxy Radical Hydrogen-Atom Abstraction, Beta-Scission, and Cyclization. *J Am Chem Soc,* 103(21), 6447-6455; doi: 10.1021/Ja00411a032.
37. Morita E, Schroder JM, and Christophers E (1990) Production of 15-hydroxyeicosatetraenoic acid by purified human eosinophils and neutrophils. *Scand J Immunol,* 32(5), 497-502; doi: 10.1111/j.1365-3083.1990.tb03190.x.
38. Nauseef WM and Borregaard N (2014) Neutrophils at work. *Nat Immunol,* 15(7), 602-11; doi: 10.1038/ni.2921.
39. Radmark O, Werz O, Steinhilber D, and Samuelsson B (2007) 5-Lipoxygenase: regulation of expression and enzyme activity. *Trends Biochem Sci,* 32(7), 332-41; doi: 10.1016/j.tibs.2007.06.002.
40. Lepley RA, Muskardin DT, and Fitzpatrick FA (1996) Tyrosine kinase activity modulates catalysis and translocation of cellular 5-lipoxygenase. *J Biol Chem,* 271(11), 6179-6184; doi: 10.1074/jbc.271.11.6179.
41. Willenberg I, Meschede AK, Gueler F, Jang MS, Shushakova N, and Schebb NH (2015) Food Polyphenols Fail to Cause a Biologically Relevant Reduction of COX-2 Activity. *PLoS One,* 10(10), e0139147; doi: 10.1371/journal.pone.0139147.
42. Akiyama T, Ishida J, Nakagawa S, Ogawara H, Watanabe S, Itoh N, Shibuya M, and Fukami Y (1987) Genistein, a specific inhibitor of tyrosine-specific protein kinases. *J Biol Chem,* 262(12), 5592-5; doi: 10.1016/S0021-9258(18)45614-1.
43. He C, Wu Y, Lai Y, Cai Z, Liu Y, and Lai L (2012) Dynamic eicosanoid responses upon different inhibitor and combination treatments on the arachidonic acid metabolic network. *Mol Biosyst,* 8(5), 1585-94; doi: 10.1039/c2mb05503a.
44. Carter GW, Young PR, Albert DH, Bouska J, Dyer R, Bell RL, Summers JB, and Brooks DW (1991) 5-lipoxygenase inhibitory activity of zileuton. *J Pharmacol Exp Ther,* 256(3), 929-37.
45. Evans JF, Ferguson AD, Mosley RT, and Hutchinson JH (2008) What's all the FLAP about?: 5-lipoxygenase-activating protein inhibitors for inflammatory diseases. *Trends Pharmacol Sci,* 29(2), 72-8; doi: 10.1016/j.tips.2007.11.006.
46. Gerstmeier J, Weinigel C, Rummler S, Radmark O, Werz O, and Garscha U (2016) Time-resolved in situ assembly of the leukotriene-synthetic 5-lipoxygenase/5-lipoxygenase-activating protein complex in blood leukocytes. *FASEB J,* 30(1), 276-85; doi: 10.1096/fj.15-278010.
47. Schewe T, Sadik C, Klotz LO, Yoshimoto T, Kuhn H, and Sies H (2001) Polyphenols of cocoa: Inhibition of mammalian 15-lipoxygenase. *Biol Chem,* 382(12), 1687-1696; doi: 10.1515/Bc.2001.204.
48. Maccarrone M, Lorenzon T, Guerrieri P, and Agro AF (1999) Resveratrol prevents apoptosis in K562 cells by inhibiting lipoxygenase and cyclooxygenase activity. *Eur J Biochem,* 265(1), 27-34; doi: 10.1046/j.1432-1327.1999.00630.x.
49. Kikuta Y, Kusunose E, Endo K, Yamamoto S, Sogawa K, Fujiikuriyama Y, and Kusunose M (1993) A Novel Form of Cytochrome-P-450 Family-4 in Human Polymorphonuclear Leukocytes - Cdna Cloning and Expression of Leukotriene-B4 Omega-Hydroxylase. *J Biol Chem,* 268(13), 9376-9380; doi: 10.1016/S0021-9258(18)98360-2.
50. Christmas P, Jones JP, Patten CJ, Rock DA, Zheng YM, Cheng SM, Weber BM, Carlesso N, Scadden DT, Rettie AE, et al. (2001) Alternative splicing determines the function of CYP4F3 by switching substrate specificity. *J Biol Chem,* 276(41), 38166-38172; doi: 10.1074/jbc.M104818200.

51. Hatzelmann A and Ullrich V (1988) The omega-hydroxylation of arachidonic-acid by human polymorphonuclear leukocytes. *Eur J Biochem,* 173(2), 445-452; doi: 10.1111/j.1432-1033.1988.tb14019.x.

52. Mitjavila MT and Moreno JJ (2012) The effects of polyphenols on oxidative stress and the arachidonic acid cascade. Implications for the prevention/treatment of high prevalence diseases. *Biochem Pharmacol,* 84(9), 1113-22; doi: 10.1016/j.bcp.2012.07.017.

53. Biais B, Krisa S, Cluzet S, Da Costa G, Waffo-Teguo P, Merillon JM, and Richard T (2017) Antioxidant and Cytoprotective Activities of Grapevine Stilbenes. *J Agric Food Chem,* 65(24), 4952-4960; doi: 10.1021/acs.jafc.7b01254.

54. Willenberg I, Brauer W, Empl MT, and Schebb NH (2012) Development of a rapid LC-UV method for the investigation of chemical and metabolic stability of resveratrol oligomers. *J Agric Food Chem,* 60(32), 7844-50; doi: 10.1021/jf302136t.

55. Soleas GJ, Yan J, and Goldberg DM (2001) Ultrasensitive assay for three polyphenols (catechin, quercetin and resveratrol) and their conjugates in biological fluids utilizing gas chromatography with mass selective detection. *J Chromatogr B Biomed Sci Appl,* 757(1), 161-72; doi: 10.1016/S0378-4347(01)00142-6.

56. Walle T, Hsieh F, DeLegge MH, Oatis JE, Jr., and Walle UK (2004) High absorption but very low bioavailability of oral resveratrol in humans. *Drug Metab Dispos,* 32(12), 1377-82; doi: 10.1124/dmd.104.000885.

57. Gresele P, Pignatelli P, Guglielmini G, Carnevale R, Mezzasoma AM, Ghiselli A, Momi S, and Violi F (2008) Resveratrol, at concentrations attainable with moderate wine consumption, stimulates human platelet nitric oxide production. *J Nutr,* 138(9), 1602-8; doi: 10.1093/jn/138.9.1602.

58. Hosoda K, Furuta T, Yokokawa A, and Ishii K (2010) Identification and quantification of daidzein-7-glucuronide-4'-sulfate, genistein-7-glucuronide-4'-sulfate and genistein-4',7-diglucuronide as major metabolites in human plasma after administration of kinako. *Anal Bioanal Chem,* 397(4), 1563-72; doi: 10.1007/s00216-010-3714-8.

59. Williamson G (2017) The role of polyphenols in modern nutrition. *Nutr Bull,* 42(3), 226-235; doi: 10.1111/nbu.12278.

Chapter 4

Development of a Quantitative Multi-omics Approach for the Comprehensive Analysis of the Arachidonic Acid Cascade in Immune Cells

Oxylipins derived from the cyclooxygenase (COX) and lipoxygenase (LOX) pathways of the arachidonic acid (ARA) cascade are essential for the regulation of the inflammatory response and many other physiological functions. Comprehensive analytical methods comprised of oxylipin and protein abundance analysis are required to fully understand mechanisms leading to changes within these pathways. Here, we describe the development of a quantitative multi-omics approach combining liquid-chromatography tandem mass spectrometry based targeted oxylipin metabolomics and proteomics. As the first targeted proteomics method to cover these pathways, it enables the quantitative analysis of all human COX (COX-1 and -2) and relevant LOX pathway enzymes (5-, 12-, 15-LOX, 15-LOX-2 and FLAP) in parallel to the analysis of 198 oxylipins with the targeted oxylipin metabolomics method from a single sample. The detailed comparison between MRM³ and classical MRM based detection in proteomics showed increased selectivity for MRM³ while MRM performed better in terms of sensitivity (LLOQ: 16 – 122 pM vs. 75 – 840 pM for the same peptides), linear range (up to 1.5 – 7.4 µM vs. 4 – 368 nM) and multiplexing capacities. Thus, the MRM mode was more favorable for this pathway analysis. With this sensitive multi-omics approach we comprehensively characterize oxylipin and protein patterns in the human monocytic cell line THP-1 and differently polarized primary macrophages. Finally, the quantification of changes in protein and oxylipin levels induced by lipopolysaccharide stimulation and pharmaceutical treatment demonstrates its usefulness to study molecular modes of action involved in the modulation of the ARA cascade.

Hartung NM, Mainka M, Pfaff R, Kuhn M, Biernacki S, Zinnert L, Schebb NH (2022) *submitted for publication*

Author contributions: NMH designed research, performed experiments and wrote the manuscript; MM designed research and performed experiments, RP, MK, SB, LZ performed experiments; NHS designed research and wrote the manuscript.

4.1 Introduction

The cyclooxygenase (COX) and lipoxygenase (LOX) pathways of the arachidonic acid (ARA) cascade play important roles in inflammation (simplified overview in **Fig. 4.1**).

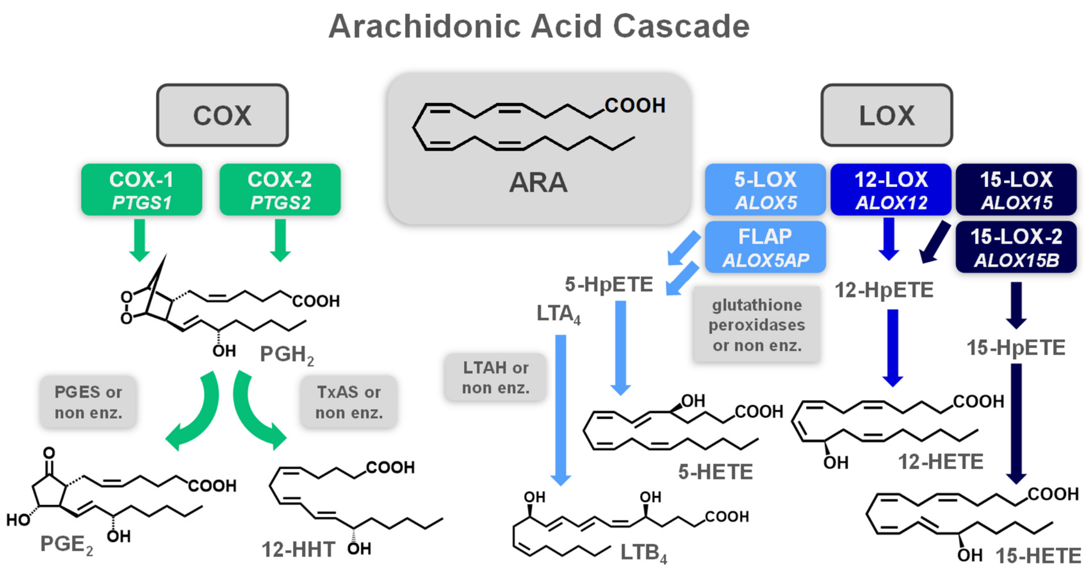

Fig. 4.1: Simplified overview of the cyclooxygenase (COX) and lipoxygenase (LOX) branches of the arachidonic acid (ARA) cascade. COX catalyze the formation of prostaglandin (PG) H_2 which is further converted by downstream enzymes or non-enzymatically, e.g., to PGE_2 by PGE synthases or to 12 hydroxy-heptadecatrienoic acid (12-HHT) by thromboxane A synthase (TxAS). The different LOX isoforms each oxidize ARA regiospecifically to hydroperoxy-eicoatetraenoic acids (HpETE) or leuktotriene A_4 (LTA_4) in case of 5-LOX supported by the 5-LOX activating protein (FLAP). The primary products are reduced to their respective hydroxy eicoatetraenoic acids (HETE) by e.g. glutathione peroxidases or rapidly hydrolyzed to LTB_4 in case of LTA_4. (Gene names are notes under the enzyme/protein names in italic)

The formed eicosanoids and other oxylipins are potent lipid mediators of the immune response [1]. Through the initial oxidation of polyunsaturated fatty acids, such as ARA, via one of the two COX enzymes the unstable prostaglandin (PG) H_2 is formed and can be further converted by downstream enzymatic or non-enzymatic reactions, e.g., to PGE_2 or 12-hydroxyheptadeca-trienoic acid (12-HHT) [2, 3]. Formed in immune cells, PGE_2 acts as a pro-inflammatory signaling molecule by, e.g., stimulating the upregulation of pro-inflammatory cytokines or enhancing blood flow through augmented atrial vasodilation [4, 5]. Increased PGE_2 levels are often associated with upregulated

COX-2 (derived from the *PTGS2* gene) abundance that is induced by pro-inflammatory stimuli such as gram-negative pathogens [5]. Though biological functions of 12-HHT are not yet fully understood, recent studies have found this oxylipin to be involved i.a. in the mediation of allergic inflammation [6]. As chemical breakdown product of PGH_2 it is an established marker of COX activity [7]. The several LOX isoforms catalyze the stereo- and regiospecific formation of hydroperoxy fatty acids as primary products that are – in the cell – rapidly reduced to hydroxy fatty acids, e.g., hydroxyeicosatetraenoic acids (HETE) formed from ARA [8]. The LOX branch of the ARA cascade is also involved in inflammation regulation. 5-LOX catalyzes the formation of pro-inflammatory and chemotactic leukotrienes (LT), such as ARA derived LTB_4. The multiple hydroxylated fatty acids formed via consecutive LOX activity are believed to elicit anti-inflammatory properties involved in the active resolution of inflammation [8, 9] but remain controversially discussed [10]. The multitude of products arising from the many ARA cascade enzymes, crosstalk between the different branches and various structurally distinct fatty acid substrates make a comprehensive oxylipin metabolomics platform necessary for thorough investigation of the oxylipin pattern. However, in order to fully comprehend the mechanisms leading to changes on metabolite levels, the additional investigation of gene expression, i.e., protein abundance is indispensable.

In the recent years, interest in multi-omics techniques as tools to achieve systemic understanding of biological changes has drastically increased, i.e., metabolomics, proteomics, transcriptomics [11, 12]. While liquid-chromatography (LC) tandem mass spectrometry (MS/MS) is the standard method for quantitative targeted oxylipin analysis [13], the LC-MS/MS-based analysis of proteins has emerged in the recent years and is often conducted as high throughput screenings allowing only relative quantification. Though the investigation of ARA cascade enzymes with proteomic tools has been reported [14-18], also in combination with metabolomics analyses [19, 20], a method for its quantitative analysis has not yet been described. Therefore, it was our goal to develop a targeted proteomics method comprising the important COX and

LOX mediated signaling pathways, and expand our existing oxylipin metabolomics platform, establishing a comprehensive and quantitative multi-omics tool to thoroughly investigate the ARA cascade.

Our targeted proteomics approach allows the analysis of human COX and LOX enzymes for the first time in a quantitative manner, and together with our oxylipin metabolomics method, is a valuable tool to characterize the ARA cascade from a single sample. This is demonstrated by characterizing the COX and LOX pathways in different human immune cells, showing correlations between oxylipin and protein abundances as well as quantitative changes upon pharmacological intervention.

4.2 Experimental Section

4.2.1 Chemicals and Biological Material

FCS (superior standardized) was purchased from Biochrom (Berlin, Germany), 1,25-dihydroxyvitamin D_3 (VD_3), ML351 as well as oxylipin standards were purchased from Cayman Chemical (Ann Arbor, MI, USA; local supplier: Biomol, Hamburg, Germany). HEK293 cells derived recombinant human transforming growth factor-β1 (TGF-β1), recombinant human colony stimulating factors CSF-1 (M-CSF), CSF-2 (GM-CSF), IFNγ and IL-4 produced in *E.coli* were obtained from PeproTech Germany (Hamburg, Germany). Lymphocyte separation medium was purchased at PromoCell (Heidelberg, Germany). Human AB serum was provided by the blood donation center University Hospital Düsseldorf (Düsseldorf, Germany). Protease-inhibitor mix M (AEBSF, Aprotinin, Bestatin, E-64, Leupeptin and Pepstatin A), resazurin as well as MS approved trypsin (> 6.000 U/g, from porcine pancreas) were from SERVA Electrophoresis GmbH (Heidelberg, Germany). Unlabeled AQUA peptide standards were obtained from Thermo Life Technologies GmbH (Darmstadt, Germany), unlabeled and heavy labeled (lys: uniformly labeled (U)-$^{13}C_6$; U-$^{15}N_2$; arg: U-$^{13}C_6$; U-$^{15}N_4$) peptide standards were purchased from JPT Peptides (Berlin, Germany).

Acetonitrile (HPLC-MS-grade), acetone (HPLC grade) methanol and acetic acid (Optima LC/MS grade) were obtained from Fisher Scientific (Schwerte, Germany). Dithiothreitol was from AppliChem (Darmstadt, Germany). Tris(hydroxymethyl)aminomethane (TRIS), ammonium bicarbonate, sodium deoxycholate and urea were obtained from Carl Roth. RPMI 1640, L-glutamine and penicillin/streptomycin (5000 units penicillin and 5 mg streptomycin/mL), lipopolysaccharide (LPS) from *E.coli* (0111:B4), dextran500 from *Leuconostoc spp*., iodoacetamide, dimethylsulfoxide (DMSO), dexamethasone, indomethacin, celecoxib, PF-4191834 as well as all other chemicals were purchased from Sigma (Schnellendorf, Germany).

4.2.2 Cell Cultivation

THP-1 cells were obtained from the German Collection of Microorganisms and Cell Cultures GmbH (DSMZ, Braunschweig, Germany) and were maintained in bicarbonate buffered RPMI medium supplemented with 10% FCS, 100 U/mL penicillin, 100 µg/mL streptomycin (P/S, 2%) and 2 mM L-glutamine (1%) in 60.1 cm² dishes in a humidified incubator at 37°C and 5% CO_2. For experiments, cells were seeded at densities of 0.125 mio cells/mL and differentiated with 50 nM VD_3 (0.1% DMSO) and 1 ng/mL TGF-β1 for 72 h.

Primary human macrophages were prepared as described [21]. In brief, peripheral blood monocytic cells (PBMC) were isolated from buffy coats obtained from blood donations at the University Hospital Düsseldorf. Blood samples were drawn with the informed consent of the patients. The study was approved by the Ethical Committee of the University of Wuppertal. PBMC were isolated by dextran (5%) sedimentation for 45 min and subsequent centrifugation (1 000 × *g* without deceleration, 10 min, 20 °C) on lymphocyte separation medium. The leucocyte ring was isolated and washed twice with PBS. Cells were seeded in 60.1 mm² dishes and left to adhere for 1 h after resuspension in serum free RPMI medium (2% P/S, 1% L-glutamine) in a humidified incubator at 37°C and 5% CO_2 (8 dishes per donor). Cells were washed and RPMI medium (2% P/S, 1% L-glutamine) supplemented with 5% human AB serum was added. For polarization towards M1- or M2-like macrophages, the medium was additionally supplemented with 10 ng/mL CSF-2 or CSF-1 for 8 days and treated with 10 ng/mL IFNγ or IL-4 for the final 48 h. No cytokines were added to generate M0 like macrophages.

Platelets were isolated from EDTA-blood as described by the platelet-rich plasma method [22].

4.2.3 Cell Culture Experiments

For the experiments of the THP-1 cells or primary macrophages with test compounds cell culture medium was replaced 7 h before the end of the differentiation with serum-free 50 mM TRIS buffered RPMI medium (2% P/S, 1% L-glutamine) and the pharmacological inhibitors or DMSO (0.1%) as control were added. Cytotoxic effects of the test compounds at the used concentrations were excluded by resazurin (alamar blue) assay [23] (**Fig. 7.11**). After 1 h of preincubation, cells were additionally treated with 1 µg/mL LPS for 6 h. In case of the THP-1 cells, all adherent and non-adherent cells were harvested by scraping in the cell culture medium. Primary macrophages were harvested by cold shock method [21]. The harvested cell pellets were frozen at -80 °C until use.

4.2.4 Quantification of Oxylipin and Protein Levels by LC-MS/MS

Oxylipin and protein levels were determined from one cell pellet. Cells were resuspended in PBS containing 1% protease inhibitor mix and antioxidant solution [24],[25], sonicated and protein content was determined via bicinchoninic acid assay [26]. Internal standards (IS) for oxylipin analysis were added to the cell lysate before proteins were precipitated in methanol at -80 °C for at least 30 min. The supernatant after centrifugation (20 000 × *g*, 10 min, 4 °C) served as sample for oxylipin analysis, which was further carried out as described [24, 25], while the protein levels were later measured in the precipitated protein pellet after freezing at -80 °C. For targeted LC-MS/MS based proteomics analysis the protein pellet was resuspended in 5% (*w/v*) sodium deoxycholate containing 1% protease inhibitor mix and precipitated again in four volumes of ice-cold acetone after centrifugation (15 000 × *g*, 20 min, 4 °C). Further steps were carried out as described [18].

The oxylipins and peptides were measured via LC-MS/MS as previously described for the oxylipins with slight modifications [24, 25, 27]. The oxylipins were separated on a 1290 Infinity II LC system (Agilent, Waldbronn, Germany), equipped with a Zorbax Eclipse Plus C18 reversed phase column (2.1 × 150 mm, particle size 1.8 µm, pore size 95 Å, Agilent) at 40 °C, with an upstream inline filter (3 mm, 1290 infinity II inline filter, Agilent) and a SecurityGuard Ultra C18 cartridge as precolumn (2.1 × 2 mm, Phenomenex LTD, Aschaffenburg, Germany). They were separated with a gradient composed of 0.1% acetic acid mixed with 5% mobile phase B (mobile phase A) and acetonitrile /methanol/acetic acid (800/150/1, *v*/*v*/*v*; mobile phase B) at a flow rate of 0.3 mL/min: 21% B at 0 min, 21% B at 1.0 min, 26% B at 1.5 min, 51% B at 10 min, 66% B at 19 min, 98% B at 25.1 min, 98% B at 27.6 min, 21% B at 27.7 min and 21% B at 31.5 min. The LC was coupled with a 5500 QTRAP mass spectrometer operated in negative electrospray ionization ESI(-) mode (Sciex, Darmstadt, Germany). The MS was set as follows: ion spray voltage: -4500 V, capillary temperature: 650°C, curtain gas N_2: 50 psi, nebulizer gas (GS1) N_2: 30 psi, drying gas (GS2) N_2: 70 psi, generated with N_2 generator NGM 33 (cmc Instruments, Eschborn, Germany), Collisionally activated dissociation (CAD) gas: high. Declustering potentials (DP), entrance potentials (EP) collision cell exit potentials (CXP) and collision energies (CE) were optimized for each of the oxylipins.

The peptides were separated on 1290 Infinity II LC systems (Agilent), equipped with a Zorbax Eclipse Plus C18 reversed phase column (2.1 × 150 mm, particle size 1.8 µm, pore size 95 Å, Agilent) at 40 °C, with an upstream inline filter (3 mm, 1290 infinity II inline filter, Agilent) and SecurityGuard Ultra C18 cartridge as precolumn (2.1 × 2 mm, Phenomenex LTD). They were chromatographically separated with a gradient composed of 95/5% water/acetonitrile (mobile phase A) and 5/95% water/acetonitrile (mobile phase B), both containing 0.1% acetic acid at a flow rate of 0.3 mL/min as follows: 0% B at 0 min, 0% B at 1 min, 35% B at 30.5 min, 100% B at 30.6 min, 100% B at 33.5 min, 0% B at 33.7 min, and 0% B at 36 min. The LC system was coupled to a 6500+ hybrid triple quadrupole linear ion trap mass spectrometer (QTRAP; Sciex) in ESI(+)-mode, with the following settings: ion spray voltage: 5500 V, capillary temperature: 550 °C, curtain gas N_2: 50 psi, nebulizer gas (GS1) N_2: 60 psi, drying gas (GS2) N_2: 60 psi, generated with N_2 generator Eco Inert-ESP (DTW, Bottrop, Germany). DP, EP and CXP were set to 40 V, 10 V and 10 V, respectively, and CE was optimized for each of the peptides (**Tab. 4.1**, **Tab. 4.2**, **Tab. 7.14**). CAD gas was set to medium. Analyst (Sciex, version 1.7) was used for instrument control and data acquisition and Multiquant (Sciex, version 3.0.2) software was used for data analysis.

The oxylipin and peptide/protein concentrations were quantified using external calibrations with IS and they were normalized to the absolute protein content determined with bicinchoninic acid assay [26]. For the quantification of protein abundance levels, two calibration series were prepared: for all COX/LOX peptides and for the peptides of the housekeeping proteins (**Tab. 4.1**, **Tab. 4.2**, **Tab. 7.14**). The calibrations were prepared using unlabeled and heavy labeled (lys: uniformly labeled (U)-$^{13}C_6$; U-$^{15}N_2$; arg: U-$^{13}C_6$; U-$^{15}N_4$) peptide standards as IS from JPT Peptides (Berlin, Germany). The absolute concentration of selected COX/LOX peptides (DCPTPMGTK, FDPELLFNK, LILIGETIK, DDGLLVWEIAR, TGTLAFER, LWEIIAR, EITEIGLQGAQDR, ELLIVPGQVVDR, VSTGEAFGAGTWDK) in the calibration solution was validated with unlabeled AQUA peptide standards (> 97% purity, 25-30% concentration precision, Thermo Life Technologies GmbH, Darmstadt, Germany). The concentration was corrected in case of deviations > 10% between both standards.

4.3 Results

The ARA cascade plays a key role in the regulation of many different physiological processes. In order to understand the crosstalk between the different enzymatic pathways of the ARA cascade and modulation thereof, quantitative information for both oxylipin levels as well as enzyme/protein abundance is needed.

For this reason, we extended our targeted oxylipin metabolomics method [24, 25, 27] and combined it with a new developed analytical approach, allowing to quantify the enzymes of the ARA cascade. Combining targeted LC-MS/MS based proteomics and oxylipin metabolomics the multi-omics methodology allows to quantify the abundance of all relevant enzymes of the COX and the LOX pathways (COX-1 and -2, 5-LOX, 12-LOX, 15-LOX, 15-LOX-2 and FLAP) and oxylipin levels from a single sample down to pM ranges.

4.3.1 Targeted Oxylipin Metabolomics LC-MS/MS Method

In order to comprehensively characterize changes in the ARA cascade on metabolite level, our existing targeted oxylipin metabolomics method [24, 25] was extended by 54 oxylipins. The resulting targeted LC-MS/MS based oxylipin metabolomics platform allows to quantitatively measure 198 oxylipins (using 29 IS) derived from twelve different polyunsaturated fatty acid precursors formed via the three enzymatic branches of the ARA cascade as well as autoxidation. A detailed description of all method parameters including the preparation of calibrations series and verification of the standard concentrations [28] can be found in the supplemental information (**Appendix**).

In our dual LC-MS/MS based approach, oxylipins were extracted from the methanolic supernatant resulting after sonication and precipitation of the cell samples, and enzyme/protein levels were quantified in the precipitated protein residue, thus, only a *single* sample is required for quantitatively assessing the ARA cascade on metabolite and gene expression levels in biological samples.

4.3.2 Targeted Proteomics LC-MS/MS/(MS) Method

The enzyme abundance is measured in form of representative peptides with amino acid (aa) sequences specific to the target enzyme. Based on an *in silico* tryptic digestion of the COX and LOX enzymes two proteotypic peptides with unique [29, 30] aa sequences were selected per enzyme from the multitude of theoretically possible peptides (**Tab. 7.13**). The results from the *in silico* digestion were narrowed down by a defined set of criteria [18] including fixed peptide lengths (7 – 22 aa) as well as acceptable calculated cleavage probabilities [31] (e.g. ≥ 70% using cleavage prediction with decision trees [32]) and predicted retention times (3 – 30 min) [33]. Possible variations in relevant splice variants [34] were considered as well as the presence of max. two unfavored aa (C, M, N, Q, W). Peptides containing single nucleotide polymorphisms [34] or posttranslational modifications were excluded [34, 35]. After the *in silico* peptide selection and evaluation of three to five candidates in digested cell matrix, the MS/MS parameters were optimized and two peptides per protein were finally selected (**Tab. 4.1**, **Tab. 4.2**, **Tab. 7.14**).

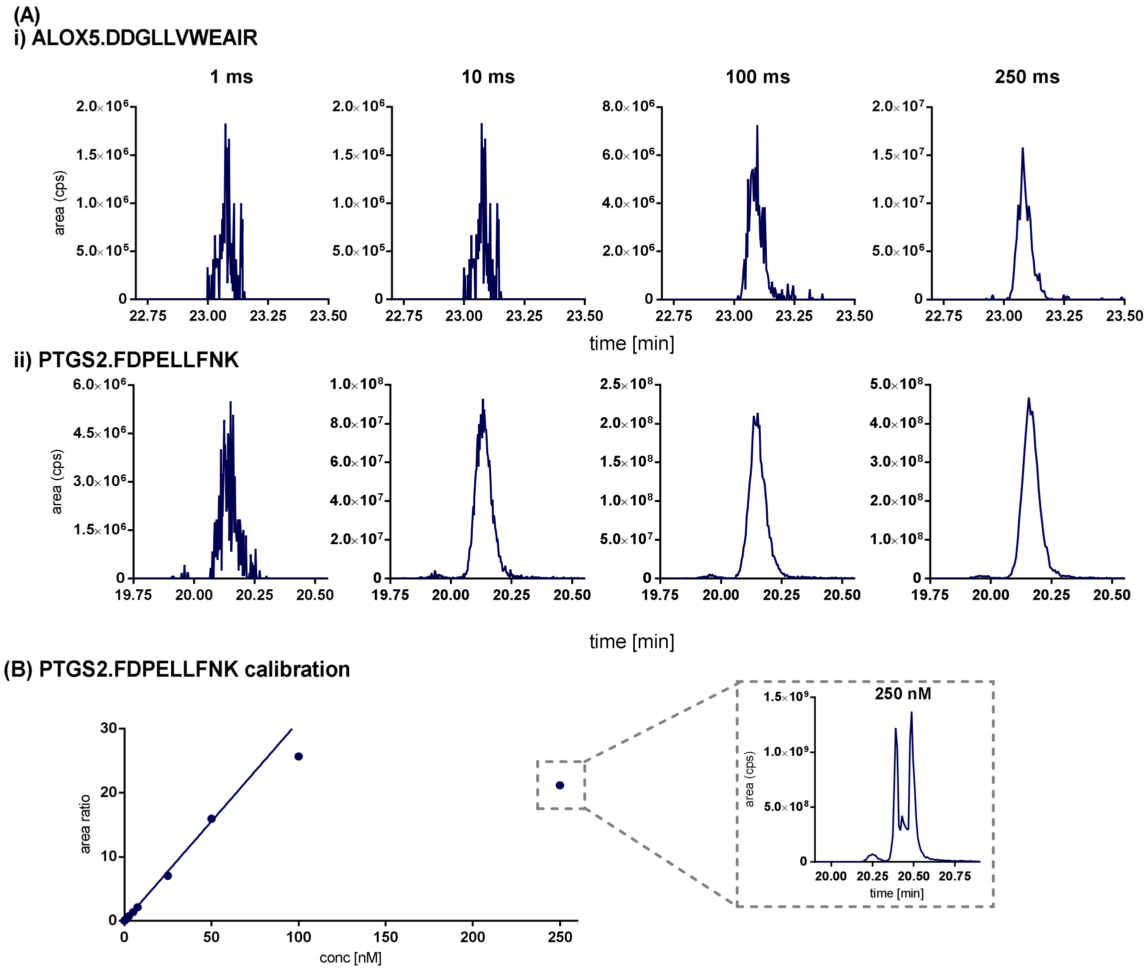

Fig. 4.2: Optimization of QTRAP fill time for MS³ experiments and evaluation of linear range in MS³. **(A)** Longer fixed fill times (FFT) result in increased signal intensity and thus, improved signal-to noise ratios. Shown are 25 nM standards of **(A) i)** DDGLLVWEAIR (5-LOX) and **(A) ii)** FDPELLFNK (COX-2). **(B)** The calibration range in MS³ is limited due to overfilling of the ion trap at higher concentrations resulting in poor peak shape, shown exemplarily for the COX-2 peptide FDPELLFNK.

In MS³ mode the triple quadruple QTRAP instrument uses the linear ion trap (LIT) in Q3 for a second fragmentation of the CAD fragment ions. With the aim of achieving higher selectivity and thus, sensitivity for quantification of the peptides in complex biological matrices by this additional fragmentation, we chose an MS³ approach for the targeted proteomics method. For each peptide the CE of multiple CAD fragment ions was optimized and two to three of the most intense fragment ions, ideally with *m/z* exceeding the precursor ion *m/z* (e.g. a transition from a double charge precursor to a single charged fragment), were chosen for further evaluation in MS³ mode. Their excitation energies (AF2) were optimized in 0.01 V steps and the final CAD fragment ions for the MS^3 method were selected based on the highest sensitivities and/or lack of matrix interference in digested cell lysates for each peptide (**Tab. 4.1**).

The fixed fill time (FFT) for the LIT had a major impact on the signal intensity which increased with longer FFTs (**Fig. 4.2 (A)**). The maximum FFT of 250 ms provided the highest sensitivities and was thus used for all peptides (except abundant TGTLAFER: 100 ms and IS peptides: 25 ms). In order to allow the simultaneous analysis of all peptides with acceptable cycle times and thus, data points per peak, the analytical run was split into 10 periods with separate MS experiments. Despite excellent chromatographic separation (**Tab. 4.1**, **Fig. 4.3 (A) i)**), with average peak widths at half maximum height (FWHM) of 4.9 s, the number of initially selected peptides was reduced to one peptide per protein for the MRM^3 method based on its sensitivity and retention time. At a LIT scan rate of 10 000 Da/s, a total cycle time of 372 – 572 ms for each of the eight MS^3 experiments resulted and thus 9 – 12 data points over the FWHM of the peak. The peptides of four housekeeping proteins were measured in two periods set in MRM mode with resulting cycle times of 150 and 450 ms at constant dwell times of 20 ms. For data evaluation, MRM^3 transitions were constructed from the MS^3 spectra by the Multiquant 3.0.2 software. Assessing the MRM^3 transitions of one MS^3 fragment ion compared to the sum of multiple MS^3 fragment ions showed higher signal intensity for the use of multiple fragment ions (**Fig. 4.6**). Thus, for the final method the ten most abundant MS^3 fragment ions of the analyte peptides and five of the IS peptides were selected for data analysis.

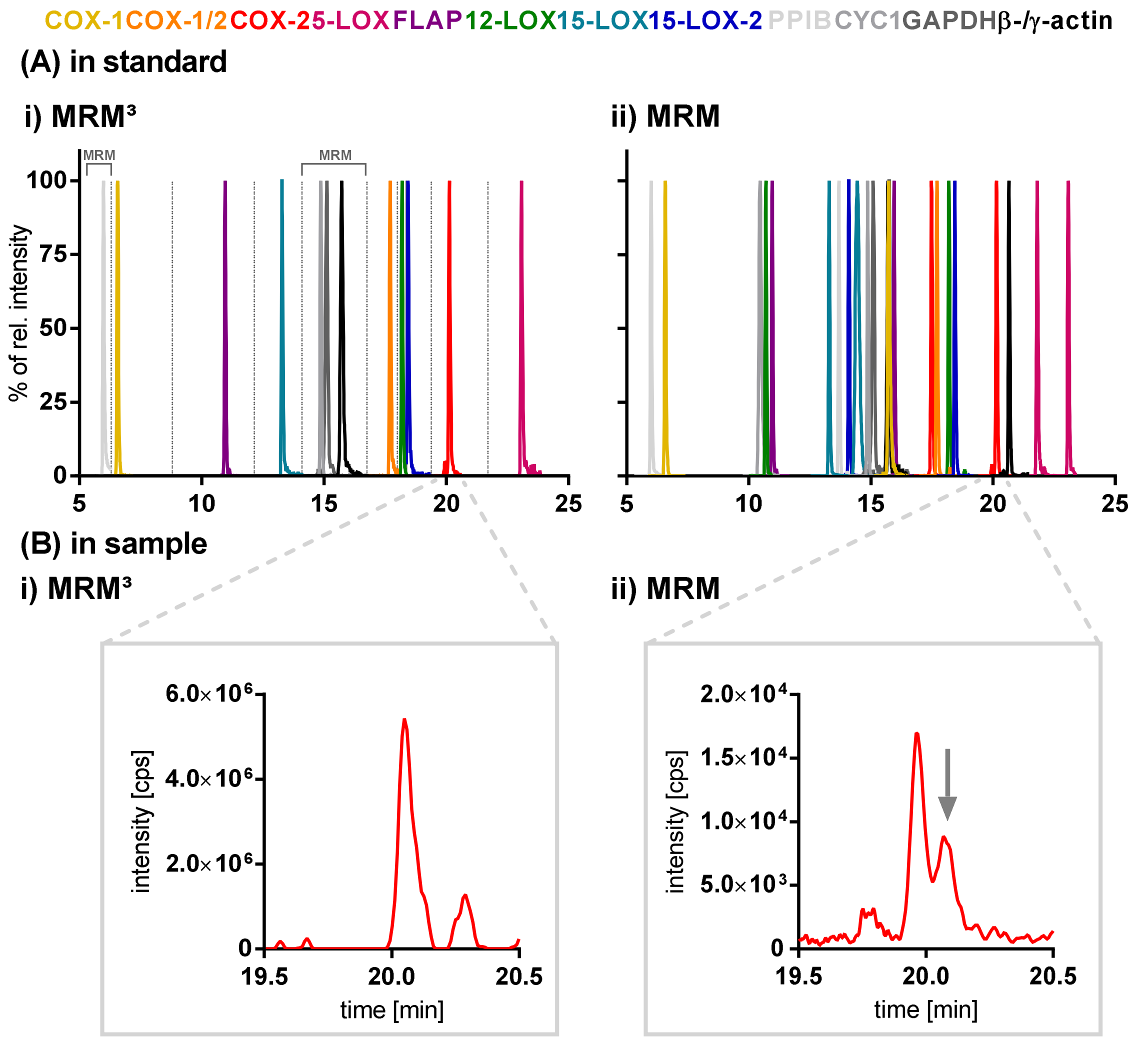

Fig. 4.3: Chromatographic separation of the peptides from the COX and LOX pathway enzymes/proteins as well as housekeeping peptides with detection in **i)** MRM³ and **ii)** MRM mode on an LC-MS/MS QTRAP system. Shown are **(A)** a mix of peptide standards (25-100 nM) as well as **(B)** the signal of COX-2 peptide FDPELLFNK in THP-1 cells. The cells were differentiated for 72 h with vitamin D3 (50 nM) and TGF-β1 (1 ng/mL) and treated with LPS (1 µg/mL) for 6 h.

The MS^3 approach was compared to scheduled MRM detection. Here, the windows were set to ± 45 s at the expected retention time and a cycle time of 0.4 s resulting in comparable average 14 data points over FWHM of the chromatographic peaks. Two peptides per protein were included in the method comprising again all COX and relevant LOX pathway enzymes as well as four housekeeping proteins, resulting in a total of 23 peptides (**Fig. 4.3 (A) ii)**, **Tab. 4.2**, **Tab. 7.14**).

The additional fragmentation in MS^3 increased selectivity allowing separation of the analyte from interfering matrix signals. This is shown in **Fig. 4.3 (B) i), ii)** for the low abundant COX-2 peptide FDPELLFNK in differentiated (50 nM VD_3 and 1 ng/mL TGF-β1, 72 h) and LPS-stimulated (1 µg/mL, 6 h) THP-1 cells. The MRM^3 method enables sensitive detection and quantification of COX and LOX peptides in the medium to high pM range (31 – 560 pM). However, the MRM method was more sensitive with up to 10-fold lower limits of detection (LOD) ranging from 4.2 pM – 56 pM and lower limits of quantification (LLOQ) in the range of 16 – 122 pM for the same peptides (**Fig. 7.10**, **Tab. 4.1**, **Tab. 4.2**). Overfilling of the trap at higher concentrations results in a breakdown of the MS signal (**Fig. 4.2 (B)**) and restricts the calibration range of the MRM^3 method to 4.0 – 368 nM depending on the peptide (**Tab. 4.1**). This limits the linear working range of the MRM^3 method to only two to three orders of magnitude. Here, the MRM method also shows a clear advantage allowing linear calibration over approx. five orders of magnitude from the pM LLOQ up to the low µM range (**Tab. 4.2**). Thus, MRM is generally advantageous. If the analyte signal is interfered in matrix, MRM^3 provides an additional level of selectivity and is useful for complicated biological matrices while MRM is more sensitive and allows analysis within a large linear range.

The dual approach of targeted oxylipin metabolomics and proteomics allows the analysis of oxylipin concentrations and protein levels in *one* sample. This powerful tool was applied to comprehensively analyze the ARA cascade in immune cells.

Tab. 4.1 (pages 90 – 91): MRM³ method parameters for **(A)** unlabeled and **(B)** heavy labeled (lys: U-$^{13}C_6$; U-$^{15}N_2$; arg: U-$^{13}C_6$; U-$^{15}N_4$) peptides of COX-1, COX-2, 5-LOX, FLAP, 12-LOX, 15-LOX and 15-LOX-2. The unlabeled and corresponding heavy labeled peptides from one protein were measured together in one time period covering each retention time (RT). RT are shown as mean ± SD, set of n = 19 calibrators. Shown are Q1 *m/z* and collisionally activated dissociation fragments (Q3) as well as selected MS³ fragments together with their respective collision (CE) and excitation energies (AF2). The linear trap (LIT) excitation time was set to 25 ms (standard setting) with fixed fill times of 250 ms (maximum) for all peptides (TGTLAFER = 100 ms, IS peptides: 25 ms) at a scan rate of 10 000 Da/s. The MS³ fragments were isolated from the MS³ spectra with an isolation window of ± 0.5 Da. The ratio between the sum of **(A)** 10 MS³ fragments of the unlabeled peptide and **(B)** 5 MS³ fragments of the heavy labeled peptide is used for quantification. The spiking levels of the heavy labeled peptides (concentrations in vial) are shown in **(B)**. The linear calibration range as well as limits of detection (LOD), lower limits of quantification (LLOQ) and LOD of the peptides and enzymes on column are shown for **(A)** unlabeled peptides. The accuracy of the calibrators was within a range of ± 15% (± 20% for LLOQ). Additionally, peptides of four housekeeping proteins (GAPDH, PPIB, β-/γ-actin, CYC1) were measured in MRM mode as separate periods with set dwell times of 20 ms and the parameters specified in **Tab. 7.14**.

(A)

Protein	Peptide	mode	Transition (Q1→Q3)	Q1 *m/z*	Q3 *m/z*	*m/z* of MS³ fragment ions summed for MRM³	Time period [min]	RT [min]	CE (V)	AF2 (V)	Calibration Range [nM]	LOD [nM]	LLOQ [nM]	LOD on column [pg] peptide	LOD on column [pg] enzyme
PPIB	IGDEDVGR	MRM	*	*	*	-	0.00 - 6.61	5.99 ± 0	*	-	*	-	-	-	-
COX-1	DCPTPMGTK	MS³	$M^{2+} \rightarrow y_7^+$	503.7	731.4	713.4 (b_7^+), 644.3, 695.3, 533.3 (y_5^+), 515.3 (y_5^+ - H_2O), 567.4, 585.3 (b_6^+), 608.3, 677.3, 387.2	6.61 - 9.10	6.92 ± 0.01	19	0.08	0.079 - 31	0.031	0.079	0.15	11
FLAP	TGTLAFER	MS³	$M^{2+} \rightarrow y_5^+$	447.7	635.4	617.3 (b_5^+), 416.2, 277.2, 287.3, 600.4, 382.2, 434.3, 522.3 (y_4^+), 461.2 (b_4^+), 332.2 (b_3^+)	9.10 - 12.45	11.30 ± 0.01	24	0.08	1.5 - 368	1.1	1.5	4.90	100
15-LOX	EITEIGLQGAQDR	MS³	$M^{3+} \rightarrow y_5^+$	477.2	546.3	528.3 (b_5^+), 511.2, 330.1, 384.1, 401.2, 215.2, 244.1, 290.1 (y_2^+), 372.2 (b_4^+), 418.2 (y_3^+)	12.45 - 14.40	13.63 ± 0.01	21	0.07	0.84 - 113	0.56	0.84	4.00	211
CYC1	DVCTFLR							14.85 ± 0.03							
GAPDH	GALQNIIPASTGAAK	MRM	*	*	*	-	14.40 - 17.03	15.09 ± 0.03	*	-	*	-	-	-	-
β-/γ-actin	VAPEEHPVLLTEAPLNPK							15.68 ± 0.04							
COX-1/2	LILIGETIK	MS³	$M^{2+} \rightarrow y_7^+$	500.3	773.3	755.5 (b_7^+), 609.4, 496.3, 361.2 (y_3^+), 310.3, 547.3 (y_5^+), 383.3, 451.3, 514.3 (b_5^+), 591.4	17.03 - 18.26	18.03 ± 0.01	23	0.12	0.13 - 4	0.053	0.13	0.27	18
12-LOX	LWEIIAR	MS³	$M^{2+} \rightarrow y_5^+$	450.8	601.4	583.4 (b_5^+), 472.3 (y_4^+), 338.3, 342.2, 229.3, 310.3, 359.2 (y_3^+), 356.2 (b_3^+), 243.1 (b_2^+), 409.4	18.26 - 18.62	18.51 ± 0.01	21	0.07	0.075 - 25	0.050	0.075	0.23	19
15-LOX-2	ELLIVPGQVVDR	MS³	$M^{2+} \rightarrow y_7^+$	669.4	770.4	752.4 (b_7^+), 283.1(b_3^+), 596.38 (b_6^+), 382.2 (b_4^+), 464.4, 436.6, 365.4, 337.2 (y_6^{++}), 481.3 (b_5^+), 587.5	18.62 - 19.59	18.76 ± 0.01	30	0.13	0.44 - 22	0.22	0.44	1.5	83
COX-2	FDPELLFNK	MS³	$M^{2+} \rightarrow y_7^{++}$	561.8	430.7	634.4 (y_5^+), 227.1 (b_2^+), 521.3 (y_4^+), 340.2 (b_3^+), 408.2 (y_3^+), 763.4 (y_6^+), 261.2 (y_2^+), 745.3,	19.59 - 21.90	20.44 ± 0.01	25	0.05	0.084 - 42	0.042	0.084	0.24	15
5-LOX	DDGLLVWEIAR	MS³	$M^{2+} \rightarrow y_5^+$	643.8	674.4	359.2 (y_3^+), 387.2 (b_3^+), 316.1 (b_2^+), 656.4 (b_5^+), 324.5, 638.4, 612.4, 595.4, 344.4, 510.4	21.90 - 36.00	23.38 ± 0.01	25	0.11	0.49 - 122	0.37	0.49	2.4	144

Tab. 4.1 continued.

(B)

Protein	Peptide	mode	Transition (Q1→Q3)	Q1 *m/z*	Q3 *m/z*	*m/z* of MS³ fragment ions summed for MRM³	Time period [min]	RT [min]	CE (V)	AF2 (V)	Spiking level in vial [nM]
PPIB	IGDEDVGR	MRM	*	*	*	-	0.00 - 6.61	5.99 ± 0.01	*	-	50
COX-1	DCPTPMGTK	MS³	$M^{2+} \rightarrow y_7^+$	507.7	739.4	652.3, 721.4 (b_7^+), 703.3, 387.2, 541.3 (y_5^+)	6.61 - 9.10	6.92 ± 0.01	19	0.1	25
FLAP	TGTLAFER	MS³	$M^{2+} \rightarrow y_5^+$	452.7	645.4	627.3 (b_5^+), 425.2, 277.2, 287.3, 391.2	9.10 - 12.45	11.30 ± 0.01	24	0.1	25
15-LOX	EITEIGLQGAQDR	MS³	$M^{3+} \rightarrow y_5^+$	480.6	556.3	538.3 (b_5^+), 372.2 (b_4^+), 521.2, 330.1, 226.1	12.45 - 14.40	13.63 ± 0.01	21	0.1	25
CYC1	DVCTFLR	MRM	*	*	*	-	14.40 - 17.03	14.85 ± 0.03	*	-	50
GAPDH	GALQNIIPASTGAAK							15.09 ± 0.03			50
β-/γ-actin	VAPEEHPVLLTEAPLNPK							15.68 ± 0.04			100
COX.1/3	LILIGETIK	MS³	$M^{2+} \rightarrow y_7^+$	504.3	781.5	496.3, 451.1, 310.2, 763.5 (b_7^+), 555.3 (y_5^+)	17.03 - 18.26	18.03 ± 0.01	23	0.1	25
12-LOX	LWEIIAR	MS³	$M^{2+} \rightarrow y_5^+$	455.8	611.3	593.4 (b_5^+), 482.3 (y_4^+), 338.3, 351.2, 238.2	18.26 - 18.62	18.51 ± 0.01	21	0.1	25
15-LOX-2	ELLIVPGQVVDR	MS³	$M^{2+} \rightarrow y_7^+$	674.4	780.4	283.1 (b_3^+), 762.4 (b_7^+), 382.2 (b_4^+), 365.4, 337.2	18.62 - 19.59	18.76 ± 0.01	30	0.1	25
COX-2	FDPELLFNK	MS³	$M^{2+} \rightarrow y_7^{++}$	565.8	434.8	642.4 (y_5^+), 227.1 (b_2^+), 771.4 (y_6^+), 529.3 (y_4^+), 340.2 (b_3^+)	19.59 - 21.90	20.44 ± 0.01	25	0.1	25
5-LOX	DDGLLVWEIAR	MS³	$M^{2+} \rightarrow y_5^+$	648.8	684.4	369.2 (y_3^+), 387.2 (b_3^+), 648.5, 352, 466.2	21.90 - 36.00	23.38 ± 0.01	25	0.1	25

* : details are specified in **Tab. 7.14**.

Tab. 4.2 (pages 93 – 95): MRM method parameters for **(A)** unlabeled and **(B)** heavy labeled (lys: U-$^{13}C_6$; U-$^{15}N_2$; arg: U-$^{13}C_6$; U-$^{15}N_4$) peptides of COX-1, COX-2, 5-LOX, FLAP, 12-LOX, 15-LOX and 15-LOX-2. For each peptide, different collisionally activated dissociation fragment ions used for qualification and quantification (top) with their Q1 and Q3 *m/z* are shown with retention time (RT, mean ± SD, set of n = 23 calibrators), relative ratios to quantifier transition as well as collision energies (CE). For unlabeled peptides **(A)** the linear calibration range is shown for quantifier transitions as well as the transitions of the corresponding heavy labeled peptides used as internal standards (IS) for quantification, limits of detection (LOD), lower limits of quantification (LLOQ) and LOD of the peptides and enzymes on column. Accuracy of calibrators was within a range of ± 15% (20% for LLOQ). The heavy labeled peptides are spiked at 25 nM for all peptides (concentration in vial).

(A)

Gene / Protein (UniProtKB No.)	Peptide	Transitions	Q1 *m/z*	Q3 *m/z*	RT [min]	Rel. Ratio to quantifier [%]	CE (V)	IS Transitions	Calibration Range [nM]	LOD [pM]	LLOQ [pM]	LOD on column peptide [fg]	LOD on column enzyme [pg]
PTGS1 / Cyclooxygenase-1	**DCPTPMGTK**	$M^{2+} \rightarrow y_7^+$	503.7	731.4			19						
(COX-1; P23219)		$M^{2+} \rightarrow b_2^+$	503.7	276.1	6.92 ± 0.01	59	20	$M^{2+} \rightarrow y_7^+$	0.016 - 1570	7.9	16	37	2.7
		$M^{2+} \rightarrow y_5^+$	503.7	533.3		43	31						
	AEHPTWGDEQLFQTTR	$M^{3+} \rightarrow y_5^+$	639.3	652.3			26						
		$M^{3+} \rightarrow y_4^+$	639.3	505.3	16.06 ± 0.03	57	28	$M^{3+} \rightarrow y_5^+$	0.50 - 5000	250	500	2394	86
		$M^{3+} \rightarrow y_6^+$	639.3	765.4		55	28						
PTGS2 / Cyclooxygenase-2	**FDPELLFNK**	$M^{2+} \rightarrow y_7^{++}$	561.8	430.7			25						
(COX-2; P35354)		$M^{2+} \rightarrow y_7^+$	561.8	860.4	20.44 ± 0.02	36	25	$M^{2+} \rightarrow y_7^{++}$	0.021 - 2111	4.2	21	24	1.5
		$M^{2+} \rightarrow b_2^+$	561.8	263.1		25	24						
	NAIMSYVLTSR	$M^{2+} \rightarrow y_8^+$	627.8	956.3			29						
		$M^{2+} \rightarrow b_3^+$	627.8	299.1	17.81 ± 0.02	92	27	$M^{2+} \rightarrow y_8^+$	0.25 - 5000	100	250	627	34
		$M^{2+} \rightarrow y_9^+$	627.8	1069.6		43	27						
PTGS1 / COX-1	**LILIGETIK**	$M^{2+} \rightarrow y_7^+$	500.3	773.3			23						
& PTGS2 / COX-2		$M^{2+} \rightarrow b_2^+$	500.3	227.2	18.03 ± 0.02	62	22	$M^{2+} \rightarrow y_7^+$	0.027 - 2660	13	27	66	4.6
		$M^{2+} \rightarrow y_5^+$	500.3	547.3		30	25						
ALOX5 / 5-Lipoxygenase	**DDGLLVWEAIR**	$M^{2+} \rightarrow y_6^+$	643.8	773.4			30						
(5-LOX; P09917)		$M^{2+} \rightarrow y_7^+$	643.8	886.5	23.38 ± 0.01	81	28	$M^{2+} \rightarrow y_6^+$	0.122 - 1219	49	122	313	19
		$M^{2+} \rightarrow y_5^+$	643.8	674.4		85	25						
	NLEAIVSVIAER	$M^{2+} \rightarrow y_7^+$	657.4	773.5			28						
		$M^{2+} \rightarrow y_{10}^+$	657.4	1086.6	22.12 ± 0.01	66	30	$M^{2+} \rightarrow y_6^+$	0.25 - 5000	100	250	656	39
		$M^{2+} \rightarrow y_8^+$	657.4	886.5		43	30						
ALOX5AP / Arachidonate 5-lipoxygenase-activating protein	**TGTLAFER**	$M^{2+} \rightarrow y_5^+$	447.7	635.4			22						
		$M^{2+} \rightarrow y_3^+$	447.7	451.2	11.30 ± 0.02	70	24	$M^{2+} \rightarrow y_4^+$	0.074 - 7366	37	74	165	3.4
		$M^{2+} \rightarrow y_6^+$	447.7	736.4		55	20						
(FLAP; P20292)	**YFVGYLGER**	$M^{2+} \rightarrow y_7^+$	552.3	793.4			24						
		$M^{2+} \rightarrow b_2^+$	552.3	311.1	16.27 ± 0.03	67	24	$M^{2+} \rightarrow y_7^+$	0.010 - 5000	5.0	10	28	0.45
		$M^{2+} \rightarrow y_6^+$	552.3	694.4		69	26						

Tab. 4.2 continued.

(A)

Gene / Protein (UniProtKB No.)	Peptide	Transitions	Q1 *m/z*	Q3 *m/z*	RT [min]	Rel. Ratio to quantifier [%]	CE (V)	IS Transitions	Calibration Range [nM]	LOD [pM]	LLOQ [pM]	LOD on column peptide [fg]	LOD on column enzyme [pg]
ALOX12 /12-Lipoxygenase	**LWEIIAR**	$M^{2+} \rightarrow y_5^+$	450.8	601.4			21						
(12-LOX; P18054)		$M^{2+} \rightarrow b_2^+$	450.8	300.2	18.51 ± 0.02	32	17	$M^{2+} \rightarrow y_6^+$	0.025 - 5000	10	25	45	3.8
		$M^{2+} \rightarrow y_6^+$	450.8	787.4		21	21						
	AVLNQFR	$M^{2+} \rightarrow y_5^+$	424.2	677.4			19						
		$M^{2+} \rightarrow y_4^+$	424.2	564.3	11.07 ± 0.02	47	21	$M^{2+} \rightarrow y_5^+$	0.050 - 5000	25	50	106	9.5
		$M^{2+} \rightarrow y_3^+$	424.2	450.3		6	19						
ALOX15 / 15-Lipoxygenase	**EITEIGLQGAQDR**	$M^{2+} \rightarrow y_8^+$	715.4	844.4			34						
(15-LOX; P16050)		$M^{2+} \rightarrow y_5^+$	715.4	546.3	13.62 ± 0.01	38	32	$M^{2+} \rightarrow y_8^+$	0.113 - 5629	56	113	402	21
		$M^{2+} \rightarrow y_9^+$	715.4	957.5		29	35						
	GFPVSLQAR	$M^{2+} \rightarrow y_7^{++}$	487.8	385.7			20						
		$M^{2+} \rightarrow y_5^+$	487.8	574.3	14.78 ± 0.01	28	29	$M^{2+} \rightarrow y_7^{++}$	0.25 - 5000	100	250	487	37
		$M^{2+} \rightarrow y_7^+$	487.8	770.5		18	24						
ALOX15B / 15-Lipoxygenase-2	**ELLIVPGQVVDR**	$M^{2+} \rightarrow y_7^+$	669.4	770.4			30						
(15-LOX-2; O15296)		$M^{2+} \rightarrow b_5^+$	669.4	568.4	18.76 ± 0.02	32	24	$M^{2+} \rightarrow y_7^+$	0.044 - 4391	22	44	147	8.3
		$M^{2+} \rightarrow y_8^+$	669.4	869.5		32	29						
	VSTGEAFGAGTWDK	$M^{2+} \rightarrow y_7^+$	713.3	734.3			36						
		$M^{2+} \rightarrow y_8^+$	713.3	881.4	14.42 ± 0.02	83	36	$M^{2+} \rightarrow y_7^+$	0.25 - 5000	100	250	712	38
		$M^{2+} \rightarrow y_9^+$	713.3	952.5		79	35						

Tab. 4.2 continued.

(B)

Gene / Protein (UniProtKB No.)	**Peptide**	**Transitions**	**Q1 *m/z***	**Q3 *m/z***	**RT [min]**	**Rel. Ratio to quantifier [%]**	**CE (V)**
PTGS1 / Cyclooxygenase-1 (COX-1; P23219)	**DCPTPMGTK**	$M^{2+} \rightarrow y_7^{+}$	507.7	739.4			19
		$M^{2+} \rightarrow b_2^{+}$	507.7	276.1	6.92 ± 0.01	59	20
		$M^{2+} \rightarrow y_7^{++}$	507.7	370.2		17	23
	AEHPTWGDEQLFQTTR	$M^{3+} \rightarrow y_5^{+}$	642.6	662.4			26
		$M^{3+} \rightarrow y_4^{+}$	642.6	515.3	16.06 ± 0.03	53	28
		$M^{3+} \rightarrow y_6^{+}$	642.6	775.4		50	28
PTGS2 / Cyclooxygenase-2 (COX-2; P35354)	**FDPELLFNK**	$M^{2+} \rightarrow y_7^{++}$	565.8	434.8			25
		$M^{2+} \rightarrow y_7^{+}$	565.8	868.5	20.44 ± 0.02	34	25
		$M^{2+} \rightarrow y_4^{+}$	565.8	529.3		6	33
	NAIMSYVLTSR	$M^{2+} \rightarrow y_8^{+}$	632.8	966.3			29
		$M^{2+} \rightarrow b_3^{+}$	632.8	299.2	17.81 ± 0.02	92	27
		$M^{2+} \rightarrow y_7^{+}$	632.8	835.5		70	30
PTGS1 / COX-1 & PTGS2 / COX-2	**LILIGETIK**	$M^{2+} \rightarrow y_7^{+}$	504.3	781.5			23
		$M^{2+} \rightarrow y_6^{+}$	504.3	668.4	18.03 ± 0.02	23	24
		$M^{2+} \rightarrow y_8^{+}$	504.3	894.6		4	24
ALOX5 / 5-Lipoxygenase (5-LOX; P09917)	**DDGLLVWEAIR**	$M^{2+} \rightarrow y_6^{+}$	648.8	783.4			30
		$M^{2+} \rightarrow y_7^{+}$	648.8	896.5	23.38 ± 0.01	78	28
		$M^{2+} \rightarrow y_5^{+}$	648.8	684.4		83	25
	NLEAIVSVIAER	$M^{2+} \rightarrow y_6^{+}$	662.4	684.4			28
		$M^{2+} \rightarrow y_8^{+}$	662.4	896.5	22.12 ± 0.01	76	30
		$M^{2+} \rightarrow y_4^{+}$	662.4	498.3		36	28
ALOX5AP / Arachidonate 5-lipoxygenase-activating protein (FLAP; P20292)	**TGTLAFER**	$M^{2+} \rightarrow y_4^{+}$	452.7	532.2			24
		$M^{2+} \rightarrow y_5^{+}$	452.7	645.4	11.30 ± 0.02	44	22
		$M^{2+} \rightarrow y_3^{+}$	452.7	461.2		32	24
	YFVGYLGER	$M^{2+} \rightarrow y_7^{+}$	557.3	803.4			24
		$M^{2+} \rightarrow b_2^{+}$	557.3	311.1	16.27 ± 0.03	66	24
		$M^{2+} \rightarrow y_6^{+}$	557.3	704.4		72	26
ALOX12 /12-Lipoxygenase (12-LOX; P18054)	**LWEIIAR**	$M^{2+} \rightarrow y_6^{+}$	455.8	797.5			21
		$M^{2+} \rightarrow y_4^{+}$	455.8	482.3	18.51 ± 0.02	87	21
		$M^{2+} \rightarrow y_3^{+}$	455.8	369.2		44	21
	AVLNQFR	$M^{2+} \rightarrow y_5^{+}$	429.2	687.4			19
		$M^{2+} \rightarrow y_3^{+}$	429.2	460.3	11.07 ± 0.02	7	19
		$M^{2+} \rightarrow z_4^{+}$	429.2	557.3		6	28
ALOX15 / 15-Lipoxygenase (15-LOX; P16050)	**EITEIGLQGAQDR**	$M^{2+} \rightarrow y_8^{+}$	720.4	854.4			34
		$M^{2+} \rightarrow y_5^{+}$	720.4	556.3	13.62 ± 0.01	39	32
		$M^{2+} \rightarrow y_9^{+}$	720.4	967.5		30	35
	GFPVSLQAR	$M^{2+} \rightarrow y_7^{++}$	492.8	390.7			20
		$M^{2+} \rightarrow y_5^{+}$	492.8	584.3	14.78 ± 0.01	28	29
		$M^{2+} \rightarrow y_6^{+}$	492.8	683.4		10	30
ALOX15B / 15-Lipoxygenase-2 (15-LOX-2; O15296)	**ELLIVPGQVVDR**	$M^{2+} \rightarrow y_7^{+}$	674.4	780.4			30
		$M^{2+} \rightarrow y_8^{+}$	674.4	879.5	18.76 ± 0.02	30	29
		$M^{2+} \rightarrow b_5^{+}$	674.4	568.4		30	24
	VSTGEAFGAGTWDK	$M^{2+} \rightarrow y_7^{+}$	717.3	742.4			36
		$M^{2+} \rightarrow y_8^{+}$	717.3	889.4	14.42 ± 0.02	74	36
		$M^{2+} \rightarrow y_{12}^{++}$	717.3	624.3		58	30

4.3.3 Analysis of the ARA Cascade in Immune Cells

The lipid mediators formed in the ARA cascade are an essential part of the immune system and function i.a. as signaling molecules between different types of immune cells in the host defense. Using the developed LC-MS/MS targeted oxylipin metabolomics and proteomics platform, the ARA cascade was comprehensively analyzed in human macrophages for the first time with this novel approach.

The monocytes from the THP-1 cell line were examined during differentiation to macrophage-like cells with 50 nM VD_3 and 1 ng/mL TGF-β1 for 72 h. This process induced the *ALOX5* gene expression along with its product formation (5-HETE and LTB_4; **Fig. 4.4 (A) i), ii)**). While other LOX were not present, COX-1 and FLAP levels increased by 17 and 32-fold, respectively, after differentiation. Additional treatment of the macrophages with 1 µg/mL LPS for 6 h stimulated *PTGS2* gene expression and formation of PGE_2 and 12-HHT which was below the detection limit in THP-1 cells bearing COX-1 alone (THP-1 monocytes and macrophages; **Fig. 4.4 (A) i), ii)**). The COX-2 protein level increased strongly after LPS (1 µg/mL) treatment and peaked at approx. 80 fmol/mg protein after 6 – 8 h where it declined to 40 fmol/mg protein after 24 h (**Fig. 4.4 (A) iii)**). Pretreatment of the THP-1 macrophages with dexamethasone suppressed the induction of *PTGS2* gene expression (i.e. COX-2 abundance) and concomitant prostanoid synthesis with potencies (IC_{50}) of 3.4 nM (COX-2; 95% CI: 2.3 – 4.9 nM) and 1.2 nM (PGE_2; 95% CI: 0.9 – 1.6 nM), respectively (**Fig. 4.4 (A) iv)**). The 5-LOX inhibitor PF4191834 suppressed 5-HETE formation with a potency (IC_{50}) of 26 nM (95% CI: 12 – 53 nM) and did not affect *ALOX5* gene expression (**Fig. 4.4 (A) v)**).

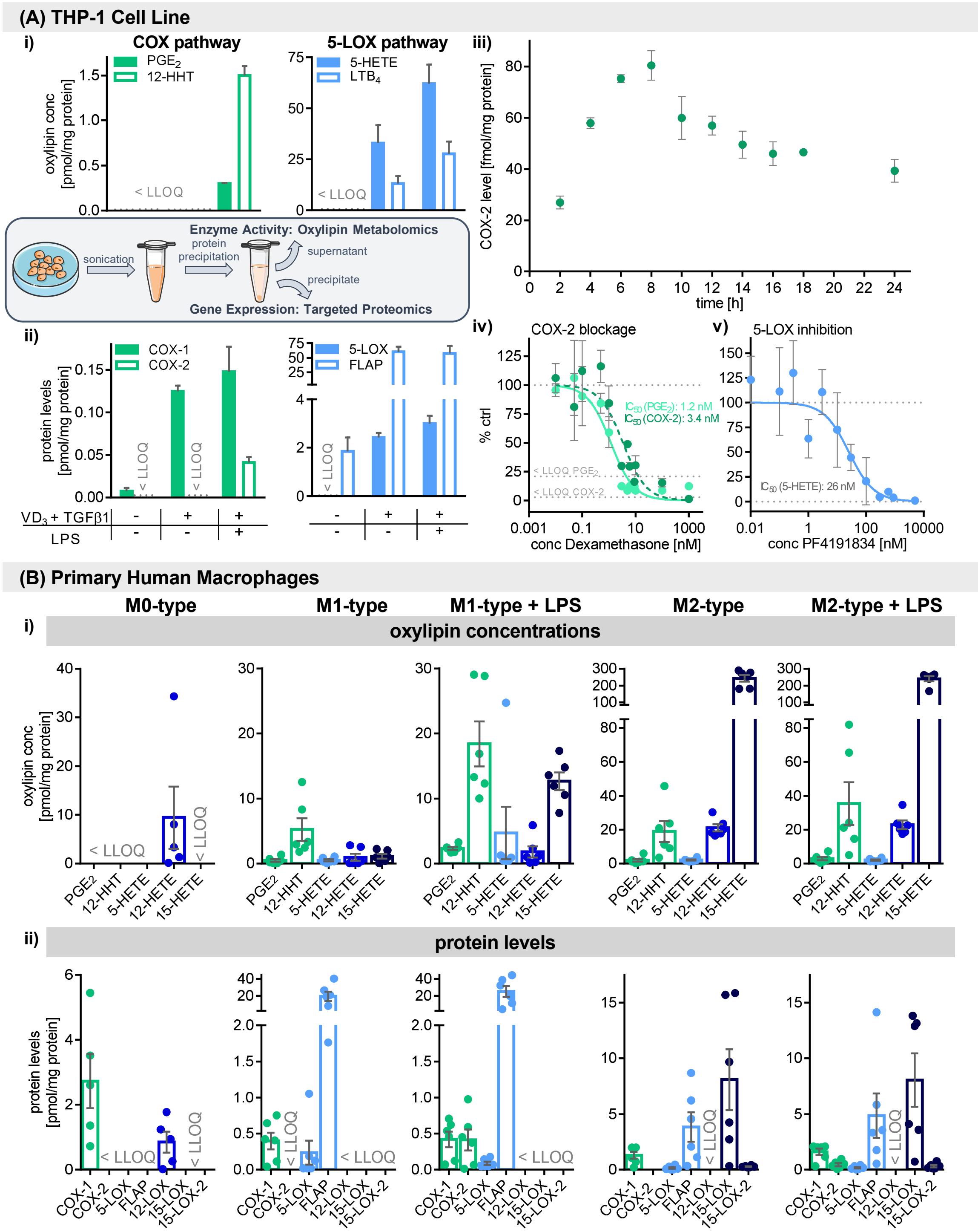
(A) THP-1 Cell Line
i)
COX pathway
PGE2
12-HHT
oxylipin conc [pmol/mg protein]
< LLOQ
5-LOX pathway
5-HETE
LTB4
iii)
COX-2 level [fmol/mg protein]
time [h]
Enzyme Activity: Oxylipin Metabolomics
sonication
protein precipitation
supernatant
precipitate
Gene Expression: Targeted Proteomics
ii)
COX-1
COX-2
protein levels [pmol/mg protein]
5-LOX
FLAP
VD3 + TGFβ1
LPS
iv)
COX-2 blockage
% ctrl
IC50 (PGE2): 1.2 nM
IC50 (COX-2): 3.4 nM
< LLOQ PGE2
< LLOQ COX-2
conc Dexamethasone [nM]
v)
5-LOX inhibition
IC50 (5-HETE): 26 nM
conc PF4191834 [nM]
(B) Primary Human Macrophages
M0-type
M1-type
M1-type + LPS
M2-type
M2-type + LPS
i)
oxylipin concentrations
PGE2
12-HHT
5-HETE
12-HETE
15-HETE
ii)
protein levels
COX-1
COX-2
5-LOX
FLAP
12-LOX
15-LOX
15-LOX-2

Fig. 4.4 (page 97):Comprehensive characterization of immune cells using combined targeted oxylipin metabolomics and proteomics: **(A)** THP-1 cell line and **(B)** primary human macrophages.

(A) i) Oxylipin concentrations and **ii)** enzyme levels in monocytic and macrophage like THP-1 cell line with and without LPS stimulation. Cells were differentiated to macrophages with 50 nM 1,25-dihydroxyvitamin D_3 (VD_3) and 1 ng/mL TGF-β1 for 72 h, with or without LPS stimulation (1 µg/mL) for 6 h (mean ± SD, n = 3). **(A) iii)** COX-2 abundance following time-dependent LPS stimulation (1 µg/mL). Shown are mean ± SD, n = 3. The potencies (IC_{50}) of COX-2 and 5-LOX inhibition by **(A) iv)** dexamethasone, calculated based on PGE_2 formation and COX-2 abundance, and **(A) v)** 5-LOX inhibitor PF4191834, calculated based on 5-HETE formation, relative to control incubations (0.1% DMSO). Shown are mean ± SD, n=3 – 6.

Correlation of **(B) i)** oxylipin formation and **ii)** enzyme levels in human macrophages derived from primary blood monocytic cells. Cells were differentiated with 10 ng/mL CSF-2 (M1-like cells) or CSF-1 (M2-like cells) for 8 days. For the final 48 h, they were treated with 10 ng/mL IFNγ (M1-like cells) or IL-4 (M2-like cells) and with or without 1 µg/mL LPS for the final 6 h. For M0-like cells, the adhered monocytes were left untreated for 7 days. Shown are mean ± SEM, n=5 – 6.

In the next step, we investigated the expression of ARA cascade genes and oxylipin formation in differently polarized primary human macrophages. The different types of polarization led to distinct oxylipin and protein patterns (**Fig. 4.4 (B) i), ii)**). In M0-like macrophages, which were derived from primary monocytic cells and incubated without cytokines for eight days, only COX-1 and 12-LOX as well as its product 12-HETE were detected. However, the presence of both enzymes is most likely attributed to platelet contamination since they are highly abundant in these cells (**Tab. 7.15**). Relevant amounts of COX-1, 5-LOX and FLAP (0.4 ± 0.1, 0.4 ± 0.2 and 19 ± 6 pmol/mg protein, respectively) were found in the macrophages polarized towards M1-like cells (10 ng/mL CSF-2 and 10 ng/mL IFNγ) with the targeted proteomics method. Oxylipins formed via these pathways (PGE_2, 12-HHT and 5-HETE) as well as 12- and 15-HETE were detected at low levels (≤ 5 pmol/mg protein) in the cells (**Fig. 4.4 (B) i), ii)**, **Tab. 7.16**). Stimulation with 1 µg/mL LPS led to strong elevation of oxylipin concentrations, e.g. 4-fold increase of PGE_2 and 12-HHT as well as an approx. 10-fold increase of 5- and 15-HETE. *PTGS2* gene expression was induced by LPS while the protein levels of COX-1 and FLAP were not modulated, and 5-LOX was slightly reduced.

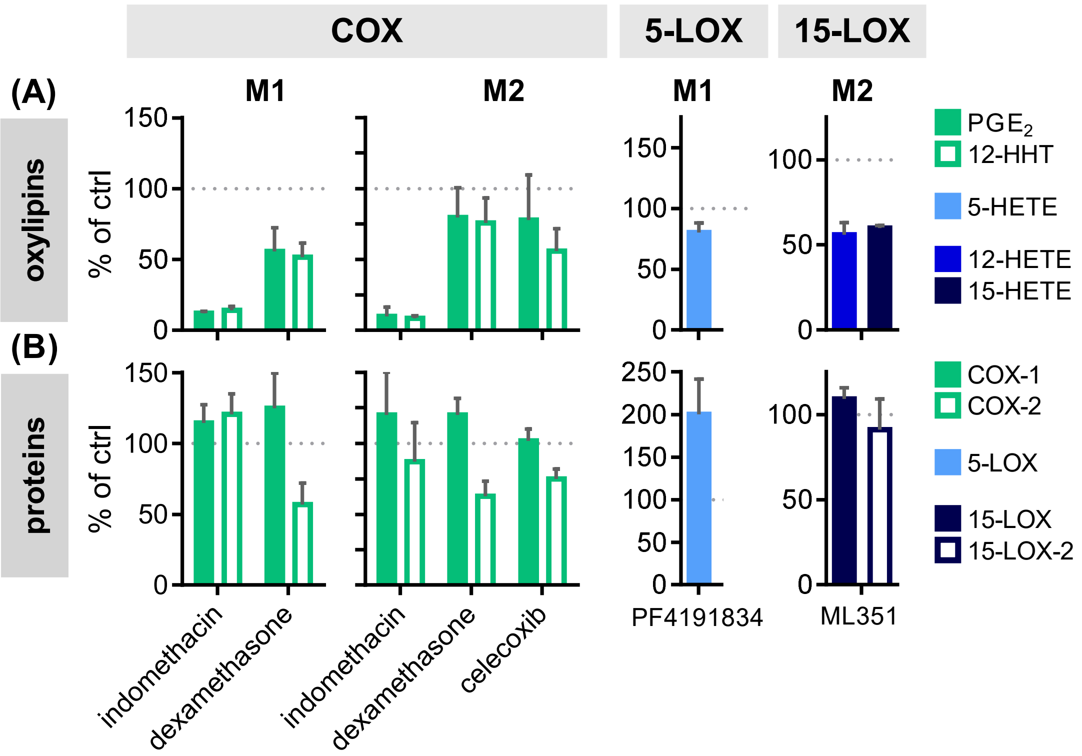

Fig. 4.5: Investigation of ARA cascade modulation in human macrophages using LC-MS/MS based targeted **(A)** oxylipin metabolomics and **(B)** proteomics. Primary blood monocytic cells were differentiated to macrophages with 10 ng/mL CSF-2 (M1-like cells) or CSF-1 (M2-like cells) for 8 days and with 10 ng/mL IFNγ (M1-like cells) or IL-4 (M2-like cells) for the final 48 h. The cells were incubated with the different drugs at the following concentrations for the final 7 h during additional LPS stimulation (1 µg/mL) for the final 6 h: 1 µM COX-1/2 inhibitor indomethacin, 100 nM dexamethasone, 5 µM COX2 inhibitor celecoxib, 5 µM 5-LOX inhibitor PF4191834, 10 µM 15-LOX inhibitor ML351 or 0.1% DMSO as control. Relative product formation was calculated based on the mean of 2 controls per donor. Shown are mean ± SEM, n = 2 – 5 donors.

LC-MS analysis of the M2-like macrophages showed an extensive protein pattern: COX-1, 5-LOX, FLAP as well as 15-LOX and 15-LOX-2 were present. High levels of 15-HETE (243 ± 20 pmol/mg protein) as well as moderate levels of 12-HETE (21 ± 2 pmol/mg) and 12-HHT (19 ± 6 pmol/mg protein) dominated the oxylipin profile while PGE_2 and 5-HETE were found at approx. 2 pmol/mg protein (**Fig. 4.4 (B) i), ii)**, **Tab. 7.16**). Interestingly, the additional LPS treatment only led to an approx. 2-fold increase of PGE_2 and 12-HHT concentrations but did not affect any of the oxylipins from the LOX pathways. Apart from COX-2 induction the levels of the ARA cascade enzymes were not changed by LPS (**Fig. 4.4 (B) i), ii)**). While the COX-2 levels were similar in both

(LPS-stimulated) M1- and M2-like cells, 5-LOX and FLAP levels were 2- and 5-fold higher in M1 and COX-1 levels were higher in M2-like macrophages. However, all of the analyzed oxylipins were higher concentrated in M2-like macrophages with the most pronounced differences between M1- and M2-like cells found for 15-HETE (> 200-fold) and 12-HETE (approx. 20-fold) followed by PGE_2, 12-HHT and 5-HETE (all approx. 4-fold).

The ARA cascade is an important target of pharmaceuticals because of its pivotal role in the regulation of the immune response and inflammation. We applied the multi-omics LC-MS/MS based approach on the quantitative characterization of pharmaceutical modulation of the ARA-cascade to demonstrate its usefulness in drug development (**Fig. 4.5**, **Tab. 7.17**). For the experiments, the primary human macrophages polarized towards M1- or M2-like phenotype were pre-incubated with the test compounds at sub-cytotoxic levels (**Fig. 7.11**) for 1 h before LPS was added for the remaining 6 h. The COX-1/-2 inhibitor indomethacin strongly reduced the PGE_2 and 12-HHT concentrations in both M1- and M2-like macrophages without relevantly modulating the COX-1 or -2 levels. Dexamethasone treatment also led to lowered concentrations of PGE_2 and 12-HHT with a more pronounced effect in M1 (approx. 50% inhibition) compared to M2-like cells (approx. 20% inhibition). The decrease of prostanoid concentrations occurred together with a decrease of the COX-2 levels which was similar in both types (approx. 40% inhibition) and did not affect COX-1. Both indomethacin and dexamethasone also markedly reduced 15-HETE formation in M1-like macrophages but had no effect in the M2-like cells. The celecoxib treatment of M2-like macrophages led to a moderate inhibition of the PGE_2 and 12-HHT formation while the concentrations of LOX products slightly increased. COX-2, 15-LOX and 15-LOX-2 levels were slightly reduced, and the selective COX-2 inhibitor did not affect COX-1 (**Fig. 4.5**, **Tab. 7.17**).

The 5-LOX inhibitor PF4191834 hardly reduced the 5-HETE concentration in the M1-like macrophages. The PGE_2 and 12-HHT concentrations were unaffected by PF4191834 while the 12- and 15-HETE concentrations were slightly reduced. Regarding the 15-LOX pathway, ML351 led to a marked inhibition of both 12- and 15-HETE formation without affecting 15-LOX and 15-LOX-2 levels. 5-LOX abundance was strongly reduced (23 ±4% of control) with only a slight effect on the 5-HETE concentration. In these incubations the PGE_2 and 12-HHT concentrations were moderately increased and the COX-1 and -2 levels were slightly elevated (**Fig. 4.5**, **Tab. 7.17**).

Conclusively, we combined our targeted oxylipin metabolomics method allowing the quantitative investigation of 198 oxylipins with an LC-MS/MS based targeted proteomics method comprising all COX and relevant LOX pathway enzymes as well as four housekeeping proteins. While the more selective detection can be achieved with the novel MRM^3 detection method, the MRM approach is characterized by higher sensitivity (in low pM range) and greater linear range up to µM concentrations. With our sensitive multi-omics approach we were able to determine the oxylipin and protein levels of immune cells in a single sample. We successfully used this approach to thoroughly characterize the ARA cascade in different immune cells and demonstrated that quantitative changes induced by pharmaceutical modulation can be determined on protein and metabolite levels.

4.4 Discussion

Oxylipins formed in the ARA cascade act as potent lipid mediators regulating many physiological functions. In order to profoundly evaluate and understand modulation of this important signaling pathway, it is crucial to investigate not only changes in metabolite concentrations, i.e. eicosanoids and oxylipins, but also on enzyme levels in parallel. Therefore, we developed a multi-omics approach comprising both LC-MS/MS based targeted oxylipin metabolomics and proteomics which can be used to quantitatively assess oxylipin and protein levels in a *single sample*.

LC-MS/MS based targeted oxylipin metabolomics is currently a well-established approach for investigating the ARA cascade [13]. Our existing platform [24, 25, 27] was further extended by 54 analytes allowing the parallel quantification of 198 oxylipins via 29 IS derived from twelve different polyunsaturated fatty acid precursors formed via the three enzymatic branches of the ARA cascade and autoxidation (**section 0, Tab. 7.12**). With that coverage, this method is currently the most comprehensive method and covers oxylipins from the most precursor fatty acids [13]. Many groups reported targeted LC-MS/MS methods consisting of 10 – 100 oxylipins [13, 36], while few are able to quantify more than 100 oxylipins [37-39]. Quantitative methods comprising over 150 oxylipins are rare [40], a method with > 200 oxylipins has only been described for relative quantification by Bao et al. [41]. Our comprehensive targeted oxylipin metabolomics method allows quantitative characterization of the complex cross-talk between the different branches of the ARA cascade and downstream products which is indispensable for a thorough understanding thereof.

The developed targeted proteomics method allows the quantitative analysis of all COX (COX-1 and -2) as well as relevant enzymes of the LOX pathway (5-LOX, 12-LOX, 15-LOX, 15-LOX-2 and FLAP) and four housekeeping proteins (β-/γ-actin, PPIB, GAPDH, CYC1). This is the first LC-MS/MS(/MS) based method for the targeted analysis of the COX and LOX pathways of the ARA cascade.

In targeted proteomics, different MS modes can be used for detection on hybrid triple quadrupole-LIT mass spectrometers. In MRM mode the analytes are quantified via the pair of a precursor and a specific fragment ion resulting from CAD induced fragmentation. In MRM³ these CAD ions are again fragmented in the LIT and an ion chromatogram is reconstructed from the secondary fragment ions [42]. We compared both approaches in detail. The LIT fill time had a strong effect on sensitivity of the MRM^3 mode. FFT was preferred over dynamic fill time (DFT) due to its better signal reproducibility and accuracy based on the resulting identical cycle times for every sample [43]. The signal intensity increased with longer FFT (**Fig. 4.2 (A)**) in line with literature [43, 44]. Long FFTs, however, have the drawback of a more rapid exhaustion of LIT capacity and breakdown of the MS signal (**Fig. 4.2 (B)**). This generally limited the upper calibration range of our MRM^3 method to low (4 nM) or medium (368 nM) nM concentrations (corresponding to 0.28 – 9.5 µg/mL enzyme equivalent; **Tab. 4.1**), comparable to other proteomics applications of MRM^3 where linearity was reported for concentrations up to 0.5 – 20 µg/mL [42, 43, 45]. Using MRM, however, robust quantification is possible over a concentration range of five orders of magnitude up to low µM concentrations (**Tab. 4.2**, **Tab. 7.14**).

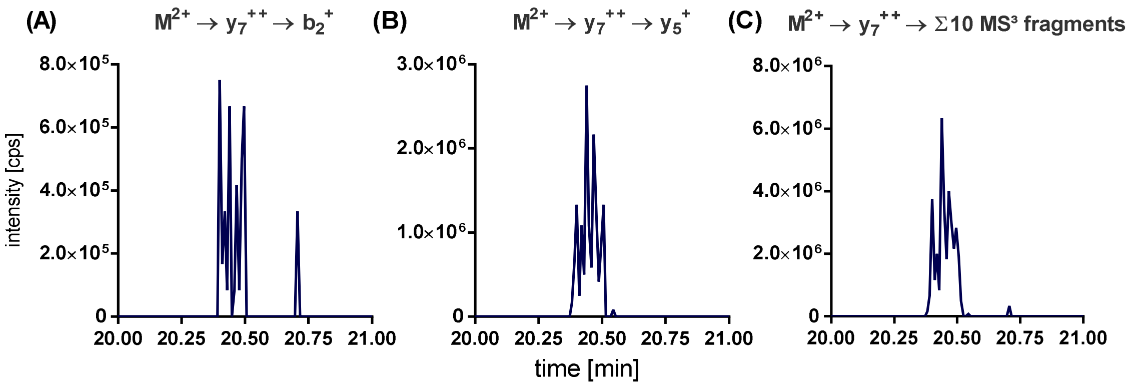

Fig. 4.6: Improving MRM^3 analysis. Summing multiple MS^3 fragments improves sensitivity for analysis and thus enables lower LLOQs in MRM^3 analysis. Shown is a standard of FDPELLFNK (COX-2; 84 pM) measured in MRM^3 mode. The signal intensities of **(A)**, **(B)** individually isolated MS^3 fragments is lower compared to **(C)** the sum of 10 MS^3 fragments.

Summing the ten most abundant fragment ions from the MS^3 spectra as “MRM^3” during data evaluation enhanced sensitivity (**Fig. 4.6**). In MRM^3, the LODs of the COX and LOX peptides were in the low to medium pM range (equivalent to 11 – 209 pg enzyme on column) and the LLOQs ranged from 75 – 840 pM, corresponding to 5 – 63 ng/mL enzyme equivalent (**Tab. 4.1**, **Fig. 7.10**). Other groups reported LLOQs in a similar range for MRM^3 based quantification on comparable instruments, e.g., several proteins were quantified down to concentrations between 10 and 80 ng/mL in human serum [42], the LLOQs of two inflammation markers were 7.8 and 156 ng/mL in plasma [45] and aquaprorin-2 water channel protein could be measured at levels down to 0.5 ng/mL in human urine (corresponding to 5 ng/mL in the measuring solution) [43]. Here, the LLOQs were two up to ten-fold lower in comparison to MRM-based quantification in matrix [42, 43, 45]. MS^3 leads to lower signal intensities than MRM due to inevitable losses during each fragmentation step. Thus, the sensitivity gain of MRM^3 strongly depends on noise reduction in biological matrices – the increased selectivity compensates the signal intensity loss [46]. The MRM detection of standards was up to ten-fold more sensitive compared to MRM^3 (**Tab. 4.1**, **Tab. 4.2**, **Fig. 7.10**) and provided sufficient sensitivity and selectivity in cell matrix. However, the additional MS^3 filtering stage proved helpful to separate the COX-2 peptide FDPELLFNK from closely eluting background matrix in THP-1 cells (**Fig. 4.3 (B) i), ii)**).

A relevant parameter for quantitative analysis is the number of data points per peak which is defined by the instrument cycle time. In order to enable MRM^3, the MS method was subdivided into ten time periods (**Fig. 4.3 (A) i), Tab. 4.1**) in order to keep these within an accepted range of 10 – 15 data points per peak. Summing the excitation time (25 ms for each MS^3 fragmentation), FFT (250/100 and 25 ms) and individual scan times per peptide (450 – 700 Da), the cycle times per period in the MRM^3 method were all below 600 ms, thus, allowing the detection of acceptable 9 – 12 data points per peak. The long cycle times of the LIT have already been addressed as drawback of MRM^3 methodology drastically limiting the number of concurrently measurable analytes [46, 47] and thus, multiplexing capacities. This might be one of the reasons why MRM^3 has not (yet) been employed for the analysis of (highly) multiplexed methods, e.g., the targeted analysis of pathway proteomes.

In our view, due to these drawbacks: i) limited linear range, ii) higher LLOQs and iii) limited multiplexing capacities based on the long cycle times and the use of time periods, the MRM^3 method is not favored for routine analysis of pathway proteomes such as the ARA cascade. However, it serves as complimentary method, in case of heavy matrix background interference disturbing MRM analysis.

Combining this targeted proteomics approach with our oxylipin metabolomics method, we comprehensively characterized the ARA cascade in immune cells for the first time solely by LC-MS/MS in a single sample. This is especially advantageous for experiments with limited biological material such as primary human cells or tissue also known as single platform-multi-omics [48].

The analysis of monocytic THP-1 cells showed that differentiation with VD_3 and TGFβ1 to macrophage-like cells led to the induction of *ALOX5* gene expression together with a drastic increase in levels of oxylipins (**Fig. 4.4 (A) i), ii)**). VD_3/TGFβ1 based differentiation and concomitant increase of *ALOX5* gene activity have been described for several myeloid cell lines (HL-60, Mono Mac 6, THP-1) [49-52]. Concomitant upregulation of the FLAP protein or mRNA levels (**Fig. 4.4 (A) iii)**) was also reported during similar treatments in peripheral blood monocytic cells [53] or the monocytic cell line U937 [54].

The LPS treatment induced upregulation of COX-2 abundance together with increased product formation (**Fig. 4.4 (A) i) – iii)**). With the quantitative multi-omics approach, we could show a dose-dependent inhibition of LPS-induced PGE_2 formation <u>and</u> *PTGS2* gene expression by dexamethasone for the first time. Both determined IC_{50} were similar (IC_{50} = 1.2 nM and 3.4 nM; **Fig. 4.4 (A) iv)**). This is consistent with the described mechanism of dexamethasone i.a. preventing the *PTGS2* gene expression by its mRNA destabilization [55] and concomitantly reducing PGE_2 formation. The remarkable potencies of dexamethasone in THP-1 macrophages were well within the range determined for inhibited PGE_2 formation (IC_{50} = 1.6 nM, 95% CI: 1.4 – 1.9 nM) in LPS stimulated human monocytes [56]. No IC_{50} values have been determined for the inhibition of the *PTGS2* gene expression with the commonly used semi-quantitative western blot method (relevant inhibition detected at 3 nM – 1µM)

[56, 57], thus, the novel targeted proteomics method offers new opportunities for such detailed characterization. The competitive 5-LOX inhibitor PF4191834 strongly inhibited 5-LOX product formation in differentiated and LPS-treated THP-1 cells without affecting *ALOX5* gene expression (IC_{50} (5-HETE) = 26 nM, **Fig. 4.4 (A) v)**) fivefold more potently than in human whole blood assay (IC_{50} (LTB_4) = 130 ± 10 nM) [58]. The commonly used iron-ligand inhibitor zileuton as well as the FLAP inhibitor MK886 had only low inhibitory potential in this cell model which might be caused by interreferences induced by the VD_3/TGFβ1 and/or LPS treatment.

The novel multi-omics approach allows to obtain true *quantitative* information on the oxylipin concentrations and enzyme abundance levels with sensitive LC-MS/MS methods. For the first time, differently polarized primary human macrophages were characterized with this unique approach and displayed distinct oxylipin and protein patterns for each type (**Fig. 4.4 (B) i), ii)**). In the non-CSF treated macrophages (M0-like cells) only COX-1, 12-LOX and its product 12-HETE were found. This pattern strongly resembles that of platelets (**Tab. 7.15**) [59] which often contaminate monocyte preparations. The presence of other enzymes (5-LOX, FLAP and 15-LOX-2) and oxylipins at very low abundances as previously reported in M0-like macrophages [21] could not be supported.

5-LOX and FLAP were detected in M1- (CSF-2 and IFNγ-treated) and M2-like (CSF-1 and IL-4 treated) macrophages together with the corresponding oxylipins formed via this pathway (**Fig. 4.4 (B) i), ii), Tab. 7.16**). Varying 5-LOX levels between M1- and M2-like macrophages have been described [21, 60, 61] and thus, might be donor-dependent. However, the relatively low 5-HETE concentrations in both macrophage types suggest only low 5-LOX activity and the detected 5-HETE levels could also result from autoxidation. Similarly, the data from the multi-omics investigation showing low levels of 12- and 15-HETE in M1-like macrophages could not be associated to LOX enzyme activity, since 12- and 15-LOX as well as 15-LOX-2 were below the detection limits and thus, might be also formed autoxidatively (**Fig. 4.4 (B) i), ii), Tab. 7.16**). The correlation between the 10-fold increased 15-HETE concentration and LPS-stimulated COX-2 upregulation in our work is consistent with previous studies demonstrating that 15-HETE is a side product of COX(-2) [62, 63]. In the M2-like macrophages the multi-omics approach showed that high 15-HETE concentrations dominated their lipid mediator profile which coincided with the presence of 15-LOX and 15-LOX-2 in these cells. This is expected because IL-4 is used during differentiation to M2-like macrophages, causing a strong elevation of 15-LOX and 15-LOX-2 abundances [21, 64, 65]. The dual reaction specificity of 15-LOX [66, 67] giving rise to both 15-HETE as well as 12-HETE also explains the formation of the second most abundant oxylipin 12-HETE in M2-like macrophages which was detected in parallel with the targeted oxylipin metabolomics method. Constitutive *PTGS1* gene expression and LPS induced *PTGS2* expression were measured in both macrophage types. COX-2 abundances in both macrophage types were comparable, but LPS stimulation led to a more pronounced increase in product synthesis (PGE_2 and 12-HHT) in M1- vs. M2-like macrophages (**Fig. 4.4 (B) i), ii), Tab. 7.16**). Higher PGE_2 formation in M1-like cells is also in line with previous reports [21, 60].

The dual targeted oxylipin metabolomics and proteomics approach also allows the detailed investigation of quantitative changes induced by pharmaceuticals on both metabolite and enzyme levels of the ARA cascade (**Fig. 4.5**, **Tab. 7.17**). The COX inhibitors hampered the synthesis of PGE_2 and 12-HHT in M1- and M2-like macrophages. Indomethacin almost completely blocked product formation – inhibiting COX-1 and COX-2 [68] without affecting the enzyme abundance. Dexamethasone and celecoxib showed less inhibitory effects on product formation due to their specificity to only target COX-2 by direct specific inhibition in case of celecoxib [68] or reduction of its expression by the glucocorticoid dexamethasone [55]. The effect of the latter is also reflected in the results of the targeted proteomics analysis: markedly decreased COX-2 protein levels in M1- and M2-like macrophages (**Fig. 4.5 (B)**). Interestingly, 15-HETE formation was reduced to a similar extent as the COX pathway products in indomethacin- or dexamethasone-treated M1-, but not in the M2-like macrophages. This again demonstrated that 15-HETE must be predominately formed as COX product in M1-like macrophages as byproduct to prostaglandin synthesis [62, 63] while 15-HETE is mainly produced in M2-like macrophages by 15-LOX and 15-LOX-2. The finding underlines that the complexity of the ARA cascade can only be addressed with the use of comprehensive methods such as our multi-omics approach. It also showed that the other prominent LOX pathway products were hardly affected by the COX inhibitors, and only celecoxib caused a notable shunt (increased formation) towards the formation of the hydroxy-fatty acids (**Tab. 7.17**). The 5-LOX inhibitor PF4191834 hardly inhibited the 5-HETE formation in M1-like macrophages without a substrate shunt towards the other enzymes (**Fig. 4.5 (A)**, **Tab. 7.17**) at a concentration forty-fold above the reported IC_{50} in human whole blood [58]. These results from the multi-omics analysis thus indicate that 5-LOX is hardly active in M1-like macrophages and that 5-HETE seems to be predominantly formed by autoxidation. The determined oxylipin pattern in M2-like macrophages again highlighted the dual reaction specificity of the 15-LOX [66, 67] as its inhibitor ML351 reduced both 12- and 15-HETE concentrations to the same extent. It showed only minimal inhibitory activity towards the other ARA cascade enzymes as described [69] and rather promoted a substrate shunt towards the COX products. The parallel analysis of the cells with the targeted proteomics method supported that the inhibitor acted only on enzyme activity as the 15-LOX level remained unchanged (**Fig. 4.5**, **Tab. 7.17**).

With our comprehensive multi-omics approach we showed clear correlations between the product and enzyme patterns in different human immune cells. Quantitative changes induced by different pharmaceuticals were assessed on both oxylipin as well as protein levels providing insights into their modes of action on the modulation of the ARA cascade.

4.5 Conclusion

Our new multi-omics approach comprised of targeted oxylipin metabolomics and proteomics allows the quantitative investigation of 198 oxylipins and all COX (COX-1 and -2), relevant LOX pathway enzymes (5-, 12-, 15-LOX, 15-LOX-2 and FLAP) as well as four housekeeping proteins from a single sample per LC-MS/MS. MRM based detection in proteomics is more favorable compared to MRM³ for investigation of the ARA cascade in immune cells due to its higher sensitivity, greater linear range and higher multiplexing capacities. However, in case of matrix interference MRM³ can be helpful. The application of the combined sensitive oxylipin metabolomics and proteomics approach to different human immune cells proved its usefulness in the thorough characterization of the ARA cascade. Here, it allowed the examination of quantitative changes induced by pharmaceuticals on oxylipin and enzyme abundance levels. Thus, this multi-omics strategy is an indispensable tool to study molecular modes of action involved in the modulation of the ARA cascade and can be used in the future for the investigation e.g. of novel pharmaceuticals or phytochemicals.

4.6 References

1. Gabbs M, Leng S, Devassy JG, Monirujjaman M, and Aukema HM (2015) Advances in Our Understanding of Oxylipins Derived from Dietary PUFAs. *Adv Nutr,* 6(5), 513-540; doi: 10.3945/an.114.007732.
2. Yu R, Xiao L, Zhao G, Christman JW, and van Breemen RB (2011) Competitive Enzymatic Interactions Determine the Relative Amounts of Prostaglandins E_2 and D_2. *J Pharmacol Exp Ther,* 339(2), 716-725; doi: 10.1124/jpet.111.185405.
3. Matsunobu T, Okuno T, Yokoyama C, and Yokomizo T (2013) Thromboxane A synthase-independent production of 12-hydroxyheptadecatrienoic acid, a BLT2 ligand. *J Lipid Res,* 54(11), 2979-2987; doi: 10.1194/jlr.M037754.
4. Ricciotti E and FitzGerald GA (2011) Prostaglandins and Inflammation. *Atertio Thromb Vasc Biol,* 31(5), 986-1000; doi: 10.1161/Atvbaha.110.207449.

5. Sheppe AEF, Edelmann MJ, and Ottemann KM (2021) Roles of Eicosanoids in Regulating Inflammation and Neutrophil Migration as an Innate Host Response to Bacterial Infections. *Infect Immun,* 89(8), e00095-21; doi: 10.1128/IAI.00095-21.
6. Okuno T and Yokomizo T (2021) Metabolism and biological functions of 12(S)-hydroxyheptadeca-5Z,8E,10E-trienoic acid. *Prostaglandins Other Lipid Mediat,* 152, 106502; doi: 10.1016/j.prostaglandins.2020.106502.
7. Rund KM, Nolte F, Doricic J, Greite R, Schott S, Lichtinghagen R, Gueler F, and Schebb NH (2020) Clinical blood sampling for oxylipin analysis – effect of storage and pneumatic tube transport of blood on free and total oxylipin profile in human plasma and serum. *Analyst,* 145(6), 2378-2388; doi: 10.1039/C9AN01880H.
8. Kuhn H, Banthiya S, and van Leyen K (2015) Mammalian lipoxygenases and their biological relevance. *Biochim Biophys Acta, Mol Cell Biol Lipids,* 1851(4), 308-330; doi: 10.1016/j.bbalip.2014.10.002.
9. Serhan CN, Chiang N, and Van Dyke TE (2008) Resolving inflammation: dual anti-inflammatory and pro-resolution lipid mediators. *Nat Rev Immunol,* 8(5), 349-61; doi: 10.1038/nri2294.
10. Schebb NH, Kühn H, Kahnt AS, Rund KM, O'Donnell VB, Flamand N, Peters-Golden M, Jakobsson P-J, Weylandt KH, Rohwer N, et al. (2022) Formation, Signaling and Occurrence of Specialized Pro-Resolving Lipid Mediators—What is the Evidence so far? *Front Pharmacol,* 13; doi: 10.3389/fphar.2022.838782.
11. Pinu FR, Beale DJ, Paten AM, Kouremenos K, Swarup S, Schirra HJ, and Wishart D (2019) Systems Biology and Multi-Omics Integration: Viewpoints from the Metabolomics Research Community. *Metabolites,* 9(4), 76; doi: 10.3390/metabo9040076.
12. Canzler S, Schor J, Busch W, Schubert K, Rolle-Kampczyk UE, Seitz H, Kamp H, von Bergen M, Buesen R, and Hackermüller J (2020) Prospects and challenges of multi-omics data integration in toxicology. *Arch Toxicol,* 94(2), 371-388; doi: 10.1007/s00204-020-02656-y.
13. Gladine C, Ostermann AI, Newman JW, and Schebb NH (2019) MS-based targeted metabolomics of eicosanoids and other oxylipins: Analytical and inter-individual variabilities. *Free Radical Biol Med,* 144, 72-89; doi: 10.1016/j.freeradbiomed.2019.05.012.
14. Hanáková Z, Hošek J, Kutil Z, Temml V, Landa P, Vaněk T, Schuster D, Dall'Acqua S, Cvačka J, Polanský O, et al. (2017) Anti-inflammatory Activity of Natural Geranylated Flavonoids: Cyclooxygenase and Lipoxygenase Inhibitory Properties and Proteomic Analysis. *J Nat Prod,* 80(4), 999-1006; doi: 10.1021/acs.jnatprod.6b01011.
15. Rodríguez-Blanco G, Zeneyedpour L, Duijvesz D, Hoogland AM, Verhoef EI, Kweldam CF, Burgers PC, Sillevis Smitt P, Bangma CH, Jenster G, et al. (2018) Tissue proteomics outlines AGR2 AND LOX5 as markers for biochemical recurrence of prostate cancer. *Oncotarget,* 9(92); doi: 10.18632/oncotarget.26342.
16. Codreanu SG, Hoeksema MD, Slebos RJC, Zimmerman LJ, Rahman SMJ, Li M, Chen S-C, Chen H, Eisenberg R, Liebler DC, et al. (2017) Identification of Proteomic Features To Distinguish Benign Pulmonary Nodules from Lung Adenocarcinoma. *J Proteome Res,* 16(9), 3266-3276; doi: 10.1021/acs.jproteome.7b00245.
17. Jethwaney D, Islam MR, Leidal KG, de Bernabe DB-V, Campbell KP, Nauseef WM, and Gibson BW (2007) Proteomic analysis of plasma membrane and secretory vesicles from human neutrophils. *Proteome Sci,* 5(1), 12; doi: 10.1186/1477-5956-5-12.

18. Hartung NM, Ostermann AI, Immenschuh S, and Schebb NH (2021) Combined Targeted Proteomics and Oxylipin Metabolomics for Monitoring of the COX-2 Pathway. *Proteomics,* 21(3-4), 1900058; doi: 10.1002/pmic.201900058.
19. Sabido E, Quehenberger O, Shen Q, Chang CY, Shah I, Armando AM, Andreyev A, Vitek O, Dennis EA, and Aebersold R (2012) Targeted Proteomics of the Eicosanoid Biosynthetic Pathway Completes an Integrated Genomics-Proteomics-Metabolomics Picture of Cellular Metabolism. *Mol Cell Proteomics,* 11(7); doi: 10.1074/Mcp.M111.014746.
20. Tahir A, Bileck A, Muqaku B, Niederstaetter L, Kreutz D, Mayer RL, Wolrab D, Meier SM, Slany A, and Gerner C (2017) Combined Proteome and Eicosanoid Profiling Approach for Revealing Implications of Human Fibroblasts in Chronic Inflammation. *Anal Chem,* 89(3), 1945-1954; doi: 10.1021/acs.analchem.6b04433.
21. Ebert R, Cumbana R, Lehmann C, Kutzner L, Toewe A, Ferreirós N, Parnham MJ, Schebb NH, Steinhilber D, and Kahnt AS (2020) Long-term stimulation of toll-like receptor-2 and -4 upregulates 5-LO and 15-LO-2 expression thereby inducing a lipid mediator shift in human monocyte-derived macrophages. *Biochim Biophys Acta, Mol Cell Biol Lipids,* 1865(9), 158702; doi: 10.1016/j.bbalip.2020.158702.
22. Dhurat R and Sukesh M (2014) Principles and methods of preparation of platelet-rich plasma: A review and author's perspective. *J Cutan Aesthet Surg,* 7(4), 189-197; doi: 10.4103/0974-2077.150734.
23. O'Brien J, Wilson I, Orton T, and Pognan F (2000) Investigation of the Alamar Blue (resazurin) fluorescent dye for the assessment of mammalian cell cytotoxicity. *Eur J Biochem,* 267(17), 5421-5426; doi: 10.1046/j.1432-1327.2000.01606.x.
24. Rund KM, Ostermann AI, Kutzner L, Galano JM, Oger C, Vigor C, Wecklein S, Seiwert N, Durand T, and Schebb NH (2018) Development of an LC-ESI(-)-MS/MS method for the simultaneous quantification of 35 isoprostanes and isofurans derived from the major n3- and n6-PUFAs. *Anal Chim Acta,* 1037, 63-74; doi: 10.1016/j.aca.2017.11.002.
25. Kutzner L, Rund KM, Ostermann AI, Hartung NM, Galano JM, Balas L, Durand T, Balzer MS, David S, and Schebb NH (2019) Development of an Optimized LC-MS Method for the Detection of Specialized Pro-Resolving Mediators in Biological Samples. *Front Pharmacol,* 10; doi: 10.3389/fphar.2019.00169.
26. Smith PK, Krohn RI, Hermanson GT, Mallia AK, Gartner FH, Provenzano MD, Fujimoto EK, Goeke NM, Olson BJ, and Klenk DC (1985) Measurement of protein using bicinchoninic acid. *Anal Biochem,* 150(1), 76-85; doi: 10.1016/0003-2697(85)90442-7.
27. Koch E, Mainka M, Dalle C, Ostermann AI, Rund KM, Kutzner L, Froehlich L-F, Bertrand-Michel J, Gladine C, and Schebb NH (2020) Stability of oxylipins during plasma generation and long-term storage. *Talanta,* 217, 121074; doi: 10.1016/j.talanta.2020.121074.
28. Hartung NM, Mainka M, Kampschulte N, Ostermann AI, and Schebb NH (2019) A strategy for validating concentrations of oxylipin standards for external calibration. *Prostaglandins Other Lipid Mediat,* 141, 22-24; doi: 10.1016/j.prostaglandins.2019.02.006.
29. Johnson M, Zaretskaya I, Raytselis Y, Merezhuk Y, McGinnis S, and Madden TL (2008) NCBI BLAST: a better web interface. *Nucleic Acids Res,* 36(suppl_2), W5-W9; doi: 10.1093/nar/gkn201.
30. Schaeffer M, Gateau A, Teixeira D, Michel PA, Zahn-Zabal M, and Lane L (2017) The neXtProt peptide uniqueness checker: a tool for the proteomics community. *Bioinformatics,* 33(21), 3471-3472; doi: 10.1093/bioinformatics/btx318.

31. Gasteiger E, Hoogland C, Gattiker A, Duvaud Se, Wilkins MR, Appel RD, and Bairoch A, (2005) Protein Identification and Analysis Tools on the ExPASy Server, in The Proteomics Protocols Handbook, Walker JM, Editor. Humana Press: Totowa, NJ, 571-607.
32. Fannes T, Vandermarliere E, Schietgat L, Degroeve S, Martens L, and Ramon J (2013) Predicting Tryptic Cleavage from Proteomics Data Using Decision Tree Ensembles. *J Proteome Res,* 12(5), 2253-2259; doi: 10.1021/pr4001114.
33. Krokhin OV and Spicer V (2009) Peptide Retention Standards and Hydrophobicity Indexes in Reversed-Phase High-Performance Liquid Chromatography of Peptides. *Anal Chem,* 81(22), 9522-9530; doi: 10.1021/ac9016693.
34. The UniProt Consortium (2018) UniProt: a worldwide hub of protein knowledge. *Nucleic Acids Res,* 47(D1), D506-D515; doi: 10.1093/nar/gky1049.
35. Hornbeck PV, Zhang B, Murray B, Kornhauser JM, Latham V, and Skrzypek E (2015) PhosphoSitePlus, 2014: mutations, PTMs and recalibrations. *Nucleic Acids Res,* 43(D1), D512-D520; doi: 10.1093/nar/gku1267.
36. Liakh I, Pakiet A, Sledzinski T, and Mika A (2020) Methods of the Analysis of Oxylipins in Biological Samples. *Molecules,* 25(2), 349; doi: 10.3390/molecules25020349.
37. Song J, Liu X, Wu J, Meehan MJ, Blevitt JM, Dorrestein PC, and Milla ME (2013) A highly efficient, high-throughput lipidomics platform for the quantitative detection of eicosanoids in human whole blood. *Anal Biochem,* 433(2), 181-188; doi: 10.1016/j.ab.2012.10.022.
38. Chen G-y and Zhang Q (2019) Comprehensive analysis of oxylipins in human plasma using reversed-phase liquid chromatography-triple quadrupole mass spectrometry with heatmap-assisted selection of transitions. *Anal Bioanal Chem,* 411(2), 367-385; doi: 10.1007/s00216-018-1446-3.
39. Astarita G, McKenzie JH, Wang B, Strassburg K, Doneanu A, Johnson J, Baker A, Hankemeier T, Murphy J, Vreeken RJ, et al. (2014) A Protective Lipidomic Biosignature Associated with a Balanced Omega-6/Omega-3 Ratio in fat-1 Transgenic Mice. *PLoS One,* 9(4), e96221; doi: 10.1371/journal.pone.0096221.
40. Quehenberger O, Dahlberg-Wright S, Jiang J, Armando AM, and Dennis EA (2018) Quantitative determination of esterified eicosanoids and related oxygenated metabolites after base hydrolysis. *J Lipid Res,* 59(12), 2436-2445; doi: 10.1194/jlr.D089516.
41. Bao Q, Liu Y, Song H, Yang N, Ai D, Zhu Y, and Zhang X (2018) Spectrum evaluation-assisted eicosanoid metabolomics for global eicosanoid profiling in human vascular endothelial cells. *Clin Exp Pharmacol Physiol,* 45(1), 98-108; doi: 10.1111/1440-1681.12825.
42. Fortin T, Salvador A, Charrier JP, Lenz C, Bettsworth F, Lacoux X, Choquet-Kastylevsky G, and Lemoine J (2009) Multiple Reaction Monitoring Cubed for Protein Quantification at the Low Nanogram/Milliliter Level in Nondepleted Human Serum. *Anal Chem,* 81(22), 9343-9352; doi: 10.1021/ac901447h.
43. Jaffuel A, Lemoine J, Aubert C, Simon R, Léonard J-F, Gautier J-C, Pasquier O, and Salvador A (2013) Optimization of liquid chromatography–multiple reaction monitoring cubed mass spectrometry assay for protein quantification: Application to aquaporin-2 water channel in human urine. *J Chromatogr,* 1301, 122-130; doi: 10.1016/j.chroma.2013.05.068.
44. Korte R and Brockmeyer J (2016) MRM3-based LC-MS multi-method for the detection and quantification of nut allergens. *Anal Bioanal Chem,* 408(27), 7845-7855; doi: 10.1007/s00216-016-9888-y.

45. Jeudy J, Salvador A, Simon R, Jaffuel A, Fonbonne C, Léonard J-F, Gautier J-C, Pasquier O, and Lemoine J (2014) Overcoming biofluid protein complexity during targeted mass spectrometry detection and quantification of protein biomarkers by MRM cubed (MRM3). *Anal Bioanal Chem,* 406(4), 1193-1200; doi: 10.1007/s00216-013-7266-6.
46. Lemoine J, Fortin T, Salvador A, Jaffuel A, Charrier J-P, and Choquet-Kastylevsky G (2012) The current status of clinical proteomics and the use of MRM and MRM3 for biomarker validation. *Expert Rev Mol Diagn,* 12(4), 333-342; doi: 10.1586/erm.12.32.
47. Schmidlin T, Garrigues L, Lane CS, Mulder TC, van Doorn S, Post H, de Graaf EL, Lemeer S, Heck AJR, and Altelaar AFM (2016) Assessment of SRM, MRM3, and DIA for the targeted analysis of phosphorylation dynamics in non-small cell lung cancer. *Proteomics,* 16(15-16), 2193-2205; doi: 10.1002/pmic.201500453.
48. Blum BC, Mousavi F, and Emili A (2018) Single-platform 'multi-omic' profiling: unified mass spectrometry and computational workflows for integrative proteomics–metabolomics analysis. *Mol Omics,* 14(5), 307-319; doi: 10.1039/C8MO00136G.
49. Brungs M, Radmark O, Samuelsson B, and Steinhilber D (1994) On the Induction of 5-Lipoxygenase Expression and Activity in HL-60 Cells: Effects of Vitamin D3, Retinoic Acid, DMSO and TGFβ. *Biochem Biophys Res Commun,* 205(3), 1572-1580; doi: 10.1006/bbrc.1994.2846.
50. Brungs M, Radmark O, Samuelsson B, and Steinhilber D (1995) Sequential Induction Of 5-Lipoxygenase Gene-Expression And Activity In Mono-Mac-6 Cells By Transforming Growth-Factor-Beta And 1,25-Dihydroxyvitamin-D3. *Proc Natl Acad Sci U S A,* 92(1), 107-111; doi: 10.1073/pnas.92.1.107.
51. Wöbke TK, von Knethen A, Steinhilber D, and Sorg BL (2013) CD69 Is a TGF-β/1α,25-dihydroxyvitamin D3 Target Gene in Monocytes. *PLoS One,* 8(5), e64635; doi: 10.1371/journal.pone.0064635.
52. Schlag K, Steinhilber D, Karas M, and Sorg BL (2020) Analysis of proximal ALOX5 promoter binding proteins by quantitative proteomics. *FEBS J,* 287(20), 4481-4499; doi: 10.1111/febs.15259.
53. Coffey MJ, Gyetko M, and Peters-Golden M (1993) 1,25-Dihydroxyvitamin D3 upregulates 5-lipoxygenase metabolism and 5-lipoxygenase activating protein in peripheral blood monocytes as they differentiate into mature macrophages. *J Lipid Mediators,* 6(1-3), 43-51.
54. Gingras M-C and Margolin JF (2000) Differential expression of multiple unexpected genes during U937 cell and macrophage differentiation detected by suppressive subtractive hybridization. *Exp Hematol,* 28(1), 65-76; doi: 10.1016/S0301-472X(99)00126-5.
55. Lasa M, Brook M, Saklatvala J, and Clark AR (2001) Dexamethasone Destabilizes Cyclooxygenase 2 mRNA by Inhibiting Mitogen-Activated Protein Kinase p38. *Mol Cell Biol,* 21(3), 771-780; doi: 10.1128/MCB.21.3.771-780.2001.
56. Willenberg I, Meschede AK, and Schebb NH (2015) Determining cyclooxygenase-2 activity in three different test systems utilizing online-solid phase extraction-liquid chromatography-mass spectrometry for parallel quantification of prostaglandin E(2), D(2) and thromboxane B(2). *J Chromatogr A,* 1391, 40-8; doi: 10.1016/j.chroma.2015.02.059.
57. Laufer S, Zechmeister P, and Klein T (1999) Development of an in-vitro test system for the evaluation of cyclooxygenase-2 inhibitors. *Inflammation Res,* 48(3), 133-138; doi: 10.1007/s000110050436.
58. Masferrer JL, Zweifel BS, Hardy M, Anderson GD, Dufield D, Cortes-Burgos L, Pufahl RA, and Graneto M (2010) Pharmacology of PF-4191834, a Novel, Selective Non-

Redox 5-Lipoxygenase Inhibitor Effective in Inflammation and Pain. *J Pharmacol Exp Ther,* 334(1), 294; doi: 10.1124/jpet.110.166967.

59. O'Donnell VB, Murphy RC, and Watson SP (2014) Platelet Lipidomics. *Circul Res,* 114(7), 1185-1203; doi: 10.1161/CIRCRESAHA.114.301597.
60. Werner M, Jordan PM, Romp E, Czapka A, Rao Z, Kretzer C, Koeberle A, Garscha U, Pace S, Claesson H-E, et al. (2019) Targeting biosynthetic networks of the proinflammatory and proresolving lipid metabolome. *FASEB J,* 33(5), 6140-6153; doi: 10.1096/fj.201802509R.
61. Werz O, Gerstmeier J, Libreros S, De la Rosa X, Werner M, Norris PC, Chiang N, and Serhan CN (2018) Human macrophages differentially produce specific resolvin or leukotriene signals that depend on bacterial pathogenicity. *Nat Comm,* 9(1), 59; doi: 10.1038/s41467-017-02538-5.
62. Hecker M, Ullrich V, Fischer C, and Meese CO (1987) Identification of novel arachidonic acid metabolites formed by prostaglandin H synthase. *Eur J Biochem,* 169(1), 113-123; doi: 10.1111/j.1432-1033.1987.tb13587.x.
63. O'Neill GP, Mancini JA, Kargman S, Yergey J, Kwan MY, Falgueyret JP, Abramovitz M, Kennedy BP, Ouellet M, and Cromlish W (1994) Overexpression of human prostaglandin G/H synthase-1 and -2 by recombinant vaccinia virus: inhibition by nonsteroidal anti-inflammatory drugs and biosynthesis of 15-hydroxyeicosatetraenoic acid. *Mol Pharmacol,* 45(2), 245-254.
64. Wuest SJA, Crucet M, Gemperle C, Loretz C, and Hersberger M (2012) Expression and regulation of 12/15-lipoxygenases in human primary macrophages. *Atherosclerosis,* 225(1), 121-127; doi: 10.1016/j.atherosclerosis.2012.07.022.
65. Snodgrass RG, Zezina E, Namgaladze D, Gupta S, Angioni C, Geisslinger G, Lütjohann D, and Brüne B (2018) A Novel Function for 15-Lipoxygenases in Cholesterol Homeostasis and CCL17 Production in Human Macrophages. *Front Immunol,* 9(1906); doi: 10.3389/fimmu.2018.01906.
66. Kühn H, Barnett J, Grunberger D, Baecker P, Chow J, Nguyen B, Bursztyn-Pettegrew H, Chan H, and Sigal E (1993) Overexpression, purification and characterization of human recombinant 15-lipoxygenase. *Biochim Biophys Acta, Lipids Lipid Metab,* 1169(1), 80-89; doi: 10.1016/0005-2760(93)90085-N.
67. Kutzner L, Goloshchapova K, Heydeck D, Stehling S, Kuhn H, and Schebb NH (2017) Mammalian ALOX15 orthologs exhibit pronounced dual positional specificity with docosahexaenoic acid. *Biochim Biophys Acta, Mol Cell Biol Lipids,* 1862(7), 666-675; doi: 10.1016/j.bbalip.2017.04.001.
68. Willenberg I, Meschede AK, Gueler F, Jang MS, Shushakova N, and Schebb NH (2015) Food Polyphenols Fail to Cause a Biologically Relevant Reduction of COX-2 Activity. *PLoS One,* 10(10), e0139147; doi: 10.1371/journal.pone.0139147.
69. Rai G, Joshi N, Jung JE, Liu Y, Schultz L, Yasgar A, Perry S, Diaz G, Zhang Q, Kenyon V, et al. (2014) Potent and Selective Inhibitors of Human Reticulocyte 12/15-Lipoxygenase as Anti-Stroke Therapies. *J Med Chem,* 57(10), 4035-4048; doi: 10.1021/jm401915r.

Chapter 5

Concluding Remarks and Future Perspectives

This thesis sets the basis for a comprehensive analysis of the arachidonic acid (ARA) cascade through establishing a targeted proteomics method and the extension of the existing targeted oxylipin metabolomics platform.

Changes in the oxylipin pattern associated with disease, inflammation, medication or nutrition are particularly relevant. However, with the oxylipin analysis alone no conclusions can be drawn regarding the mechanisms responsible for the changes of the oxylipin pattern in cell culture or *in vivo* experiments since, e.g., direct enzyme inhibition as well as decreased gene expression resulting in attenuated enzyme abundance can both lead to reduced oxylipin levels. The accompanying analysis of enzyme/protein levels in order to address this question is often carried out by traditional bioanalytical methods such as immuno-blotting which only leads to semi-quantitative results.

The liquid chromatography-tandem mass spectrometry (LC-MS/MS) based targeted proteomics method developed during this thesis (*chapters 2 and 4*) enables quantitative analysis of multiple proteins in parallel to oxylipin analysis with high sensitives in one sample. The establishment of such a method requires careful development. Next to helpful *in silico* tools, experimental confirmation is essential for the selection of appropriate proteotypic peptides representing the proteins of interest for the method. The plethora of peptides formed during tryptic digestion of biological samples, detectable in the MS with many isobaric or nearly isobaric signals, necessitate strategies to ensure correct identification, realized here via retention time alignment with the internal standard and comparison of area ratios between multiple transitions in the sample and a standard. With the detailed workflow presented in *chapter 2*, a targeted proteomics method was established for the quantitative analysis of all COX (COX-1 and -2) and in *chapter 4* for relevant enzymes/proteins of the LOX pathway (5-, 12-, 15-LOX, 15-LOX-2 and FLAP), which is the first quantitative targeted proteomics method for the analysis of the human COX and LOX pathways.

Efforts to further enhance the sensitivity of targeted methods include, e.g., the use of nano-LC which reduces ion suppression effects [1] or mass separation from co-eluting matrix by additional fragmentation in hybrid triple quadrupole linear ion trap mass spectrometers (multiple reaction monitoring cubed, MRM^3) [2]. However, the comparison of the latter approach to conventional MRM detection in this thesis revealed higher limits of quantification, reduced linear ranges and limited multiplexing capacities, underlining the fact that sensitivity improvements with MRM^3 strongly depend on the matrix, i.e., the degree of background interference that is reduced by increasing selectivity.

In order to increase the informative value, the analytical scope of the method can be further extended to other enzymes either directly involved in oxylipin formation, such as prostaglandin E synthases and CYP enzymes, to enzymes/proteins upstream of the ARA cascade, e.g., lipid-liberating phosphor-lipases, oxylipin receptors or immunomodulating cytokines. Additionally, untargeted analysis with high-resolution MS instruments and database supported identifications (discovery proteomics) [3] can aid in the search of relevant enzymes/proteins undergoing abundance changes during treatments with test compounds and they can subsequently be added to the targeted proteomics method.

Targeted oxylipin metabolomics platforms cover a wide range of structurally diverse compounds, owing to the multitude of enzymes involved in the ARA cascade and autoxidative reactions leading to their formation as well as the many precursor fatty acids as potential substrates. Furthermore, especially very low concentrations of many analytes (low nM to pM range) with at the same time large abundance differences throughout all oxylipins and the presence of many regio- and stereoisomers make their analysis challenging. Recently, additional analytical tools are being applied such as comprehensive LC or ion mobility spectrometry as well as chiral LC to further enhance separation allowing to understand the highly regio- and stereospecific bioactivities of oxylipins [4-6]. The discovery of new oxylipin structures as well as the commercial availability of standards makes continuous updates of the analytical scope of the method necessary [7-9]. About 20 years ago, a novel class of multiple hydroxylated fatty acids termed specialized pro-resolving mediators (SPM) was discovered which is hypothesized to contribute to the active resolution of inflammation [10]. Today, the enzymatic formation routes of SPM, their occurrence in tissues and blood and thus, their biological relevance is controversially discussed [11]. In order to be able to further elucidate their formation routes and biological functions [12, 13], several SPM including lipoxins, maresins, protectins and resolvins were added to the method during the course of this thesis [9]. With the commercial availability of several additional compounds, e.g., prostanoid and resolvin standards, as well as diastereomers of analytes, e.g.*,* 15-(*R*) PGE_2, the method was later further extended (*chapter 4*). Allowing the quantitative analysis of 198 oxylipins (and 28 additional isoprostanes [8]) it is currently the most comprehensive targeted oxylipin metabolomics platform.

Not only the availably but also the quality of analytical standards is highly relevant for accurate quantitative analysis, since quantification is based on external calibrations. Varying concentrations of few oxylipins reported from different labs in, e.g., human plasma and also found during inter-lab comparisons of the same samples are likely attributed to differences in the analytical standards used for quantification. During the course of this thesis a strategy was developed allowing to characterize the quality of oxylipin standards. For this, the areas resulting from MS measurements in selected ion monitoring (SIM) mode and, if possible, UV absorption of regular standards are compared to few standards with verified concentrations and similar structures (e.g. hydroxy-fatty acids) [14]. Though diverging concentrations can be adjusted with the calculated correction factors, standards in verified quality are only available for few analytes and the portfolios of the manufacturers need to be extended to ensure comparable and meaningful results.

Next to the analytical tools, meaningful biological systems are required for the investigation of ARA cascade modulation. Due to the important role of oxylipins in inflammation signaling, human immune cells are highly relevant for the investigation of the ARA cascade. Immortal monocytic cell lines such as THP-1 or Mono-Mac-6 are well-established models that are easy to maintain, however, the altered metabolism of cancerous cells may not fully represent the *in vivo* status [15, 16]. Primary cells freshly isolated from human blood (e.g., neutrophils or monocytes) as *ex vivo* systems have higher physiological relevance and can also reveal inter-individual differences. The characterization of the COX and LOX pathways in THP-1 cells and primary macrophages in *chapter 4* demonstrates how the ARA cascade can be selectively modulated with pharmaceuticals. Moreover, the crosstalk and influence between different cell types can be investigated in human whole blood assays containing multiple blood cells (i.e. monocytes, neutrophils, platelets).

Human primary neutrophils serve as relevant biological systems, especially for the investigation of the 5-LOX pathway. The interactions of dietary ingredients with the oxylipin formation in this pathway were investigated in *chapter 3*. Resveratrol, ε-viniferin and a resveratrol imine analogue markedly inhibited the 5-LOX activity in a cell-free enzyme assay as well as in human neutrophils while genistein only inhibited product formation in the cells. However, the targeted metabolomics method revealed complex interactions in the neutrophils including other enzyme targets of the test compounds, e.g., the inhibition of COX activity by resveratrol, and substrate shunts towards unaffected enzymes leading to a parallel increase of, e.g., 15-HETE concentrations by ε-viniferin. These results highlight the diverse network of biochemical reactions within the ARA cascade and the importance of a comprehensive analysis of the total oxylipin pattern.

Several polyphenols were demonstrated to interfere with the ARA cascade enzymes (especially COX-2) in cell-free *in vitro* assays and biological test systems [17-21]. It was suspected that this effect contributes to the anti-inflammatory properties which are discussed as possible mechanisms [22] of the beneficial health effects reported for the intake of fruits and vegetables in many epidemiological studies [23-25]. However, the actual mechanisms leading to these are much more complex. *In vivo*, the effect mechanisms of polyphenols are affected by numerous factors including bioavailability, metabolization and synergistic effects of multiple polyphenols or with the food matrix as well as parallel interactions with multiple metabolic pathways and individual genetic profiles [26]. Thus, also polyphenol metabolites and mixtures need to be considered regarding their potential contribution to ARA cascade modulation and further studies are necessary to characterize the overall effects of dietary polyphenols from fruits and vegetables on human health more deeply.

Conclusively, the targeted proteomics method developed in this thesis provides a new valuable analytical tool for a better understanding of mechanisms involved in the modulation of the ARA cascade. Applied here for the thorough analysis of human immune cells, it was demonstrated how the combination of sensitive targeted oxylipin metabolomics and proteomics presents novel opportunities in oxylipin research.

5.1 References

1. Wilson SR, Vehus T, Berg HS, and Lundanes E (2015) Nano-LC in proteomics: recent advances and approaches. *Bioanalysis,* 7(14), 1799-1815; doi: 10.4155/bio.15.92.
2. Fortin T, Salvador A, Charrier JP, Lenz C, Bettsworth F, Lacoux X, Choquet-Kastylevsky G, and Lemoine J (2009) Multiple Reaction Monitoring Cubed for Protein Quantification at the Low Nanogram/Milliliter Level in Nondepleted Human Serum. *Anal Chem,* 81(22), 9343-9352; doi: 10.1021/ac901447h.
3. Domon B and Aebersold R (2010) Options and considerations when selecting a quantitative proteomics strategy. *Nat Biotechnol,* 28(7), 710-721; doi: 10.1038/nbt.1661.

4. Hinz C, Liggi S, Mocciaro G, Jung S, Induruwa I, Pereira M, Bryant CE, Meckelmann SW, O'Donnell VB, Farndale RW, et al. (2019) A Comprehensive UHPLC Ion Mobility Quadrupole Time-of-Flight Method for Profiling and Quantification of Eicosanoids, Other Oxylipins, and Fatty Acids. *Anal Chem,* 91(13), 8025-8035; doi: 10.1021/acs.analchem.8b04615.
5. Blum M, Dogan I, Karber M, Rothe M, and Schunck W-H (2019) Chiral lipidomics of monoepoxy and monohydroxy metabolites derived from long-chain polyunsaturated fatty acids[S]. *J Lipid Res,* 60(1), 135-148; doi: 10.1194/jlr.M089755.
6. Toewe A, Balas L, Durand T, Geisslinger G, and Ferreirós N (2018) Simultaneous determination of PUFA-derived pro-resolving metabolites and pathway markers using chiral chromatography and tandem mass spectrometry. *Anal Chim Acta,* 1031, 185-194; doi: 10.1016/j.aca.2018.05.020.
7. Ostermann AI, Willenberg I, and Schebb NH (2015) Comparison of sample preparation methods for the quantitative analysis of eicosanoids and other oxylipins in plasma by means of LC-MS/MS. *Anal Bioanal Chem,* 407(5), 1403-14; doi: 10.1007/s00216-014-8377-4.
8. Rund KM, Ostermann AI, Kutzner L, Galano JM, Oger C, Vigor C, Wecklein S, Seiwert N, Durand T, and Schebb NH (2018) Development of an LC-ESI(-)-MS/MS method for the simultaneous quantification of 35 isoprostanes and isofurans derived from the major n3- and n6-PUFAs. *Anal Chim Acta,* 1037, 63-74; doi: 10.1016/j.aca.2017.11.002.
9. Kutzner L, Rund KM, Ostermann AI, Hartung NM, Galano JM, Balas L, Durand T, Balzer MS, David S, and Schebb NH (2019) Development of an Optimized LC-MS Method for the Detection of Specialized Pro-Resolving Mediators in Biological Samples. *Front Pharmacol,* 10; doi: 10.3389/fphar.2019.00169.
10. Serhan CN, Hong S, Gronert K, Colgan SP, Devchand PR, Mirick G, and Moussignac RL (2002) Resolvins: a family of bioactive products of omega-3 fatty acid transformation circuits initiated by aspirin treatment that counter proinflammation signals. *J Exp Med,* 196(8), 1025-37; doi: 10.1084/jem.20020760.
11. Schebb NH, Kühn H, Kahnt AS, Rund KM, O'Donnell VB, Flamand N, Peters-Golden M, Jakobsson P-J, Weylandt KH, Rohwer N, et al. (2022) Formation, Signaling and Occurrence of Specialized Pro-Resolving Lipid Mediators—What is the Evidence so far? *Front Pharmacol,* 13; doi: 10.3389/fphar.2022.838782.
12. Ebert R, Cumbana R, Lehmann C, Kutzner L, Toewe A, Ferreirós N, Parnham MJ, Schebb NH, Steinhilber D, and Kahnt AS (2020) Long-term stimulation of toll-like receptor-2 and -4 upregulates 5-LO and 15-LO-2 expression thereby inducing a lipid mediator shift in human monocyte-derived macrophages. *Biochim Biophys Acta, Mol Cell Biol Lipids,* 1865(9), 158702; doi: 10.1016/j.bbalip.2020.158702.
13. Kutzner L, Goloshchapova K, Rund KM, Jübermann M, Blum M, Rothe M, Kirsch SF, Schunck W-H, Kühn H, and Schebb NH (2020) Human lipoxygenase isoforms form complex patterns of double and triple oxygenated compounds from eicosapentaenoic acid. *Biochim Biophys Acta, Mol Cell Biol Lipids,* 1865(12), 158806; doi: 10.1016/j.bbalip.2020.158806.
14. Hartung NM, Mainka M, Kampschulte N, Ostermann AI, and Schebb NH (2019) A strategy for validating concentrations of oxylipin standards for external calibration. *Prostaglandins Other Lipid Mediat,* 141, 22-24; doi: 10.1016/j.prostaglandins.2019.02.006.
15. Riddy DM, Goy E, Delerive P, Summers RJ, Sexton PM, and Langmead CJ (2018) Comparative genotypic and phenotypic analysis of human peripheral blood monocytes

and surrogate monocyte-like cell lines commonly used in metabolic disease research. *PLoS One,* 13(5), e0197177; doi: 10.1371/journal.pone.0197177.

16. Bosshart H and Heinzelmann M (2016) THP-1 cells as a model for human monocytes. *Ann Transl Med,* 4(21), 22; doi: 10.21037/atm.2016.08.53.
17. Hong J, Smith TJ, Ho C-T, August DA, and Yang CS (2001) Effects of purified green and black tea polyphenols on cyclooxygenase- and lipoxygenase-dependent metabolism of arachidonic acid in human colon mucosa and colon tumor tissues1. *Biochem Pharmacol,* 62(9), 1175-1183; doi: 10.1016/S0006-2952(01)00767-5.
18. Kutil Z, Kvasnicova M, Temml V, Schuster D, Marsik P, Cusimamani EF, Lou J-D, Vanek T, and Landa P (2015) Effect of Dietary Stilbenes on 5-Lipoxygenase and Cyclooxygenases Activities In Vitro. *Int J Food Prop,* 18(7), 1471-1477; doi: 10.1080/10942912.2014.903416.
19. Wakabayashi I and Yasui K (2000) Wogonin inhibits inducible prostaglandin E(2) production in macrophages. *Eur J Pharmacol,* 406(3), 477-81; doi: 10.1016/S0014-2999(00)00695-6.
20. Prasad NS, Raghavendra R, Lokesh BR, and Naidu KA (2004) Spice phenolics inhibit human PMNL 5-lipoxygenase. *Prostaglandins, Leukotrienes and Essential Fatty Acids,* 70(6), 521-528; doi: 10.1016/j.plefa.2003.11.006.
21. Willenberg I, Meschede AK, Gueler F, Jang MS, Shushakova N, and Schebb NH (2015) Food Polyphenols Fail to Cause a Biologically Relevant Reduction of COX-2 Activity. *PLoS One,* 10(10), e0139147; doi: 10.1371/journal.pone.0139147.
22. Garcia-Lafuente A, Guillamon E, Villares A, Rostagno MA, and Martinez JA (2009) Flavonoids as anti-inflammatory agents: implications in cancer and cardiovascular disease. *Inflamm Res,* 58(9), 537-52; doi: 10.1007/s00011-009-0037-3.
23. Wang X, Ouyang Y, Liu J, Zhu M, Zhao G, Bao W, and Hu FB (2014) Fruit and vegetable consumption and mortality from all causes, cardiovascular disease, and cancer: systematic review and dose-response meta-analysis of prospective cohort studies. *BMJ [Br Med J],* 349, g4490; doi: 10.1136/bmj.g4490.
24. Cooper AJ, Forouhi NG, Ye Z, Buijsse B, Arriola L, Balkau B, Barricarte A, Beulens JWJ, Boeing H, Büchner FL, et al. (2012) Fruit and vegetable intake and type 2 diabetes: EPIC-InterAct prospective study and meta-analysis. *Eur J Clin Nutr,* 66(10), 1082-1092; doi: 10.1038/ejcn.2012.85.
25. Aune D, Chan DSM, Vieira AR, Rosenblatt DAN, Vieira R, Greenwood DC, and Norat T (2012) Fruits, vegetables and breast cancer risk: a systematic review and meta-analysis of prospective studies. *Breast Cancer Res Treat,* 134(2), 479-493; doi: 10.1007/s10549-012-2118-1.
26. Williamson G (2017) The role of polyphenols in modern nutrition. *Nutr Bull,* 42(3), 226-235; doi: 10.1111/nbu.12278.

Summary

Eicosanoids and other oxylipins formed from polyunsaturated fatty acids via the enzymes of the arachidonic acid (ARA) cascade fulfill important biological functions. Especially their crucial roles in the mediation of inflammatory responses have made them a major target for pharmaceutical development. Most drugs are designed to exert their effects by directly inhibiting the target enzymes. However, the cellular effect mechanisms of several dietary constituents such as polyphenols which interfere with oxylipin formation are far from being understood.

In order to fully understand their modes of action it is therefore necessary not only to comprehensively investigate the oxylipin pattern but also to analyze the abundance of enzymes and proteins involved in their formation. For this reason, the aim of this thesis was the development of an analytical method allowing the quantification of the ARA cascade enzymes and the characterization of different biological systems for investigating ARA cascade modulation in parallel to oxylipin analysis.

In the first part of this thesis (*chapter 2*), a targeted proteomics method based on liquid chromatography tandem mass spectrometry (LC-MS/MS) was developed for the cyclooxygenase-2 (COX-2) pathway. The method allows an absolute quantification using external calibration with internal standards (IS) and relative quantification via the normalization to the levels of three housekeeping proteins (peptidyl-prolyl cis-trans isomerase B, PPIB; glyceraldehyde-3-phosphate dehydrogenase, GAPDH; β-/γ-actin). In this chapter, a detailed workflow for targeted proteomics method development was established: the proteins are measured in form of representative peptides which are chosen based on several criteria after *in silico* tryptic digestion. Among these, the uniqueness of the peptide sequence is the most important one providing unequivocal identification of the target protein. Additional criteria help to further

narrow down the choice of peptides to those with appropriate properties for the MS method: peptide length, cleavage probabilities, presence of posttranslational modifications or single nucleotide polymorphisms, splice variants, the occurrence of amino acids prone to modification and predicted retention times. After the following experimental evaluation of the pre-selected peptides, two to three peptides are finally chosen per protein. Three characteristic fragment ions arising from peptide backbone fragmentation are then carefully selected per peptide, the most sensitive one used as quantifier and two others as qualifier multiple reaction monitoring (MRM) transitions. The comparison of their area ratios to standards strengthens the identification in biological matrix together with the identical retention times of the co-eluting heavy labeled peptide IS. The method allows sensitive quantification of the COX-2 peptides down to a lower limit of quantification of 100 pM (equivalent to 0.5 fmol or 561 fg peptide, 34 pg COX-2 protein on column). Using a workflow comprising initial protein precipitation, reduction of disulfide bridges followed by alkylation of sulfhydryl groups before the overnight tryptic digestion as well as solid-phase extraction, the COX-2 abundance was investigated with the established method in different human cells. Strong correlations were found between the oxylipins formed via the COX pathway and the COX-2 abundance in the three colon carcinoma cell lines and primary macrophages.

With respect to their potential effects on human health, the second part of this thesis deals with the investigation of the modulating effects of polyphenols on 5-lipoxygenase (LOX) activity and the ARA cascade in human neutrophils (*chapter 3*). The mechanisms of action of a library of food polyphenols and a synthetic analogue were characterized using two assay systems. In cell-free enzyme assays and human neutrophils, resveratrol, its dimer ε-viniferin and a resveratrol imine analogue (IRA) directly inhibited 5-LOX activity with potencies (IC_{50}) in low micromolar ranges while the isoflavone genistein only showed potent inhibition of 5-LOX product formation in the cells. Inhibitory effects of this compound on all other pathways of the ARA cascade indicated by the targeted LC-MS based oxylipin metabolomics analysis suggest a global cellular interference. The modulation of the total oxylipin pattern upon resveratrol, ε-viniferin or IRA treatment not only demonstrated their inhibitory effects on the formation of downstream metabolites of the 5-LOX pathway, but also revealed their individual effects on the rest of the ARA cascade at concentrations that could be reached *in vivo* (10 µM) after consumption of polyphenol-rich food or supplements. Resveratrol also inhibited the formation of 15-LOX and COX pathway products, while the inhibition of 5-LOX with ε-viniferin and IRA lead to substrate shunts towards other enzymes. The concentrations of oxylipins formed via the COX and cytochrome P450 monooxygenase (CYP) pathways increased during treatment with IRA and ε-viniferin additionally promoted an increase in 15-LOX pathway products. This emphasizes the importance of comprehensive oxylipin analysis to understand the complex mechanisms involved in modulations of the ARA cascade.

A more thorough investigation of the COX and LOX pathways in immune cells can be achieved by parallel analysis of oxylipin <u>and</u> protein levels. For this reason, in *chapter 4* a multi-omics approach was developed enabling the quantitative analysis of 198 oxylipins (and 28 additional isoprostanes) and all COX (COX-1 and -2) and relevant LOX pathway enzymes/proteins (5-, 12-, 15-LOX, 15-LOX-2 and FLAP) via LC-MS/MS(/MS). With respect to the labor-intensive generation and limited availability of biological samples such as tissue or primary blood cells, the approach was optimized to enable both analyses from a single sample. With the aim of increasing detection sensitivities in proteomics, the MRM³ and MRM modes were compared. The additional fragmentation step provides a higher degree of selectivity in MRM³, which can be valuable to overcome matrix interferences. However, higher sensitivities (LLOQ: 16 – 122 pM vs. 75 – 840 pM for the same peptides) and greater linear ranges (up to 1.5 – 7.4 µM vs. 4 – 368 nM) together with superior multiplexing capacities made MRM the more favorable method for this pathway analysis. The crucial role of the lipid mediators formed via the COX and LOX pathways in the immune response makes it necessary to understand the mechanisms involved in their modulation. Oxylipin concentrations and protein abundances

were characterized in the human monocytic cell line THP-1 and differently polarized primary macrophages with the combined sensitive oxylipin metabolomics and proteomics approach. The differentiation of the THP-1 monocytes to macrophage-like cells led to an induction of 5-LOX and its product formation. The protein pattern of the M1-like macrophages was also characterized by 5-LOX and its activating protein (FLAP), while it was dominated by 15-LOX and 15-LOX-2 the M2-like macrophages accompanied by high levels of the oxylipins formed via these enzymes. The methodology then allowed mechanistical investigations of lipopolysaccharide stimulation inducing *PTGS2* gene expression (COX-2 enzyme) and enhancing prostanoid formation as well as pharmaceutical treatment inhibiting oxylipin formation and/or gene expression.

Overall, with the development of a targeted proteomics method this thesis contributes to a more comprehensive analysis of the ARA cascade. The combined quantitative analysis of enzyme/protein abundances and oxylipin concentrations in the multi-omics approach will promote a better understanding of mechanisms leading to changes in the ARA cascade. This is relevant for comprehending cellular effect mechanisms of, e.g., dietary constituents such as polyphenols which were shown here to modify the oxylipin pattern in human immune cells.

Appendix

Appendix of Chapter 2

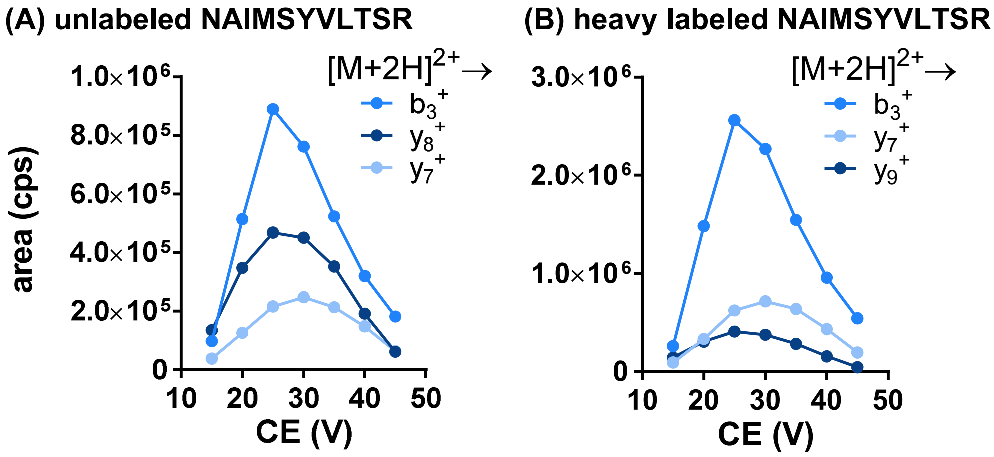

Fig. 7.1: Effect of CE optimization on intensity of **(A)** unlabeled and **(B)** heavy labeled NAIMSYVLTSR (arg: U-$^{13}C_6$; U-$^{15}N_4$) transitions.

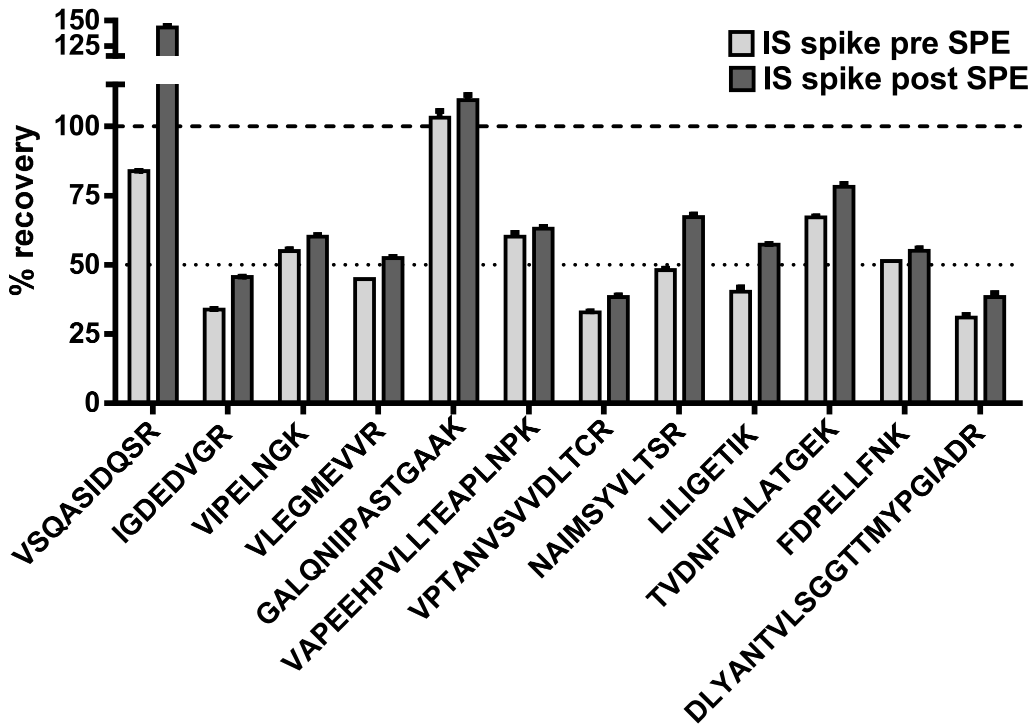

Fig. 7.2: Evaluation of loss of IS peptides during SPE in sample preparation. IS peptides were spiked to matrix of 5 mio. HCA-7 cells at 30 - 60 nM (resulting final concentration in vial) just before and after SPE. Areas were determined via LC-MS/MS and % recovery was calculated relative to an IS mix without matrix at the same concentration level from quantifier IS transitions. Shown are mean ± deviation of mean for n = 2. The mean loss during SPE was approx. 10%.

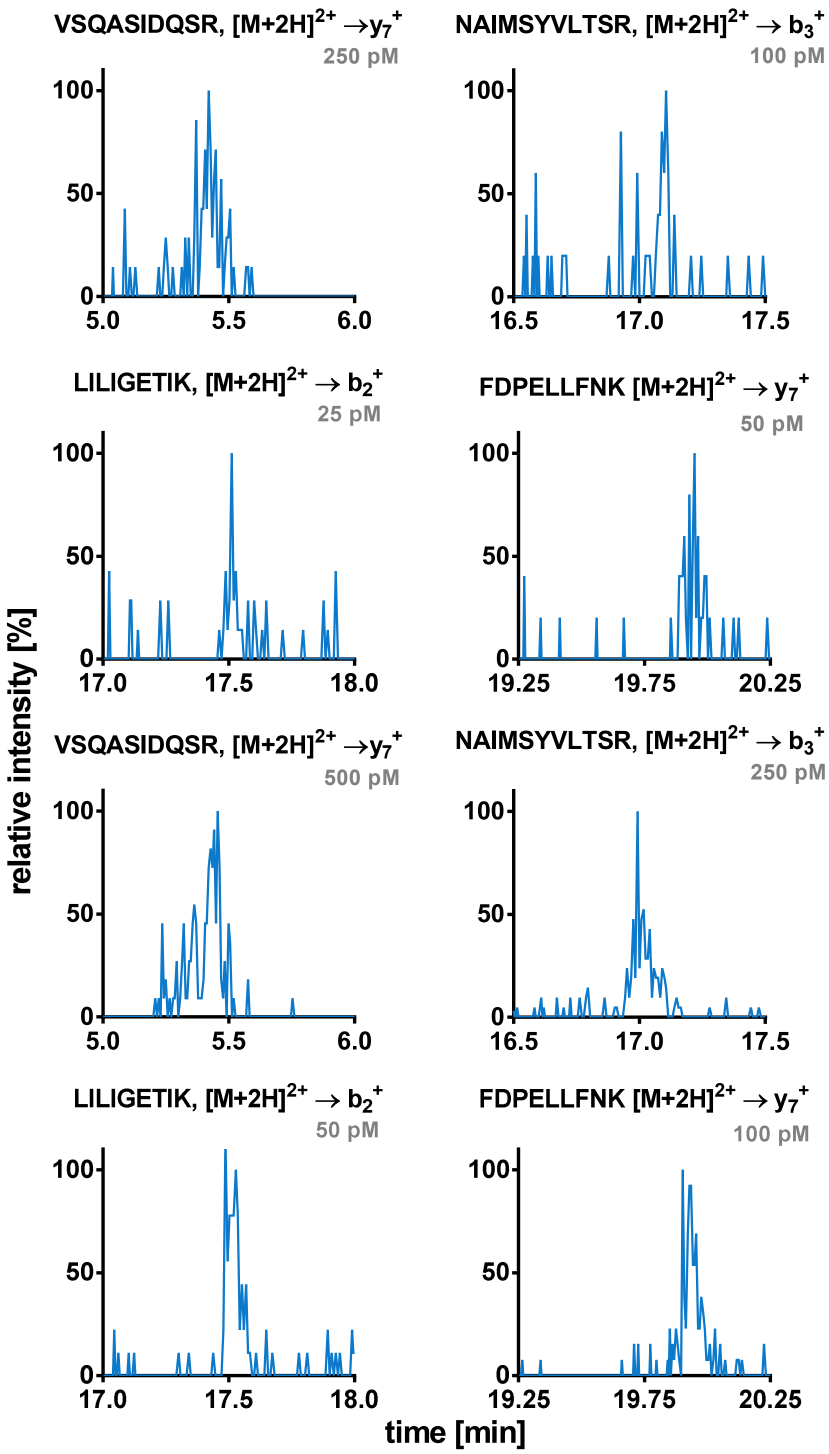

Fig. 7.3: Limits of detection (LOD) and lower limits of quantification (LLOQ) of COX-2 peptides**. (A)** LOD and **(B)** LOQ of COX-2 peptides were determined by signal-to-noise ratios of 3 (LOD) and 5 (LLOQ) and ranged from 25 – 250 pM and 50 – 500 pM with accuracies of ± 20%, respectively.

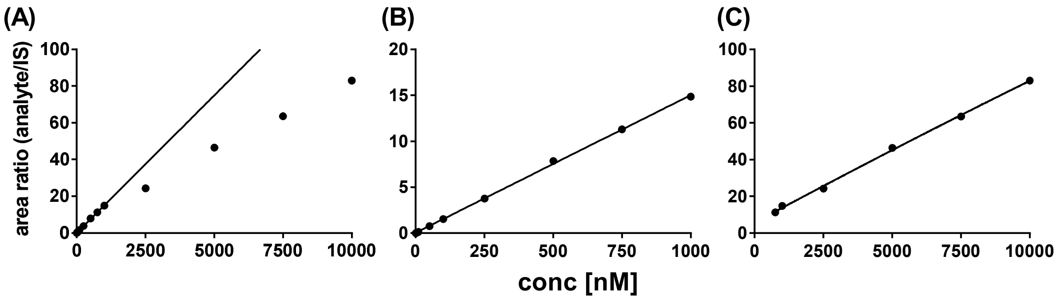

Fig. 7.4: Limited dynamic MS detector response is exemplarily shown for **(A)** VLEGMEVVR peptide. Two calibration curves were used. **(B)** Linear fit was used in a range of 1 nM – 1 µM and **(C)** quadratic fitting was used to determine concentrations above 1 µM (calibration range: 750 nM – 10 µM).

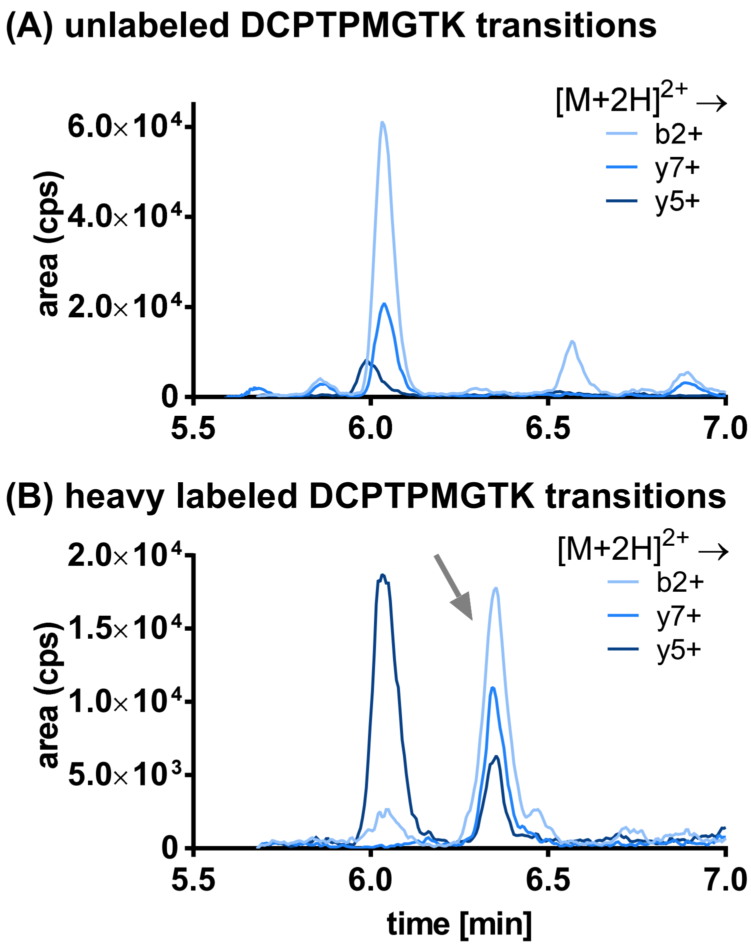

Fig. 7.5: MRM signal of the three most intense transitions of **(A)** unlabeled and **(B)** heavy labeled COX-1 specific DCPTPMGTK peptide in HCT-116 cell matrix. No signal was detected for the transition of the unlabeled peptide at the retention time indicated by the spiked heavy labeled peptide (6.38 min). Neither the exemplarily shown DCPTPMGTK nor other COX-1 specific peptides were detected in any of the investigated colon cells, while all were detected in the human macrophages incubated with or without LPS.

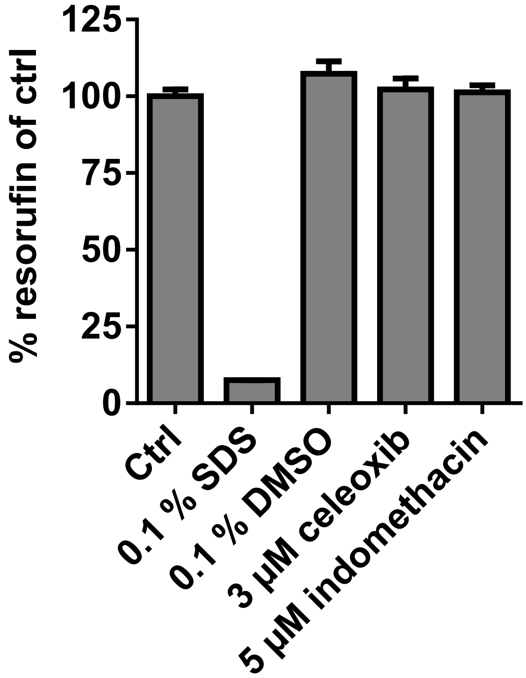

Fig. 7.6: Cell viability was determined by resazurin assay in HCA-7 cells. Cells were incubated with the test compounds celecoxib and indomethacin as well as DMSO as vehicle control and SDS as positive control at indicated concentrations for 24 h after a 24 h pre-incubation period without treatment. Dehydrogenase activity was measured as resorufin formation by fluorometric readout at 590 nm after excitation at 560 nm. Shown are mean ± SD for n = 6.

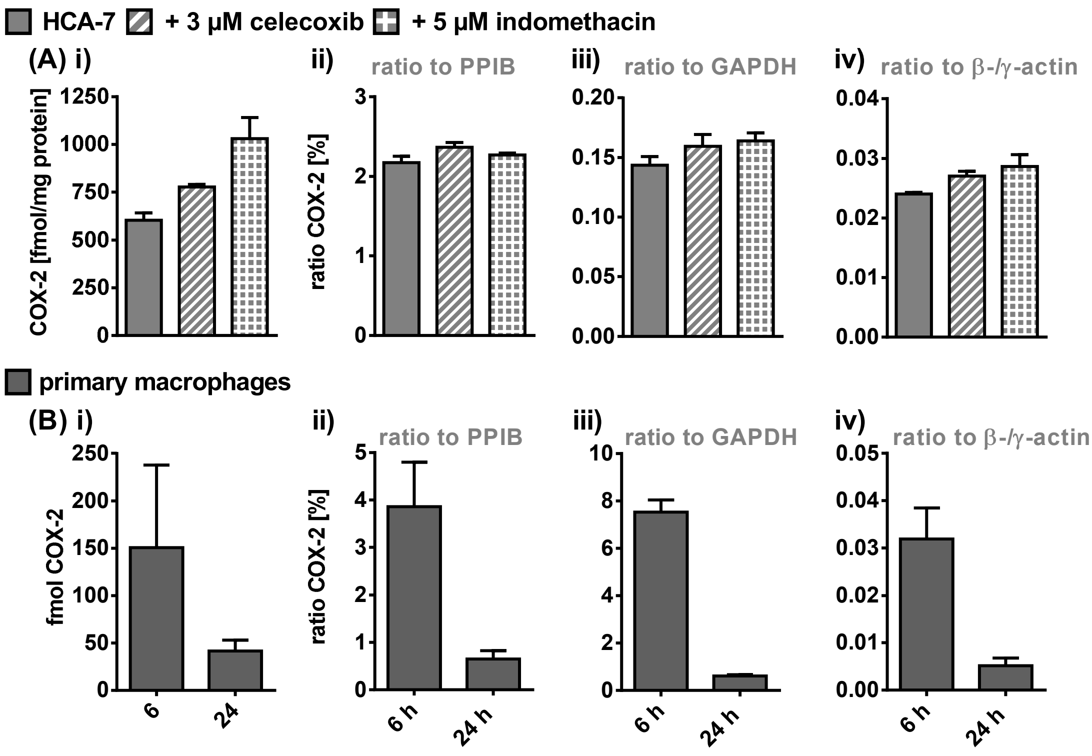

Fig. 7.7: COX-2 protein levels in **(A)** untreated HCA-7 cells, treated with 3 µM celecoxib or 5 µM indomethacin as well as in **(B)** human primary macrophages treated with 1 µg/mL LPS (for 6 h and 24 h). **(A), (B) i)** COX-2 abundance levels were determined as mean concentrations of three COX-2 specific peptides (VSQASIDQSR, NAIMSYVLTSR, FDPELLFNK) and **(A), (B) ii-iv)** normalized to mean concentrations of specific PPIB (IGDEDVGR, VLEGMEVVR, TVDNFVALATGEK), GAPDH (VIPELNGK, VPTANVSVVDLTCR, GALQNIIPASTGAAK) and β-/γ-actin peptides (VAPEEHPVLLTEAPLNPK, DLYANTVLSGGTTMYPGIADR).

Tab. 7.1: Comparison of transition rankings. PABST (PeptideAtlas Best SRM Transition) transition rank of **(A)** COX-2 and **(B)** PPIB peptides' transitions on 5500 QTRAP on SRMAtlas [37], is compared to experimental data of optimized transitions on 5500 QTRAP, ranked from most intense to least intense.

(A) Peptide	**SRM-Atlas ranking**	**Experi-mental ranking**	**Transi-tions**
VSQASIDQSR *predicted*			
	1	7	$M^{2+} \rightarrow y_7^+$
	2	**3**	$M^{2+} \rightarrow y_4^+$
	3	6	$M^{2+} \rightarrow b_3^+$
	4	**1**	$M^{2+} \rightarrow y_6^+$
	5	**2**	$M^{2+} \rightarrow y_7^+$
NAIMSYVLTSR			
	1	**2**	$M^{2+} \rightarrow y_8^+$
	2	**3**	$M^{2+} \rightarrow y_7^+$
	3	**1**	$M^{2+} \rightarrow b_3^+$
	4	7	$M^{2+} \rightarrow y_6^+$
	5	6	$M^{2+} \rightarrow y_5^+$
LILIGETIK *predicted*			
	1	**1**	$M^{2+} \rightarrow b_{2+}$
	2	**2**	$M^{2+} \rightarrow y_7^+$
	3	**3**	$M^{2+} \rightarrow y_5^+$
	4	5	$M^{2+} \rightarrow y_6^+$
	5	4	$M^{2+} \rightarrow b_{3+}$
FDPELLFNK *predicted*			
	1	**1**	$M^{2+} \rightarrow b_2^+$
	2	**2**	$M^{2+} \rightarrow y_7^+$
	3	**3**	$M^{2+} \rightarrow y_2^+$
	4	5	$M^{2+} \rightarrow y_4^+$
	5	4	$M^{2+} \rightarrow y_3^+$

(B) Peptide	**SRM-Atlas ranking**	**Experi-mental ranking**	**Transi-tions**
IGDEDVGR			
	1	**1**	$M^{2+} \rightarrow y_7^+$
	2	**2**	$M^{2+} \rightarrow y_3^+$
	3	4	$M^{2+} \rightarrow y_5^+$
	4	**3**	$M^{2+} \rightarrow y_6^+$
	5	5	$M^{2+} \rightarrow y_4^+$
VLEGMEVVR			
	1	**2**	$M^{2+} \rightarrow y_7^+$
	2	**3**	$M^{2+} \rightarrow y_6^+$
	3	**1**	$M^{2+} \rightarrow b_2^+$
	4	5	$M^{2+} \rightarrow y_3^+$
	5	4	$M^{2+} \rightarrow y_4^+$
TVDNFVALATGEK			
	1	**3**	$M^{2+} \rightarrow y_8^+$
	2	**2**	$M^{2+} \rightarrow y_7^+$
	3	4	$M^{2+} \rightarrow y_5^+$
	4	7	$M^{2+} \rightarrow y_6^+$
	5	9	$M^{2+} \rightarrow y_9^+$
	8	**1**	$M^{2+} \rightarrow b_2^+$

Tab. 7.2 (page 136): Selected proteotypic peptides (PTPs) from *in silico* tryptic digest of housekeeper proteins Peptidyl-prolyl cis-trans isomerase B (PPIB or cyclophilin B), glyceraldehyde-3-phosphate dehydrogenase (GAPDH), cytoplasmic actin 1 (β-actin) / cytoplasmic actin 2 (γ-actin). They were selected based on peptide length (7-22 aa), uniqueness, cleavage probability calculated with peptide cutter (≥ 95%) or cleavage prediction with decision trees (CP-DT; ≥ 70%), occurrence of single nucleotide polymorphisms (SNPs) or posttranslational modifications (PTMs), as well as unfavored amino acids (C, M, N, Q, W; max. 2 allowed) and predicted retention time (RT; 3 – 30 min). All of the β -actin peptides (>7 aa) share sequences with tryptic peptides of other proteins and are thus not unique. In order to narrow the specificity, PTPs were chosen which solely occur in β-actin and γ-actin. Especially for GAPDH and in β-/γ-actin it is impossible to find peptides without PTMs. Although PTMs are unfavored, they were tolerated in these cases.

Peptides	Position	[M+H]+	Length [aa]	Unique-ness[a)]	C-terminal cleavage probability[b)] [%]	Overall cleavage probability[c)] [%]	SNPs[d)]	PTMs[e)]	Un-favored aa	Pred. RT [min][f)]
PPIB (P23284)										
IGDEDVGR	52-59	860.41	8	unique, *known variant of Q9UPX8*	100	95	-	-		5.1
TVDNFVALATGEK	72-84	1364.71	13	unique	100	88	-	T72: p, T81: p, K84: ub, K84: suc	1 × N	15.2
VLEGMEVVR	172-180	1031.56	9	unique	100	87	-	-	1 × M	12.9
GAPDH (P04406)										
GALQNIIPASTGAAK	201-215	1411.79	15	unique	95	93	-	S210: p, T211: p, K215: ac, K215: ub, K215: sm, K215: sc, K215: m2	1 × N, 1 × Q	13.5
VIPELNGK	220-227	869.51	8	unique	100	96	-	N225: da, K227: ac, K227:m2, K227: ub, K227: sc	1 × N	8.8
VPTANVSVVDLTCR*	235-248	1473.77	14	unique	100	95	-	T237: p, S241: p, T246: p, C247: sc, C247: n	1 x C, 1 × N	14.4
β-Actin / γ-Actin (P60709 / P63261)										
VAPEEHPVLLTEAPL NPK	96-113	1954.06	18	P60709, P63261, *known variants of: Q6S8J3, P0CG39, P0CG38*	**ACTB:** 94; **ACTG:** 94	**ACTB:** 99; **ACTG:** 99	-	**ACTB:** T106: p, K113: ac, K113: ub, K113: sm; **ACTG:** T106: p, K113: ac, K113: ub, K113: sm	1 × N	15.9
DLYANTVLSGGTTMY PGIADR	292-312	2215.07	21	P60709, P63261	**ACTB:** 100; **ACTG:** 100	**ACTB:** 97 **ACTG:** 97	-	**ACTB:** Y294: p, T297: p, S300: p, Y306: p; **ACTG:** Y294: p, T297: p, S300: p, Y306: p	1 × M, 1 × N	19.8

[a)]from BLAST and NeXtprot; [b)]calculated from peptide cutter; [c)]calculated from CP-DT; [d)]SNPs from Uniprot; [e)]PTMs from Uniprot and Phosphosite Plus (ac – acetylation, da - deamidation, gl – glycosylation, m2 - dimethylation, n – nitrosylation, p – phosphorylation, sc- succinylation, sm - sumoylation, ub - ubiquitinylation); [f)]predicted RT from SSRCalc
-: not reported; *: carbamidomethylated cys

Tab. 7.3 (page 138): Selected proteotypic peptides (PTPs) from *in silico* tryptic digest of cyclooxygenase 1 (COX-1, prostaglandin G/H synthase 1). They were selected based on peptide length (7-22 aa), uniqueness, cleavage probability calculated with peptide cutter (≥ 5%) or cleavage prediction with decision trees (CP-DT; ≥ 70%), occurrence of single nucleotide polymorphisms (SNPs) or posttranslational modifications (PTMs), as well as unfavored amino acids (C, M, N, Q, W; max. 2 allowed) and predicted retention time (RT; 3 – 30 min).

Peptides	Position	$[M+H]^+$	Length [aa]	Uniqueness[a)]	C-terminal cleavage probability[b)] [%]	Overall cleavage probability[c)] [%]	SNPs[d)]	PTMs[e)]	Unfavored aa	Pred. RT [min][f)]
COX-1 (P23219)										
DCPTPMGTK*	157-165	1006.43	9	unique	100%	77	-	-	1 × C, 1 × M	6.50
AEHPTWGDEQLFQTTR	317-332	1915.89	16	unique	100%	85	-	-	2 × Q, 1 × W	13.90
LQPFNEYR	459-466	1066.53	8	unique	85%	91	-	-	1 × N, 1 × Q	10.30

[a)]from BLAST and NeXtprot; [b)]calculated from peptide cutter ; [c)]calculated from CP-DT ; [d)]SNPs from Uniprot; [e)]PTMs from Uniprot and Phosphosite Plus; [f)]predicted RT from SSRCalc

-: not reported
*: carbamidomethylated cys

Tab. 7.4: **(A)** Unlabeled and **(B)** heavy labeled (lys: U-$^{13}C_6$; U-$^{15}N_2$; arg: U-$^{13}C_6$; U-$^{15}N_4$) housekeeper peptides data. For each peptide, different ion types (transitions) used for qualification and quantification (bold) with their associated Q1 and Q3 *m/z* are shown with retention time (RT), relative ratios to quantifier transition as well as collision energies (CE). Retention times (RT) were calculated from sample batch. For unlabeled peptides **(A)** linear (L) and quadratic (Q) calibration ranges are shown for quantifier transitions, as well as the transitions of the corresponding heavy labeled peptides used internal standards (IS) for the quantification. Accuracy of calibrators was in a range of ± 10% (L) ± 21% (Q). The spiking levels of the heavy labeled peptides (concentrations in vial) are in shown **(B)**.

(A) Peptide	**Transitions**	**Q1 *m/z***	**Q3 *m/z***	**RT [min]**	**Rel. Ratio to quantifier [%]**	**CE (V)**	**IS Transitions**	**Range [nM]**
PPIB (P23284)								
IGDEDVGR								
	$M^{2+} \rightarrow y_7^+$	**430.7**	**747.3**	5.86 ± 0.05		**26**	**$M^{2+} \rightarrow y_7^+$**	1 - 1000 (L)
	$M^{2+} \rightarrow y_6^+$	430.7	690.3		39	26		
	$M^{2+} \rightarrow y_5^+$	430.7	575.3		35	31		
VLEGMEVVR								
	$M^{2+} \rightarrow y_7^+$	**516.3**	**819.4**	13.32 ± 0.10		**33**	**$M^{2+} \rightarrow y_7^+$**	1 - 1000 (L)
	$M^{2+} \rightarrow y_6^+$	516.3	690.4		60	36		
	$M^{2+} \rightarrow y_8^+$	516.3	932.5		7	36		
TVDNFVALATGEK								
	$M^{2+} \rightarrow y_7^+$	**682.9**	**689.4**	17.65 ± 0.09		**36**	**$M^{2+} \rightarrow y_7^+$**	1 - 1000 (L)
	$M^{2+} \rightarrow y_8^+$	682.9	788.5		79	36		
	$M^{2+} \rightarrow y_5^+$	682.9	505.3		57	33		
GAPDH (P04406)								
VIPELNGK								
	$M^{2+} \rightarrow y_6^{++}$	435.3	329.2	10.16 ± 0.14	97	38		
	$M^{2+} \rightarrow y_6^+$	**435.3**	**657.4**			**36**	**$M^{2+} \rightarrow y_6^{++}$**	10 - 1000 (L)
	$M^{2+} \rightarrow y_4^+$	435.3	431.3		5	48		
VPTANVSVVDLTCR*								
	$M^{3+} \rightarrow y_5^+$	**510.9**	**664.3**	15.39 ± 0.10		**31**	**$M^{3+} \rightarrow y_5^+$**	5 - 1000 (L)
	$M^{3+} \rightarrow y_3^+$	510.9	436.2		92	29		
	$M^{3+} \rightarrow y_4^+$	510.9	549.3		56	37		
VPTANVSVVDLTCR*								
	$M^{3+} \rightarrow y_5^+$	**510.9**	**664.3**	15.39 ± 0.10		**31**	**$M^{3+} \rightarrow y_5^+$**	750 - 10000 (Q)
	$M^{3+} \rightarrow y_3^+$	510.9	436.2		92	29		
	$M^{3+} \rightarrow y_4^+$	510.9	549.3		56	37		

Tab. 7.4 continued**.**

(A)	Peptide	Transitions	Q1 *m/z*	Q3 *m/z*	RT [min]	Rel. Ratio to quantifier [%]	CE (V)	IS Transitions	Range [nM]
	GAPDH (P04406)								
	GALQNIIPASTGAAK								
		$M^{2+} \rightarrow y_8^+$	**706.4**	**702.4**	14.62 ± 0.14		**43**	**$M^{2+} \rightarrow y_9^+$**	1 - 1000 (L)
		$M^{2+} \rightarrow y_9^+$	706.4	815.5		21	46		
		$M^{2+} \rightarrow y_{11}^+$	706.4	1042.6		7	43		
	GALQNIIPASTGAAK								
		$M^{2+} \rightarrow y_8^+$	**706.4**	**702.4**	14.62 ± 0.14		**43**	**$M^{2+} \rightarrow y_9^+$**	750 - 10000 (Q)
		$M^{2+} \rightarrow y_9^+$	706.4	815.5		21	46		
		$M^{2+} \rightarrow y_{11}^+$	706.4	1042.6		7	43		
	β-Actin / γ-Actin (P60709 / P63261)								
	VAPEEHPVLLTEAPLNPK								
		$M^{3+} \rightarrow y_5^+$	**652.0**	**568.4**	15.26 ± 0.17		**45**	**$M^{3+} \rightarrow y_6^+$**	750 - 10000 (Q)
		$M^{3+} \rightarrow y_8^+$	652.0	869.5		18	42		
		$M^{3+} \rightarrow y_{16}^{++}$	652.0	892.5		9	38		
	DLYANTVLSGGTTMYPGIADR								
		$M^{3+} \rightarrow y_6^+$	739.0	628.3	20.50 ± 0.04	335	47		
		$M^{3+} \rightarrow y_7^+$	**739.0**	**791.4**			**40**	**$M^{3+} \rightarrow y_6^+$**	750 - 10000 (Q)
		$M^{3+} \rightarrow y_8^+$	739.0	922.5		49	38		

*: carbamidomethylated cys

Tab. 7.4 contiued.

(B)	Peptide IS	Transitions	Q1 *m/z*	Q3 *m/z*	RT [min]	Rel. Ratio to quantifier [%]	CE (V)	Spiking level in vial [nM]
	PPIB (P23284)							
	IGDEDVGR							
		$M^{2+} \rightarrow y_7^+$	**435.7**	**757.3**			**21**	
		$M^{2+} \rightarrow y_6^+$	435.7	700.3	5.86 ± 0.05	44	21	30
		$M^{2+} \rightarrow y_5^+$	435.7	585.3		31	26	
	VLEGMEVVR							
		$M^{2+} \rightarrow y_7^+$	**521.3**	**829.4**			**23**	
		$M^{2+} \rightarrow y_6^+$	521.3	700.4	13.32 ± 0.10	55	26	30
		$M^{2+} \rightarrow y_8^+$	521.3	942.5		10	26	
	TVDNFVALATGEK							
		$M^{2+} \rightarrow y_7^+$	**686.9**	**697.4**			**31**	
		$M^{2+} \rightarrow y_8^+$	686.9	796.5	17.64 ± 0.09	88	31	60
		$M^{2+} \rightarrow y_5^+$	686.9	513.3		57	28	
	GAPDH (P04406)							
	VIPELNGK							
		$M^{2+} \rightarrow y_6^{++}$	**439.3**	**333.2**			**18**	
		$M^{2+} \rightarrow y_6^+$	439.3	665.4	10.16 ± 0.14	86	16	30
		$M^{2+} \rightarrow y_5^+$	439.3	568.3		9	25	
	VPTANVSVVDLTCR*							
		$M^{3+} \rightarrow y_5^+$	**514.3**	**674.3**			**21**	
		$M^{3+} \rightarrow y_3^+$	514.3	446.2	15.38 ± 0.10	82	19	60
		$M^{2+} \rightarrow y_5^+$	770.9	674.3		10	40	
	GALQNIIPASTGAAK							
		$M^{2+} \rightarrow y_9^+$	**710.4**	**1050.**[illegible]			**31**	
		$M^{2+} \rightarrow y_{11}^+$	710.4	936.6	14.62 ± 0.14	32	33	60
		$M^{2+} \rightarrow y_{10}^+$	710.4	823.5		18	33	
	β-Actin / γ-Actin (P60709 / P63261)							
	VAPEEHPVLLTEAPLNPK							
		$M^{3+} \rightarrow y_2^+$	654.7	252.2		105	45	
		$M^{3+} \rightarrow y_6^+$	**654.7**	**647.4**	15.26 ± 0.17		**30**	90
		$M^{3+} \rightarrow y_7^+$	654.7	776.4		52	30	
	DLYANTVLSGGTTMYPGIADR							
		$M^{3+} \rightarrow y_6^+$	**742.4**	**638.3**			**30**	
		$M^{3+} \rightarrow y_7^+$	742.4	801.4	20.49 ± 0.04	23	28	90
		$M^{3+} \rightarrow y_8^+$	742.4	932.5		8	28	

Tab. 7.5: COX-1 peptides data. For each unlabeled peptide, different ion types used as qualifier and quantifier (bold) transitions are shown with their associated Q1 and Q3 *m/z*, retention time (RT), relative ratios to quantifier transition as well as collision energies (CE). Retention times (RT) were calculated from sample batch.

Peptide	Transitions	Q1 *m/z*	Q3 *m/z*	RT [min]	Rel. Ratio to quantifier [%]	CE (V)
DCPTPMGTK						
	$M^{2+} \rightarrow b_2^{+}$	**503.7**	**276.1**			**20**
	$M^{2+} \rightarrow y_7^{+}$	503.7	731.4	6.45 ± 0.04	75	19
	$M^{2+} \rightarrow y_5^{+}$	503.7	533.3		42	31
LQPFNEYR						
	$M^{2+} \rightarrow b_2^{+}$	**533.8**	**242.2**			**21**
	$M^{2+} \rightarrow y_6^{+}$	533.8	825.4	11.82 ± 0.11	60	21
	$M^{2+} \rightarrow y_6^{++}$	533.8	413.2		32	24
AEHPTWGDEQLFQTTR						
	$M^{3+} \rightarrow y_{5+}$	**639.3**	**652.3**			**26**
	$M^{3+} \rightarrow y_4^{+}$	639.3	505.3	15.33 ± 0.13	69	28
	$M^{3+} \rightarrow b_{10}^{++}$	639.3	576.2		47	24

Tab. 7.6: Intra- and interday precisions COX-1/2 specific peptides, shown as relative deviation of the mean.

peptide	intraday precision [%]	interday precison [%]
VSQASIDQSR	3.0	10.3
NAIMSYVLTSR	7.3	10.6
LILIGETIK	3.9	3.3
FDPELLFNK	2.4	5.6

Tab. 7.7: Concentrations of selected prostanoids measured in human colon carcinoma cells and macrophages by targeted lipidomics (oxylipin metabolomics). All data are shown as mean ± deviation of the mean for n = 2.

	PGD_2	PGE_2	PGF_{2a}	TXB_2	12-HHT
concentration in pellet [pmol/mg protein]					
HCT-116	< LOD	0.35 ± 0.05	< LOD	< LOD	0.0292 ± 0.0004
HT-29	0.38 ± 0.06	1.8 ± 0.1	2.2 ± 0.3	0.19 ± 0.03	1.9 ± 0.2
HCA-7	0.69 ± 0.08	26 ± 2	1.9 ± 0.3	2.5 ± 0.4	5.5 ± 0.9
HCA-7 + 3 µM celecoxib	0.08 ± 0.02	4 ± 1	0.18 ± 0.05	0.12 ± 0.05	0.4 ± 0.1
HCA-7 + 5 µM indomethacin	< LOD	0.32 ± 0.01	< LOD	< LOD	0.034 ± 0.003
concentration in culture medium [nM]					
macroph. 0 h	1.14 ± 0.01	0.24 ± 0.02	0.84 ± 0.07	1.26 ± 0.05	1.89 ± 0.05
macroph. + 1 h 1 µg/mL LPS	1.19 ± 0.03	0.28 ± 0.01	1.01 ± 0.03	1.26 ± 0.01	1.37 ± 0.08
macroph. + 6 h 1 µg/mL LPS	1.80 ± 0.02	5 ± 3	7.6 ± 0.8	9.4 ± 0.8	6 ± 1
macroph. + 24 h 1 µg/mL LPS	1.46 ± 0.03	6 ± 4	14 ± 2	16 ± 1	0.3 ± 0.1
macroph. ctrl (24 h)	1.14 ± 0.07	0.28 ± 0.01	1.17 ± 0.09	1.36 ± 0.07	< LOD
medium ctrl (0 h)	0.95	0.28	0.87	1.21	2.23

Appendix of Chapter3

Tab. 7.8: Inhibition of COX-2 by selected polyphenols as described in [1]. IC_{50} values of the indicated compounds were determined on recombinant human COX-2. Data are expressed as mean and the 95% confidence interval; n=3. The IC_{50} values of most compounds were already reported in [1].

	COX-2 activity IC_{50} ± SD [µM]
genistein	> 30
IRA	> 50
resveratrol	0.4 (0.3, 0.7)
ε-viniferin	11 (3, 40)

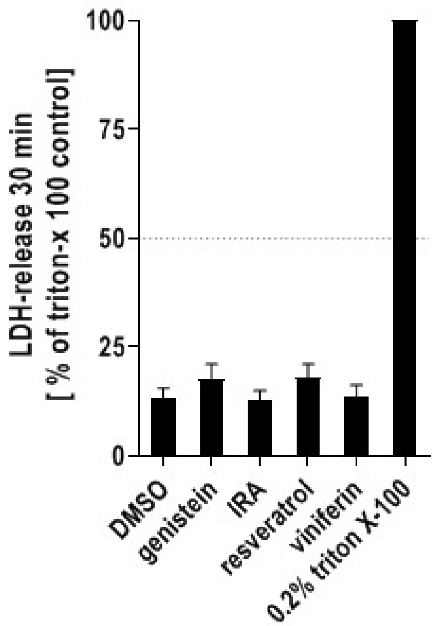

Fig. 7.8: Neutrophil cell integrity and survival measured by LDH release. Isolated human neutrophils were treated with 10 µM of the indicated compounds, DMSO (0.1%) as vehicle control and Triton-X 100 (0.2%) as positive control. LDH release was measured with PROMEGA´s CytoTox 96 Non-Radioactive Cytotoxicity Assay according to the manufacturer`s protocol. Data are expressed as percentage of positive control, mean ± SEM; n=3.

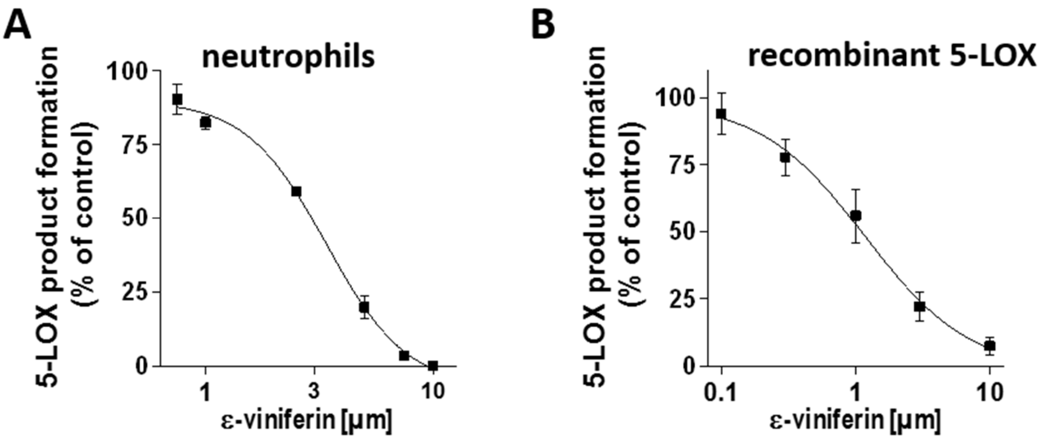

Fig. 7.9: Concentration-dependent inhibition of the 5-LOX pathway by ε-viniferin in human neutrophils and on isolated 5-LOX. Human neutrophils **(A)** and recombinant 5-LOX **(B)** were treated with indicated concentrations of ε-viniferin for 10 min at 37 °C and on ice, respectively. Subsequently, neutrophils were stimulated by Ca^{2+}-ionophore (2.5 µM), whereas recombinant 5-LOX was activated by $CaCl_2$ (2 mM) and arachidonic acid (20 µM), for 10 min at 37 °C. Metabolites were analyzed and quantified by UV-coupled HPLC using PGB_1 as internal standard. All isomers of LTB_4 and 5-H(p)ETE were considered as 5-LOX products. Data are expressed as percentage of DMSO control, mean ± SEM; n=5.

Appendix of Chapter 4

Preparation of Oxylipin Calibration Series

An oxylipin calibration series was prepared containing 54 analytes which was used in addition to the established calibration series [2]. Here, we provide a detailed description of all steps.

Before the preparation started, all reusable glass ware (e.g. volumetric flasks, volumetric pipettes, gastight syringes) was checked for residual interfering compounds by rinsing them with methanol and analyzing the rinsing solution with the targeted oxylipin metabolomics LC-MS/MS method [2-4]. Next, the retention times of the new analytes were determined using the established LC gradient. Their MS parameters were optimized using single stocks of 100 nM which were infused into the MS per flow injection mode without analytical column (0.3 mL/min, 35/65% A/B). The Q1 *m/z* were determined in Q1 scans. The Q3 *m/z* for the MRM method were selected from the recorded fragment ion spectra with collision energy (CE) ramps over a range of 20 V, under consideration of sensitivity and selectivity. Declustering potential (DP) and CE were then optimized for the selected transitions.

The single stocks of the internal standards were diluted to the anticipated working concentrations in the calibrators (20 nM, approx. equivalent to 20-times LLOQ) and analyzed with the MRM method. At this concentration 7(*S*),8(*R*),17(*S*)-TriHDHA-d5 (RvD1-d_5) was contaminated with the unlabeled analyte at concentrations >LLOQ. Therefore, we reduced the concentration of this IS by four-fold in the IS master mix and thus, no interference was found at the final calibrator concentration (5 nM).

Then, nine stock mixes ("master mixes", **Tab. 7.9**) were prepared avoiding direct light radiation. The analytes assigned to each of these either differed in retention time or *m/z*, enabling an interference-free measurement in single ion monitoring (SIM) mode for every analyte in each master mix according to Hartung et al [5]. In total, two internal standard master mixes, seven analyte master mixes and at the same time, working solutions (3-5 µM) for each analyte (for later optimization, etc.), were prepared (**Tab. 7.9**):

Standard Operating Procedure for the Preparation of Master Mixes

Pre-arrangements

- Get enough ice boxes / cold packs
- Prepare cleaning solvents
- Prepare working stocks
- Add fresh MeOH to fresh vial (volume in **Tab. 7.9**)
- Get the needed volumetric flasks (VF) and gas tight syringes (e.g. from Hamilton) ready, after they were checked for residues
- Put a bit of fresh MeOH in the clean VF
- Pipette the masters on **ice**
- Only take **5 single stock standards (STD)** out of the -80°C freezer at once

Master Mix Preparation

- *Work in groups of two, all main steps are done by partner A, unless stated otherwise*
- Warm the vial containing the single stock STD in the hand
    - Vortex
    - Draw the STD and set to correct volume with a gas tight syringe
- Show partner B the set volume
- Partner B checks it off the list or notes the actual volume
- Wipe the syringe tip with lint-free wipe (moistened with MeOH)
- Transfer volume to VF

- Give partner B the single stock STD
- Partner B: Prepare working stock
  - Add 1 µL of single stock STD with pipette to prepared vial with MeOH
  - Vortex
  - Store on ice
  - Close the single stock STD vial tightly
- Take next original vial of single stock STD and restart procedure
- Partner B: clean syringes with cleaning solvents
  - 10 x ACN I
  - 10 x ACN II
  - 10 x MeOH I
  - 10 x MeOH II
  - Dry syringe (move piston up and down)
  - Change cleaning solvents after 5 STDs
  - Wipe the syringe tip with lint-free wipe (moistened with MeOH)
- When all STDs are added to masters, warm VF with hand to RT
  - Fill to mark with MeOH
  - Mix master by turning flask upside down
  - Transfer to flasks with screwcaps
  - Store at -80°C

Tab. 7.9 (pages 149 – 150): Preparation of master mixes and working stocks from single stock standards.

	Cayman Item No.	Pre-cursor FA	Q1 *m/z*	RT [min]	single stock conc [µM]	single stock vol [µL]	master mix conc [µM]	master mix total vol [mL]	working stock volumes (STD + MeOH) [µL]
IS Master I									
15(*S*)-HETE-d_8	334720	ARA	327.2	19.88	304	32.9	5		
20-HETE-d_6	390030	ARA	325.2	17.97	306	32.7	5		
(±)9(10)-DiHOME-d_4	10009993	LA	317.2	14.84	314	31.9	5		
Leukotriene B_4-d_4	320110	ARA	339.2	13.76	734	13.6	5		
5(*S*),6(*R*),15(*S*)-TriHETE-d5 (Lipoxin A_4-d_5)	10007737	ARA	356.3	10.09	280	35.8	5	2	1 + 100
7(*S*),8(*R*),17(*S*)-TriHDHA-d_5 (Resolvin D1-d_5)	11182	DHA	380.3	10.19	262	9.5	1.25		
7(*S*),16(*R*),17(*S*)-TriHDHA-d_5 (Resolvin D2-d_5)	11184	DHA	380.2	9.40	262	38.2	5		
IS Master II									
15-deoxy-$^{\Delta12,14}$-PGJ_2-d_4	318570	ARA	319.4	17.68	312	250			1 + 100
PGE_2-d_4	314010	ARA	355.2	8.88	2805	50			1 + 600
PGD_2-d_4	312010	ARA	355.2	9.29	281	250	5	10	1 + 100
13,14-dihydro-15-keto-PGE_2-d_4	10010606	ARA	355.4	10.26	281	250			1 + 100
TxB_2-d_4	319030	ARA	373.3	7.66	267	250			1 + 100
Master I									
13,14-dihydro-15-keto-PGD_2	10007208	ARA	351.2	11.18	284	176			1 + 100
11-dehydro-2,3-dinor-TxB_2	19510	ARA	339.3	6.89	294	170			1 + 100
2,3-dinor-TxB_2	19050	ARA	341.2	5.68	292	171			1 + 100
PGD_3	12990	EPA	349.3	8.11	285	175			1 + 100
13,14-dihydro-15-keto-tetranor-PGD_2	13100	ARA	297.2	6.56	335	149			1 + 100
15-keto-PGE_1	13680	DGLA	351.3	9.96	500	100	10	5	1 + 100
PGD_1	12000	DGLA	353.2	9.36	500	100			1 + 100
13,14-dihydro-15-keto-PGD_1	10010425	DGLA	353.3	11.68	500	100			1 + 100
11-dehydro-TxB_2	19500	ARA	367	9.02	1357	37			1 + 300
11-dehydro-TxB_3	19995	EPA	365.3	7.73	273	183			1 + 100
TxB_3	19990	EPA	367.2	6.54	271	184			1 + 100
TxB_2	10007237	ARA	369.2	7.68	270	185			1 + 100
TxB_1	10006610	DGLA	371.3	7.37	500	100			1 + 100
Master II									
LTB_5	21110	EPA	333.3	11.95	299	167			
2,3-dinor-TxB_1	10006330	DGLA	343	5.17	290	172			
5(*S*),12(*R*),18(*R*)-TriHEPE (Resolvin E1)	10007848	EPA	349.3	6.25	143	351			
5(*S*),6(*R*),15(*S*)-TriHEPE (Lipoxin A_5)	10011453	EPA	349.1	8.77	285	175	10	5	1 + 100
15-keto-$PGF_{2\alpha}$	10007227	ARA	351.2	9.17	284	176			
5(*S*),6(*S*),15(*S*)-TriHETE (6(*S*)-Lipoxin A_4)	10049	ARA	351.2	10.51	284	176			
7(*R*),14(*S*)-DiHDHA (Maresin 1)	10878	DHA	359.1	13.60	277	180			
4(*S*),11(*R*),17(*S*)-TriHDHA (Resolvin D3)	13834	DHA	375.3	9.18	266	188			

Tab. 7.9 continued.

	Cayman Item No.	Pre-cursor FA	Q1 *m/z*	RT [min]	single stock conc [µM]	single stock vol [µL]	master mix conc [µM]	master mix total vol [mL]	working stock volumes (STD + MeOH) [µL]
Master III									
13,14-dihydro-15-keto-tetranor-PGE_2	13101	ARA	297	7.32	335	149	10	5	1 + 100
15-keto-PGE_2	10007215	ARA	349.2	9.50	285	175			1 + 100
PGD_2	10007202	ARA	351.2	9.37	284	176			1 + 100
8-iso-PGE_2	14350	ARA	351.4	8.69	1500	33			1 + 300
5(*S*),14(*R*),15(*S*)-TriHEPE (Lipoxin B_4)	90420	ARA	351.2	9.15	284	176			1 + 100
8-*iso*-PGE_1	13360	DGLA	353.4	8.84	1500	33			1 + 300
13,14-dihydro-PGE_1	13610	DGLA	355.4	9.81	500	100			1 + 100
20-OH-PGE_2	14950	ARA	367.2	3.74	1357	37			1 + 300
7(*S*),16(*R*),17(*S*)-TriHDHA (Resolvin D2)	10007279	DHA	375.3	9.45	266	188			1 + 100
1a,1b-dihomo-PGE_2	18665	ARA	379.4	11.40	1510	33			1 + 300
Master IV									
15-deoxy-$^{\Delta 12,14}$-PGJ_2	10007235	ARA	315.2	17.73	316	158	10	5	1 + 100
20-HEPE	19322	EPA	317.2	16.76	314	159			1 + 100
2,3-dinor-11β-$PGF_{2\alpha}$	16530	ARA	325.3	5.93	306	163			1 + 100
Δ12-PGJ_2	18550	ARA	333.3	11.89	2990	17			1 + 600
22-HDHA	19321	DHA	343.2	19.15	290	172			1 + 100
PGE_3	14990	EPA	349.3	7.74	1427	35			1 + 300
11β-$PGF_{2\alpha}$	10007224	ARA	353.3	7.82	282	177			1 + 100
11β-13,14-dihydro-15-keto $PGF_{2\alpha}$	16540	ARA	353.4	9.83	1410	35			1 + 300
13,14-dihydro-15-keto-$PGF_{2\alpha}$	10007226	ARA	353.3	10.28	282	177			1 + 100
13,14-dihydro-PGF_{2a}	16660	ARA	355.4	9.53	500	100			1 + 100
Master V									
13,14-dihydro-15-keto-PGE_2	10007214	ARA	351.2	10.29	284	176	10	5	1 + 100
2,3-dinor-6-keto-$PGF_{1\alpha}$	15120	DGLA	341.1	7.34	500	100			1 + 100
20-OH $PGF_{2\alpha}$	16950	ARA	369.3	3.59	1350	37			1 + 300
PGE_1	13010	DGLA	353.3	9.20	1500	33			1 + 300
13,14-dihydro-15-keto-PGE_1	13650	DGLA	353.3	10.81	500	100			1 + 100
9,10-DiH stearic acid	28612	OL	315.2	17.29	1504	33			1 + 300
PGB_1	11110	DGLA	335.4	12.27	1500	33			1 + 300
7(*S*),14(*S*)-DiHDHA (7-*epi*-Maresin 1)	13161	DHA	359.1	13.06	277	180			1 + 100
6,15-diketo-13,14-dihydro-$PGF_{1\alpha}$	15270	DGLA	369.3	7.72	2699	19			1 + 600
PGE_2	10007211	ARA	351.2	8.91	284	176			1 + 100
Master Rv I									
7(*S*),8(*R*),17(*S*)-TriHDHA (Resolvin D1)	25905	DHA	375.3	10.24	27	941	10	2.5	1 + 100
5(*S*),18(*R*)-DiHEPE (RvE2)	13827	EPA	333.2	11.27	299	84			
Master Rv II									
5(*S*),15(*S*)-DiHEPE (RvE4)	29590	EPA	333.2	11.85	299	84	10	2.5	1 + 100

ARA: arachidonic acid (20:4 n6), DGLA: dihomo-gamma-linolenic acid (20:3 n6), DHA: docosa-hexaenoic acid (22:6 n3), EPA: eicosapentaenoic acid (20:5 n3), LA: linoleic acid (18:2 n6), OL: oleic acid (18:1 n9)

Verification of Standard Concentrations

Only 12 analytes were available as STD with verified concentrations, i.e. MaxSpec standards (Cayman Chemical, Ann Arbor, MI, USA). In order to check the concentrations of the remaining analytes in regular quality, their SIM areas were compared to those of the MaxSpec STD, assuming comparable ionization efficiency for similar chemical structures as described [5]. For this, the master mixes were separately diluted to 100 nM and measured as triplicates in SIM mode using their Q1 *m/z* (**Tab. 7.9**). The mean SIM areas of structurally similar analytes were compared (under consideration of the actual volumes used for master preparation) and a correction factor was calculated if the difference between the analyte and the MaxSpec areas exceeded ±30%. This was the case for 21 analytes.

Preparation of Dilution Series for Calibration

The calibration series was prepared by serial dilution as follows

- *Work in groups of two, all main steps are done by partner A, unless stated otherwise*
- Get enough ice boxes / cold packs
- Get the needed volumetric flasks (VF) ready after they were checked for residues (**Tab. 7.10**)
- Add small volume of fresh MeOH in the clean VF
    - Add analyte master mixes/higher concentrated calibrator (**Tab. 7.10**)
    - Warm the flasks containing the analyte master mixes/calibrator in the hand
    - Vortex
    - Draw the volume of the analyte master mixes/calibrator with a volumetric pipette
    - Wipe the tip with lint-free wipe (moistened with MeOH)
    - Transfer volume to VF which is stored on ice and gently shake
    - Put analyte master mixes/calibrator back on ice immediately
- Partner B: Add IS
    - Warm the flasks containing the IS master mixes in the hand
    - Vortex
    - Draw volumes of IS masters with gastight syringes (**Tab. 7.10**)
    - Wipe the tip with lint-free wipe (moistened with MeOH)
    - Transfer volume to VF which is stored on ice and gently shake
- When all STDs are added to the VF, warm VF with hand to RT
    - Fill to mark with MeOH
        - **CAVE:** Calibrator 17: add exact volume of MeOH
    - Mix calibrator by turning flask upside down
- Repeat procedure until 18 calibrators are prepared (**Tab. 7.10**)
- Transfer each calibrator from VF to multiple vials
- Store at -80°C

Tab. 7.10: Preparation of new calibration series using master mixes.

calibrator no.	Analyte conc [nM]	final vol [mL]	type of STD	vol STD [mL]	vol IS master [µL] IS I	vol IS master [µL] IS II	vol MeOH [mL]	IS conc [nM]
18	1000	10	*all masters*	7 x 1	40	40	fill to	20
17	750	6.667	calibrator	5	7	7	1.65	20
16	500	25	*all masters*	7 x 1.25	100	100	fill to mark	20
15	250	20	calibrator	10	40	40		20
14	100	25	calibrator	5	80	80		20
13	50	25	calibrator	2.5	90	90		20
12	25	25	calibrator	2.5	90	90		20
11	10	25	calibrator	2.5	90	90		20
10	5	25	calibrator	2.5	90	90		20
9	2.5	25	calibrator	2.5	90	90		20
8	1	25	calibrator	2.5	90	90		20
7	0.75	20	calibrator	1.5	74	74		20
6	0.5	25	calibrator	2.5	90	90		20
5	0.25	25	calibrator 9	2.5	90	90		20
4	0.1	25	calibrator 8	2.5	90	90		20
3	0.05	20	calibrator 6	2	72	72		20
2	0.025	20	calibrator 5	2	72	72		20
1	0.01	20	calibrator 4	2	72	72		20

Preparation of RT Mixture

Few analytes with interfering MS transitions could not be fully chromatographically separated and were therefore not added to the master mixes. However, their transitions were added to the targeted oxylipin metabolomics method and a mixture of these analytes was prepared (50 nM, **Tab. 7.11**) in order to be able to monitor them in samples. This retention time mixture is regularly measured together with the calibration series.

Tab. 7.11: Analytes in the retention time mix for identification**.**

Analyte	Cayman Item No.	Pre-cursor FA	Q1 *m/z*	RT [min]	interfering oxylipin (RT [min])
11β-PGE_2	14510	ARA	351.2	9.11	LxB_4 (9.15)
15-keto-$PGF_{1α}$ *MaxSpec*	25902	DGLA	353.2	9.46	PGD_1 (9.36)
8-iso-15-keto-PGE_2	14390	ARA	349.2	9.47	15-keto-PGE_2 (9.50)
Δ12-PGD_2	12650	ARA	351.2	8.67	8-iso-PGE2 (8.69) + PGE_2 (8.91)
5(*S*),6(*R*),15(*R*)-TriHETE (15(*R*)-LxA_4)	90415	ARA	351.2	10.22	LxA_4 (10.23)
15(*R*)-PGD_2	10118	ARA	351.2	9.45	PGD_2 (9.37)
15(*R*)-PGE_2	14710	ARA	351.2	8.67	PGE_2 (9.01)
15(*R*)-$PGF_{2α}$	16740	ARA	353.2	8.48	$PGF_{2α}$ (8.65)
7(*S*),8(*R*),17(*R*)-TriHDHA (17(*R*)-RvD1)	13060	DHA	375.3	10.35	7(*S*),8(*R*),17(*S*)-TriHDHA (RvD1; 10.24)
4(*S*),11(*R*),17(*R*)-TriHDHA (17(*R*)-RvD3)	9002880	DHA	375.3	9.12	4(*S*),11(*R*),17(*S*)-TriHDHA (RvD3; 9.18)
8-iso-15(*R*)-$PGF_{2α}$	16395	ARA	353.2	8.48	$PGF_{2α}$ (8.65)

ARA: arachidonic acid (20:4 n6)
DGLA: dihomo-gamma-linolenic acid (20:3 n6)
DHA: docosahexaenoic acid (22:6 n3)

The final targeted LC-MS/MS based oxylipin metabolomics method thus allows to quantitatively measure 198 oxylipins (using 29 IS) derived from twelve different polyunsaturated fatty acid precursors formed via the three enzymatic branches of the ARA cascade as well as autoxidation. The parameters for the analysis of the prepared calibration series and analytes of the retention time mix can be found in **Tab. 7.12**.

Tab. 7.12 (pages 155 – 157): Parameters for the LC-MS/MS analysis of the oxylipins in the prepared calibration series and the retention time mix. Shown are mass transitions with Q1 and Q3 *m/z*, MS parameters including declustering potential (DP), entrance potential (EP), collision energy (CE) and collision cell exit potential (CXP), internal standards used for quantification, retention time (RT), limit of detection (LOD), lower limit of quantification (LLOQ) and upper limit of quantification (ULOQ).

Analyte	Mass transition Q1 m/z	Mass transition Q3 m/z	MS parameters DP [V]	EP [V]	CE [V]	CXP [V]	Internal standard	RT [min]	LOD [nM]	calibration range LLOQ [nM]	ULOQ [nM]
11-dehydro-2,3-dinor-TxB_2	339.3	133.0	-55	-10	-20	-7	$^2H_4$-TxB_2	6.89	0.57	0.76	762
11-dehydro-TxB_2	367.0	161.1	-70	-10	-26	-8	$^2H_4$-TxB_2	9.02	0.21	0.31	412
11-dehydro-TxB_3	365.3	161.2	-70	-10	-24	-8	$^2H_4$-TxB_2	7.73	0.74	1.84	737
11β-13,14-dihydro-15-keto $PGF_{2\alpha}$	353.4	195.0	-85	-10	-34	-7	$^2H_4$-13,14-dihydro-15-keto PGE_2	9.83	18.25	45.62	1825
11β-PGE_2	351.3	189.1	-60	-10	-24	-7	*theoretically* $^2H_4$-PGE_2 1)	9.11			
11β-$PGF_{2\alpha}$	353.3	193.1	-70	-10	-35	-12	$^2H_4$-PGE_2	7.82	0.50	0.75	1000
13,14-dihydro PGE_1	355.4	237.1	-70	-10	-37	-7	$^2H_4$-13,14-dihydro-15-keto PGE_2	9.81	0.17	0.35	698
13,14-dihydro-15-keto PGD_2	351.2	207.0	-55	-10	-25	-7	$^2H_4$-13,14-dihydro-15-keto PGE_2	11.18	0.25	0.50	1000
13,14-dihydro-15-keto-PGD_1	353.3	209.0	-65	-10	-31	-7	$^2H_4$-13,14-dihydro-15-keto PGE_2	11.68	0.25	0.50	1000
13,14-dihydro-15-keto-PGE_1	353.3	221.2	-70	-10	-29	-6	$^2H_4$-13,14-dihydro-15-keto PGE_2	10.81	0.25	0.50	1000
13,14-dihydro-15-keto-PGE_2	351.2	235.2	-75	-10	-18	-13	$^2H_4$-13,14-dihydro-15-keto PGE_2	10.29	10.00	25.00	1000
13,14-dihydro-15-keto-$PGF_{2\alpha}$	353.3	183.3	-100	-10	-35	-10	$^2H_4$-13,14-dihydro-15-keto PGE_2	10.28	0.75	1.00	1000
13,14-dihydro-15-keto-tetranor-PGD_2	297.2	109.0	-55	-10	-31	-7	$^2H_4$-13,14-dihydro-15-keto PGE_2	6.56	1.04	1.55	2070
13,14-dihydro-15-keto-tetranor-PGE_2	297.0	109.0	-70	-10	-18	-8	$^2H_4$-13,14-dihydro-15-keto PGE_2	7.32	0.39	0.79	1579
13,14-dihydro-$PGF_{2\alpha}$	355.4	193.0	-90	-10	-34	-7	$^2H_4$-13,14-dihydro-15-keto PGE_2	9.53	5.00	10.00	1000
15(*R*)-PGD_2	351.2	271.3	-80	-10	-23	-6	*theoretically 2H4-PGD2* 1)	9.45			
15(*R*)-PGE_2	351.2	271.3	-80	-10	-23	-6	*theoretically* $^2H_4$-PGE_2 1)	8.67			
15(*R*)-$PGF_{2\alpha}$	353.2	193.0	-80	-10	-33	-7	*theoretically* $^2H_4$-$PGF_{2\alpha}$ 1)	8.48			
15-deoxy-$\Delta^{12,14}$-PGJ_2	315.2	203.1	-90	-10	-28	-7	$^2H_4$-15-deoxy-Δ12,14-PGJ_2	17.73	0.75	1.00	1000
15-keto PGE_1	351.3	209.0	-90	-10	-31	-7	$^2H_4$-PGE_2	9.96	2.50	5.00	1000
15-keto PGE_2	349.2	235.1	-80	-10	-20	-7	$^2H_4$-PGE_2	9.50	0.25	0.50	750
15-keto $PGF_{2\alpha}$	351.2	219.1	-60	-10	-23	-7	$^2H_4$-PGE_2	9.17	0.50	0.75	750
15-keto-$PGF_{1\alpha}$	353.3	193.1	-70	-10	-37	-6	*theoretically* $^2H_4$-$PGF_{2\alpha}$ 1)	9.46			
1a,1b-dihomo PGE_2	379.4	261.2	-70	-10	-21	-7	$^2H_4$-PGE_2	11.40	0.03	0.06	451
2,3-dinor-11β-$PGF_{2\alpha}$	325.3	163.0	-65	-10	-19	-7	$^2H_4$-PGE_2	5.93	0.65	1.31	2613

Tab. 7.12 continued.

Analyte	Mass transition Q1 *m/z*	Q3 *m/z*	MS parameters DP [V]	EP [V]	CE [V]	CXP [V]	Internal standard	RT [min]	LOD [nM]	calibration range LLOQ [nM]	ULOQ [nM]
2,3-dinor-6-keto $PGF_{1\alpha}$	341.1	135.0	-90	-10	-31	-7	$^2H_4$-PGE_2	7.34	0.15	0.25	800
2,3-dinor-TxB_1	343.0	142.9	-70	-10	-18	-8	$^2H_4$-TxB2	5.17	1.00	2.50	750
2,3-dinor-TxB_2	341.2	167.0	-70	-10	-14	-8	$^2H_4$-TxB2	5.68	1.00	2.50	1000
20-HEPE	317.2	287.3	-70	-10	-18	-8	$^2H_6$-20-HETE	16.76	0.25	0.50	1000
20-OH $PGF_{2\alpha}$	369.3	193.0	-70	-10	-37	-7	$^2H_4$-PGE_2	3.59	1.06	1.59	2121
20-OH-PGE_2	367.2	189.1	-70	-10	-27	-8	$^2H_4$-PGE_2	3.74	0.57	1.14	2288
22-HDHA	343.2	313.2	-85	-10	-18	-7	$^2H_6$-20-HETE	19.15	0.75	1.00	1000
$^2H_4$-13,14-dihydro-15-keto PGE_2	355.4	239.1	-65	-10	-31	-7	*internal standard*	10.26			
$^2H_4$-15-deoxy-$\Delta^{12,14}$-PGJ_2	319.4	203.0	-80	-10	-31	-7	*internal standard*	17.68			
$^2H_4$-PGD_2	355.2	275.3	-80	-10	-24	-6	*internal standard*	9.35			
$^2H_4$-PGE_2	355.2	275.3	-80	-10	-24	-6	*internal standard*	8.88			
$^2H_4$-TxB_2	373.3	173.2	-85	-10	-23	-8	*internal standard*	7.66			
4(*S*),11(*R*),17(*R*)-TriHDHA (17(*R*)-RvD3)	375.3	147.0	-80	-10	-24	-10	*theoretically* $^2H_5$-7(*S*),16(*R*),17(*S*) -TriHDHA (RvD2) [1)]	9.12			
4(*S*),11(*R*),17(*S*)-TriHDHA (RvD3)	375.3	147.0	-80	-10	-24	-10	$^2H_5$-7(*S*),16(*R*),17(*S*) -TriHDHA (RvD2)	9.18	0.25	0.50	1000
5(*S*),12(*R*),18(*R*)-TriHEPE (RvE1)	349.3	195.0	-80	-10	-22	-10	$^2H_5$-7(*S*),16(*R*),17(*S*) -TriHDHA (RvD2)	6.25	0.25	0.50	1000
5(*S*),14(*R*),15(*S*)-TriHEPE (LxB_4)	351.2	221.0	-70	-10	-21	-13	$^2H_5$-5(*S*),6(*R*),15(*S*)-TriHETE (LxA_4)	9.15	0.50	0.75	1000
5(*S*),15(*S*)-DiHEPE (RvE4)	333.2	115.0	-80	-10	-19	-7	$^2H_4$-LTB_4	11.85	0.25	0.50	1000
5(*S*),18(*R*)-DiHEPE (RvE2)	333.2	253.3	-80	-10	-19	-9	$^2H_4$-LTB_4	11.27	4.63	9.26	1852
5(*S*),6(*R*),15(*R*)-TriHETE (15(*R*)-LxA4)	351.2	235.1	-70	-10	-18	-15	*theoretically* $^2H_5$-5(*S*),6(*R*),15(*S*)-TriHETE (LxA_4) [1)]	10.22			
5(*S*),6(*R*),15(*S*)-TriHEPE (LxA_5)	349.1	215.0	-70	-10	-24	-13	$^2H_5$-5(*S*),6(*R*),15(*S*)-TriHETE (LxA_4)	8.77	1.00	2.50	1000
5(*S*),6(*S*),15(*S*)-TriHETE (6(*S*)-LxA_4)	351.2	235.1	-70	-10	-18	-5	$^2H_5$-5(*S*),6(*R*),15(*S*)-TriHETE (LxA_4)	10.51	0.75	1.00	1000
6,15-diketo-13,14-dihydro $PGF_{1\alpha}$	369.3	267.0	-70	-10	-31	-7	$^2H_4$-PGE_2	7.72	45.49	75.82	3033
7(*R*),14(*S*)-DiHDHA (MaR1)	359.1	250.2	-80	-10	-19	-14	$^2H_4$-LTB_4	13.60	0.75	1.00	1000
7(*S*),14(*S*)-DiHDHA (7-*epi*-MaR1)	359.1	250.1	-80	-10	-20	-5	$^2H_4$-LTB_4	13.06	0.50	0.75	1000
7(*S*),16(*R*),17(*S*)-TriHDHA (RvD2)	375.3	141.0	-80	-10	-21	-8	$^2H_5$-7(*S*),16(*R*),17(*S*) -TriHDHA (RvD2)	9.45	0.75	1.00	1000

Tab. 7.12 continued.

Analyte	Mass transition Q1 *m/z*	Q3 *m/z*	MS parameters DP [V]	EP [V]	CE [V]	CXP [V]	Internal standard	RT [min]	LOD [nM]	calibration range LLOQ [nM]	ULOQ [nM]
7(*S*),8(*R*),17(*R*)-TriHDHA (17(*R*)-RvD1)	375.3	141.0	-70	-10	-19	-15	*theoretically* $^{2}H_5$-7(*S*),8(*R*),17(*S*)-TriHDHA (RvD1) [1)]	10.35			
7(*S*),8(*R*),17(*S*)-TriHDHA (RvD1)	375.3	141.0	-70	-10	-19	-8	$^{2}H_5$-7(*S*),8(*R*),17(*S*)-TriHDHA (RvD1)	10.24	0.05	0.10	1000
8-iso-15(*R*)-$PGF_{2\alpha}$	353.2	193.0	-80	-10	-33	-7	*theoretically* $^{2}H_4$-$PGF_{2\alpha}$ [1)]	8.48			
8-*iso*-15-keto PGE_2	349.4	235.0	-65	-10	-19	-7	*theoretically* $^{2}H_4$-PGE_2 [1)]	9.47			
8-*iso*-PGE_1	353.4	235.0	-80	-10	-19	-7	$^{2}H_4$-PGE_2	8.84	0.25	0.50	500
8-*iso*-PGE_2	351.4	271.2	-55	-10	-23	-7	$^{2}H_4$-PGE_2	8.69	0.10	0.25	500
9,10-DiH-stearic acid	315.2	170.8	-85	-10	-35	-9	$^{2}H_4$-9,10-DiHOME	17.29			
LTB_5	333.3	195.2	-80	-10	-21	-8	$^{2}H_4$-LTB_4	11.95	0.25	0.50	1000
PGB1	335.4	221.0	-85	-10	-28	-7	$^{2}H_4$-15-deoxy-Δ12,14-PGJ_2	12.27	0.05	0.10	750
PGD_1	353.3	317.2	-80	-10	-19	-6	$^{2}H_4$-PGD_2	9.36	0.05	0.10	250
PGD_2	351.2	271.3	-80	-10	-23	-6	$^{2}H_4$-PGD_2	9.37	0.75	1.00	750
PGD_3	349.3	269.2	-80	-10	-21	-6	$^{2}H_4$-PGD_2	8.11	0.50	0.75	1000
PGE_1	353.3	317.2	-80	-10	-19	-6	$^{2}H_4$-PGE_2	9.20	0.05	0.10	250
PGE_2	351.2	271.3	-80	-10	-23	-6	$^{2}H_4$-PGE_2	8.91	0.25	0.50	750
PGE_3	349.3	269.2	-80	-10	-21	-6	$^{2}H_4$-PGE_2	7.74	0.37	0.73	1462
TxB_1	371.3	171.2	-90	-10	-33	-10	$^{2}H_4$-TxB2	7.37	0.40	0.80	1608
TxB_2	369.2	169.1	-80	-10	-24	-7	$^{2}H_4$-TxB2	7.68	0.25	0.50	1000
TxB_3	367.3	169.3	-90	-10	-33	-8	$^{2}H_4$-TxB2	6.54	3.23	4.30	4301
Δ12-PGD_2	351.3	233.1	-60	-10	-18	-7	*theoretically* $^{2}H_4$-PGD_2 [1)]	8.67			
Δ12-PGJ_2	333.3	189.2	-70	-10	-21	-8	$^{2}H_4$-15-deoxy-Δ12,14-PGJ_2	11.89	0.86	1.28	1712

[1)] preparation of indepentent calibration necessary due to interferences

Further Supplementary Tables and Figures

Tab. 7.13 (page 159): Proteotypic peptides for targeted proteomics method. The proteotypic peptides (PTPs) were selected from an in silico tryptic digest of 5-LOX, FLAP, 12-LOX, 15-LOX, 15-LOX-2 and CYC1. The peptides were selected based on peptide length (7-22 aa), uniqueness, cleavage probability calculated with peptide cutter (≥ 90%) or cleavage prediction with decision trees (CP-DT; ≥ 70%), occurrence of single nucleotide polymorphisms (SNPs), variation in splice variants or posttranslational modifications (PTMs), as well as unfavored amino acids (C, M, N, Q, W; max. 2) and predicted retention time (RT; 3 – 30 min).

Peptides	Position	$[M+H]^+$	Length [aa]	Uniqueness[a)]	C-terminal cleavage probability[b)] [%]	Overall cleavage probability[c)] [%]	SNPs[d)]	varination in splice variants[e)]	PTMs[f)]	Unfavored aa	Pred. RT [min][g)]
Lipoxygenase (5-LOX, P09917, gene: ALOX5)											
DDGLLVWEAIR	473-483	1286.7	11	unique	100%	98%	-	differs in isoform delta-10-13	-	1 × W	23.50
NLEAIVSVIAER	641-652	1313.7	12	unique	100%	97%	-	missing in isomform delta-10-13 & missing in alpha-10	-	1 × N	20.40
5-Lipoxygenase-activating protein (FLAP, P20292, gene: ALOX5AP)											
TGTLAFER	45-52	894.0	8	unique	94%	98%	-	-	-	-	10.80
YFVGYLGER	97-105	1103.2	9	unique	100%	97%	-	-	-	-	15.50
12-Lipoxygenase (12-LOX, P18054, gene: ALOX12)											
LWEIIAR	467-473	900.1	7	unique	100%	97%	-	-	-	1 × W	16.70
AVLNQFR	622-628	847.0	7	unique	100%	90%	-	-	-	1 × N; 1 × Q	10.40
15-Lipoxygenase (15-LOX, P16050, gene: ALOX15)											
EITEIGLQGAQDR	501-513	1429.7	13	unique	100%	97%	-	-	-	2 × Q	12.80
GFPVSLQAR	514-522	974.5	9	unique	100%	96%	-	-	-	1 × Q	12.00
15-Lipoxygenase-2 (15-LOX-2, O15296, gene: ALOX 15B)											
VSTGEAFGAGTWDK	7-21	1425.5	14	unique	90%	94%	-	-	-	1 × W	13.40
ELLIVPGQVVDR	418-429	1337.6	12	unique	100%	95%	-	missing in isoform O15296-2 (15-LOX2sv-b) and O15296-4 (15-LOX2sv-a)	-	1 × Q	17.40
Cytochrome C1 (CYC1, P08574, gene: CYC1)											
HLVGVCYTEDEAK	134-146	1520.7	13	unique	82%	92%	-	-	-	1 × C	8.70
DVCTFLR	269-275	910.4	7	unique	100%	99%	-	-	-	1 × C	13.00

[a)]from BLAST and NeXtprot; [b)]calculated from peptide cutter; [c)]calculated from CP-DT; [d)]SNPs from Uniprot; [e)]splice variants from Uniprot; [f)]PTMs from Uniprot and Phosphosite Plus; [g)]predicted RT from SSRCal; -: not reported; *: carbamidomethylated cys

Tab. 7.14: Parameters for analysis of housekeeper peptides via LC-MS/MS. **(A)** Unlabeled and **(B)** heavy labeled (lys: U-$^{13}C_6$; U-$^{15}N_2$; arg: U-$^{13}C_6$; U-$^{15}N_4$) peptide data for housekeeper peptides GAPDH, PPIB, β-/γ-actin, CYC1, updated from Hartung et al [6]. For each peptide, different CAD fragment ions used for qualification and quantification (top) with their Q1 and Q3 *m/z* are shown with retention time (RT, mean ± SD, n =12), relative ratios to quantifier transition as well as collision energies (CE). For unlabeled peptides **(A)** linear calibration range is shown for quantifier transitions, as well as the transitions of the corresponding heavy labeled peptides used as internal standards (IS) for the quantification, limits of detection (LOD) and lower limits of quantification (LLOQ). Accuracy of calibrators was within a range of ± 20%. The spiking levels of the heavy labeled peptides (concentrations in vial) are in shown **(B)**.

(A)

Gene / Protein (UniProtKB No.)	Peptide	Transitions	Q1 *m/z*	Q3 *m/z*	RT [min]	Rel. Ratio to quantifier [%]	CE (V)	IS Transitions	Calibration Range [µM]
ACTB & ACTG1 / β-Actin & γ-Actin	**VAPEEHPVLLTEAPLNPK**	$M^{3+} \rightarrow y_5^{+}$	652.0	568.4		100	45		
		$M^{3+} \rightarrow y_{16}^{++}$	652.0	892.5	15.70 ± 0.04	86	38	$M^{3+} \rightarrow y_6^{+}$	0.01 ± 10
(P60709 / P63261)		$M^{3+} \rightarrow y_8^{+}$	652.0	869.5		45	42		
	DLYANTVLSGGTTMYPGIADR	$M^{3+} \rightarrow y_6^{+}$	739.0	628.3		100	47		
		$M^{3+} \rightarrow y_7^{+}$	739.0	791.4	20.66 ± 0.01	64	40	$M^{3+} \rightarrow y_6^{+}$	0.01 ± 10
		$M^{3+} \rightarrow y_8^{+}$	739.0	922.5		31	38		
PPIB / Peptidyl-prolyl cis-trans isomerase B	**IGDEDVGR**	$M^{2+} \rightarrow y_7^{+}$	430.7	747.3		100	26		
		$M^{2+} \rightarrow y_6^{+}$	430.7	690.3	5.99 ± 0.01	27	26	$M^{2+} \rightarrow y_7^{+}$	0.01 ± 10
		$M^{2+} \rightarrow y_5^{+}$	430.7	575.3		19	31		
(PPIB; P23284)	**VLEGMEVVR**	$M^{2+} \rightarrow y_7^{+}$	516.3	819.4		100	33		
		$M^{2+} \rightarrow y_6^{+}$	516.3	690.4	13.69 ± 0.02	41	36	$M^{2+} \rightarrow y_7^{+}$	0.01 ± 7.5
		$M^{2+} \rightarrow y_8^{+}$	516.3	932.5		12	36		
GAPDH / Glycer-aldehyde-3-phosphate dehydrogenase	**VPTANVSVVDLTCR**	$M^{3+} \rightarrow y_5^{+}$	510.9	664.3		100	31		
		$M^{3+} \rightarrow y_3^{+}$	510.9	436.2	15.75 ± 0.02	48	29	$M^{3+} \rightarrow y_5^{+}$	0.01 ± 10
		$M^{3+} \rightarrow y_4^{+}$	510.9	549.3		50	37		
	GALQNIIPASTGAAK	$M^{2+} \rightarrow y_8^{+}$	706.4	702.4		100	43		
(GAPDH; P04406)		$M^{2+} \rightarrow y_9^{+}$	706.4	815.5	15.10 ± 0.03	38	46	$M^{2+} \rightarrow y_9^{+}$	0.01 ± 10
		$M^{2+} \rightarrow y_{11}^{+}$	706.4	1042.6		19	43		
CYC1 / Cytochrome c1	**HLVGVCYTEDEAK**	$M^{3+} \rightarrow y_6^{+}$	507.6	692.3		100	22		
		$M^{3+} \rightarrow y_7^{+}$	507.6	855.4	10.42 ± 0.07	82	16	$M^{3+} \rightarrow y_6^{+}$	0.01 ± 10
(CYC1; P08574)		$M^{3+} \rightarrow b_6^{+}$	507.6	666.3		58	20		
	DVCTFLR	$M^{2+} \rightarrow y_5^{+}$	455.7	696.4		100	20		
		$M^{2+} \rightarrow y_5^{++}$	455.7	348.7	14.86 ± 0.03	45	18	$M^{2+} \rightarrow y_5^{+}$	0.01 ± 10
		$M^{2+} \rightarrow y_4^{+}$	455.7	536.3		40	22		

Tab. 7.14 continued.

(B)

Gene / Protein (UniProtKB No.)	Peptide	Transitions	Q1 *m/z*	Q3 *m/z*	RT [min]	Rel. Ratio to quantifier [%]	CE (V)	Spiking level in vial [nM]
ACTB & ACTG1 / β-Actin & γ-Actin (P60709 / P63261)	**VAPEEHPVLLTEAPLNPK**	$M^{3+} \rightarrow y_6^{+}$	654.7	647.4		100	30	
		$M^{3+} \rightarrow y_7^{+}$	654.7	776.4	15.70 ± 0.04	98	30	100
		$M^{3+} \rightarrow y_2^{+}$	654.7	252.2		81	45	
	DLYANTVLSGGTTMYPGIAD	$M^{3+} \rightarrow y_6^{+}$	742.4	638.3		100	30	
		$M^{3+} \rightarrow y_7^{+}$	742.4	801.4	20.66 ± 0.01	50	28	100
		$M^{3+} \rightarrow y_8^{+}$	742.4	932.5		20	28	
PPIB / Peptidyl-prolyl cis-trans isomerase B (PPIB; P23284)	**IGDEDVGR**	$M^{2+} \rightarrow y_7^{+}$	435.7	757.3		100	21	
		$M^{2+} \rightarrow y_6^{+}$	435.7	700.3	5.99 ± 0.01	31	21	50
		$M^{2+} \rightarrow y_5^{+}$	435.7	585.3		17	26	
	VLEGMEVVR	$M^{2+} \rightarrow y_7^{+}$	521.3	829.4		100	23	
		$M^{2+} \rightarrow y_6^{+}$	521.3	700.4	13.69 ± 0.02	40	26	50
		$M^{2+} \rightarrow y_8^{+}$	521.3	942.5		13	26	
GAPDH / Glycer-aldehyde-3-phosphate dehydrogenase (GAPDH; P04406)	**VPTANVSVVDLTCR**	$M^{3+} \rightarrow y_5^{+}$	514.3	674.3		100	21	
		$M^{2+} \rightarrow y_5^{+}$	770.9	674.3	15.75 ± 0.02	5	40	50
		$M^{3+} \rightarrow y_3^{+}$	514.3	446.2		46	19	
	GALQNIIPASTGAAK	$M^{2+} \rightarrow y_9^{+}$	710.4	823.5		100	31	
		$M^{2+} \rightarrow y_{11}^{+}$	710.4	1050.6	15.10 ± 0.03	40	33	50
		$M^{2+} \rightarrow y_{10}^{+}$	710.4	936.6		22	33	
CYC1 / Cytochrome c1 (CYC1; P08574)	**HLVGVCYTEDEAK**	$M^{3+} \rightarrow y_6^{+}$	510.2	700.3		100	22	
		$M^{3+} \rightarrow y_7^{+}$	510.2	863.4	10.42 ± 0.07	80	16	50
		$M^{3+} \rightarrow b_6^{+}$	510.2	666.3		61	20	
	DVCTFLR	$M^{2+} \rightarrow y_5^{+}$	460.7	706.4		100	20	
		$M^{2+} \rightarrow y_5^{++}$	460.7	353.7	14.86 ± 0.03	40	18	50
		$M^{2+} \rightarrow y_4^{+}$	460.7	546.3		36	22	

Tab. 7.15: Protein levels in human platelets. Platelet-rich plasma was generated from EDTA-blood after centrifugation and platelets were then isolated from the platelet-rich plasma after subsequent centrifugation. Protein levels were quantified via LC-MS/MS based targeted proteomics, shown are mean ± SEM in pg/mg protein from n=3 donors.

	Protein abundance levels [pg/mg] total protein in human platelets						
donor	**COX-1**	**COX-2**	**5-LOX**	**FLAP**	**12-LOX**	**15-LOX**	**15-LOX-2**
A	1.2	<LLOQ	<LLOQ	<LLOQ	0.7	<LLOQ	<LLOQ
B	1.6				0.6		
C	0.5				0.4		

Tab. 7.16: Investigation of the ARA cascade in primary human macrophages. **(A)** Oxylipin concentrations and **(B)** protein levels in human macrophages derived from primary blood monocytic cells. Cells were differentiated with 10 ng/mL CSF-2 (M1-like cells) or CSF-1 (M2-like cells) for 8 days. For the final 48 h, they were treated with 10 ng/mL IFNγ (M1-like cells) or IL-4 (M2-like cells) and with or without 1 µg/mL LPS for the final 6 h. For M-like cells, the adhered monocytes were left untreated for 8 days (mean ± SEM, n=5-6). All data was obtained by LC-MS/MS based targeted oxylipin metabolomics and proteomics.

(A) Oxylipin concentrations [pmol/mg protein]

	M0	**M1**	**M1 + LPS**	**M2**	**M2 + LPS**
PGE_2	< LLOQ	0.6 ± 0.2	2.3 ± 0.5	2.0 ± 0.8	3 ± 1
12-HHT	< LLOQ	5 ± 1	18 ± 5	19 ± 6	35 ± 13
5-HETE	< LLOQ	0.5 ± 0.1	5 ± 3	2.1 ± 0.4	2.1 ± 0.4
12-HETE	9 ± 6	1.0 ± 0.5	2 ± 3	21 ± 2	23 ± 3
15-HETE	< LLOQ	1.1 ± 0.4	13 ± 3	243 ± 20	241 ± 15

(B) Protein levels [pmol/mg protein]

	M0	**M1**	**M1 + LPS**	**M2**	**M2 + LPS**
COX-1	2.7 ± 0.8	0.4 ± 0.1	0.4 ± 0.1	1.3 ± 0.3	1.6 ± 0.3
COX-2	< LLOQ	< LLOQ	0.4 ± 0.1	< LLOQ	0.5 ± 0.1
5-LOX	< LLOQ	0.4 ± 0.2	0.13 ± 0.02	0.18 ± 0.08	0.3 ± 0.1
FLAP	< LLOQ	19 ± 6	25 ± 7	4 ± 1	4.9 ± 2
12-LOX	0.8 ± 0.3	< LLOQ	< LLOQ	< LLOQ	< LLOQ
15-LOX	< LLOQ	< LLOQ	< LLOQ	8 ± 3	8 ± 2
15-LOX-2	< LLOQ	< LLOQ	< LLOQ	0.28 ± 0.03	0.3 ± 0.1

Tab. 7.17 (page 164 – 166): Modulation of the ARA cascade in primary human macrophages. Effects of ARA cascade modulation on **(A)** oxylipin concentrations and **(B)** protein levels of the COX, 5- ,12-, 15-LOX and 15-LOX-2 pathways in human macrophages derived from primary blood monocytic cells. Cells were differentiated with 10 ng/mL CSF-2 (M1-like cells) or CSF-1 (M2-like cells) for 8 days and with 10 ng/mL IFNγ (M1-like cells) or IL-4 (M2-like cells) for the final 48 h. The cells were incubated with the different pharmaceuticals at the following concentrations for the final 7 h during additional LPS stimulation (1 µg/mL) for the final 6 h: 1 µM COX-1/2 inhibitor indomethacin, 100 nM dexamethasone, 5 µM COX-2 inhibitor celecoxib, 5 µM 5-LOX inhibitor PF4191834, 10 µM 15-LOX inhibitor ML351 or 0.1% DMSO as control.

The concentrations of **(A) i)** oxylipins and **(B) i)** proteins were determined in each sample and **(A) ii), (B) ii)** calculated relative to the mean of both controls per donor as well as **(A) iii)**, **(B) iii)** the overall means ± SEM/mean deviation per test compound. In case the concentrations of analytes were < LLOQ and ≥ LOD the LOD was used and for concentrations < LOD the half LLOQ was used for relative calculation. All data was obtained by LC-MS/MS based targeted oxylipin metabolomics and proteomics.

			(A) i) Oxylipin conc [pmol/mg protein]					(B) i) Protein levels [pmol/mg protein]						
	Donor	Incubation	12-HHTrE	PGE_2	5-HETE	12-HETE	15-HETE	COX-1	COX-2	5-LOX	FLAP	12-LOX	15-LOX	15-LOX-2
M1 + 1 µg/mL LPS	A	Ctrl. 1	17	0.61	0.26	0.33	7.4	0.39	0.12	0.15	24	< LOD	< LOD	< LOD
		Ctrl. 2	18	0.71	0.32	0.21	5.2	0.61	0.17	0.24	41			
		Indomethacin	1.4	0.077	0.26	0.19	0.43	0.62	0.20	0.23	41			
		Dexamethasone	16	0.77	0.26	0.26	3.6	0.59	0.077	0.28	39			
		PF4191834	18	0.88	0.25	0.16	2.8	0.65	0.14	0.46	43			
	B	Ctrl. 1	20	1.2	0.49	2.0	18	0.41	0.22	0.086	21	< LOD	< LOD	< LOD
		Ctrl. 2	20	1.1	0.58	1.7	17	0.48	0.27	0.11	27			
		Indomethacin	4.3	0.18	0.49	1.2	1.5	0.63	0.36	0.15	35			
		Dexamethasone	13	0.55	0.54	1.0	9.3	0.87	0.24	0.22	49			
		PF4191834	15	0.89	0.52	0.25	11	0.74	0.29	0.30	38			
	C	Ctrl. 1	30	2.4	0.69	0.26	16	1.2	0.56	0.22	49	< LOD	< LOD	< LOD
		Ctrl. 2	22	1.9	0.77	0.21	12	0.94	0.41	0.27	47			
		Indomethacin	3.6	0.25	0.71	0.44	0.81	1.1	0.49	0.20	49			
		Dexamethasone	16	1.4	1.2	0.20	7.8	0.93	0.17	0.30	46			
		PF4191834	40	2.8	0.44	0.14	11	1.1	0.38	0.31	44			
	D	Ctrl. 1	37	5.4	1.9	0.17	18	1.3	0.75	0.44	41	< LOD	< LOD	< LOD
		Ctrl. 2	29	4.3	1.7	0.26	18	1.1	0.58	0.35	29			
		Indomethacin	4.3	0.42	2.0	0.35	1.1	1.0	0.60	0.32	24			
		Dexamethasone	14	2.1	5.5	0.22	5.7	1.2	0.25	0.64	31			
		PF4191834	32	3.4	1.3	0.34	13	1.1	0.43	0.56	18			
M2 +1 µg/mL LPS	A	Ctrl .1	38	2.3	0.42	10	114	2.0	0.29	0.13	4.2	< LOD	17	0.26
		Ctrl. 2	38	2.0	0.47	10	110	2.2	0.31	0.12	4.6		18	0.24
		Dexamethasone	25	2.2	0.53	12	125	2.0	0.15	0.14	3.8		18	0.31
	B	Ctrl .1	29	2.8	0.50	11	143	1.4	0.20	0.062	2.7	< LOD	17	0.17
		Ctrl. 2	39	3.4	0.82	11	154	1.5	0.19	0.10	3.1		19	0.18
		ML351	37	3.8	0.63	5.3	94	2.0	0.36	< LOD	3.5		22	0.25
	C	Ctrl .1	27	2.4	1.5	16	56	0.75	0.26	0.064	3.4	< LOD	0.38	0.079
		Ctrl. 2	29	2.9	1.3	19	65	0.40	0.20	0.044	2.4		0.24	0.049
		Dexamethasone	21	1.7	1.4	14	67	0.62	0.15	0.082	3.2		0.46	0.086
	D	Ctrl .1	35	3.1	2.3	27	232	0.51	0.15	0.10	1.8	< LOD	1.2	0.18
		Ctrl. 2	30	3.2	3.2	31	247	0.68	0.15	0.10	2.1		1.0	0.15
		Celecoxib	13	1.5	4.0	29	296	0.55	0.12	0.080	1.8		0.89	0.11
	E	Ctrl .1	41	1.9	3.0	41	435	0.91	0.15	0.075	1.0	< LOD	4.5	0.15
		Ctrl. 2	35	2.2	2.0	31	344	0.78	0.13	0.054	0.6		3.3	0.14
		Dexamethason	23	0.91	3.5	50	516	1.3	0.10	0.12	1.0		9.6	0.23
		ML351	51	3.9	1.7	27	233	0.81	0.19	0.032	0.8		4.4	0.13
	F	Ctrl .1	17	1.2	1.9	21	368	0.72	0.10	0.10	2.7	< LOD	2.0	0.48
		Ctrl. 2	14	0.71	2.4	19	295	0.75	0.11	0.13	3.0		2.3	0.52
		Indomethacin	0.84	< LOD	2.5	19	291	0.83	0.070	0.086	2.7		2.3	0.40
		Dexamethasone	8.6	0.51	2.8	26	389	0.75	0.032	0.084	2.6		2.7	0.53
		ML351	16	0.95	2.1	8.7	202	0.79	0.070	< LOD	2.7		2.0	0.29
	G	Ctrl .1	45	2.7	2.3	27	346	0.75	0.24	0.056	1.1	< LOD	4.0	0.16
		Ctrl. 2	41	2.5	2.0	31	362	0.85	0.28	0.043	0.9		4.4	0.17
		Indomethacin	3.8	0.086	3.0	39	441	1.4	0.37	0.10	3.3		5.9	0.21
		Dexamethasone	53	3.5	2.9	45	444	1.1	0.24	0.10	1.5		5.2	0.14
		Celecoxib	31	2.8	3.9	59	493	0.88	0.18	0.080	2.0		3.0	0.10
		ML351	100	7.9	1.3	17	200	1.3	0.48	< LOD	2.2		4.5	0.12
	H	Ctrl .1	55	4.3	1.6	23	309	1.3	0.36	0.081	2.2	< LOD	6.8	0.40
		Ctrl. 2	53	4.5	1.8	23	356	1.3	0.38	0.082	2.9		4.2	0.34
		Indomethacin	5.9	1.0	2.1	21	290	0.94	0.20	0.085	2.5		2.7	0.34

Tab. 7.17 continued.

	Donor	Incubation	(A) ii) Relative oxylipin conc (% of ctrl)					(B) ii) Relative protein levels (% of ctrl)						
			12-HHTrE	PGE_2	5-HETE	12-HETE	15-HETE	COX-1	COX-2	5-LOX	FLAP	12-LOX	15-LOX	15-LOX-2
M1 + 1 µg/mL LPS	A	Ctrl. 1	96	93	89	121	118	77	85	77	74	< LOD	< LOD	< LOD
		Ctrl. 2	104	107	111	79	82	123	115	123	126			
		Indomethacin	8	12	92	70	7	124	140	118	124			
		Dexamethasone	90	117	92	96	57	118	53	142	118			
		PF4191834	105	133	89	59	45	131	96	232	132			
	B	Ctrl. 1	99	104	92	108	104	92	90	86	87	< LOD	< LOD	< LOD
		Ctrl. 2	101	96	108	92	96	108	110	114	113			
		Indomethacin	21	16	92	65	8	143	150	147	147			
		Dexamethasone	66	49	101	54	53	197	101	218	206			
		PF4191834	72	80	97	13	63	167	118	302	160			
	C	Ctrl. 1	116	113	94	110	116	111	116	91	102	< LOD	< LOD	< LOD
		Ctrl. 2	84	87	106	90	84	89	84	109	98			
		Indomethacin	14	12	97	185	6	107	102	84	102			
		Dexamethasone	60	68	158	83	55	88	36	125	95			
		PF4191834	153	131	61	57	78	103	79	126	92			
	D	Ctrl. 1	112	112	107	78	99	108	113	111	118	< LOD	< LOD	< LOD
		Ctrl. 2	88	88	93	122	101	92	87	89	82			
		Indomethacin	13	9	111	162	6	83	90	81	68			
		Dexamethasone	42	44	307	101	32	97	38	160	89			
		PF4191834	97	70	74	160	73	90	65	141	53			
M2 +1 µg/mL LPS	A	Ctrl .1	100	107	94	99	101	94	96	105	96	< LOD	98	103
		Ctrl. 2	100	93	106	101	99	106	104	95	104		102	97
		Dexamethasone	65	102	119	116	112	98	52	112	86		101	125
	B	Ctrl .1	85	91	76	103	96	95	104	78	91	< LOD	97	96
		Ctrl. 2	115	109	124	97	104	105	96	122	109		103	104
		ML351	109	122	95	49	63	138	186	20	119		124	142
	C	Ctrl .1	98	91	107	91	92	130	113	119	117	< LOD	123	124
		Ctrl. 2	102	109	93	109	108	70	87	81	83		77	76
		Dexamethasone	75	65	102	78	111	107	66	152	110		146	135
	D	Ctrl .1	107	97	85	93	97	85	100	98	92	< LOD	111	109
		Ctrl. 2	93	103	115	107	103	115	100	102	108		89	91
		Celecoxib	40	46	147	98	124	93	82	80	92		83	68
	E	Ctrl .1	108	92	120	115	112	107	109	116	125	< LOD	115	102
		Ctrl. 2	92	108	80	85	88	93	91	84	75		85	98
		Dexamethason	60	44	138	139	133	156	71	185	133		245	160
		ML351	133	191	65	75	60	96	138	25	110		113	89
	F	Ctrl .1	110	125	88	105	111	97	99	85	95	< LOD	92	96
		Ctrl. 2	90	75	112	95	89	103	101	115	105		108	104
		Indomethacin	5	5	116	93	88	113	66	76	96		108	80
		Dexamethasone	56	53	128	128	117	102	30	74	93		125	107
		ML351	103	100	97	43	61	108	67	14	95		93	59
	G	Ctrl .1	104	105	107	93	98	94	91	113	113	< LOD	96	95
		Ctrl. 2	96	95	93	107	102	106	109	87	87		104	105
		Indomethacin	9	2	136	135	124	175	141	199	334		142	125
		Dexamethasone	122	133	131	155	125	138	94	195	147		124	84
		Celecoxib	71	109	179	207	139	110	68	161	198		72	61
		ML351	231	303	61	58	56	157	184	33	221		106	74
	H	Ctrl .1	101	98	93	98	93	99	98	99	86	< LOD	124	108
		Ctrl. 2	99	102	107	102	107	101	102	101	114		76	92
		Indomethacin	11	23	123	91	87	72	53	104	100		49	92

Tab. 7.17 continued.

M1 + LPS	(A) iii) Mean of relative oxylipin conc (% of ctrl) 12-HHTrE	PGE_2	5-HETE	12-HETE	15-HETE
Ctrl.	100 ± 4	100 ± 4	100 ± 3	100 ± 6	100 ± 5
Indomethacin	14 ± 3	12 ± 1	98 ± 4	121 ± 31	7 ± 1
Dexamethasone	52 ± 10	56 ± 17	132 ± 50	67 ± 11	39 ± 6
PF4191834	107 ± 17	103 ± 17	80 ± 8	72 ± 31	65 ± 7
M2 +LPS					
Indomethacin	8 ± 2	10 ± 6	125 ± 6	106 ± 14	100 ± 12
Dexamethasone	76 ± 18	80 ± 21	124 ± 23	123 ± 25	120 ± 22
Celecoxib	56 ± 16	78 ± 32	163 ± 16	152 ± 55	131 ± 8
ML351	144 ± 30	179 ± 46	80 ± 10	56 ± 7	60 ± 1

M1 + LPS	(B) iii) Mean of protein levels (% of ctrl) COX-1	COX-2	5-LOX	FLAP	12-LOX	15-LOX	15-LOX-2
Ctrl.	100 ± 5	100 ± 5	100 ± 6	100 ± 6			
Indomethacin	114 ± 13	120 ± 14	107 ± 16	110 ± 17	< LOD	< LOD	< LOD
Dexamethasone	125 ± 25	57 ± 15	161 ± 20	127 ± 27			
PF4191834	123 ± 17	90 ± 11	200 ± 41	109 ± 23			
M2 +LPS							
Indomethacin	120 ± 30	87 ± 28	126 ± 37	177 ± 79		100 ± 27	99 ± 13
Dexamethasone	120 ± 12	63 ± 11	144 ± 23	114 ± 12		148 ± 25	122 ± 13
Celecoxib	102 ± 8	75 ± 7	121 ± 41	145 ± 53	< LOD	78 ± 6	65 ± 3
ML351	125 ± 14	144 ± 28	23 ± 4	136 ± 29		109 ± 6	91 ± 18

≤ 25%	≤ 50%	≤ 75%	≥ 125%	≥150%	≥175%	≥200%	of control

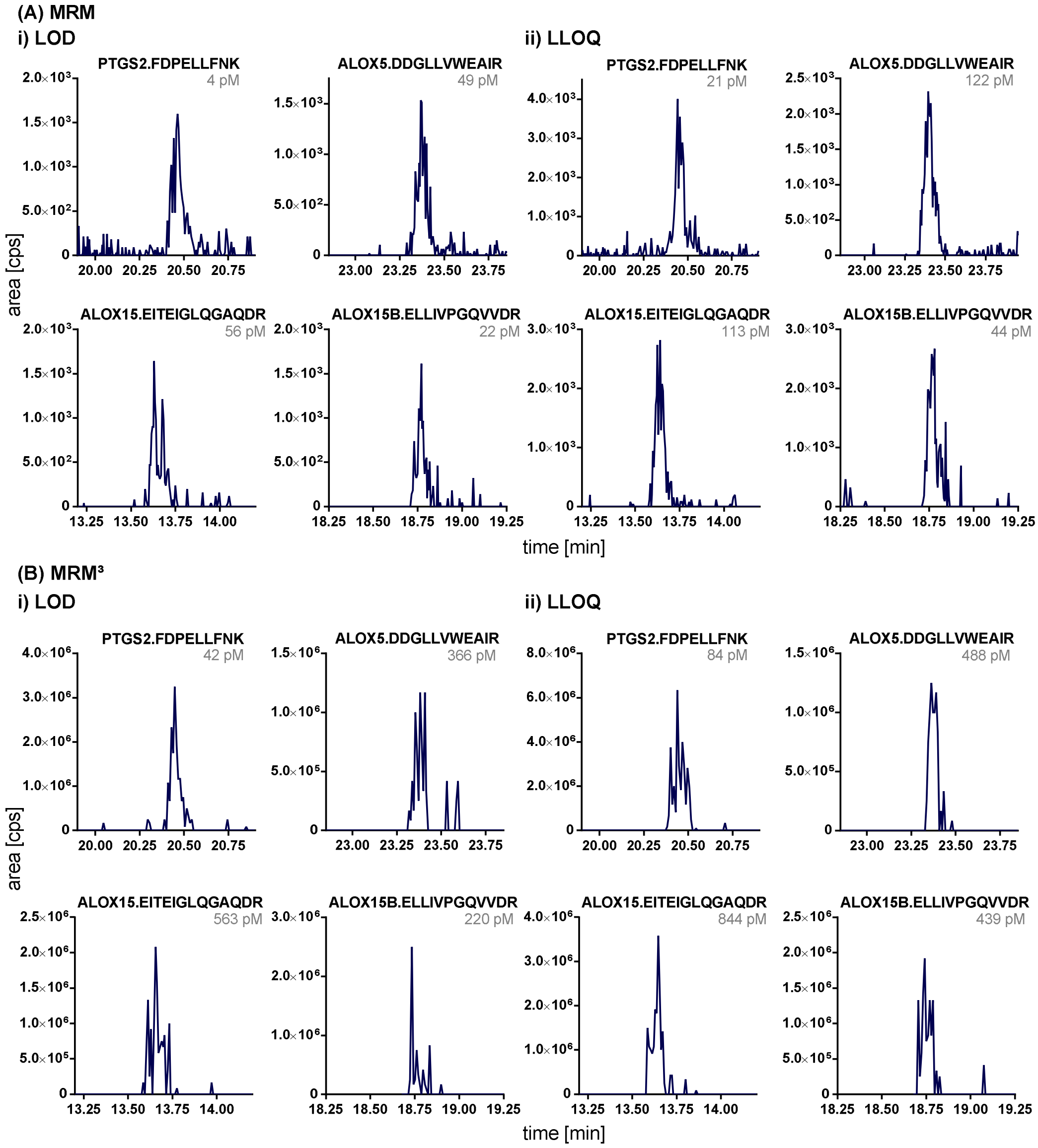

Fig. 7.10: Comparison of MRM and MRM³ sensitivities. Comparison of **(A)** MRM and **(B)** MRM³ modes regarding **i)** limits of detection (LOD) and **ii)** lower limits of quantification (LLOQ) for peptides of COX-2 (FDPELLFNK), 5-LOX (DDGLLVWEAIR), 15-LOX (EITEIGLQGAQDR) and 15-LOX-2 (ELLIVPGQVVDR). LOD was set to S/N ≥ 3 and LLOQ to S/N ≥ 5 and accuracies within ± 20%.

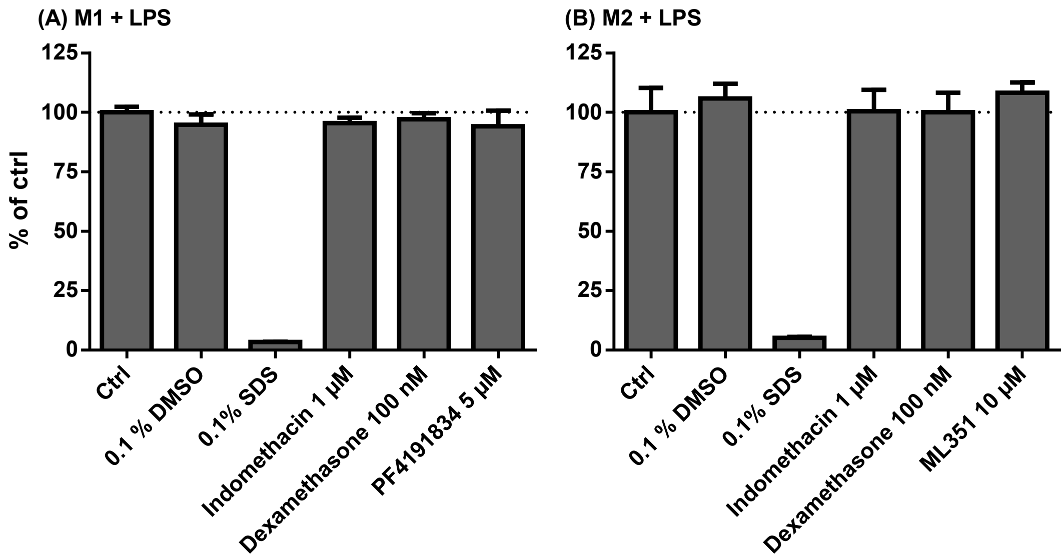

Fig. 7.11: Cell viability assay. Cell viability was determined by resazurin assay in human primary macrophages. Cells were differentiated with **(A)** 10 ng/mL CSF-2 (M1-like cells) or **(B)** CSF-1 (M2-like cells) for 8 days and with 10 ng/mL IFNγ (M1-like cells) or IL-4 (M2-like cells) for the final 48 h. The cells were incubated with the different test compounds at the indicated concentrations for the final 7 h during additional 1 µg/mL LPS stimulation for the final 6 h. DMSO served as vehicle control and SDS as positive control. Dehydrogenase activity was measured as resorufin formation by fluorometric readout at 590 nm after excitation at 560 nm [7]. Shown are mean ± SD for n = 6-12 technical replicates from a pool of 5 donors.

References

1. Willenberg I, Meschede AK, Gueler F, Jang MS, Shushakova N, Schebb NH (2015) Food Polyphenols Fail to Cause a Biologically Relevant Reduction of COX-2 Activity. PLoS One, 10 e0139147, doi: 10.1371/journal.pone.0139147.
2. Koch E, Mainka M, Dalle C, Ostermann AI, Rund KM, Kutzner L, Froehlich L-F, Bertrand-Michel J, Gladine C, and Schebb NH (2020) Stability of oxylipins during plasma generation and long-term storage. Talanta, 217, 121074; doi: 10.1016/j.talanta.2020.121074.
3. Rund KM, Ostermann AI, Kutzner L, Galano JM, Oger C, Vigor C, Wecklein S, Seiwert N, Durand T, and Schebb NH (2018) Development of an LC-ESI(-)-MS/MS method for the simultaneous quantification of 35 isoprostanes and isofurans derived from the major n3- and n6-PUFAs. Anal Chim Acta, 1037, 63-74; doi: 10.1016/j.aca.2017.11.002.
4. Kutzner L, Rund KM, Ostermann AI, Hartung NM, Galano JM, Balas L, Durand T, Balzer MS, David S, and Schebb NH (2019) Development of an Optimized LC-MS Method for the Detection of Specialized Pro-Resolving Mediators in Biological Samples. Front Pharmacol, 10; doi: 10.3389/fphar.2019.00169.
5. Hartung NM, Mainka M, Kampschulte N, Ostermann AI, and Schebb NH (2019) A strategy for validating concentrations of oxylipin standards for external calibration.

Prostaglandins Other Lipid Mediat, 141, 22-24; doi: 10.1016/j.prostaglandins.2019.02.006.

6. Hartung NM, Ostermann AI, Immenschuh S, and Schebb NH (2021) Combined Targeted Proteomics and Oxylipin Metabolomics for Monitoring of the COX-2 Pathway. Proteomics, 21(3-4), 1900058; doi: 10.1002/pmic.201900058.
7. O'Brien J, Wilson I, Orton T, and Pognan F (2000) Investigation of the Alamar Blue (resazurin) fluorescent dye for the assessment of mammalian cell cytotoxicity. Eur J Biochem, 267(17), 5421-5426; doi: 10.1046/j.1432-1327.2000.01606.x.

Abbreviations

12-HHT	12-hydroxyheptadecatrienoic acid
AF2	excitation energy
VD_3	1,25-dihydroxyvitamin D_3
ACN	acetonitrile
aa	amino acid
ARA	arachidonic acid
BCA	bicinchoninic acid
BHT	butylated hydroxytoluene
CP-DT	cleavage prediction with decision trees
CXP	collision cell exit potential
CE	collision energy
CAD	collisionally activated dissociation
COX	cyclooxygenase
CYC1	cytochrome c1
CYP	cytochrome P450 monoxygenase
DP	declustering potential
DiHOME	dihydroxyoctadecenoic acid
DiHETrE	dihydroxyeicosatrienoic acid
DHA	docosahexaenoic acid
DFT	dynamic fill time
EPA	eicosapentaenoic acid
ESI	electrospray ionization
EP	entrance potential
EGCG	epigallocatechin-gallate
EpETrE	epoxyeicosatrienoic acid
EpOME	epoxyoctadecenoic acid
FLAP	five lipoxygenase activating protein
FFT	fixed fill time
FWHM	full width at half maximum
ALOX5	gene of the 5-lipoxgenase enzyme (5-LOX)
PTGS1/2	genes of the prostaglandin G/H synthase 1/2 proteins (COX-1/-2)
GAPDH	glyceraldehyde-3-phosphate dehydrogenase
GM-CSF	granulocyte-macrophage colony-stimulating factor
HPLC	high performance liquid chromatography
H(p)ETE	hydro(pero)xyeicosatetraenoic acid
HDHA	hydroxydocosahexaenoic acid
HEPE	hydroxyeicosapentaenoic acid

HETE	hydroxyeicosatetraenoic acid
HODE	hydroxyoctadecadienoic acid
iNOS	inducible NO synthase
IFN	interferon gamma
IL	interleukin
IS	internal standard
IsoP	isoprostane
LDH	lactate dehydrogenase
LT	leukotriene
LOD	limit of detection
LIT	linear ion trap
LM	lipid mediator
LPS	lipopolysaccharide
Lx	lipoxin
LOX	lipoxygenase
LC	liquid chromatography
LLOQ	lower limit of quantification
M-CSF	macrophage-colony stimulating factor
MS	mass spectrometry
m/z	mass-to-charge ratio
MAPEG	membrane associated proteins in eicosanoid and glutathione metabolism
MeOH	methanol
MRM	multiple reaction monitoring
MRM^3	multiple reaction monitoring cubed
P/S	penicillin/streptomycin
PPIB	peptidyl-prolyl cis-trans isomerase B
PBMC	peripheral blood monocytic cells
PBS	phosphate buffered saline
PUFA	polyunsaturated fatty acids
PTM	postranslational modification
PG	prostaglandin
PTP	proteotypic peptide
Rv	resolvin
IRA	resveratrol imine analogue
RT	retention time
SRM	selected reaction monitoring
SAV	single amino acid variant
SIM	single ion monitoring
nsSNP	single nucleotide polymorphism
SDC	sodium deoxycholate

SPM	specialized pro-resolving mediator
SSRCalc	Sequence Specific Retention Calculator
STD	standard
Tx	thromboxane
TXAS	thromboxane synthase
TGF-β1	transforming growth factor beta 1
TRIS	tris(hydroxymethyl)aminomethane
U	uniformely labeled

Acknowledgement

This thesis was carried out from April 2017 to October 2021 at the Institute for Food Toxicology (University of Veterinary Medicine Hannover) and at the Chair of Food Chemistry (University of Wuppertal) in the research group of Prof. Dr. Nils Helge Schebb.

Now, facing its completion, I want to express my gratitude to everybody who worked with and supported me during this time, colleagues and cooperation partners, as well as family and friends who accompanied and encouraged me along the way to successfully finalize this thesis.

First of all, I want to thank my supervisor Prof. Dr. Nils Helge Schebb for giving me the opportunity to work in his group on an interesting and multi-faceted project focusing on instrumental analytical methods and biological questions addressed with different cell culture experiments. I thank him for the valuable scientific discussions and advice, his encouragement and support throughout the whole time of my thesis. I am also grateful for the opportunities I was given to participate in many national and international conferences where I had the chance to present my work and discuss it with other scientists.

I further thank Prof. Dr. Julia Bornhorst for introducing me to various cell culture techniques and giving advice in the lab and beyond as well as for being a board member of the PhD committee.

I am grateful for the financial support in form of a Kekulé fellowship that I received from the Fonds der Chemischen Industrie (Frankfurt am Main, Germany).

For the successful collaboration I want to thank Prof. Dr. Ulrike Garscha and a special thanks goes to Dr. Jana Fischer for performing lab the experiments with neutrophils that led to the results presented in chapter 3.

I also thank Prof. Dr. Stephan Immenschuh and his team for the friendly cooperation and for providing samples of primary human macrophages used in chapter 2.

Further, I would like to thank Sebastian Biernacki and Michael Kuhn for their diligent work during their master theses and partly as research assistant that led to valuable contributions to this thesis.

I also want to acknowledge Anne Kaufmann and Lilli Zinnert for contributing to this thesis as student research associates and always being open to learn.

I would like to acknowledge Prof. Dr. Kietzmann and Prof. Dr. Bettina Seeger who enabled uncomplicated transition of the group from the University of Veterinary Medicine in Hannover to the University of Wuppertal.

For initially sparking my interest in chemistry and science with numerous exiting experiments in class I want to thank my former chemistry teacher Mrs. Cibis. I thank Dr. Anja These for her contagious fascination of research during my master thesis which paved the way for my own research interest and scientific work.

A special thanks goes to my colleagues of the AG Schebb with whom I shared many funny, joyful and stressful moments at work and beyond with many unforgettable memories. It was a great pleasure to work with you in the last years.

I thank Dr. Katharina Rund who for her endless energy and motivation, for always taking time to help or give advice and digging out useful things from her office when needed. Thank you for sharing your delicious food, anecdotes of train travel and late walks home together after work with long talks before separating at “the corner”.

Many thanks go to Malwina Mainka for mastering the challenges of the standard verification and “PG Kali” with me and taking the first steps together in working with primary macrophages. Thank you for sharing candy and spending many funny procrastination breaks in our office together, initiating furniture shopping trips and sharing the struggles of aging.

Elisabeth Koch, I thank for her critical and honest opinion and making sure that everything is in the right place of the lab, but most importantly for her talent for jokes and her humor. Thank you for exchanging recipes, providing n3 supplements and oil as well as never missing out on a “(großer) gemischter Vorspeisenteller” while testing restaurants together in Wuppertal.

I want to thank Dr. Nadja Kampschulte for her support in tackling technical challenges and managing numerous topics in the lab, particularly cleaning out unnecessary items. Thank you for keeping track of new *-omics* terms, creating a good mood during work (not only with musical entertainment from the sound board), mutual compliments and letting me ride with you and Rufus in the rain.

I would like to thank Rebecca Pfaff for learning how to generate primary macrophages together with me and for her (late-night) assistance in the cell culture.

I thank Dr. Laura Kutzner for her excellent scientific advice and tolerating my coaching and inspiration attempts that hopefully did not remain without effect.

Dr. Annika Ostermann I would like to thank for introducing me to the first steps in proteomics, her valuable scientific opinion and pleasant bike rides home together while working in Hannover.

I want to like to thank Michelle Wiebel for giving excellent touristic advice to discover Wuppertal and the surrounding area and Laura Carpanedo for reactivating my French skills and the friendly greetings in the hall.

Further, I thank all current and former members of the group for the pleasant working atmosphere, respectful interaction and constant helpfulness. Especially Dieter Riegel, Claudia Steinhage and Marion Fischer who taught me many helpful tips and tricks for the practical lab courses and Sabine Scalet for her patience in dealing with bureaucracy.

I also would like to thank the group members AG B(ornhorst) for the nice working atmosphere, and especially Dr. Merle Nicolai and Vivien Michaelis for the fun celebration of the last “normal” rhenish carnival together.

My former colleagues at the University of Veterinary Medicine in Hannover I also want to thank for the pleasant working environment. Particularly, I thank Dr. Michael Empl for his jokes and endless conversations as well as Dr. Tina

Kostka and Dr. Maren Schenke for unforgettable game nights with pizza and döner.

During the course of my thesis I made new friends in Hannover and Wuppertal with whom I enjoyed the time outside of work. In particular, I want to thank Dumar, Can-Nur, Sofia and Andres with whom I shared wonderful dance evenings and delicious meals in Hannover. I thank Terris for showing me Wuppertal's hidden gems and expanding my knowledge in film and music.

Most importantly, I would like to extend my gratitude to my family and friends who always encouraged me along the way. I very much thank Fousi for his constant support, endless patience and always being there for me. I am extremely grateful for the unconditional support of my parents and I thank them and my sister Michelle for always encouraging and believing in me.

THANK YOU!

Curriculum Vitae

Der Lebenslauf ist in der Online-Version aus Gründen des Datenschutzes nicht enthalten.

Der Lebenslauf ist in der Online-Version aus Gründen des Datenschutzes nicht enthalten.

List of Publications

Publications in peer-reviewed Journals

Within the Scope of this Thesis

Hartung NM, Mainka M, Pfaff R, Kuhn M, Biernacki S, Zinnert L, Schebb NH (2022) Development of a quantitative multi-omics approach for the comprehensive analysis of the arachidonic acid cascade in immune cells, *submitted for publication*

Hartung NM, Ostermann AI, Immenschuh S, Schebb NH (2021) Combined targeted proteomics and oxylipin metabolomics for monitoring of the COX-2 pathway. *Proteomics*, 21 (3-4), 1900058; doi: 10.1002/pmic.201900058.

Hartung NM*, Fischer J*, Ostermann AI, Willenberg I, Rund KM, Schebb NH, Garscha U (2019) Impact of food polyphenols on oxylipin biosynthesis in human neutrophils. *Biochim Biophys Acta, Mol Cell Biol Lipids*, 1864 (10), 1536-1544; doi: 10.1016/j.bbalip.2019.05.002.
*Authors contributed equally to this work.

Further Publications

Mainka M, Pfaff R, Hartung NM, Schebb NH (2022) Sterol derivatives specifically increase anti-inflammatory oxylipin formation in M2-like macrophages by LXR mediated induction of 15-lipoxygenase LOX, *submitted for publication*

Kopczynski D, Hentschel A, Coman C, Schebb NH, Hornemann T, Mashek DG, Hartung NM, Shevchuk O, Schött HF, Lorenz K, Torta F, Burla B, Zahedi RP, Sickmann A, Kreutz MR, Ejsing CS, Medenbach J and Ahrends R (2020) Simple Targeted Assays for Metabolic Pathways and Signaling: A Powerful Tool for Targeted Proteomics. *Anal Chem*, 92 (20), 13672 – 13676; doi: 10.1021/acs.analchem.0c02793.

Rohwer N, Kühl AA, Ostermann AI, Hartung NM, Schebb NH, Zopf D, McDonald FM, Weylandt KH (2020) Effects of chronic low-dose aspirin treatment on tumor prevention in three mouse models of intestinal tumorigenesis. *Cancer Med*, 9 (7), 2535–2550; doi: 10.1002/cam4.2881.

Jung S, Lauter J, Hartung NM, These A, Hamscher G, Wissemann V (2020) Genetic and chemical diversity of the toxic *herb Jacobaea vulgaris Gaertn. (syn. Senecio jacobaea L.*) in Northern Germany. *Phytochemistry*, 172,112235; doi: 10.1016/j.phytochem.2019.112235.

Kutzner L, Rund KM, Ostermann AI, Hartung NM, Galano JM, Balas L, Durand T, Balzer MS, David S, Schebb NH (2019) Development of an optimized LC-MS method for the detection of specialized pro-resolving mediators in biological samples. *Front Pharmacol,* 10, 169; doi: 10.3389/fphar.2019.00169.

Hartung NM*, Mainka M*, Kampschulte N, Ostermann AI, Schebb NH (2019) A strategy for validating concentrations of oxylipin standards for external calibration. *Prostaglandins Other Lipid Mediators*, 141, 22-24; doi: 10.1016/ j.prostaglandins.2019.02.006.
*Authors contributed equally to this work.

Ostermann AI, Greupner T, Kutzner L, Hartung NM, Hahn A, Schuchardt JP, Schebb NH (2018) Intra-individual variance of human plasma oxylipin pattern: Low inter-day variability in fastened blood samples versus high variability during the day. *Anal Methods,* 10, 4935 – 4944; doi: 10.1039/c8ay01753k.

Ostermann AI, Reutzel M, Hartung N, Franke N, Kutzner L, Schoenfeld K, Weylandt KH, Eckert GP, Schebb NH (2017) A Diet Rich in Omega-3 Fatty Acids Enhances Expression of Soluble Epxide Hydrolase in Murine Brain. *Prostaglandins Other Lipid Mediators*, 133, 79-87; doi: 10.1016/j.prostaglandins.2017.06.001.

Zhang Y, Hartung NM, Fraatz MA, Zorn H (2015) Quantification of key odor-active compounds of a novel nonalcoholic beverage produced by fermentation of wort by shiitake (*Lentinula edodes*) and aroma genesis studies. *Food Res Int*, 70, 23−30; doi: 10.1016/j.foodres.2015.01.019.

ORAL PRESENTATIONS

Hartung NM (2021) Untersuchung der Wirkung von Polyphenolen auf Cyclooxygenasen und Lipoxygenasen mittels targeted Proteomics und Metabolomics Methoden, 49. Deutscher Lebensmittelchemikertag (online), Germany.

Hartung NM (2019) Targeted proteomics and lipidomics for investigating the modulation of cyclooxygenase-2 expression and activity, Stipendiatentreffen des Verbandes der Chemischen Industrie in Frankfurt am Main, Germany.

Hartung NM (2019) Optimization of an LC-MS targeted proteomics approach for investigation of cyclooxygenase 2, 52. DGMS-Jahrestagung in Rostock, Germany.

Hartung NM (2018) Targeted Metabolomics zur Untersuchung der Modulation der 5-Lipoxygenase Aktivität durch Lebensmittel, 28. Doktorandenseminar des AK Separation Science der GDCh Fachgruppe Analytische Chemie in Hohenroda, Germany.

POSTER PRESENTATIONS

Hartung NM, Immenschuh S, Schebb NH (2020) Characterization of cyclooxygenase expression and activity in different cell lines using targeted proteomics and lipidomics, Virtual 18th Winter Eicosanoid Conference, USA.

Hartung NM, Immenschuh S, Schebb NH (2019) Method development for an LC-MS targeted proteomics approach for investigating the arachidonic acid-cascade, 8. Berliner LC-MS/MS Symposium in Berlin, Germany.

Hartung NM, Immenschuh S, Schebb NH (2019) Investigation of cyclooxygenase 2 expression by LC-MS targeted proteomics, Regionalverbandstagung Nordrhein-Westfalen der Lebensmittelchemischen Gesellschaft in Wuppertal, Germany.

Hartung NM, Immenschuh S, Schebb NH (2019) Development of a targeted proteomics method for investigation of cyclooxygenase-2 expression, Proteomic Forum 2019, XIII. Annual Congress of the European Proteomics Association in Potsdam, Germany.

Hartung NM, Ostermann AI, Schebb NH (2018), LC-MS/MS approach for investigation of cyclooxygenase-2 expression, Lipidomics Forum in Dortmund, Germany.

Hartung NM, Ostermann AI, Schebb NH (2018), Analysis of cyclooxygenase-2 expression by means of LC-MS/MS, 47. Deutscher Lebensmittelchemikertag in Berlin, Germany.

Mainka M, Hartung NM, Kampschulte N, Ostermann AI, Schebb NH (2018) Is in, what's on? - Verification of concentrations of commercially available standards for quantification of oxylipins, 47. Deutscher Lebensmittelchemikertag in Berlin, Germany.

Hartung NM, Ostermann AI, Schebb NH (2018), LC-MS/MS based analysis of cyclooxygenase 2 expression and activity, 7th European Workshop on Lipid Mediators in Brussels, Belgium.

Mainka M, Hartung NM, Kampschulte N, Ostermann AI, Schebb ,NH (2018) Challenges in absolute quantification of oxylipins – A strategy for the preparation of standard series and verification of concentrations, 7th European Workshop on Lipid Mediators in Brussels, Belgium.

Hartung NM, Fischer J, Garscha U, Schebb NH (2018) Modulating Effects of Food Polyphenols on 5-Lipoxygenase Activity, The 17th International Winter Eicosanoid Conference in Baltimore, MD, USA.

Hartung NM, Fischer J, Garscha U, Schebb NH (2017) Modulation of 5-Lipoxygenase Activity by Food Polyphenols, 46. Deutscher Lebensmittelchemikertag in Würzburg, Germany.